Noble gas isotope investigation of unconventional hydrocarbon reservoirs and related subsurface environments

David Byrne

St Peter's College

University of Oxford

A thesis submitted for the degree of

Doctor of Philosophy

Michaelmas 2018

Abstract

Unconventional petroleum reservoirs represent complex subsurface fluid environments. Investigating the behaviour of these systems has important consequences for our energy production, environmental impact, and has the potential to further our general understanding of subsurface fluid behaviour in low-porosity systems. This study utilises noble gas isotopes in produced gases as geochemical tracers to investigate several facets of unconventional petroleum systems and related regimes. Firstly, the behaviour of source-rocks during natural gas generation is investigated in the Eagle Ford Shale (South Texas, USA). Here, clear relationships are shown between the noble gas composition and parameters for thermal maturity, including δ^{13}C of methane. This allows new constraints to be placed on the behaviour of gas during generation and leads to novel approaches for quantifying the extent of gas generation within and expulsion from source-rocks. Secondly, the migration of hydrocarbons from source-rock to reservoir is investigated in a series of related samples from the Haynesville play area (East Texas, USA). Migrated samples from conventional reservoirs are shown to have much higher abundances of atmosphere-derived and radiogenic noble gas isotopes. These observations are used to test conceptual models of subsurface gas flow and ultimately to quantify the relative volumes of gas, water and rock encountered during migration. Finally, we investigate the behaviour of geothermal fluids in Iceland, using a similar approach but applying it to another low-porosity subsurface environment. Here, atmosphere-derived noble gas isotopes display solubility-dependent fractionation patterns, likely as a result of geothermal boiling and degassing at depth. The data and interpretations presented in this study greatly expand our understanding of noble gas behaviour in low-porosity rocks, and highlight new potential for their use as tracers in subsurface environments.

Extended Abstract

The recent proliferation of unconventional shale gas reservoirs as an energy resource enables a more detailed investigation of the geochemical behaviour of these systems. In addition, it provides an opportunity to improve our understanding of other low-permeability crustal fluid systems at depth. Organic-rich shales are not only the source-rocks in conventional petroleum systems, but potential seals, which may be important for the trapping and storage of CO_2 and/or nuclear waste.

In this study we measure noble gas isotopes in produced natural gases and geothermal fluids, in order to better understand their evolution and behaviour. Noble gases are ideal tracers of fluid provenance and physical processes in the subsurface due to their inert nature. Using 3 case studies, we investigate several aspects of different subsurface fluid regimes.

Firstly, the behaviour of source-rocks during natural gas generation is investigated in the Eagle Ford Shale (South Texas, USA). The Eagle Ford is an unconventional source-rock reservoir, which generates hydrocarbon gas at a range of depths. As hydrocarbon generation is controlled primarily by temperature this range of depths equates to different stages of hydrocarbon generation across the basin. Noble gas concentrations and isotopic characteristics were determined in 10 natural gas samples, along with the concentrations and δ^{13}C and δD of hydrocarbon gases. The large range in thermal maturity exhibited across the basin, as demonstrated by the range in δ^{13}C of methane from -37.8 to -47.5‰ VPDB, allows us to constrain the evolution of the noble gas signature within a source-rock during hydrocarbon generation and expulsion. For the first time, we show that ^{36}Ar concentrations in hydrocarbon gases are not simply controlled by solubility exchange with formation water. Instead, they are shown to decrease dramatically (from 2.6×10^{-7} to 7.0×10^{-9}cm^{3}STPcm^{-3}) with increasing thermal maturity, which we attribute to a dilution effect as more short-chain hydrocarbon compounds are generated through cracking of kerogen and secondary cracking of oil. We develop a model that combines ^{36}Ar concentrations with δ^{13}C data in order to quantify the retention capacity for generated hydrocarbons, and show that between 40 to 80% of the hydrocarbons generated by the Eagle Ford shale are retained within the formation. We also calculate that radiogenic ^{4}He concentrations within the Eagle Ford are well in excess of that which could have accumulated internally since deposition and requires contributions from external ^{4}He sources.

Secondly, the migration of hydrocarbons from source-rock to reservoir is investigated in a series of related samples from the Haynesville play area (East Texas, USA). The migration of hydrocarbons from source-rock to reservoir represents one of the critical stages of petroleum system evolution, but is challenging to study geochemically and thus remains poorly understood. By analysing samples produced from genetically-related unconventional source-rock reservoirs and overlying conventional reservoirs we can directly assess the effects of migration on noble gas composition, and infer the processes that caused them. We present new noble gas isotope and abundance data from 27 natural gas wells within the Haynesville basin, including (n=8) from the unconventional Haynesville source-rock. In addition, we report data from samples derived from the overlying conventional reservoirs within Cotton Valley (n=5), Travis Peak (n=9), and James Lime (n=5). Samples consist primarily of methane (>70%), with small contributions from longer chain hydrocarbons, and other gases such as CO_2 and N_2. Noble gas abundances for both atmosphere-derived and radiogenic isotopes are significantly higher in conventional reservoirs, clearly reflecting the effects of the migration process. We present a model that can be used to constrain the volumes of rock and groundwater encountered by the conventional gas accumulation during migration. Specifically we observe progressive incorporation of mantle-sourced ^{3}He and radiogenic ^{4}He and ^{40}Ar with increasing migration distance from the source-rock. This results in a counterintuitive distribution of ^{3}He/^{4}He values, with the greatest contributions of mantle He observed in the shallowest reservoirs. We interpret this to be due to mixing between a pristine source-rock signature and an endmember characterised by elevated ^{3}He/^{4}He and ^{40}Ar/^{36}Ar, likely representative of mantle-enriched groundwater circulating in the wider hydrogeological system of the basin. In order to ascertain the processes controlling the introduction of these external noble gases into the impermeable source-rock, we model the flux of He across the basin using a finite-difference approximation of the advection-dispersion-reaction equation. We find that whilst the Haynesville source-rock is relatively impermeable to groundwater advection, groundwater flow in the overlying sandstones can transport mantle ^{3}He and radiogenic ^{4}He. Vertical diffusion from the adjacent strata can then introduce the external signatures into the source-rock.

Finally, we present a case study of geothermal fluids in Iceland, extending the models developed in previous chapters to related volcanic systems. Whilst noble gases have been used in this environment for determining mantle isotope systematics before, the potential of using inter-elemental atmosphere-derived noble gas models is under-utilised. We present new data for complete noble gas isotope and abundance data (He, Ne, Ar, Kr, Xe) from 29 geothermal gases: 16 from geothermal power boreholes and 13 from naturally-degassing fumaroles. Samples are taken from both

the Northern Rift Zone (NRZ) and Western Rift Zone (WRZ) of Iceland. Helium isotope ratios are MORB-like in the NRZ, with values in excess of MORB up to $16.92R_a$ in the WRZ. Neon isotopes show enrichment in primordial $^{20}Ne/^{22}Ne$, plotting close to the solar-air mixing line. Helium and neon isotope systematics are decoupled, consistent with previous studies. Argon, krypton and xenon isotopes are indistinguishable from air. Atmosphere-derived noble gas (ANG) isotopes (^{20}Ne, ^{36}Ar, ^{84}Kr, ^{130}Xe) are strongly correlated and show evidence for solubility-controlled fractionation. A pure air-saturated water source for these ANG isotopes is not consistent with our observations, and instead a small (10%) external contribution with a similar composition to that observed in sediments is required. Multiple-stage gas-water equilibration is required to explain the observed magnitudes of ANG fractionation, supporting repeated boiling/condensation/degassing episodes in the subsurface geothermal system. Concentrations and stable isotope ratios of other major geochemical species show relationships with $^3He/^4He$ ratios. In some cases (δD and $\delta^{18}O$ of H_2O) this is likely to be a superficial relationship due to the geographic distribution of MORB vs OIB signals. However, other observed correlations (e.g. δD and $\delta^{13}C$ of methane) may be indicative of deeper source or process controls.

Overall, the data and interpretations presented in this study greatly expand our understanding of noble gas behaviour in low-porosity rocks, and highlight new potential for their use as tracers in subsurface environments.

Acknowledgements

This thesis is, naturally, the result of contributions from a number of people, some of whom are just as much (if not more) deserving of its authorship as myself. Fortunately the world is not fair in this regard, and so I get to put my name on the cover and they will have to make do with being mentioned here.

First and foremost this project would never have been completed without a lot of hard work and patience on the part of my supervisors, the formidable trio of Peter Barry, Michael Lawson and Chris Ballentine. I'm indebted to Chris for providing a world-class laboratory, letting me break things in it, and for knowing all there is to know about noble gases. I owe Mike for all of his work targeting and securing sampling opportunities, and his encyclopaedic knowledge of all things petroleum geochemistry. I would like to thank Pete for undertaking the unenviable task of training me in mass spectrometry, our awesome field trips, and his daily guidance and motivation to drive the project forward when I was frequently doing my utmost to avoid it.

I have been lucky enough to work with a lot of great scientists over the course of this project. This includes all the members of the Noble Lab past and present who shared in the fun and frustration of labwork, especially Oliver, Michael, Jennifer, Darren, Annie, James, Rosie and Becca. I'd also like to thank Mike Formolo for his insight, and help in obtaining background data and information release. I'm also grateful to Sæmi Halldórsson for fieldwork opportunities, samples, and an education in some of the more obscure genres of music.

I would never have considered undertaking a PhD in geochemistry were it not for my experiences at undergraduate level. For this I must thank Nigel Woodcock, whose infectious enthusiasm for geology and passion for teaching it first led me to fall in love with the subject. I am also grateful to Sambuddha Misra for his continued mentorship on all aspects of the life scientific, and to Team Rainbow for enduring my friendship throughout our time as undergrads.

At Oxford, I was unfortunate enough to have many close friends in the Earth Sciences department, without whom this thesis would likely have been completed in half the time. Some of the worst offenders in this regard include Duane, Tim, Jo, Sean, Vicky and Marta (+ Nomi and Tom!). Special contempt must be reserved for William Nash for our endless discussions over politics, chess, philosophy, or

whatever it was we weren't supposed to be working on. I must admit however that his spectacular demonstration of time management during thesis writing was somewhat instructive. Jon Wade deserves a mention for welcoming me into the World of Wade, which may not have been the most productive office but was certainly the most fun. Some of the few people who may have had a positive impact on my studies are my long-suffering officemates Maria and Afsaneh, for attempting to limit the time I spent watching/playing various sports in the office. I would also like to thank Mel Murphy for helping me not to lose sight of myself, and Elizabeth Crowley for cultivating the oasis of sanity that is the Earth Sciences library.

Science can be thirsty work, and to that end I thank Ian Stuart of the Harcourt Arms for providing a welcoming haven from the stress of the lab, and ensuring that I was suitably refreshed throughout the course of my studies. I also thank the other members of Jazz Valhalla, Jamie, Nick and Pete, for our regular jam sessions, which were perhaps more therapeutic than they were musically accomplished.

I can't imagine what the last few years would have been like without Arola, whose love and support are, as I'm so often reminded, far more than I deserve. Finally, I should thank Mum and Dad for their sacrifices in providing me with every opportunity I could wish for, and for their unfailing belief in me despite all evidence to the contrary.

Declaration

I declare that this thesis has been composed by myself and that the work has not been submitted for any other degree or professional qualification. I confirm that the work submitted is my own, except where work which has formed part of jointly-authored publications has been included. My contributions to these publications have been explicitly indicated below. I confirm that appropriate credit has been given within this thesis where reference has been made to the work of others.

The work presented in Chapter 1, section 1.3 was previously published in *Geological Society of London Special Publications*, Vol. 468 as "Noble gases in conventional and unconventional petroleum systems" by **Byrne, D. J.**, Barry, P. H., Lawson, M., and Ballentine, C. J.. I carried out the compilation and interpretation of data, and wrote the manuscript.

The work presented in Chapter 2 was previously published in *Geochimica et Cosmochimica Acta*, Vol. 241, as "Determining gas expulsion vs retention during hydrocarbon generation in the Eagle Ford Shale using noble gases" by **Byrne, D. J.**, Barry, P. H., Lawson, M., and Ballentine, C. J.. I carried out noble gas analyses, led interpretation and model development, and wrote the manuscript.

The work presented in Chapter 3 has been prepared for submission as "Tracing subsurface fluid flow in the East Texas Basin using noble gas isotopes" by **Byrne, D. J.**, Barry, P. H., Lawson, M., and Ballentine, C. J.. I carried out noble gas analyses, led interpretation and model development, and wrote the manuscript.

Contents

Appendices

List of Figures

List of Tables

List of Abbreviations

ANG . . . . . Atmosphere-derived noble gas

API . . . . . American petroleum institute gravity units

ASW . . . . . Air-saturated water

MORB . . . . Mid-ocean ridge basalt

OIB . . . . . Ocean island basalt

$\mathbf{R}_a$ . . . . . Atmospheric helium isotope ratio

SEM . . . . . Secondary electron multiplier

STP . . . . . Standard temperature and pressure of 273.15K and 10^5Pa

TOC . . . . . Total organic content

1 Introduction

Contents

1.1 Motivation

This project was conceived with the aim of applying and adapting the techniques of noble gas isotope geochemistry into a relatively new and rapidly evolving field. The use of noble gas isotopes to investigate petroleum systems in the subsurface dates back decades (Zartman et al., 1961; Wasserburg et al., 1963). However the landscape of hydrocarbon production has been revolutionised in recent years with the advent of unconventional production (also known as shale gas or shale oil). From being a

minor component of energy output ten years ago, unconventional production now accounts for 50% of U.S. oil production and 60% of natural gas production, with projections set to increase this share in the coming years (EIA, 2018). Given the likely continued significance of these energy resources, understanding their behaviour is crucial for safe and effective operation. Unconventional systems represent a fundamentally different method of hydrocarbon extraction from a fundamentally different subsurface environment. As such, it is relatively poorly understood from a geochemical perspective. Given the potential of noble gases as tracers, it is timely to revisit and revise their use in petroleum systems for this new era.

The findings from the noble gas analysis of produced unconventional gases are also likely to have implications in related fields. Unconventional hydrocarbons are produced directly from the organic-rich source-rocks in which they are generated. Source-rocks represent a previously unobserved part of the deep hydrogeological regime, one wherein the migration of crustal fluids has important consequences for the interactions between the interior and surface volatile reservoirs of the Earth (Ballentine et al., 2005). Understanding the fundamental processes affecting fluids in low-porosity source-rocks will also lead to a better understanding of other subsurface engineering projects, such as CO_2 sequestration (Gilfillan et al., 2009), or nuclear waste storage (Hendry et al., 2015). In terms of environmental impact, noble gases are ideal tracers of contamination, and are already being used to assess the potential causes of fugitive gas in drinking water aquifers (Darrah et al., 2014; Harkness et al., 2017; Barry et al., 2018b), resulting from concerns about the impact of oil and gas production on drinking water (Osborn et al., 2011). Finally, as source-rocks are the origin of hydrocarbons occurring in conventional reservoirs, better-constraining their behaviour will likely have implications for understanding conventional petroleum systems.

1.2 Overview

Chapter 1 of this thesis provides a comprehensive literature review and summary of noble gas isotope analytical methods used for the acquisition of the majority of the

data acquired as part of this project. The main original contributions contained in this thesis comprise 3 chapters, each focussing on a particular case study.

Chapter 2 focuses on understanding the generation of hydrocarbons using noble gases. Production from unconventional source-rock reservoirs allows us for the first time to sample natural hydrocarbons from their locus of generation. Hydrocarbon generation is a gradual process, driven by temperature and time. We utilise a sample suite from the Eagle Ford shale, in South Texas, USA. As the Eagle Ford Formation has been buried to variable depths across the play, we can effectively sample different points in the hydrocarbon generation process all from the same reservoir. Using high-precision noble gas isotope measurements in conjunction with traditional stable isotope geochemistry represents the first step in understanding these environments.

In Chapter 3, we focus on hydrocarbon migration - the movement of oil or gas from the source-rock into a conventional reservoir. This is a crucial process in the evolution of a petroleum system, but is challenging to study using geochemical methods. Using a sample suite from East Texas, USA, where we can directly relate unconventional production from the Haynesville source-rock with conventional production from a series of overlying reservoirs, we can investigate the differences between source-rock and reservoir and use these to better understand the process of migration.

In Chapter 4, we aim to take some of the concepts explored in the previous chapters and apply them to a new environment. Iceland has been the focus of many geochemical studies, including noble gas analyses (Marty et al., 1991; Poreda et al., 1992; Hilton et al., 1998; Füri et al., 2010; Barry et al., 2014; Halldórsson et al., 2016). However, these studies have almost exclusively focused on using the light noble gases to understand mantle endmember compositions and their relationships. We exploit the ability to measure the full suite of noble gases and explore the potential for using the solubility-dependent of atmosphere-derived noble gases to investigate the phase partitioning behaviour in geothermal fluids. The boiling, condensation, and degassing of these fluids is important both for controlling the surface chemistry of Iceland, but also in powering its geothermal power, the

boreholes of which account for many of our measured samples. This is a concept that has been investigated extensively using many other geochemical tools (Arnason, 1977; Arnórsson et al., 1983; Stefánsson and Barnes, 2016; Stefánsson et al., 2017), and we demonstrate that noble gases can provide invaluable constraints on the behaviour of these systems as part of an ongoing collaborative approach.

The impact of this study and the outlook for future work is summarised in Chapter 5.

An additional study of smaller scope is included in Appendix A. Here we investigate the phenomenon of excess atmospheric krypton and xenon abundances observed in many hydrocarbon systems. We report noble gas isotope and abundance data from natural gases produced from 2 distinct hydrocarbon fields, the Hogsback field in Wyoming, USA, and the Sable Island field in the Scotian Basin. Both of these fields contain gas sourced from type III kerogen and we test the hypothesis that kerogen type is a controlling factor for the presence of Kr and Xe enrichments. We conclude that this is not the case. By comparing datasets from other studies we also show that neither fluid type (oil vs gas) or migration (conventional vs unconventional reservoirs) appears to control the presence of heavy noble gas enrichments.

1.3 Literature Review

The study of the origin and post-generation history of hydrocarbons in sedimentary basins has been the subject of thousands of investigations worldwide, both by the academic and industrial communities. Many studies have tried to better understand or characterise the elements or processes that occur within a given hydrocarbon system (e.g. Waples, 1994; Hindle, 1997). In a frontier basin, initial studies may focus on predicting whether a particular package of Earth's crust has the necessary elements of sufficient quality and distribution to generate and store hydrocarbons over geological timescales (e.g. Blanc and Connan, 1994; Whiticar, 1994). In better studied basins, efforts are likely to focus on defining the robustness of critical hydrocarbon play elements. The application of geochemical techniques has been at the forefront of many of these studies by: (i) providing time and temperature

constraints on basin evolution (Sweeney and Burnham, 1990; Crowhurst et al., 2002; Stolper et al., 2014), (ii) determining the depositional environment, age, thermal maturity and type of organic matter of key source-rock intervals (Hughes et al., 1995), and (iii) linking hydrocarbons in reservoirs to the source-rock responsible for their generation (Dow, 1974; Stahl, 1978; Philp, 1993). However, the physical histories of accumulated hydrocarbons have proven to be more difficult to understand.

The noble gases have found strong application as physical tracers in a wide range of geochemical fields (Ozima and Podosek, 2002; Porcelli et al., 2002; Burnard et al., 2013). Thanks to their chemical inertness, they are unaffected by biological activity, chemical alteration, or redox reactions that complicate many other tracer systems. This means that only physical processes, such as mixing, dissolution, phase partitioning, and diffusion are recorded by the noble gases. This, coupled with the fact that the different components of the Earth's noble gas inventory (atmosphere, crust and mantle) are isotopically distinct and well-constrained, means that the inputs into and the processes occurring within any given system can be accurately deduced. Given these properties, noble gas geochemistry has the theoretical potential to help constrain physical processes and timescales associated with hydrocarbon fluid generation, migration and storage in petroleum systems.

In a typical noble gas investigation of a petroleum system, samples are taken from the produced hydrocarbon and measured for their noble gas composition. From here a range of different models can be applied to investigate different characteristics of the system, from gas, oil, and water interactions to the timing of migration and accumulation. The development of these quantitative noble gas models has happened alongside improvements in analytical technology, allowing measurement of more noble gas isotopes with greater accuracy and precision, and from this an increased understanding of the processes affecting the noble gases within the subsurface. Consequently noble gases now provide a powerful tool that can reveal information about the subsurface inaccessible by other analytical techniques. For complementary information we refer readers to comprehensive reviews by Ballentine et al., 2002, and Holland and Gilfillan, 2013 for detailed discussion.

1.3.1 Definitions

We use the term 'petroleum system' in the sense defined by Magoon and Dow, 1994, and provide a schematic representation in Fig. 1.1. It is considered to encompass a unit of active source-rock, all related hydrocarbon accumulations, and the geological features and processes that are necessary for the hydrocarbon accumulations to exist. This comprises a series of elements and processes; elements include the source-rock, migration pathway, reservoir, and trap, whereas processes include hydrocarbon generation, migration, and the geological processes affecting the system. As such, the petroleum system can cover a large geographic, stratigraphic, and temporal range and significant differences may exist between different systems.

We discuss both conventional and unconventional hydrocarbon systems. Conventional hydrocarbon systems comprise of (i) a source-rock of sufficient quality and distribution that is buried to temperatures and pressures necessary to result in the generation of and expulsion of hydrocarbons from the source-rock, (ii) secondary migration of hydrocarbons along carrier beds to a reservoir rock in a configuration that traps hydrocarbons either stratigraphically or structurally, and (iii) an overlying low permeability seal rock that results in the accumulation of hydrocarbons within the reservoir rock. Whilst the term 'unconventional' has been applied to petroleum exploitation environments ranging from tar sands to ultra-deep water production, we use the term here in a stricter sense to apply to source-rock reservoirs such as gas-shales (Curiale and Curtis, 2016). These are traditionally unconventional in that they produce directly from the source-rocks that generate the petroleum, with very little secondary migration. The low porosity and permeability of these rocks means that they typically require advanced production techniques such as hydraulic fracturing or directional drilling to produce economically. A schematic representation of conventional and unconventional production is shown in Fig. 1.1.

Noble gas isotope ratio measurements are typically reported simply as raw ratios, unlike most other geochemical isotope ratios, which use permil (‰) notation (Hoefs, 1997). Using the raw ratios is more convenient when relatively large isotopic variations are common (Porcelli et al., 2002). Although using raw ratios

eliminates the requirement for a universal standard, samples in natural systems are often compared to air, which is well mixed and defined in Tables 1.1 and 1.2. In subsurface fluid systems it is also common to use air-saturated water (ASW) as a standard, which is well defined over a range of temperatures and salinities (Table 1.3). Helium isotope ratios ($^3He/^4He$) are usually reported relative to the air ratio (R_a). Quantities of noble gases are typically reported in cm^3 standard temperature and pressure (cm^3STP or ccSTP), due to the small amounts of noble gases usually present in geochemical systems. The cm^3STP unit can be directly converted to moles using the molar gas volume (22400cm^3 at STP of 273.15K and 10^5Pa) (Burnard et al., 2013).

Element	Volume mixing ratio
He	$5.24(\pm0.05) \times 10^{-6}$
Ne	$1.818(\pm0.004) \times 10^{-5}$
Ar	$9.34(\pm0.01) \times 10^{-3}$
Kr	$1.14(\pm0.01) \times 10^{-6}$
Xe	$8.7(\pm0.1) \times 10^{-8}$

Table 1.1: The volume mixing ratios for the noble gases in dry air. Data from Porcelli et al., 2002

1.3.2 Origin of terrestrial noble gases

Primordial noble gases

Primordial elements are those indigenous to Earth, incorporated during planetary formation. The noble gases are highly volatile, and thus difficult to entrain during planetary accretion (Pepin, 1991). This results in a bulk Earth that is depleted in noble gases by several orders of magnitude compared to the proto-solar nebula from which the planet was formed (Wieler, 2002; Grimberg et al., 2006). Some of the noble gas isotopes (e.g. ^{20}Ne, ^{36}Ar, ^{84}Kr, ^{130}Xe) are not produced on Earth in significant quantities, and thus their provenance in terrestrial reservoirs is assumed to be 100% primordial (Burnard et al., 1997; Moreira et al., 1998). The isotopic composition of possible accretionary precursors such as the protosolar nebula and carbonaceous chondrites have been compared with the terrestrial inventory of the

Isotope	Relative abundance
^{4}He	$1.399(\pm 0.013) \times 10^{-6}$
^{3}He	$\equiv 1$
^{20}Ne	$\equiv 1$
^{21}Ne	9.80 ± 0.08
^{22}Ne	0.0290 ± 0.0003
^{36}Ar	$\equiv 1$
^{38}Ar	0.1885 ± 0.0003
^{40}Ar	298.56 ± 0.31
^{78}Kr	0.6087 ± 0.0020
^{80}Kr	3.9599 ± 0.002
^{82}Kr	20.217 ± 0.004
^{83}Kr	20.136 ± 0.021
^{84}Kr	$\equiv 100$
^{86}Kr	30.524 ± 0.025
^{124}Xe	2.337 ± 0.008
^{126}Xe	2.180 ± 0.011
^{128}Xe	47.15 ± 0.07
^{129}Xe	649.6 ± 0.9
^{130}Xe	$\equiv 100$
^{131}Xe	521.3 ± 0.8
^{132}Xe	660.7 ± 0.5
^{134}Xe	256.3 ± 0.4
^{136}Xe	217.6 ± 0.3

Table 1.2: The isotopic ratios of noble gases in air. Data from Porcelli et al., 2002; Lee et al., 2006

Element	Concentration (cm^3STPg^{-1})		
	Freshwater 10^oC	Freshwater 20^oC	Seawater 10^oC
He	4.73×10^{-8}	4.65×10^{-8}	4.04×10^{-8}
Ne	2.06×10^{-7}	1.93×10^{-7}	1.70×10^{-7}
Ar	3.91×10^{-4}	3.23×10^{-4}	3.11×10^{-4}
Kr	9.21×10^{-8}	7.27×10^{-8}	7.26×10^{-8}
Xe	1.34×10^{-8}	9.24×10^{-9}	1.04×10^{-8}

Table 1.3: The equilibrium concentrations of the noble gases in air-saturated water at atmospheric pressure for selected salinities and temperatures, calculated from Henry's constant equations in Fernández-Prini et al., 2003, and Setschenow coefficient equations in Smith and Kennedy, 1983.

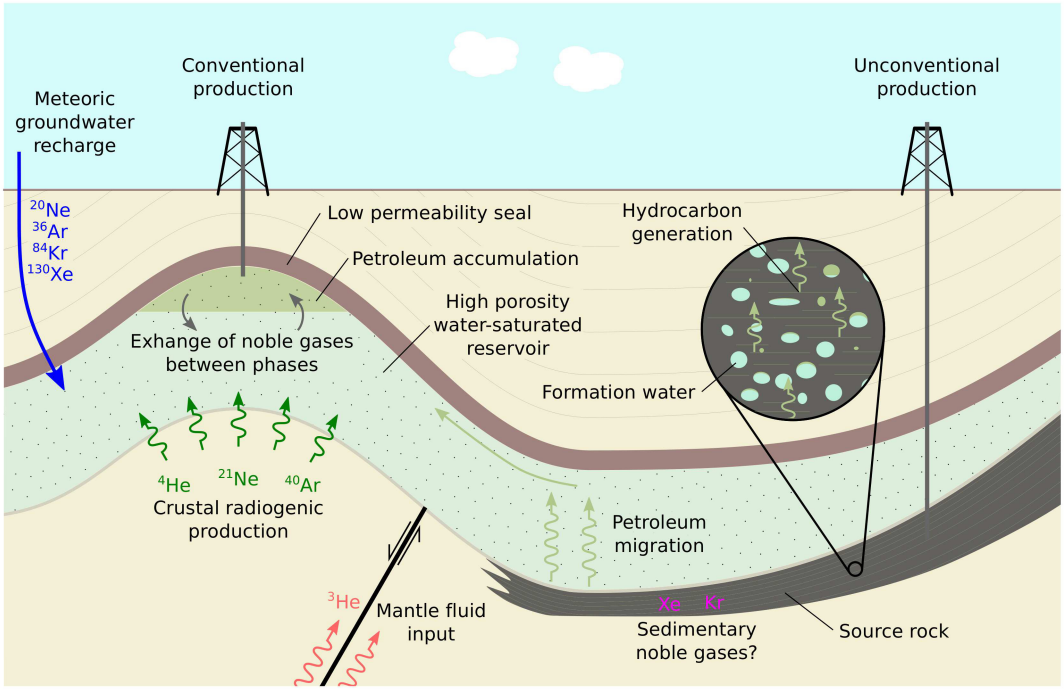

Figure 1.1: A schematic conceptual model of the sources of noble gases in petroleum systems, modified from Ballentine and O'Nions, 1992. For each input, the major characteristic isotopes are shown, although in reality each source will have varying contributions from a range of isotopes. Groundwater is usually considered to be ubiquitous in the subsurface, although the provenance of the water (meteoric recharge or formation water) and the connectivity of different sources can vary. Meteoric groundwater recharge has air-saturated water (ASW) composition and air-like isotopic ratios; the isotopes shown have no significant mantle or radiogenic sources, and so are considered characteristic of the subsurface noble gas component. Crustal radiogenic production occurs throughout the crust, though the produced isotopes can be transported via groundwater flow. Phase equilibrium between groundwater and any hydrocarbon accumulation is rapid on a geological timescale, and is the primary conduit for introducing noble gases into the hydrocarbon phase.

primordial gases to reconstruct the origin and processes responsible for delivery of volatiles to Earth on its formation (e.g. Ballentine et al., 2005; Ballentine and Holland, 2008; Holland et al., 2009; Marty, 2012; Halliday, 2013). These models of planetary noble gas acquisition successfully explain the modern terrestrial inventory for all of the primordial noble gases except Xe, whose apparent depletion in the Earth is still the subject of much debate (Sanloup et al., 2005; Lee and Steinle-Neumann, 2006; Pepin and Porcelli, 2006). The recent discovery of the progressive isotopic fractionation of atmospheric Xe during the Archaean supports gradual

depletion from the atmosphere occurring until approximately 2.1Ga, although the exact mechanisms responsible are still unclear (Pujol et al., 2011; Avice et al., 2018; Bekaert et al., 2018).

Production of noble gases

Noble gases are produced both directly and indirectly from radioactive processes occurring within the Earth. The partitioning of different radioactive elements into chemically and physically distinct parts of the planet is the cause of much of the heterogeneity in the terrestrial noble gas reservoirs. The most productive radioactive elements in terms of abundance and decay rate (U, Th, K) are highly incompatible in the Earth's mantle, meaning that the crust is typically associated with much higher levels of noble gas production (Ballentine and Burnard, 2002).

Noble gas production proceeds by 3 mechanisms: radiogenic, nucleogenic, and fissiogenic. The laws governing the pathways and rates of radioactive decay are well understood, allowing theoretical production rates to be accurately calculated in any system if the parent isotope concentration and half-life (decay constant) is known (Rutherford, 1906; Pierce et al., 1964). This is the basis of a number of successful dating tools such as Kr-Ar dating, Ar-Ar dating and ^{4}He dating (Merrihue and Turner, 1966; Farley, 2002; Renne et al., 2010).

Radiogenic production. Radiogenically produced isotopes are those produced as direct daughter products of radioactive decay. For the modern Earth, the most significant radioactive decay pathway is the U, Th series. The initial decay of ^{235}U, ^{238}U and ^{232}Th is by α-decay, significant in terms of noble gas production because an α-particle is equivalent to a ^{4}He nucleus. The vast majority of α-particles ionise the surrounding material upon ejection, collecting electrons to form a ^{4}He atom. Elevated U, Th concentrations are therefore associated with helium that is isotopically enriched in ^{4}He. The incompatibility of both U, Th in the mantle means that they, and consequently ^{4}He, are highly enriched in continental crust.

Similarly, high crustal concentrations of ^{40}K lead to elevated ^{40}Ar when ^{40}K decays by electron capture. The subsequent release of radiogenic ^{40}Ar into the

atmosphere has drastically altered the isotopic composition of atmospheric argon over Earth history. Whilst the majority of primordial argon is ^{36}Ar (the proto-solar nebula has a $^{40}Ar/^{36}Ar \approx 3.0 \times 10^{-4}$), the atmospheric $^{40}Ar/^{36}Ar$ ratio in the modern atmosphere is 298.6 because of radiogenic ^{40}Ar enrichment (Göbel et al., 1978; Anders and Grevesse, 1989; Lee et al., 2006).

Nucleogenic production. In addition to α-particles the emission of neutrons is also a direct result of radioactivity. Nucleogenic production is the interaction of both these particles with the nuclei of nearby atoms, leading to the formation of new elements in Wetherill reactions (Wetherill, 1954).

Most commonly the impact of an α-particle into a nucleus is followed by the emission of a neutron in an (α, n) reaction, effectively adding 2 protons and 1 neutron to the nucleus of the affected atom. Noble gases formed in measurable quantities in this fashion include ^{21}Ne, which is derived from the (α, n) reaction of ^{18}O, ($^{18}O(\alpha, n)^{21}Ne$) as well as ^{22}Ne, which is formed indirectly via the β^+ decay of the short-lived ^{22}Na produced by (α, n) reaction with ^{19}F ($^{19}F(\alpha, n)^{22}Na(\beta^+)^{22}Ne$).

Alternatively, an incident neutron can cause a nucleus to emit an α-particle, effectively removing 2 protons and 1 neutron in a (n, α) reaction. This pathway provides a further source of ^{21}Ne, produced by the $^{24}Mg(\alpha, n)^{21}Ne$ reaction, as well as a small contribution to ^{3}He, produced by the $^{6}Li(\alpha, n)^{3}He$ reaction.

As nucleogenic reactions require a source of α-particles and neutrons, their production rates are tightly coupled with nearby radioactivity, primarily U, Th. Both α-particles and neutrons have a limited range in typical crustal rock after being ejected from the parent nucleus, with typical ranges of 15-45μm and 10-100cm respectively (Ziegler, 1977; Martel et al., 1990). As such, heterogeneities on the mineral-scale can have measurable effects on the relative production of different isotopes. Notably, observed radiogenic $^{21}Ne/^{22}Ne$ values from the modern crust are incompatible with those predicted from average crust ^{18}O and ^{19}F concentrations. This has led to the inference that the O/F concentration in the modern crust is

systematically lower in phases associated with high U, Th concentrations (Kennedy et al., 1990; Hiyagon and Kennedy, 1992).

Fissiogenic production. A further source of noble gas production is as a result of the fission of heavy, unstable nuclei. The systematics of this process are more complex than simple radioactive decay, but the production rates of different isotopes can still be relatively well-constrained (Wieler and Eikenberg, 1999). The dominant fission process in noble gas production is the spontaneous fission of ^{238}U, which produces ^{129,131,132,134,136}Xe, as well as smaller amounts of ^{83,84,86}Kr. The spontaneous fission of ^{232}Th, and the neutron-induced fission of ^{238}U, ^{235}U, and ^{232}Th also make minor contributions to the production of these fissiogenic Xe and Kr isotopes (Ballentine and Burnard, 2002).

The production rates of fissiogenic isotopes are much lower than those of radiogenic or nucleogenic isotopes (Table 1.4). As such, fissiogenic Xe excesses are only observed in samples that have been isolated for significant periods of time (Reynolds, 1963; Holland et al., 2013).

1.3.3 Physical chemistry of noble gases in fluids

Henry's law

The dissolution of noble gases into fluids (water, oil, and gas) has been reviewed by Ballentine et al., 2002. Dissolution follows Henry's law, which states that the concentration of a gas in solution is directly proportional to the partial pressure of that gas in the gas phase. This can be formulated for any noble gas i, assuming ideal gas behaviour in both the gas and fluid phases (Eq. 1.1).

$$p_i = K_i x_i \tag{1.1}$$

Where p_i is the partial pressure, x_i is the mole fraction in solution, and K_i is the Henry's constant. Henry's constants are specific to the solute, and are temperature and salinity dependent; their units depend on the units used to measure the partial pressure and concentration in the fluid phase.

Isotope	Present day production rate ($cm^3STPkg^{-1}yr^{-1}$)
^{3}He	2.49×10^{-18}
^{4}He	3.31×10^{-10}
^{20}Ne	1.47×10^{-18}
^{21}Ne	1.51×10^{-17}
^{22}Ne	3.03×10^{-17}
^{36}Ar	2.38×10^{-18}
^{38}Ar	1.09×10^{-18}
^{40}Ar	6.05×10^{-11}
^{83}Kr	5.86×10^{-21}
^{84}Kr	2.12×10^{-20}
^{86}Kr	1.39×10^{-19}
^{131}Xe	7.89×10^{-20}
^{132}Xe	5.24×10^{-19}
^{134}Xe	7.50×10^{-19}
^{136}Xe	9.09×10^{-19}

Table 1.4: Present day production rates for the radiogenic noble gases in typical continental crust. Data from Ballentine and Burnard, 2002.

The Henry's constants of noble gases in water have been determined empirically over a temperature range from the freezing point to the critical point of water (Crovetto et al., 1982; Smith, 1985), and equations have been formulated using a compilation of empirical data that allow the calculation of Henry's constants at any temperature (Fernández-Prini et al., 2003). Determination of the Henry's constant for oil faces the further complexity of the natural variation in oil composition. This work is limited to just one study of two oils with API gravities of 25^o and 31^o (Kharaka and Specht, 1988). The solubility of the noble gases was shown to be affected by the API gravity, but it is likely that the solubility is also controlled by properties other than bulk density (e.g., concentration of polar compounds, trace element concentrations). Hence the Henry's constant for oils remains a key uncertainty in models that apply these constraints.

Non-ideality

Henry's law can be modified to account for non-ideal behaviour in the gas and fluid phases by taking into account both the gas phase fugacity coefficient, and the liquid phase activity coefficient (Eq. 1.2).

$$\Phi_i p_i = \gamma_i K_i x_i \tag{1.2}$$

Where Φ_i is the fugacity coefficient, and γ_i is the activity coefficient; a deviation of either of these from unity represents non-ideal behaviour. Fugacity is pressure and temperature dependent, and can be calculated from empirical measurements of real molar volume (Dymond and Smith, 1980). Activity is dependent on temperature and salinity, with the relationship formulated in the Setschenow equation (Eq. 1.3).

$$\gamma_i = e^{Ck_i(T)} \tag{1.3}$$

Where C is the concentration of salt in the solution, and k_i is the temperature dependent Setschenow coefficient. The response of Ar to changes in salinity is independent of the electrolyte species, and this relationship is assumed to be true for the other noble gases (Ben-Naim and Egel-Thal, 1965). The Setschenow coefficients have been determined empirically for the noble gases over a range of temperatures from 270-340K (Smith and Kennedy, 1983). Unfortunately, the temperatures encountered in subsurface environments often greatly exceed this range, with the onset of oil formation occurring at temperatures of approximately 350K, and secondary cracking to gas being above 420K (Waples, 1980). As such, the extrapolation of curves fitted to the empirical data must be used to account for salinity effects on noble gas solubility in the range of interest of most hydrocarbon systems, and represents a potential source of error in any derivative product. Recent work on noble gas partitioning in CO_2-water systems show measurable deviations from predicted behaviours in high-pressure environments (Warr et al., 2015b). In most petroleum system investigations these deviations from ideality are unlikely to affect the general outcomes of any models, but care must be taken when considering

the precision with which they can be applied. Further work involving a combination of empirical and model data will be crucial to refine these models in the future.

1.3.4 Terrestrial noble gas inventories

The atmosphere

Although small in size compared to the solid Earth, the majority of the Earth's primordial noble gases are held in the atmosphere (Porcelli and Ballentine, 2002). The creation and evolution of the atmosphere is complex, and not yet fully understood. Whilst it is likely that terrestrial bodies such as the Earth are able to gravitationally capture volatiles from the proto-solar nebula during formation (Pepin, 2006), the atmosphere is clearly distinct from a solar composition (Brown, 1949). Alternative proposed methods of acquiring noble gases include adsorption onto accumulating dust (Marrocchi et al., 2005; Marrocchi et al., 2011), or the implantation by solar wind (Podosek et al., 2000). A contribution of volatile-rich cometary material brought in during the late heavy bombardment has also been suggested as a source of atmospheric noble gases (Owen et al., 1992; Dauphas, 2003; Holland et al., 2009).

The reasons for the atmosphere's distinct noble gas composition are likely due to the atmospheric losses experienced by the Earth during its early history. Whether this occurred by aggregate catastrophic loss, or gradual escape of volatiles, is still debated (Pepin, 2006; Pepin and Porcelli, 2006; Tucker and Mukhopadhyay, 2014). However, the atmospheric composition of noble gases has been remarkably constant over geological timescales. Whilst degassing of the solid Earth at volcanoes and mid-ocean ridges releases mantle noble gases into the atmosphere, it is in such small quantities as to be insignificant even over billions of years. However, exceptions to this include isotopes with high radiogenic production such as ^{40}Ar, which are produced within the Earth to such an extent that solid Earth degassing can influence atmospheric concentrations (Allègre et al., 1996). Helium is gravitationally unbound in the atmosphere. However, the loss into space is balanced by a volcanic degassing flux from mid-ocean ridge, ocean-island, and subduction-related volcanism,

resulting in an assumed steady-state helium concentration in the atmosphere (Torgersen, 1989; Lupton and Evans, 2013). When considering most fluids in the crust, and groundwater in particular, it is reasonable to assume that the atmospheric noble gas composition has been constant over the timescale of their introduction into the subsurface.

The hydrosphere

When in direct contact with the atmosphere, water will rapidly equilibrate with air according to the processes detailed in the previous section. The solubilities of the noble gases vary by element, meaning that at equilibrium the elemental composition of the water is not air-like (Kipfer et al., 2002). However, isotopic ratios of the individual noble gases are not significantly affected by equilibrium partitioning. As the rules governing this partitioning and the variation with respect to temperature, pressure, and salinity are well known, it is possible to calculate the air-saturated water composition in any given environment. This composition is crucial for noble gas analysis of hydrocarbon reservoirs, as a common assumption in modelling and analysis is that all atmospherically derived noble gases in the subsurface will be delivered in known quantities dissolved as air-saturated water (ASW) through hydrocarbon-water interaction and noble gas partitioning.

One complication to this arises from empirical measurements of atmosphere-derived noble gas concentrations in meteoric groundwater that have often been found to be higher than the values predicted by Henry's law equilibration. This phenomenon is commonly referred to as 'excess air' (Herzberg and Mazor, 1979; Heaton and Vogel, 1981). The behaviour of this excess air component is generally consistent, with neon being the most strongly affected, and the heavier noble gases proportionally less so. Theoretical models describing processes by which this can occur have been developed, and refined over time to more closely match observations (Stute et al., 1995; Ballentine and Hall, 1999; Aeschbach-Hertig et al., 2000). Whilst these models differ slightly, they are based on the principle that excess air is introduced into groundwater by the entrapment of air bubbles during fluctuations

of the water table. A close fit to experimental observations is found by modeling a closed-system equilibration of these bubbles (Aeschbach-Hertig et al., 2008). Within petroleum systems deposited under marine conditions, the groundwater is likely to have a marine noble gas composition (Kipfer et al., 2002) and excess air within these systems are not expected.

The mantle

The Earth's mantle contains a high proportion of primordial noble gases. It is introduced to the surface in CO_2-rich volcanic gases that can permeate through the crust or get released at mid-ocean ridges and volcanoes. The measured compositions of these gases have distinctive high but variable $^3He/^4He$ ratios. For example, the well-mixed asthenospheric upper mantle, as sampled by depleted mid-ocean ridge basalt (MORB) mantle ranges from 7-9 R_a (Graham, 2002), where the sub-continental lithospheric mantle is defined as 6.1 $\pm$ 2.1 (Day et al., 2015). In contrast, many mantle plume regions extend as high as $\approx 50 R_a$ (Stuart et al., 2003). Likewise, the mantle is marked by high $^{20}Ne/^{22}Ne$ ratios and $^{40}Ar/^{36}Ar$ ratios (Sarda et al., 1988; Staudacher et al., 1989). Addition of mantle noble gases into subsurface hydrocarbon accumulations, while not useful in the context of origin and history of hydrocarbon gases, may be useful for constraining the origin of non-hydrocarbon gases that in some cases accumulate concurrently in the subsurface - particularly CO_2 and N_2 (Ballentine and Sherwood Lollar, 2002; Ballentine et al., 2005; Gilfillan et al., 2009).

The crust

Due to their incompatibility in the mantle, the major radioactive elements involved in noble gas production were partitioned heavily into the Earth's crust during planetary formation. These elements which include U, Th, and K, initiate the decay chains that produce the radiogenic noble gas isotopes, principally ^4He, ^{40}Ar, ^{21}Ne, ^{22}Ne, and to a lesser extent some Xe and Kr isotopes. Whilst the crust is a complex and heterogeneous system with inputs from many sources, crustal fluids are often characterised by high concentrations of these radiogenic isotopes.

These isotopes are produced within the minerals that make up the crust, but can be released into the surrounding fluid systems (Bach et al., 1999). The extent of this release is controlled by a number of factors including grain size, temperature, and mineral alteration (Honda et al., 1982; Brooker et al., 1998; Baxter et al., 2002). Lighter isotopes are more readily released at lower temperatures, and as such the ratios of radiogenic isotopes (e.g. $^{4}He/^{21}Ne^{*}$, $^{4}He/^{40}Ar^{*}$) can be used to determine temperatures of release (Torgersen et al., 1992).

In general, higher concentrations of radiogenically produced noble gas isotopes reflect older systems that have been isolated for longer periods of time. Data from fracture fluids in mines in Precambrian shields show concentrations that would have taken billions of years to accumulate (Holland et al., 2013).

1.3.5 Introduction of noble gases into the petroleum system

Source-rock formation

The genesis of the petroleum system begins with the deposition of an organic carbon rich sedimentary rock. Typically >1% total organic carbon (TOC) is considered sufficient for a source-rock (Gluyas and Swarbrick, 2013), although this can vary. As organic carbon comes in a variety of forms, each of which has distinct chemical behaviour in a petroleum system, these source-rocks are typically classified according to their kerogen composition, as outlined in Table 1.5. The type of organic matter that makes up source-rocks is of particular importance because it is this that ultimately determines how oil or gas prone a source-rock is likely to be, as well as the volume of hydrocarbons that can be generated from the source-rock on a gram for gram basis (Peters and Cassa, 1994). Laboratory simulation of this naturally occurring process has been extensively investigated in hydrous pyrolysis experiments, in which immature source-rock is heated under controlled conditions to simulate the naturally-occurring process of petroleum formation (Peters, 1986; Peters et al., 2015). These and other experimental studies suggest that the presence of water may be required during catagenesis and hydrocarbon generation to produce

the compositions that we observe in nature (Lewan, 1993). Noble gases are more soluble in oil than in water, and thus the formation of a liquid petroleum phase within the source-rock will cause the partitioning of noble gases between it and the surrounding water phase that remains in the rock (Ballentine et al., 1991). The water in this context is likely to not represent a significant volume given the prior compaction and lithification of the source-rock. Given sufficient pressure generated during the generation of hydrocarbons, oil may escape from the source-rock and as such noble gases in the escaping fluid will evolve separately (described below) to the noble gas signature of any retained oil. The extent of kerogen decomposition can further affect the partitioning of noble gases, as the solubility of noble gases has been shown to be positively correlated with the API of the oil (Kharaka and Specht, 1988). Given continued burial and increase in temperature, the retained oil itself will begin to crack to gaseous hydrocarbons. The onset of gas generation will further complicate this phase partitioning, as the noble gases have a strong affinity for the gas phase when it is present. Furthermore, it is unclear how the alteration of the source-rock composition will affect the noble gases stored within; it is possible that any component adsorbed onto the organic carbon could be released during thermal degradation.

Kerogen type	Primary organic matter source	Depositional environment	Principal generated hydrocarbons
Type I (Sapropelic)	Algae	Lacustrine	Oil
Type II (Planktonic)	Plankton	Marine	Oil + Gas
Type III (Humic)	Plants	Terrestrial	Gas (+ Coal)

Table 1.5: The classification of source-rocks, after Gluyas and Swarbrick, 2013

Most noble gas studies to date have focussed on characterising or modelling the inheritance and evolution of noble gases during migration and accumulation in conventional reservoirs. However, key gaps exist in our understanding of hydrocarbon generation and expulsion from source-rocks, and there have been very few studies to date that have studied the evolution of noble gases during hydrocarbon generation. Questions such as the role of water during hydrocarbon

generation, the relative volumes of expelled versus retained oil and gas, and the mechanisms of storage within the source-rocks (adsorption or as free gas within porosity or fractures), remain elusive.

Primary migration

Primary migration is the initial expulsion of the generated hydrocarbons out of the source-rock and into the surrounding crust. This occurs by thermally activated diffusion of hydrocarbons through the residual organic-matter network (Stainforth and Reinders, 1990). The rate of primary migration is an important control on the total hydrocarbons produced from the source-rock, as well as the extent of secondary cracking. The effects of primary migration on the noble gas composition of the hydrocarbon phase are unclear. Although a thermal-diffusive release mechanism may impart a mass-dependent kinetic fractionation signature onto the noble gases, it has not been identified in real-world samples. It is possible that the effect is small compared to that of other subsurface processes. Such processes include the interaction of noble gases co-transported in or with hydrocarbons with other fluids or the mechanisms and timescales associated with the movement of hydrocarbons within the crust.

Secondary migration

The principal mechanism driving secondary migration is the buoyancy force due to the density difference between petroleum and the surrounding water. This driving force is balanced by the resistance provided from capillary entry pressure, a function of the surrounding pore-size and permeability (Schowalter, 1979). Empirical investigations into this process suggest that secondary migration likely occurs along restricted pathways, often along structural boundaries, and proceeds rapidly on geological timescales (Dembicki and Anderson, 1989). Fig. 1.1 shows the migration of hydrocarbons through a groundwater-saturated reservoir, and the potential inputs of noble gas sources into the same groundwater. Once in contact the noble gases are expected to equilibrate between the two phases quickly relative to geological timescales (Ballentine et al., 2002).

Secondary migration can occur laterally for up to 100's of kilometres and vertically through kilometres of groundwater-saturated strata (Demaison and Huizinga, 1991) and have profound effects on the noble gases in the system. The migrating hydrocarbons can undergo phase partitioning with this surrounding groundwater, and as the noble gases are more soluble in hydrocarbons than in water, this can strip the groundwater of much of its noble gases (Ballentine et al., 1996). This occurs via well-defined Henry's-law solubility-dependent partitioning, and forms the basis of a series of models that investigate hydrocarbon migration using the varying solubilities of the noble gases (Zartman et al., 1961; Bosch and Mazor, 1988; Ballentine et al., 1991). While this has yet to be discussed or tested in studies performed to date, the evolution of noble gas signatures in hydrocarbons in conventional systems is therefore likely to be dependent on the mechanism and length scales of migration. In systems where migration occurs short over distances, it is possible that hydrocarbons may encounter relatively limited volumes of water with which to interact and partition noble gases (e.g. Ballentine et al., 1996). In contrast, migration within hydrocarbon systems such as those of the foreland basins of the Western Canadian Sedimentary basin may occur over tens or hundreds of kilometres and as such will encounter significantly greater volumes of water. However, to date there has been no thorough investigation into the effects of secondary migration distance upon noble gas composition - if any such pattern exists it could prove an invaluable tool in retroactively assessing migration distances and pathways.

The general effects of secondary migration on noble gases can be considered by comparing the conventional systems with unconventional systems where no secondary migration takes place. Fig. 1.2 shows an overlapping but distinct grouping of conventional and unconventional systems with respect to [^{4}He] concentrations. Conventional systems tend to have higher [^{4}He] concentrations, which we speculate could be due to interaction with large-scale aquifer systems during secondary migration. Previous studies of conventional systems have shown some to contain concentrations of radiogenic noble gases far higher than that possible by local production, requiring input from regional systems (Ballentine et al., 1991).

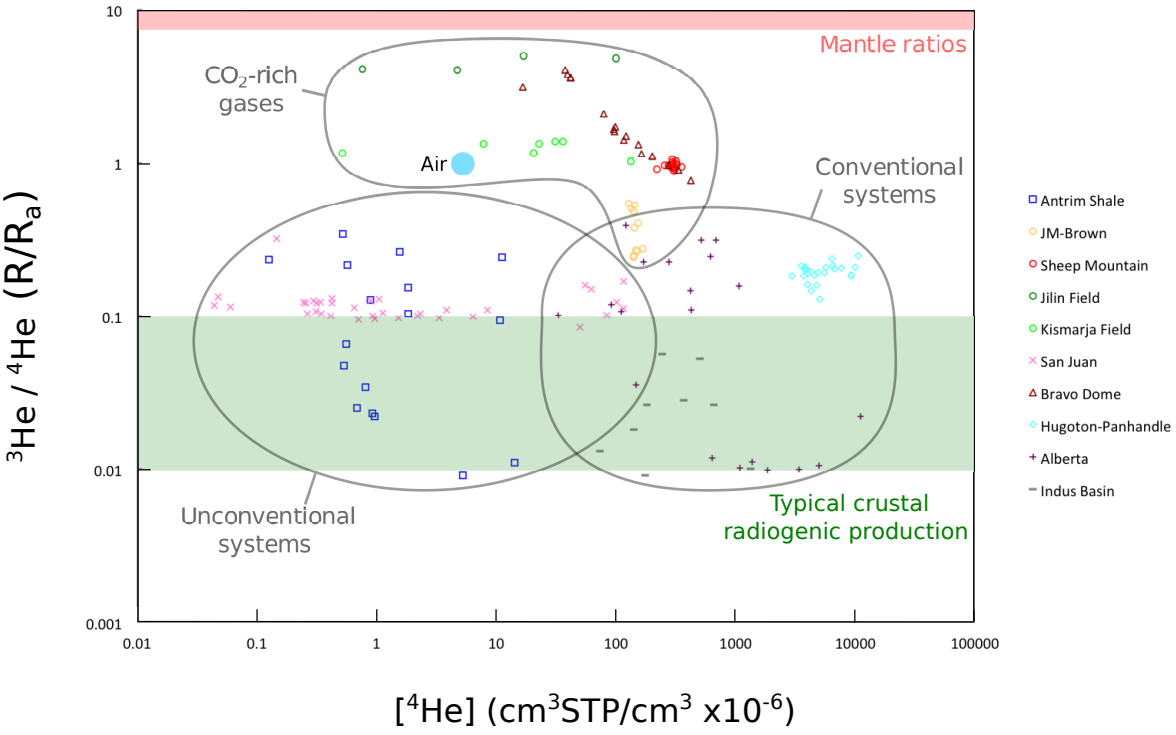

Figure 1.2: Helium isotope ratio and concentration measurements from selected noble gas studies of petroleum systems. $^3He/^4He$ ratios are reported relative to the atmospheric ratio R_a. The observed range of $^3He/^4He$ ratios and ^4He concentrations is controlled by the regional geology and tectonic regime of the petroleum systems. The $^3He/^4He$ ratio of a system is usually thought to comprise of 2-endmember mixing between crustal fluids with a ratio of 0.01-0.02R_a, and mantle fluids, which have a ratio of >8R_a. Presence of even small contributions of mantle fluids therefore increases $^3He/^4He$ ratios above normal crustal values, and is a feature of extensional tectonic regimes (Marty et al., 1993). Concentrations of ^4He are affected by several factors: radiogenic production of ^4He occurs over time, meaning that older systems will have accumulated more ^4He; the regional hydrogeology can also transport ^4He dissolved in groundwater into the petroleum accumulations; finally, concentrations of all noble gases will be affected by the extent of secondary cracking of hydrocarbons, as this effectively increases the relative volume of hydrocarbon gases in the sample and dilutes the helium concentration. As is evident from the data, different systems show distinct ratios and concentrations, and different amounts of scatter show variations in homogeneity. Mixing lines are apparent in some systems, such as the mantle-CO_2 rich Bravo Dome; others show little or no pattern. Data are broadly clustered according to the type of the system, conventional or unconventional, and CO_2-rich. Data sources: Antrim Shale (Wen et al., 2015b); San Juan coalbed methane (Zhou et al., 2005); JM-Brown, Sheep Mountain, Jilin and Kismarja fields (Gilfillan et al., 2008); Alberta field (Hiyagon and Kennedy, 1992); Indus Basin (Battani et al., 2000); Hugoton-Panhandle field (Ballentine and Sherwood Lollar, 2002); Bravo Dome (Ballentine et al., 2005).

Accumulation

The final stage in a conventional petroleum system is the migration of the hydrocarbons into a suitable structural or stratigraphic trap, with a low porosity seal allowing an accumulation to form (Downey, 1984). Once in an accumulation, there are still several processes that can allow further alteration of the noble gas composition. The structure and fluid flow pathways that focused the hydrocarbon migration into the trap are likely to allow fluids from other sources to also arrive at the same location. It is therefore not unusual to see mixing and interaction with CO_2-rich mantle-derived fluids, especially in tectonically active areas (Hooker et al., 1985; Gilfillan et al., 2008; Gilfillan et al., 2009). These mantle fluids have a distinct elevated $^3He/^4He$ ratio, and so their presence in the hydrocarbon accumulation is often, though not always, easily identified. Continued subsurface flow of and interaction with groundwater can also transport noble gases from other parts of the crust. In many cases this can lead to high concentrations of crustal radiogenic noble gases that require contributions from a large fetch area or catchment (Ballentine et al., 1991; Ballentine et al., 1996; Ballentine and Sherwood Lollar, 2002).

Tertiary migration

Once in an accumulation, it is possible for the hydrocarbons to leak gradually through the seal, or through mechanical structures such as faults (Wiprut and Zoback, 2000). Evidence for this is apparent in the many natural hydrocarbon seeps found both onshore and on the seafloor (Bojesen-Koefoed et al., 1999; Hornafius et al., 1999; Holzner et al., 2008). It is possible to identify this loss of hydrocarbons within the noble gas signature using a mass-balance approach if the input of noble gases into the accumulation is well constrained. This is particularly notable in systems that are filled to structural spill. A recent study by Barry et al., 2016 demonstrated the sensitivity of noble gases to constraining the relative hydrocarbon volumes lost from the Sleipner Vest reservoirs of the Norwegian North Sea through such a process

Unconventional systems

As the widespread commercial exploitation of unconventional systems is a relatively recent phenomenon, there is a comparatively small compilation of literature describing the geochemical behaviour of these systems (Curtis, 2002). As source-rock reservoirs typically have low porosity and hydrocarbons produced from these systems have not undergone any prior migration, we might expect the noble gas signature to be indigenous to the source-rock. However, it is clear that these are not perfectly closed systems, as many source-rock reservoirs have generated hydrocarbons that have migrated to form conventional systems (Curiale and Curtis, 2016).

The behaviour of noble gases within unconventional systems is therefore likely to be similar to that of noble gases within source-rocks, barring any drilling or production-related effects. The lack of secondary migration should simplify the factors affecting noble gases composition, as unknowns about the timing and rate of migration can be eliminated.

1.3.6 Analysis of the petroleum system using noble gases

Early noble gas investigations

The presence of significant amounts of helium in natural gases was first observed over 100 years ago (Cady and McFarland, 1906). The first isotopic measurements of noble gases were made nearly 50 years later, and established using $^{4}He/^{40}Ar$ ratios that the presence of high concentrations of radiogenic ^{4}He in natural gases was not due to increased local ^{4}He production, but due to fluid migration transporting He from off-structure (Zartman et al., 1961). Wasserburg et al., 1963 also used measurements of natural gases to make early estimates of the terrestrial ^{4}He degassing flux through the crust, and hence residence time in the atmosphere. These pioneering studies highlighted the potential utility of noble gases to study the origin and history of hydrocarbon and non-hydrocarbon fluids in sedimentary basins, and formed the foundations for future studies targeting multiple elements and processes of numerous hydrocarbon systems.

The preparation of samples for noble gas analysis requires specialised equipment and techniques compared to sample collection for traditional hydrocarbon geochemical analyses, mostly to avoid air contamination. Concentrations of noble gas species in air are significantly higher than those of typical crustal samples (especially Ar and Ne), and so even very small air admixtures can have a large impact on measured values even when present only at the ppm level (Barry et al., 2016). Furthermore, the small size of the noble gas atoms means that they have a much higher propensity to slowly leak across seals that are sufficient to hold hydrocarbon compounds. Valved high-pressure cylinders are not considered to be effective at maintaining the sample integrity required for noble gas analysis over long periods of time. Typically noble gas hydrocarbon samples are collected at low pressure in refrigeration-grade copper tubes that are either crimped or clamped to make a helium-tight seal effective during transport and storage.

Endmember mixing models

Noble gases are introduced into the petroleum system from several distinct geochemical reservoirs, each with a distinct elemental and isotopic composition. Deconvolving the contribution of different endmember compositions is a key step in beginning to understand the subsurface environment of any petroleum system, and the composition of any accumulations. The detection of mantle-rich fluids can be used to gain insight into the geological history and connectivity of any accumulation. Fig. 1.2 shows that He isotope data reveal a grouping of CO_2-rich petroleum accumulations that are associated with elevated $^3He/^4He$ isotope ratios, in which this CO_2 is postulated to have been derived from magmatic fluids passing through the petroleum system (Gilfillan et al., 2009).

For robust analysis of noble gas provenance by endmember mixing decomposition, it is first crucial that the endmembers themselves are well defined. For some systems, such as the atmosphere, this is certainly the case, however others can be more complicated. The elemental composition of air-saturated groundwater is dependent on temperature and salinity of recharge conditions, and these are

often difficult to constrain. However the isotopic composition of each element is unaffected by solubility partitioning, and for He and Ne, their solubilities are similar enough that they can be considered equivalent in certain situations. Radiogenic production ratios are well-known for average crust, although local parent-isotope concentrations can cause significant deviations in some isotope ratios (Ballentine and Burnard, 2002). For the mantle, isotope ratios (e.g., $^{3}He/^{4}He$) are reasonably well constrained for different mantle compositions (MORB, OIB) and the fact that these are orders of magnitude different to crustal endmembers makes the uncertainty in them less significant.

Processes that can isotopically or elementally fractionate noble gases, such as those detailed in the following sections, must be identified and taken into account. For this reason, it is preferable to use isotopic ratios of the same element rather than elemental ratios when calculating mixing fractions, as they are less affected by solubility or mass dependent fractionation. As such, mantle contributions to a petroleum system are usually deduced from $^{3}He/^{4}He$ ratios (Eq. 1.4), and radiogenic contributions from $^{20}Ne/^{22}Ne$ and $^{21}Ne/^{22}Ne$ ratios.

$$R_{sample} = f_{mantle}R_{mantle} + f_{radiogenic}R_{radiogenic} \tag{1.4}$$

Example equation for deconvolving mantle helium contributions, where R denotes a $^{3}He/^{4}He$ ratio, and f is the fractional contribution to the measured sample.

A further important use for calculations is the identification of any air contamination in a sample, as even ppm levels of air within a sample can impact measurements. Due to the varying concentrations of the noble gases in typical crustal samples and air, certain isotopes are more sensitive to air contamination. For example, the $^{4}He/^{20}Ne$ ratio is often used to identify atmospheric He contamination, as all of the ^{20}Ne is assumed to be originally atmospheric in origin. A $^{4}He/^{20}Ne$ close to the air value of 0.32 suggests atmospheric contamination, as crustal samples typically have values many orders of magnitude higher (Ballentine et al., 1996). However, as Ar is much more abundant in air than He, it takes a smaller amount of air contamination to affect the $^{40}Ar/^{36}Ar$ ratios.

Hydrocarbon-water interaction models

Water is a key component in all petroleum systems. It is present in the sediments during burial (known as 'connate' or 'formation water'), however groundwater can also migrate through the system depending on the permeability and structural configuration of reservoir lithologies or carrier beds. Understanding the interactions between hydrocarbon and water phases can help give insight into the history of the formation and migration of the hydrocarbons themselves, as well as their present water contact. The present day water contact may be particularly important in providing pressure support for the production of hydrocarbons at wells, and may have implications for water breakthrough (Toth, 1980).

The noble gases have different solubilities in fluids, with the heavier noble gases typically more soluble. This phenomenon has been demonstrated empirically in noble gas investigations of groundwaters, where Xe and Kr are enriched relative to their atmospheric abundances (Mazor, 1972). Theoretically it should be possible to predict the partitioning behaviour for the noble gases between any fluid phases in the subsurface, such as water and oil or gas. This has led to the development of models describing the partitioning of the noble gases between water and oil/gas phases in the subsurface.

These models make a series of assumptions. Firstly, they assume that the hydrocarbon phase is initially devoid of noble gases and only inherits an atmospheric noble gas inventory through interaction with air-saturated water (ASW) in the subsurface post expulsion from the source-rock (i.e. hydrocarbons in source-rocks do not contain any noble gases). These models also typically assume that an initial composition of atmosphere-derived noble gases is present in groundwater, which is well constrained over a range of temperatures and salinities (Kipfer et al., 2002). Isotopes for each gas are chosen which have no significant radiogenic production in the subsurface (^{20}Ne, ^{36}Ar, ^{84}Kr, ^{130}Xe), so that the total amount of each isotope present in the system is constant. These isotopes have previously been used as tracers in the investigation of groundwater circulation patterns (Castro et al., 1998a; Castro et al., 1998b). Helium is typically not considered in these models as ^{4}He is produced

radiogenically in large amounts, and atmosphere-derived ^{3}He in the subsurface is negligible. Furthermore, the solubilities of He and Ne are often indistinguishable at crustal pressures and temperatures, meaning that little new information would be gained regardless. In systems with negligible fissiogenic Xe, ^{132}Xe is often used instead of ^{130}Xe, as it is present in higher quantities at atmospheric ratios. The result from these assumptions is that measurement of the atmosphere-derived noble gas isotopes in one phase of the subsurface system allows the volume ratios and partitioning behaviour of the entire system to be reconstructed.

The fundamentals of this approach were originally laid out by Bosch and Mazor, 1988, who used the isotope ratios of atmosphere-derived Ne/Ar, Kr/Ar, and Xe/Ar to predict partitioning patterns in water-oil and water-gas systems. Ballentine et al., 1996 used atmosphere-derived ^{20}Ne/^{36}Ar ratios measured in the North Sea Magnus oilfield to quantitatively estimate oil/water volume ratios (V_o/V_w). The technique is similarly applicable to predict gas/water volume ratios (V_g/V_w) in gas-dominated petroleum systems, as shown in the following equation.

$$\frac{V_g}{V_w} = \frac{\left(\frac{^{20}Ne}{^{36}Ar}\right)_{asw}}{\left(\frac{^{20}Ne}{^{36}Ar}\right)_g} - \frac{K^{Ar}}{K^{Ne}} \tag{1.5}$$

Where K_i is the Henry's coefficient of noble gas i in water at reservoir conditions, and the subscript asw refers to the air-saturated water composition of groundwater recharge. For oil-water systems V_o/V_w is calculated analogously to the above equation, but using the ratio of the Henry's coefficients of oil and water, instead of simply water.

This concept was modified by (Zaikowski and Spangler, 1990), who used Ne/Ar ratios combined with absolute ^{36}Ar concentrations to predict the evolution of groundwater in contact with varying gas volumes. Using absolute concentrations has the added complexity of uncertainties that arise from the conversion of concentration at STP to reservoir temperature and pressure than using ratios, but can provide an additional constraint on water-gas ratio volumes. Furthermore, at gas/water ratios of over 0.01, effectively 100% of the noble gases are partitioned into the gas

phase, making ratios insensitive to changes in V_g/V_w. Concentrations however will still be diluted by the addition of more hydrocarbons, making them more effective at determining V_g/V_w in these scenarios. The formulation for calculating V_g/V_w using concentrations is as follows.

$$\frac{V_g}{V_w} = \frac{C^i_{asw}}{C^i_g} - \frac{1}{K_i} \tag{1.6}$$

Where C is the concentration of the noble gas i in a particular phase, and K_i is the Henry's coefficient in water at reservoir conditions. Units for Henry's coefficient must be chosen to complement the units used for concentrations in the water and gas phases. For oil-water systems, again the ratio of Henry's coefficients is used.

The models and equations described thus far are applicable to a simple 2-phase static closed system. In reality, petroleum systems are often more complex, exhibiting open system behaviour in the form of reservoir leakage, gradual noble gas stripping by previous migrating hydrocarbons and dual hydrocarbon phase accumulations (e.g. reservoired oil with a gas cap). These more complex scenarios can be accounted for by using mass-balance for hydrocarbon loss and/or partitioning, or Rayleigh fractionation to describe gradual processes (Zhou et al., 2005). The context of the specific system will dictate which model is most appropriate. For example, Barry et al., 2016 use compound models to describe volume ratio interactions in both open and closed systems from the Sleipner field, North Sea.

A graphical representation of this approach is shown in Fig. 1.3, illustrating the different distributions of atmosphere-derived noble gases for both gas-water and oil-water systems. Examples of data from previous studies are shown in Fig. 1.4, which shows the observed ranges of $^{20}Ne/^{36}Ar$ from real world gas and oil systems. It is also clear that whilst the behaviour $^{84}Kr/^{36}Ar$ and $^{130}Xe/^{36}Ar$ should follow directly from the measured $^{20}Ne/^{36}Ar$, it is frequently observed at elevated levels and therefore usually not considered for quantitative volume ratio calculations.

The practical applications of this approach include measuring the extent of groundwater interaction with a known hydrocarbon phase, which can provide insight into migration patterns and regional subsurface fluid flow regimes (Bosch

and Mazor, 1988; Ballentine et al., 1996). The extent of groundwater interaction also has implications for the quality of the hydrocarbons present. The dissolution and removal of soluble hydrocarbons by persistent groundwater flow (also known as 'water-washing') can have a negative impact on the quality of the accumulated oil (Lafargue and Barker, 1988). Furthermore, the movement of groundwater through the system can introduce and maintain microbial communities, which can biodegrade oil, or produce microbial methane (Leahy and Colwell, 1990; Horstad et al., 1992).

The accuracy and precision that arise from the application of this technique is somewhat limited by its input parameters. As detailed in previous sections, the Henry's law solubility of noble gases is dependent on temperature, pressure, salinity (for water), and API gravity (for oil). These relationships are non-linear and must be empirically derived, with some parameters often needing to be extrapolated from empirical data to match reservoir conditions. Additionally, the initial composition of air-saturated groundwater is similarly dependent on temperature and salinity conditions when it is formed at the surface during aquifer recharge. As groundwater associated with hydrocarbon systems can be millions of years old, it can be difficult to predict what these surface conditions would have been, but the generic assumption is made that perturbations in the noble gas composition caused by petroleum system processing is far larger than any uncertainty in initial composition. As the increase in quality data sets from case studies increases, it is interesting to note that data inversion techniques are starting to be used to reconstruct surface conditions and demonstrate that some systems can preserve these signals over many millions of years (Barry et al., 2017).

Dating by radiogenic ingrowth

The dating of groundwaters using the decay and production of noble gas isotopes is a well-established technique, albeit with many assumptions. Whilst several different methods exist, each appropriate for different timescales or systems, the most widely investigated, and most appropriate for typical basinal fluid timescales, is the accumulation of stable radiogenic ^{4}He and ^{40}Ar (Torgersen and Clarke, 1985;

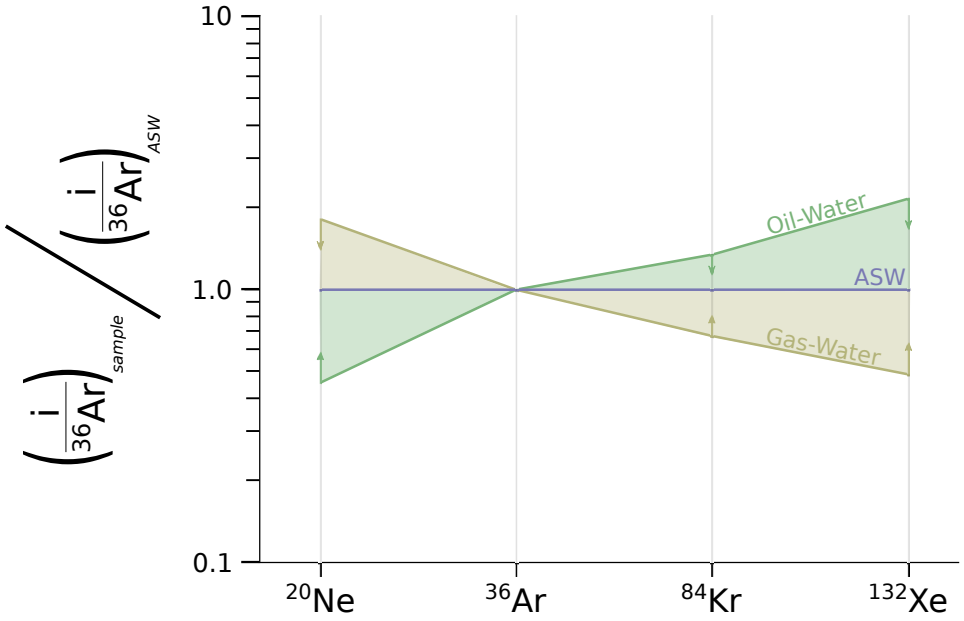

Figure 1.3: Model for the distribution of atmosphere-derived noble gases (ANG) in subsurface partitioning between water and oil/gas phases, after Bosch and Mazor, 1988. All values are normalised to the air-saturated water (ASW) reference, which is assumed to be the initial composition of groundwater in the subsurface. Upon first interaction with a small gas volume ($V_g/V_w \approx 0$) the different solubilities of the noble gases cause different amounts of exsolution into the gas. The composition of the gas volume at $V_g/V_w = 0$ will be that defined by the gas-water interaction line. As the gas volume, and consequently V_g/V_w increases, the proportion of noble gases in the gas volume increases, and the composition of the gas will evolve back towards the initial ASW values, as shown by the arrows. In a closed system, the gas remains in contact with the water, and as V_g/V_w increases the noble gases will eventually be ≈100% in the gas phase, resulting in the gas phase having the initial ASW composition. In an open system, where gas is able to escape, the remaining water can become highly fractionated, and eventually the noble gases exsolving from this water will evolve to compositions beyond the ASW line. In this way the ANG's can be used to assess to what extent a system is open or closed (i.e. how much gas is potentially escaping from the system). Furthermore, quantitative V_g/V_w ratios can be calculated from this method (see text). In an oil system, the same method applies. The initial gas-water and oil-water interaction lines were calculated for an initial ASW composition of zero salinity at STP (Kipfer et al., 2002), and the phase partitioning occurring at a reservoir temperature of 100^{o}C. Choosing different initial ASW and reservoir conditions can substantially affect the magnitude of fractionation upon partitioning.

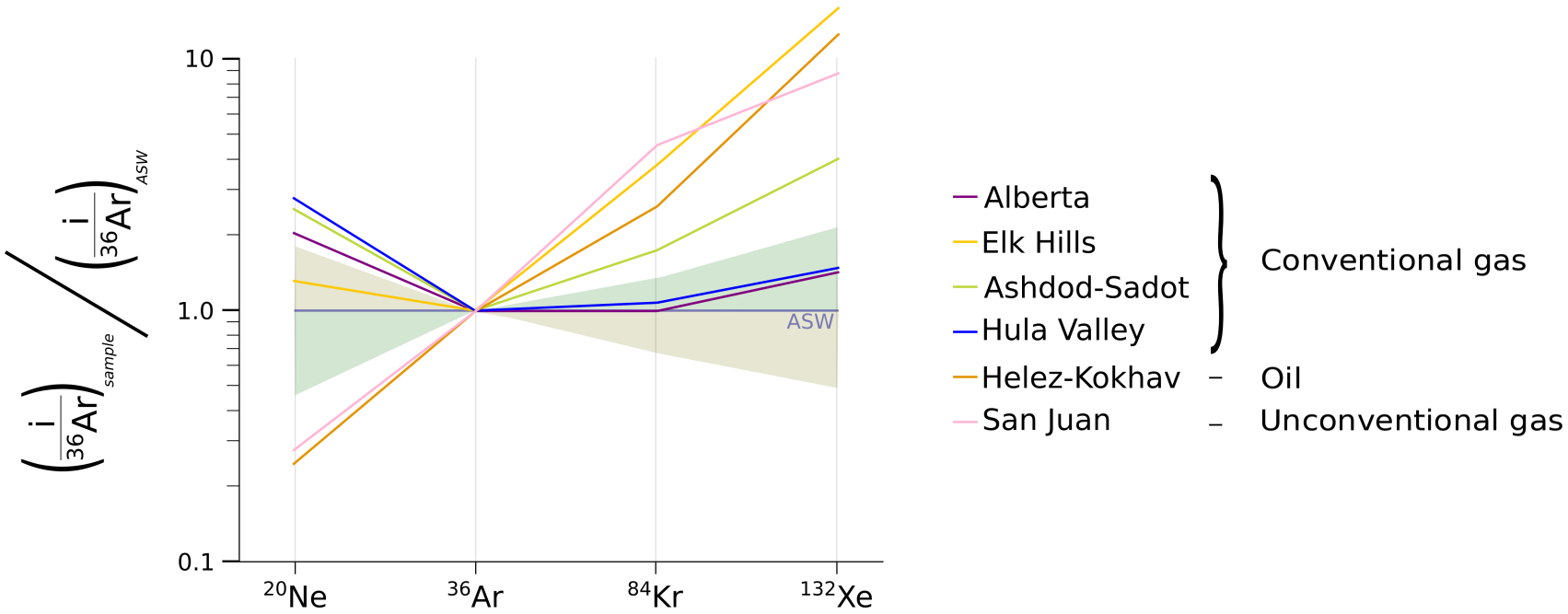

Figure 1.4: Selected data displayed on the ANG composition chart described in Fig. 1.3. Shaded areas correspond to the gas-oil and water-oil partitioning lines described in Fig. 1.3, although as these lines are sensitive to temperature, pressure and salinity both in the reservoir and at initial groundwater recharge conditions, the actual partitioning lines will vary for each system. The Hula Valley and Ashdod-Sadot systems (Bosch and Mazor, 1988) show similar elevated $^{20}Ne/^{36}Ar$ ratios suggesting gas-water partitioning with small Vg/Vw, although enrichments in Kr and Xe vary. The Helez-Kokhav oil system (Kennedy et al., 1990) shows partitioning in the direction of the oil-water line, suggesting a low V_o/V_w. The San Juan coalbed methane (Zhou et al., 2005) shows a gas system fractionated strongly away from the gas-water line past the ASW reference. This is potentially indicative of an open system with significant gas loss, or some other mechanism fractionating the noble gases. The Elk Hills system (Torgersen and Kennedy, 1999) shows $^{20}Ne/^{36}Ar$ values expected for a gas system, although the $^{84}Kr/^{36}Ar$ and $^{130}Xe/^{36}Ar$ are highly enriched. The Alberta system (Hiyagon and Kennedy, 1992) is described in the caption to Fig. 1.2. A common observation amongst the different systems is an enrichment in atmospheric Kr and Xe compared to the values predicted from the $^{20}Ne/^{36}Ar$ partitioning. The extent of this enrichment is variable, although it is often suggested to derive from an adsorbed component within the source-rock.

Marty et al., 1993; Tolstikhin et al., 1996; Castro et al., 1998a; Castro et al., 1998b; Mahara et al., 2009). A similar technique using fissiogenic Xe production is possible, but is only applicable in very old samples (>100Ma) due to the slow accumulation rate (Holland et al., 2013). By using the partitioning laws described in the previous section, it is possible to indirectly date the groundwater associated with a petroleum system by measuring the noble gases in the hydrocarbon phase (Zhou and Ballentine, 2006). The importance of groundwater involvement in petroleum systems is detailed in the above section, and constraining the age is a crucial step in resolving the groundwater-hydrocarbon interaction.

The basis for all of these models is to deconvolve the noble gases produced in situ within the system from those present initially in the groundwater, and those brought in from external fluxes. The in situ concentration is then compared with the theoretical production rates (calculated from parent isotope concentrations and decay constants) to give the necessary time for this concentration to accumulate.

$$[^4He]_{total} = [^4He]_{in-situproduction} + [^4He]_{asw} + [^4He]_{externalflux} \tag{1.7}$$

Where total is the total reconstructed concentration in associated groundwater, ASW is the initial concentration in air-saturated groundwater recharge, in situ production is the amount produced in place over the lifetime of the system, and external flux denotes the amount brought in from external sources. The closure age of the system can then be calculated using the following parameterization, after Torgersen, 1980.

$$[^4He]_{in-situproduction} = \frac{\rho J \Lambda (1-\phi)}{\phi} \times t \tag{1.8}$$

Where ρ is the density of the rock, J is the in situ production of ^{4}He (in cm^3STPg^{-1}), Λ is a parameter describing the efficiency of transfer of produced ^{4}He from mineral to surrounding fluid, where $0 \leq \Lambda \leq 1$, and Φ is porosity. The residence time of the groundwater in the system is t. Λ is thought to be approximately 1 over geological timescales (Ballentine and Burnard, 2002). J is

calculated as a function of the concentrations of U and Th in the surrounding rocks, after Craig and Lupton, 1976.

$$J(^4He) = 0.2355 \times 10^{-6} \times [U](1 + 0.123(\frac{[Th]}{[U]} - 4)) \tag{1.9}$$

Analogous equations can be formulated for the production of ^{40}Ar, or any other radiogenic or nucleogenic isotope.

The principal uncertainty in groundwater dating is the term accounting for external flux of radiogenically produced isotopes. Radiogenic concentrations in excess of those that can be reasonably explained by in situ production are frequently observed in groundwater and hydrocarbon systems (Torgersen and Ivey, 1985; Takahata and Sano, 2000). Several studies suggest that this is due to a universal continental degassing flux from the deep crust, whilst others have suggested a more variable input from old isolated fluid bodies or mineral degassing during alteration (Torgersen and Clarke, 1985; Solomon et al., 1996; Tolstikhin et al., 1996; Patriarche et al., 2004) or due to thermal perturbation of old continental crust (Ballentine et al., 2002; Lowenstern et al., 2014). The exact impacts of these various factors are probably dependent on basin-scale hydrogeological behaviours, and as such knowledge of the basin structure and history are crucial during these calculations and subsequent interpretations.

Zhou and Ballentine, 2006 considered data from 3 previous studies to investigate ^{4}He ages of hydrocarbon associated groundwater In the San Juan basin, biogenic coalbed methane play ^{4}He ages were found to be dependent on distance from recharge at the basin margin. Making an argument that the biogenic degradation of the coal is related to groundwater age enabled a biogenic gas production rate to be calculated, and is in reasonable agreement with biogenic gas production rates estimated using a similar approach in the Antrim Shales, Illinois basin, USA (Schlegel et al., 2011). ^{4}He ages from the North Sea Magnus oilfield gave values of ~2Ma, which when compared with the age of the reservoir (~150Ma) to suggest the influence of formation water has been relatively minor. The He-rich Hugoton-Panhandle gas field in the Southern US yielded slightly older ^{4}He groundwater

ages of around 4Ma. This is still relatively young compared to the estimated age of the petroleum system, and is interpreted to be more representative of the ages of groundwaters bringing in the high He concentrations, indicating a relatively recent injection of commercial He.

Dating of groundwaters associated with natural gases in the Piceance basin, Colorado, has also been undertaken by McMahon et al., 2013. They were able to identify a range of groundwater ages using ^{4}He dating in conjunction with ^{14}C dating. This was used to show the compartmentalisation of the field into areas with different ages, with differences in gas composition between the areas. Similarly, the ^{4}He ages determined by Schlegel et al., 2011, in the Illinois basin, showed older groundwater ages associated with thermogenic methane, whilst younger ages were associated with microbially generated methane. This suggests noble gas ages have the potential to constrain the onset and extent of microbial methane generation.

Unconventional systems

The rapid expansion of unconventional source-rock reservoir hydrocarbon production over the last decade has created an opportunity for the development of new noble gas techniques to advance our understanding of the mechanisms involved in unconventional oil and gas generation, storage, and production (Curiale and Curtis, 2016). As unconventional hydrocarbons are generated and produced in situ, with no secondary migration, the pressure-temperature histories of the systems are better constrained, and the noble gas signatures are likely to be less influenced by basin-scale fluid flow regimes. Furthermore, the retention of hydrocarbons within the source-rock allows for the initial noble gas composition of hydrocarbons to be measured directly. This could have important implications for the study of conventional systems, where the initial hydrocarbon noble gas composition is often assumed to be negligible.

Tantalising insights into the potential behaviour of noble gases in source-rocks were found in an investigation into biogenic coalbed methane in the San Juan system (Zhou et al., 2005). The produced gases were observed to be highly enriched in

atmosphere derived Xe, and to a lesser extent Kr. This effect was suggested to be due to preferential sorption of heavy noble gases onto the organic-carbon rich sediments, a phenomenon that has been observed experimentally in laboratory simulations (Fanale and Cannon, 1971; Podosek et al., 1981) and observed previously in other hydrocarbon systems (Torgersen and Kennedy, 1999). Variable fractionation was also observed in both $^{20}Ne/^{22}Ne$ and $^{38}Ar/^{36}Ar$ isotope ratios, consistent with kinetic mass-dependent fractionation. This is proposed to be due to concentration gradients created during gas production imparting a diffusive effect on the produced gas.

An investigation into Marcellus shale gases by Hunt et al., 2012, showed that the gases could be separated into distinct groups with different thermal maturities, based on their radiogenic/nucelogenic noble gas contents. The $^{4}He/^{40}Ar^{*}$ and $^{21}Ne^{*}/^{40}Ar^{*}$ ratios (where * indicates the radiogenic component)both showed a distinct grouping that correlated with thermal maturity, suggesting that the temperatures experienced by the source-rocks affected the release of radiogenically produced noble gases into the surrounding fluids (e.g. Ballentine et al., 1996). Whilst there are more practical ways of identifying gas maturity, this shows the possibility for using noble gases to track the extent of gas release with temperature, unaffected by chemical or biological effects.

The Antrim shale-gas play has also been investigated by Wen et al., 2015b. Trace amounts of mantle fluids were detected using $^{3}He/^{4}He$ isotope ratios, and ^{4}He groundwater ages were relatively young ($\geq$250ka), coinciding with past glaciations. Both of these findings suggest that despite the low porosity of the rocks, groundwater and other fluids are still able to permeate the system. However, the Antrim shale is naturally fractured to a much greater extent than typical unconventional shale-gas systems, which could artificially increase permeability and hence local fluid flow (Apotria et al., 1994; Ryder, 1996). Further observations from this study include variable Ne isotopes exhibiting scatter in the mass-dependent fractionation directions, similar to the San Juan basin; whether this is a signal common to all unconventional systems is not yet known.

Measured data from unconventional studies are shown alongside those from conventional systems in figures 1.2, 1.5 and 1.6. Helium isotopes show lower ^{4}He concentrations compared to conventional systems, and no significant mantle contributions. Neon isotopes in both datasets show no significant radiogenic contribution but high levels of scatter along mass-dependent fractionation trajectories. ^{40}Ar/^{36}Ar isotopes ratios show little variation in unconventional systems, but large ranges in ^{36}Ar concentration compared to conventional systems. This pattern potentially reflects heterogeneity in production when compared to conventional accumulations, caused by lower permeability and connectivity within the source-rock reservoir. However, more datasets are needed to draw any robust conclusions. It is also important to note that both the San Juan and Antrim shale systems would be considered far from typical for unconventional source-rock reservoir production. The San Juan is a biogenic coalbed methane rather than a more common thermogenic shale gas, and the Antrim system also has a significant biogenic component, and has been highly fractured by recent glaciation events. For a detailed discussion of nomenclature and classification of unconventional systems, see Curiale and Curtis, 2016.

Studies of noble gases in produced unconventional hydrocarbons are still relatively sparse (Moore et al., 2018), there have been several noble gas studies of the groundwaters associated with unconventional systems, primarily for assessing environmental impact on aquifers. Of these, Darrah et al., 2014, Darrah et al., 2015 and Jackson et al., 2013, have shown the utility of noble gases in discriminating between anthropogenic hydrocarbon contamination of drinking water aquifers, and natural hydrocarbon migration in subsurface brines.

1.3.7 Summary

Despite years of investigation and a number of notable publications in the field, noble gases are still not used as a routine geochemical analytical tool in hydrocarbon systems, in the manner of C or H isotopes. Partly this is due to the expense and difficulty of making the measurements themselves, but it is also due to the complex

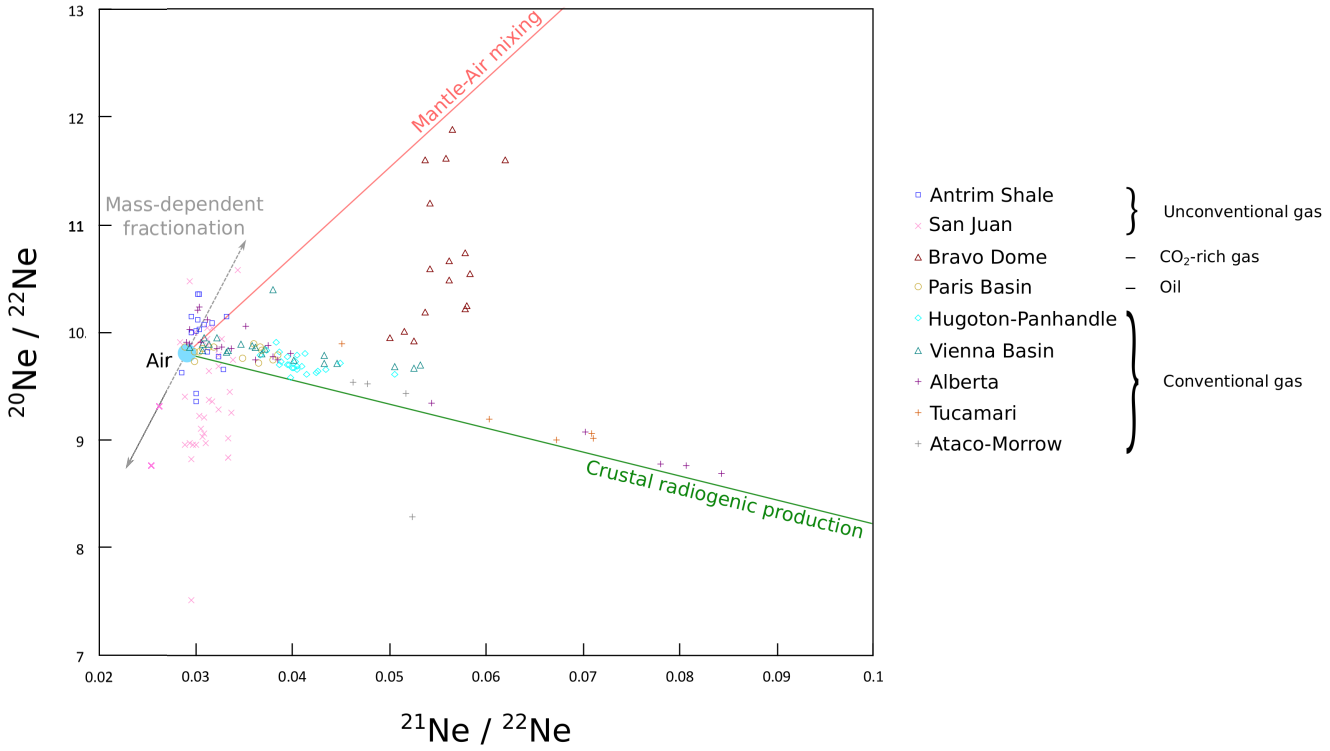

Figure 1.5: Neon 3-isotope plot for selected noble gas studies of petroleum systems. Neon isotopes are conventionally thought of as a 3-endmember mixing system, with crustal radiogenic production and mantle mixing lines shown. In crustal systems, both ^{21}Ne and ^{22}Ne are produced radiogenically, resulting in alteration of the isotope ratios along the crustal evolution line defined in Kennedy et al., 1990. The Bravo Dome system shows radiogenic ingrowth in addition to mixing with a mantle Ne endmember (Ballentine et al., 2005). Additionally, mass-dependent fractionation of the system can cause the isotopes to evolve along the mass-fractionation line in either direction, consistent with data observed in both the Antrim and San Juan systems. Both of these systems are unconventional, the San Juan being a coalbed methane system, and the Antrim a more typical shale gas play. The Bravo Dome system is rich in CO2 that is interpreted to be sourced from mantle fluids; the neon isotopes clearly show mixing with a mantle endmember. Data sources: Antrim Shale (Wen et al., 2015b); San Juan coalbed methane (Zhou et al., 2005); Bravo Dome (Ballentine et al., 2005); Paris Basin (Pinti and Marty, 1995); Vienna Basin (Ballentine and O'Nions, 1992); Alberta, Tucamari, and Ataco-Morrow (Kennedy et al., 1990).

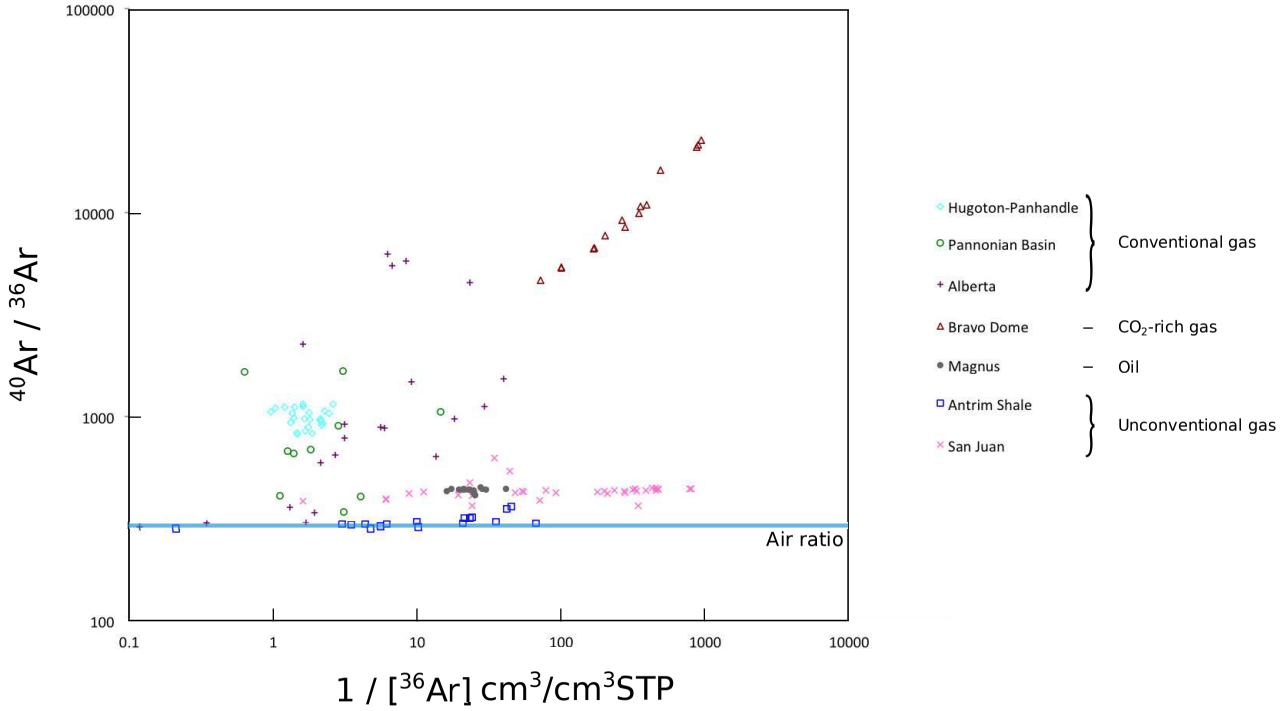

Figure 1.6: Selected examples of Ar isotope ratio and concentration measurements from previous studies. $^{40}Ar/^{36}Ar$ is plotted against $1/[^{36}Ar]$ so that mixing trajectories towards well-defined endmembers such as air are clearly apparent. Addition of pure radiogenic ^{40}Ar however will not result in straight-line mixing on this plot. The Ar isotope system is a mixing system between the air-like ratio of 298.6 (Lee et al., 2006) and addition of radiogenic ^{40}Ar, produced in the crust from ^{40}K decay. As is evident from the data shown, ratios below the air value are not usually observed. Elevated $^{40}Ar/^{36}Ar$ ratios can be caused both by radiogenic production of ^{40}Ar within the crust, as well as mixing with mantle fluids which have high levels of radiogenic ^{40}Ar. The Ar isotope system is also important for the detection of any air contamination in samples; the relatively high concentration of Ar in Air makes even small amounts of contamination drastically affect measured Ar concentrations and isotope ratios. Data sources: Magnus (Ballentine et al., 1996); Pannonian Basin (Ballentine and O'nions, 1993); Hugoton-Panhandle gas field (Ballentine and Sherwood Lollar, 2002); Alberta field (Hiyagon and Kennedy, 1992); Bravo Dome (Ballentine et al., 2005); Antrim Shale (Wen et al., 2015b); San Juan coalbed methane (Zhou et al., 2005).

nature of interpreting noble gas results and the necessity of having proper context to do so. Whilst calculating absolute V_g/V_w ratios and ^{4}He and ^{40}Ar ages represents significant progress towards quantifying fluid exchange and accumulation within a system, it is still not always intuitive what these numbers actually represent. For V_g/V_w and V_o/V_w ratios it is not necessarily the ratio of gas to water in the accumulation itself, but rather the entire history of hydrocarbon-water interaction within the system (e.g., during migration from the source-rock to the accumulation). In this way they should be considered not as an alternative to geological observations, but as an additional constraint to complement existing techniques.

A key step in the development of the noble gas toolkit is the continued acquisition and compilation of case studies. Although petroleum systems can be broadly categorised they are all unique, which potentially provides great future utility for identifying the source and history of a hydrocarbon reservoir. Comparison between different systems will allow universal patterns between similar systems to be discerned from local effects particular to that location. This in turn will allow more robust conclusions to be drawn in a more straightforward fashion from new studies.

In the study of unconventional systems, it remains unclear which questions noble gases will be most suited to answer. Will the adaptation and application of existing conventional system tools be appropriate, or will new approaches need to be formulated entirely? The isolation of any Xe-enriched sedimentary component, and the controls on this process should be a preliminary goal. This may lead to insights into the mechanisms controlling gas storage within organic-rich sediment; the importance of adsorption versus free gas stored in porosity could help explain extent of gas generation and recoverability. As previously mentioned, constraining the noble gas characteristics of source-rocks could also help refine groundwater models in conventional systems. Indeed, fluid interaction models could also have some utility in unconventional systems themselves. Previous studies have shown that despite their low permeability, groundwater-derived noble gases and mantle fluids are present within produced gases. Unconventional systems are known to expel some generated hydrocarbons, as many simultaneously act as source-rocks

for conventional accumulations (Robison, 1997). Noble gases could be used to shed light on the mechanisms controlling gas release versus retention within the source-rock, effectively helping predict the volumes of hydrocarbons present in a source-rock while simultaneously providing constraints on potential volumes in associated conventional petroleum accumulations.

The promise of being able to geochemically decode the physical structure and history of a petroleum system is a tantalising prospect. Although theoretically straightforward, this goal is complicated by the vagaries of any natural system. Completion of further data-rich studies on a wide range of different systems should be aided by improvements in experimental technology. Past investigations were typically focused on a few specific isotopes, it is now possible to routinely measure all naturally occurring noble gas isotopes in a single sample. The acquisition of accurate data for less-studied isotopes such as those of Kr and Xe could lead to development of new investigative techniques as well as the corroboration of existing ideas. Integration of this data will help investigations of individual systems to be generalised into overarching patterns applicable to all petroleum systems, at which point noble gas analysis can become less descriptive, and more predictive.

1.4 Methodology

1.4.1 Sample collection

Samples for this work were collected from 3 distinct sources: natural gas wells, geothermal wells, and fumaroles. The basic sample collection method is identical for all sample sources, and is based on the well-established technique described in Weiss, 1968. Gas is flushed through a hose and into refrigeration-grade copper tubes which are subsequently sealed using steel clamps to form a cold-weld that ensures no leaking of noble gases across the seal (even for He). For natural gas wells and geothermal wells, the gas was fed through a 2-stage regulator in order to decrease the pressure to 1-2bar, and then connected with tygon tubing to copper tubes connected in series to enable duplicate collection. The exhaust was then submerged in water to prevent the backflow of air into the copper tubes, and the

gas was flushed through for 10 minutes to ensure the complete removal of air. The copper tubes were then clamped starting from the point closest to the exhaust and working back towards the well, sealing the sample gas inside the copper tubes. For fumaroles the method is similar except that the gas is entrained into the sample apparatus using a funnel, and depending on the flow rate of gas the copper tubes may need to be flushed for a longer period of time to ensure the removal of air. An illustration of the sample collection method is provided in Fig. 1.7.

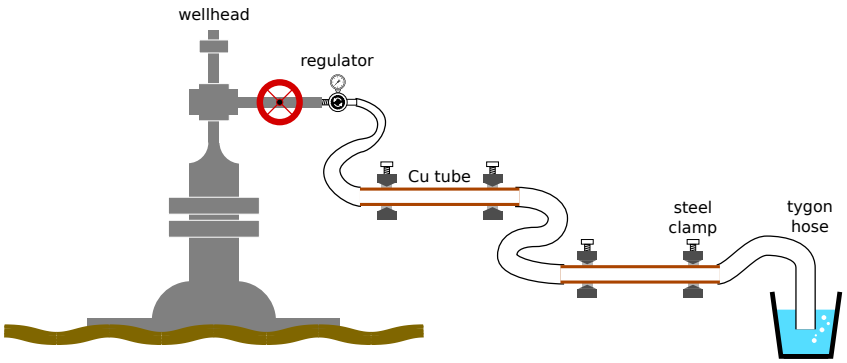

Figure 1.7: Schematic representation of noble gas sample collection from a wellhead, using 2 Cu tubes in series for duplicate collection. Gas will be stepped down from well pressure to ~2bar and flushed through the setup for ~10 minutes to remove air. Exhaust is submerged in water to exclude the possibility of air backflowing into the sample tubes. After flushing, the clamps would be closed starting from the right and moving to the left in the layout shown.

1.4.2 Sample analysis

The principal method employed in the collection of data for this thesis was the analysis of the isotopic composition of the noble gases in gas-phase samples. This was undertaken at the Noble Laboratory in the Oxford University Dept. of Earth Sciences. The equipment used consists of an extraction line attached to 2 mass spectrometers, a Helix SFT and an Argus VI, both manufactured by Thermo Fisher Scientific. The Helix SFT has a 2-collector setup including one Faraday detector and one electron multiplier (SEM), an internal volume of 1400cm^3, and a mass-resolution of ~700 for the SEM. This setup is specialised for measurement

of He isotopes, with the 2 collectors allowing simultaneous measurement of ^{4}He on the Faraday detector and the low-abundance ^{3}He on the more sensitive SEM. The high mass-resolution also allows separation of the ^{3}He peak from deuterium-substituted diatomic hydrogen (HD). The Argus VI is designed primarily for Ar isotope measurement, and combines a low internal volume of 700cm^{3} with a detector array of 5 Faradays and 1 SEM. Our measurement protocol utilises the Argus for measurement of Ne, Ar, Kr and Xe isotopes, allowing the measurement of all 23 stable noble gas isotopes in a single sample run. As Kr and Xe have 6 and 9 stable isotopes respectively, they must be measured on the Argus using peak-jumping. For comprehensive reviews of the fundamental principles of noble gas mass spectrometry see Reynolds, 1956; Nier, 1981; Stacey et al., 1981; Takaoka, 1983; Burnard and Farley, 2000 and Morgan, 2015. For papers detailing the specification and performance of the Argus and Helix SFT instruments used in this work, see Mark et al., 2009 and Mabry et al., 2012 respectively.

Prior to analysis, samples must be purified to remove all reactive gases, and then the different noble gas elements separated out cryogenically. For this purpose we use a custom-built extraction line containing a series of getters and cryogenic traps. A schematic representation of the extraction line is shown in Fig. 1.8. The extraction and purification protocol was developed during the first stage of this work, and minor subsequent refinements and modifications have been made since. The basic sample measurement protocol is as follows:

- Sample is inlet into the calibrated volume, where pressure response is measured on the 1000Torr baratron. Valve O4 is closed so as to isolate the sample in the calibrated volume plus sample pipette.
- The sample is expanded into the volume containing the Ti getter, held at 950^{o}C using an external furnace (10 mins).
- The furnace is removed and the sample is left within the Ti getter volume as it cools to room temperature (10 mins).

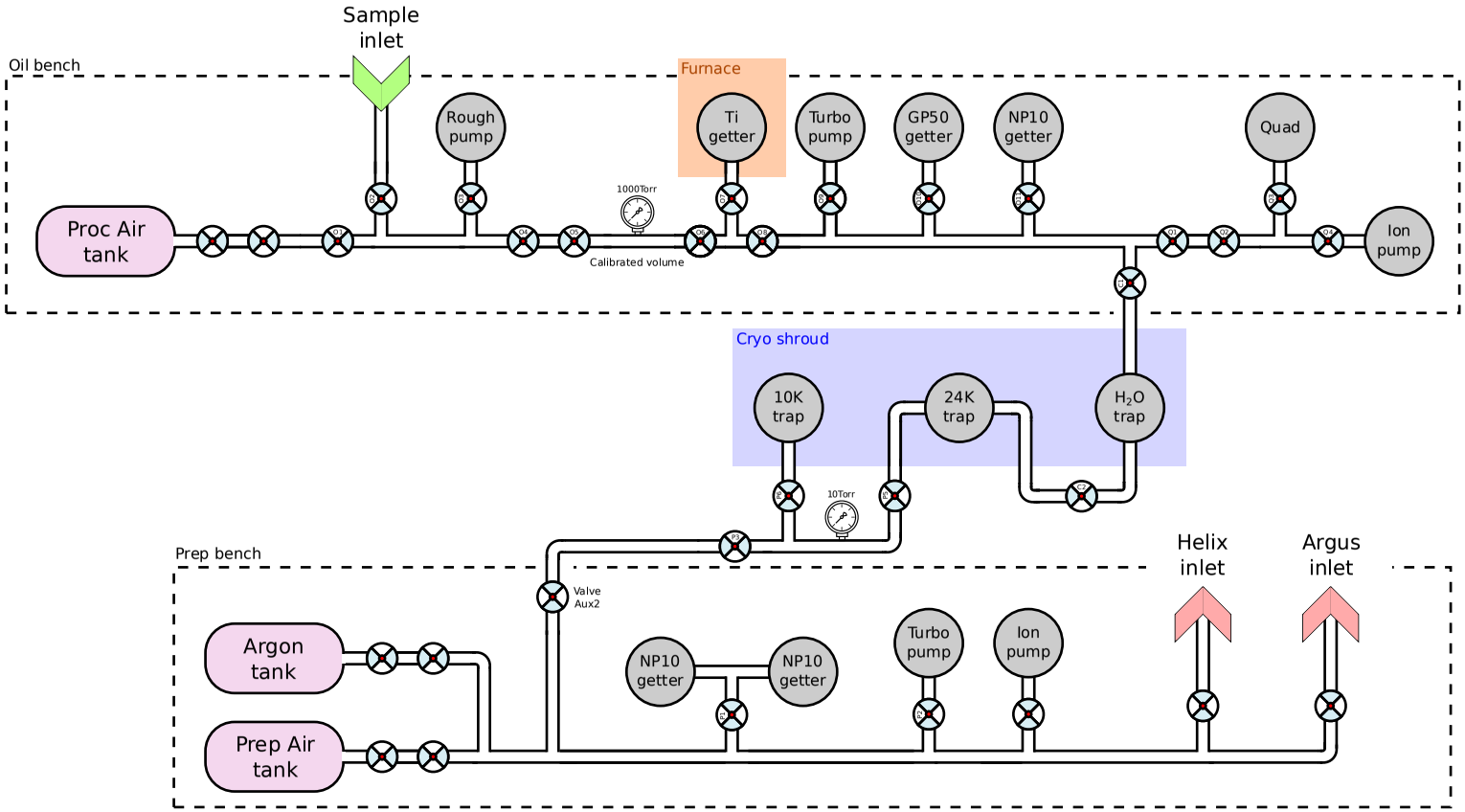

Figure 1.8: Schematic representation of the extraction line used for noble gas isotope measurements in this work. The section of the line between valves O4 and O5 is referred to as the 'calibrated volume' in the text, and has been measured to enclose 69.7cm^3. Gauge icons represent baratrons used for measuring pressure within the line.

- The sample is further expanded into the dual-getter system (SAES NP10 and GP50) for further removal of reactive gases (10 mins).
- Valve Q1 is closed so as to isolate a small aliquot of the sample in the quadrupole pipette. The remainder of the sample is expanded into the water trap, held at 180K (10 mins).
- The aliquot in the quadrupole pipette is expanded into the quadrupole and analysed for a first-order measurement of the bulk noble gas composition of the sample. This allows an estimation of the amount of sample which should be inlet into the mass spectrometers.
- The sample is expanded into the stainless-steel 24K trap(so-called due to its minimum attainable temperature), held at ~24K. This freezes Ar, Kr and Xe, but not He or Ne (10 mins).
- The sample is expanded into the charcoal 10K trap, held at ~10K. This freezes He and Ne onto the trap (10 mins).
- Valve C2 is closed to isolate the sample in the cryogenic traps. The oil bench can now be prepared to run the next sample.
- The 10K trap is raised to 34K, releasing He into the prep bench manifold (10 mins). If necessary, the amount of He can be cut down by isolating the Aux2 volume, pumping the manifold through valve P2, and subsequently re-expanding from the Aux2 volume.
- He is inlet into the Helix SFT instrument for measurement. The remaining He is pumped away.
- The 10K trap is raised to 90K, releasing Ne into the prep manifold (10 mins).
- Ne is inlet into the Argus for measurement. During measurement the 10K trap is heated to 300K and the remaining Ne pumped away. Simultaneously the 24K trap is heated to 200K, releasing the heavy noble gases.

- An aliquot of the heavy noble gases is isolated between valves P3 and Aux2. This is then expanded into the prep manifold and the air pipette. The air pipette is then isolated and the remainder of the aliquot pumped away. This cuts down the amount of Ar which is typically present in much higher abundance than the other noble gases.

- The air pipette is expanded back into the prep manifold and inlet into the Argus for measurement of Ar.

- The remaining heavy noble gases in the 24K trap are frozen back down at 52K, where Kr and Xe are frozen but Ar is not. The Ar is then pumped away through the prep manifold. To ensure complete removal of Ar, the 24K trap is cycled between 52K and 70K 3 times, each time pumping away the Ar at 52K.

- The 24K trap is finally heated to 200K, releasing Kr and Xe, which are expanded into the prep manifold and inlet into the Argus for simultaneous measurement of Kr and Xe.

The samples are normalised to the air standard by running procedural air standards from the air bottle by the sample inlet using the exact same protocol as that of sample measurements. Reproducibility of the mass spectrometers was monitored by running nightly automated standards from the prep bench air bottle. The mass resolution of the Argus is insufficient to resolve key interferences during the measurement of Ne, specifically the interferences of $^{40}Ar^{++}$ with ^{20}Ne and that of $^{44}CO_2^{++}$ with ^{22}Ne. Therefore, $^{40}Ar^{+}$ and $^{44}CO_2^{+}$ were also monitored during Ne isotope measurement. A correction factor was applied to remove the effect of $^{40}Ar^{++}$ following Niedermann et al., 1993, and $^{44}CO_2^{++}$ levels were found to be insignificant for all samples measured as part of this work.

Errors are reported associated with all noble gas isotope ratios and abundance measurements. These are derived from the external reproducibility of the daily standards run on the mass spectrometer system, as well as associated uncertainties

in parameters required to calculate concentrations or isotope ratios from raw signal intensities.

$$C_{sm} = \frac{C_{st} I_{sm} V_{st} p_{st}}{I_{st} V_{sm} p_{sm}} \tag{1.10}$$

For example, the calculation of a concentration measurement is shown in Eq. (1.10), where C is concentration, I is signal intensity as measured on the mass spectrometer, V and p are the volume and pressure of gas run, combining to represent the number of moles of gas run. The subscripts sm and st indicate the unknown sample and known standard respectively. Uncertainty in C_{sm} is calculated by standard error propagation methods (summation in quadrature) using the uncertainties in the input parameters. Uncertainty in V is typically not required as the same volume of sample and standard are run, and so V can be cancelled. Regardless the volumes of the different parts of the line used for sample input are well-calibrated. The pressure is measured on a baratron at the sample/standard inlet, which shows a digital readout and the uncertainty is taken from the last stable digit in the digital readout, which is typically $< 1\%$. The uncertainty in I comprises the internal precision taken from the extrapolation of signal measurement within the mass spectrometer, and the external reproducibility of daily air standards run. This is typically dominated by the external reproducibility, which varies for different isotopes but is typically several percent. As such the computed error in C_{sm} is typically dominated by the variability in daily standards run over the course of a sample suite being measured. This results in a similar relative error for most values reported in this thesis. This method however does not account for counting statistic effects that may be experienced when measuring extreme ratios on an SEM (such as very low ^{3}He signal in strongly radiogenic samples), as such the error may be underestimated for these extreme ratios.

2

Investigating gas generation in the Eagle Ford Shale

Contents

Abstract

The recent proliferation of tight or unconventional petroleum bearing reservoirs as an energy resource enables a more detailed investigation of the geochemical behaviour of these systems. In addition, it provides an opportunity to improve our understanding of low-permeability crustal fluid systems at depth. Organic-rich shales

are not only the source-rocks in conventional petroleum systems, but potential seals, which may be important for the trapping and storage of CO_2 and/or nuclear waste. The use of noble gas isotopes as tracers of fluid provenance and physical exchange processes is well established in other crustal fluid systems. Noble gas concentrations and isotopic characteristics were determined in 10 natural gas samples produced from the Eagle Ford shale, Texas, along with the concentration and δ^{13}C and δD of hydrocarbon gases. By sampling gases produced directly from unconventional reservoirs we are able to determine their residence time and the extent of interaction of these fluids with other fluids in the wider hydrogeological system. The large range in thermal maturity exhibited across the basin, as demonstrated by the range in δ^{13}C of methane from -37.8 to -47.5‰ VPDB, allows us to constrain the evolution of the noble gas signature within a source-rock during hydrocarbon generation and expulsion. For the first time, we show that ^{36}Ar concentrations in hydrocarbon gases are not simply controlled by solubility exchange with formation water. Instead, they are shown to decrease dramatically (from 2.6×10^{-7} to 7.0×10^{-9}cm^{3}STPcm^{-3}) with increasing thermal maturity, which we attribute to a dilution effect as more short-chain hydrocarbon compounds are generated through cracking of kerogen and secondary cracking of oil. We develop a model that combines ^{36}Ar concentrations with δ^{13}C data in order to quantify the retention capacity for generated hydrocarbons, and show that between 40 to 80% of the hydrocarbons generated by the Eagle Ford shale are retained within the formation. We also calculate that radiogenic ^{4}He concentrations within the Eagle Ford are well in excess of that which could have accumulated internally since deposition and requires contributions from external ^{4}He sources. The identification of both hydrocarbon expulsion and helium addition to nominally 'tight' formations now provides a process driven and quantitative understanding of the fluid migration dynamics and processes controlling these critical formations.

2.1 Introduction

The expansion of petroleum exploration into unconventional shale oil and gas systems has fundamentally changed the global energy outlook. Unlike conventional petroleum systems (where oil and gas migrate from a source rock into a high-porosity reservoir), unconventional systems produce directly from the source-rock itself. These source-rocks are typically low-porosity organic-rich shales, and advanced production techniques such as hydraulic fracturing are required to render them economically viable (Curtis, 2002). From a geochemical perspective, this provides an opportunity to directly sample previously inaccessible fluids which are hosted in low-porosity shales, often several kilometres below the surface. The commercial production of unconventional systems has been developed and expanded rapidly in recent years, however the mechanisms controlling the behaviour and interaction of fluids within these low permeability systems remain poorly constrained (Neuzil, 1994; Prinzhofer, 2013).

Noble gas isotopes are useful for investigating crustal fluids in hydrological, volcanic and petroleum systems (Burnard et al., 2013; Holland and Gilfillan, 2013; Byrne et al., 2017). Due to their inert nature, noble gases are unaffected by the chemical alteration, redox, or biological phenomena that complicate other geochemical tracers (Ozima and Podosek, 2002; Porcelli et al., 2002). Instead, noble gas signatures are only affected by physical processes such as mixing, diffusion, dissolution, and radiogenic production (Ballentine et al., 2002). Noble gas techniques have been previously applied to investigate the genesis and behaviour of conventional petroleum systems by constraining the timing of migration and accumulation (Torgersen and Clarke, 1985; Marty et al., 1993; Zhou and Ballentine, 2006; Zhou et al., 2012; Barry et al., 2016; Tolstikhin et al., 2017), quantifying relative volumes of gas and liquid phases present (Zartman et al., 1961; Bosch and Mazor, 1988; Zaikowski and Spangler, 1990; Ballentine et al., 1991; Ballentine et al., 1996; Barry et al., 2018b), assessing the extent of fluid leakage through reservoir seals (Barry et al., 2017), and identifying the presence and provenance of fugitive gas

contamination in aquifers (Darrah et al., 2014; Wen et al., 2016). We investigate here whether high-precision noble gas analysis of samples from unconventional fields will allow us to adapt models successfully applied in conventional systems, to develop interpretations specific to unconventional systems.

Unconventional systems present a series of new challenges in understanding fluid provenance and migration. For example, the high adsorptive capacity of the argillaceous sediments that typically make up unconventional plays (Ross and Bustin, 2007) acts to preferentially concentrate heavy noble gases (Torgersen and Kennedy, 1999; Zhou et al., 2005), thus making solubility models that assume that the only source of heavy noble gases is that derived from groundwater difficult to use quantitatively. Additionally, the lack of secondary migration in unconventional systems lends itself to the possibility of in-situ investigation of thermal history using the thermally-driven release of radiogenic isotopes from the sediment grains into the free fluid phase (Hunt et al., 2012), as well as dating by accumulation of radiogenic ^{4}He (Wen et al., 2015a).

Understanding the movement of fluids in unconventional systems is of significant importance, but remains poorly constrained. Recent work has suggested these low porosity systems may be open to both losses from the system and to contributions from underlying strata. For example, the extent of interaction between the shale gas and the overlying crust has implications for the possibility of contamination of aquifers due to hydrocarbon production (Darrah et al., 2014; Wen et al., 2016; Wen et al., 2017). Similarly, the degree to which hydrocarbons are lost from the source rock is also critical for determining volumes of petroleum released into the basin that may migrate in to conventional accumulations, as well as for making unconventional gas-in-place estimates (Ungerer et al., 1990; Ungerer, 1990; Schmoker, 2002; Jarvie et al., 2007; Clarkson et al., 2012; McGlade et al., 2013). However, recent studies also show evidence for externally-sourced groundwaters contributing significantly to the noble gas inventories of in-situ unconventional hydrocarbons (Györe et al., 2017). Such an observation has important implications for the extent of fluid interaction between low-porosity shale layers and the local hydrogeological regime, which is a

crucial parameter for understanding their effectiveness as a seal in carbon capture and storage (Barry et al., 2016) and nuclear waste disposal (Neuzil, 2013; Hendry et al., 2015). The extent of interaction between fluids within the shale and those in the surrounding stratigraphy can be defined in many ways, and broadly described as the extent of open vs closed system behaviour. For the purposes of this study concerning the behaviour of fluids during hydrocarbon generation, we consider the expulsion efficiency of methane to be defined as the quantity of methane expelled from the source-rock compared to the total amount generated.

Thermal maturity is a key concept in hydrocarbon generation, and refers to the extent of thermally-driven destruction (or 'cracking') of longer chain organic carbon compounds into shorter chains (Lewan, 1993). Low maturity hydrocarbon fluids typically consist of longer, complex oil molecules, whilst high maturity fluids consist primarily of simple gas compounds such as methane (CH_4), ethane (C_2H_6), and propane (C_3H_8). By considering samples over a significant maturity range we seek to constrain the evolution of noble gas signatures within the source rock during the hydrocarbon generation process. This allows us to address a number of key unanswered questions such as the extent to which the source rock behaves as an open or closed system during hydrocarbon generation, the influence of groundwater during the generation process, and the propensity for hydrocarbon storage within the shale versus expulsion (e.g. Bernard and Horsfield, 2014).

2.2 Geological Background

The Eagle Ford Formation comprises a series of organic-rich marls, limestones and bentonites deposited in the Maverick Basin of the Cretaceous Western interior seaway of North America during the Late Cretaceous (Cenomanian to Turonian) (Robison, 1997). The Formation underlies much of south Texas, where it has been targeted for unconventional oil and gas production since 2008, and is now one of the most prolifically produced unconventional fields worldwide (Clarke et al., 2016). Due to the regional dip of the formation to the south-east, the Eagle Ford has been buried to different levels of thermal maturity across the region, with wells to the

north-west producing oils and associated solution gases, and wells to the South-East producing drier, methane-rich gas (Donovan et al., 2016). This study targeted wells from a range of maturities across the Eagle Ford formation, and aims to use noble gas analysis to characterise the behaviour of subsurface fluids in low porosity hydrocarbon systems across a range of thermal maturity levels. We present noble gas isotope and concentration data, alongside bulk gas composition and isotopic data, from the Eagle Ford shale oil and gas play in south Texas, USA (Fig. 2.1).

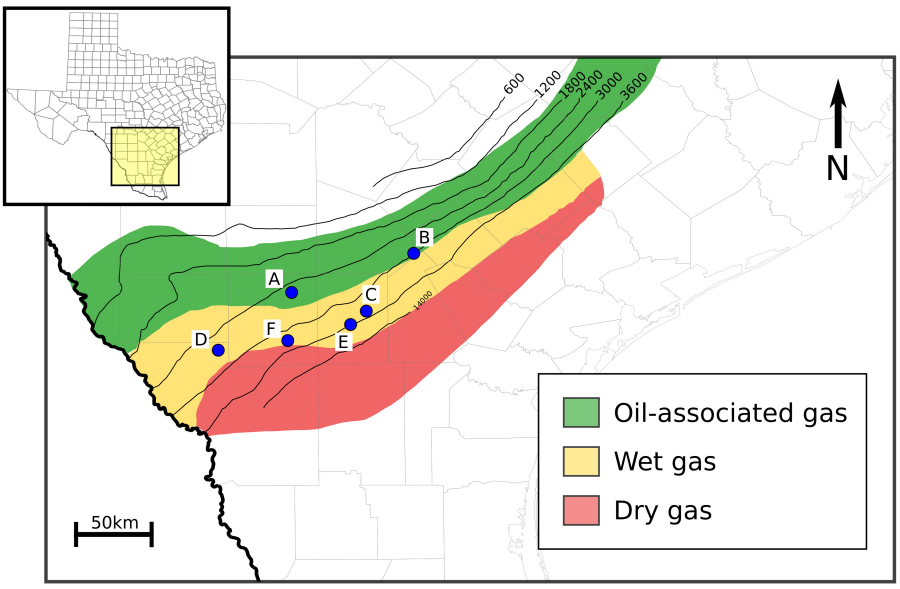

Figure 2.1: Map of the Eagle Ford shale gas play within Texas, showing wellsite locations and ranges of different types of gas production. Contours indicate the depth of the top Eagle Ford shale (m). Adapted from Zumberge et al., 2012).

2.3 Materials and Methods

Samples were collected directly from producing well heads in the Eagle Ford area; a total of 10 samples were taken from 6 different lease areas. Samples for noble gas analysis were collected in 10mm diameter, refrigeration-grade copper tubes, which were connected using tygon tubing to a 2-stage pressure regulator attached directly to the wellhead. The regulator was used to step down the pressure from the wellstream to 1-2bar. The copper tubes were then flushed with the produced gas for 10 minutes to avoid air contamination, before being sealed with stainless

steel clamps (Weiss, 1968). In addition, samples for hydrocarbon gas geochemistry analysis were collected in industry-standard 300 cm^3 valve-sealed stainless-steel cylinders, which were flushed for 5 minutes to avoid air contamination. These were then shipped to GeoMark Research LTD in Lafayette, Louisiana, USA for bulk gas composition and C and H isotope analysis of major hydrocarbon species using standard procedures that are described in detail in Zumberge et al., 2012. Noble gas isotopic analysis was carried out in the Noble Laboratory at the University of Oxford following procedures outlined in section 1.4.2.

2.4 Results

2.4.1 Bulk gas composition and stable isotopes

Results are presented for samples from 10 wells within the Eagle Ford field, major gas species composition and stable isotope results are shown in Table 2.1. The produced gases consist primarily of methane (C_1), ranging from 67 - 92 mole %, with longer chain hydrocarbons making up most of the remainder: 3.6-15.8% ethane (C_2) and 0.5-9.6% propane (C_3). There is a large range of gas dryness from 2.7 to 22.9, where gas dryness is a measure of the ratio of heavier, 'wetter' gas species relative to methane, defined as $\frac{C_1}{C_2+C_3}$ (Bernard et al., 1976). Gas dryness is often interpreted to be an indicator of hydrocarbon maturity, as at higher temperatures or over longer time periods at elevated temperatures, longer-chain hydrocarbons will 'crack' into shorter chain molecules, increasing the relative proportion of short-chain molecules such as methane (Behar et al., 1997). Minor components include CO_2 (0.7-3.9%) and N_2 (0.07-0.42%). Stable carbon and hydrogen isotopes of methane show a large range from $\delta^{13}C_{C1}$ = -47.5 to -37.8‰ VPDB and δD_{C1} = -167 to -261‰ (VSMOW). $\delta^{13}C_{C1}$ and δD_{C1} are strongly correlated (R^2=0.96), and fall within the expected range for thermogenic hydrocarbons (Schoell, 1980; Clayton, 1991; Whiticar, 1994). Like gas dryness, $\delta^{13}C$ of methane is also often considered as an indicator of hydrocarbon maturity, as during hydrocarbon generation, bonds containing the lighter ^{12}C atoms have a higher propensity to crack. As a result, the petroleum compounds formed earlier in the generation process tend to contain a

higher proportion of the lighter ^{12}C isotope relative to the rare ^{13}C isotope, and thus have lower (more negative) $\delta^{13}C$ ratios. $\delta^{13}C$ of methane in the samples shows a broad positive correlation with gas dryness, although the relationship is not linear. This behaviour is consistent with petroleum generation models that predict slightly drier gases during the early stages of petroleum formation (Lorant et al., 1998). Carbon isotope ratios for the heavier hydrocarbon species are consistently higher than methane in every sample: $\delta^{13}C_{C2}$ = -33.5 to -17.39‰ and $\delta^{13}C_{C3}$ = -29.4 to -14.0‰. As much of the following discussion and interpretation centres on variations with respect to maturity, samples are labelled A through to F, going from lowest to highest maturity as interpreted from the carbon isotope ratio of methane. We consider C-isotopes to be the most reliable indicator of maturity in this system, due to being unaffected by phase partitioning between oil and gas, as gas dryness could be (Bernard and Horsfield, 2014). Other maturity indicators such as molecular biomarker ratios are not present in the higher-maturity gases in this system. Samples from wells within the same lease, for which maturity is approximately equal, are distinguished by number (A1, A2; B1, B2 etc.).

2.4.2 Noble gas isotopic analysis

Helium

Helium isotope ratios ($^3He/^4He$) ratios are reported relative to the atmospheric ratio (where air=1R_a), and show a range from 0.015-0.16R_a (Tables 2.3 and 2.2). $^4He/^{20}Ne$ ratios are >5000 for all samples, which by comparison with the atmospheric $^4He/^{20}Ne$ of 0.32 suggests that there is negligible atmospheric He contribution. The low $^3He/^4He$ ratios suggest that the majority of the helium is derived from crustal radiogenic production, for which typically $^3He/^4He$=0.02R_a (Ballentine and Burnard, 2002). However some samples show a small and variable contribution of mantle fluids, for which sub-continental lithospheric mantle $^3He/^4He$=6.1R_a (Gautheron and Moreira, 2002; Day et al., 2015). Using a simple 2-endmember mixing model, we can quantify mantle helium contributions to ^4He of between 0.14% and 2.57%. Helium isotope ratios appear to be dependent on geographic location, with all pairs

Sample	Composition (mole%)							$\delta^{13}C$ (‰VPDB)			δD (‰VSMOW)	
	C1	C2	C3	C4+	CO_2	N_2	Gas dryness	C1	C2	C3	C1	Well depth (m)
A1	78.1	12.6	5.1	2.7	1.2	0.3	4.4	-47.5	-32.1	-29.4	-261	2700
A2	77.8	12.6	5.3	2.7	1.3	0.3	4.3	-47.4	-32.2	-29.3	-260	2700
B1	67.4	15.8	9.6	3.9	2.1	1.0	2.7	-46.1	-33.5	-28.8	-241	3120
B2	73.7	13.9	6.7	3.4	2.0	0.4	3.6	-45.9	-32.5	-29.3	-237	3100
C1	75.7	12.3	4.8	4.7	2.2	0.2	4.4	-43.1	-27.1	-23.9	-199	3600
C2	75.9	n.d.	n.d.	n.d.	n.d.	n.d.	n.d.	-43.0	n.d.	n.d.	n.d.	3610
D1	80.3	11.2	4.0	3.8	0.7	0.1	5.3	-40.7	-24.6	-22.7	-181	2960
D2	79.6	10.4	3.8	5.1	0.8	0.3	5.6	-40.7	-24.6	-22.4	-179	2990
E1	83.1	8.9	2.0	2.5	3.4	0.2	7.6	-40.3	-23.6	-19.5	-184	3770
F1	91.8	3.6	0.4	0.2	3.9	0.1	22.9	-37.8	-17.4	-14.0	-167	3690

Table 2.1: Bulk gas composition and stable isotope data for Eagle Ford gases. Errors are ±0.1% for concentrations, and ±0.1‰ for isotope ratios.

of samples from the same lease having almost indistinguishable ^{3}He/^{4}He values. Previous work has shown the presence of mantle fluids to be strongly influenced by local structural geometry, with major faults seeming to increase the presence of mantle fluids (Hooker et al., 1985; Oxburgh et al., 1986). However, the spatial resolution of this sample set is not high enough to make detailed inferences about the distribution of mantle fluids in the wider area. The presence of mantle helium in these samples is strong evidence for open system behaviour of the Eagle Ford shale over geological time. Helium concentrations (^{4}He) range from 1.39 to 5.26 $\times$ 10^{-5} cm^{3}STPcm^{-3}, and show no appreciable correlation with ^{3}He/^{4}He (Fig. 2.2).

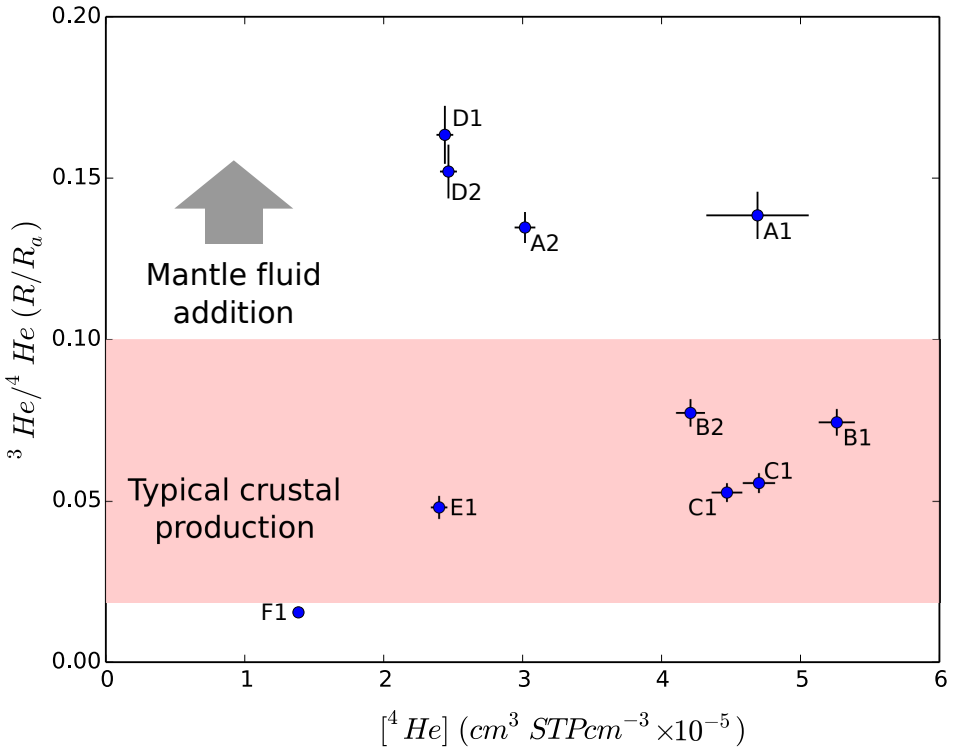

Figure 2.2: Total measured helium concentrations and isotope ratios for Eagle Ford gases. Typical crustal production ratios are around 0.02 (Ballentine and Burnard, 2002), and ratios over 0.1 can be likely attributed to mantle fluid contents. Sub-continental lithospheric mantle has a ^{3}He/^{4}He ratio of $\approx 6.1 R_a$ (Day et al., 2015).

Neon

Neon isotope ratios (^{20}Ne/^{22}Ne and ^{21}Ne/^{22}Ne) show an excess of the nucleogenically-produced ^{21}Ne and ^{22}Ne isotopes, with the trend following the empirically-derived

crustal neon production line (Kennedy et al., 1990). Although there is some scatter around this line, shown in Fig. 2.3, it is notable that previous noble gas studies of unconventional hydrocarbon systems also show a large dispersion in neon isotope ratios relative to this reference (Zhou et al., 2005; Wen et al., 2015b). It is possible that there is some variable effect of mass-dependent fractionation, unique to low-porosity unconventional systems, that results in these deviations. Neon concentrations (^{20}Ne) range from 8.7 to 55.6 $\times 10^{-10}$ cm^{3}STPcm^{-3} and are strongly dependent on maturity, with higher maturity samples having systematically lower Ne concentrations. This can be seen in the relationship of δ^{13}C and ^{20}Ne (Tables 2.1 and 2.3).

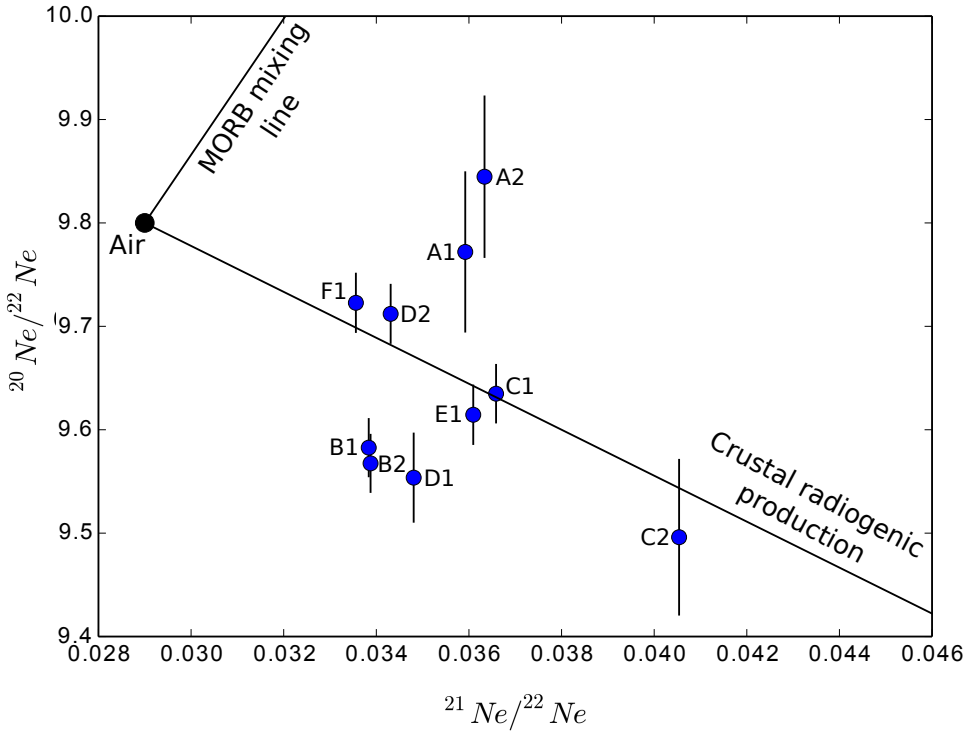

Figure 2.3: Neon isotope plot for the Eagle Ford gases. Typical crustal production ratios are taken from (Kennedy et al., 1990), and reflect an empirically observed correlation across a range of crustal fluids.

Argon

Argon isotope ratios (^{40}Ar/^{36}Ar) range from 342 to 561, all showing an excess of radiogenically-produced ^{40}Ar relative to the air value of 298.6 (Lee et al., 2006). Argon concentrations (^{36}Ar) range from 7.0 to 262 $\times 10^{-9}$ cm^{3}STPcm^{-3}, and like Ne concentrations, show a strong correlation with sample maturity as measured by δ^{13}C of methane (Fig. 2.4). Argon isotope ratios and concentrations are shown in Fig. 2.5. Whilst samples with the lowest total ^{40}Ar also tend to have low ^{40}Ar/^{36}Ar, the relationship is not clear at higher ^{40}Ar and cannot be explained solely by radiogenic production of ^{40}Ar. Oil-associated gases (either exsolved from oil during production or present as a gas cap in the reservoir (Stolper et al., 2017) (A, B), show a different trend to pure gas samples (C-F), with higher ^{40}Ar concentrations.

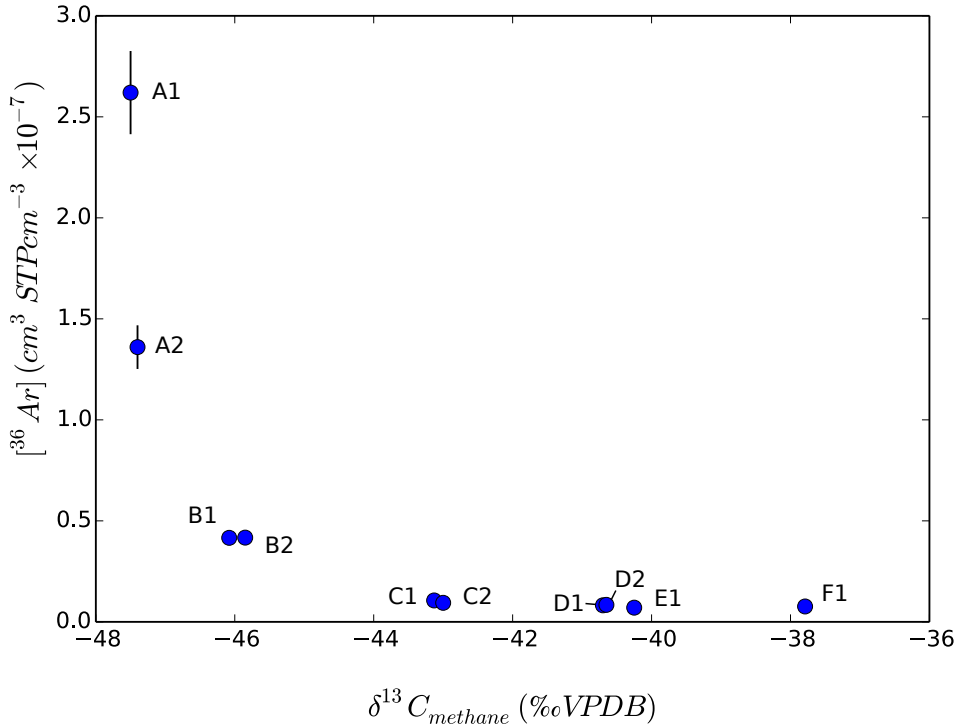

Figure 2.4: Plot illustrating the relationship between ^{36}Ar concentration and δ^{13}C of methane, which we consider to be our most reliable indicator of thermal maturity in this system.

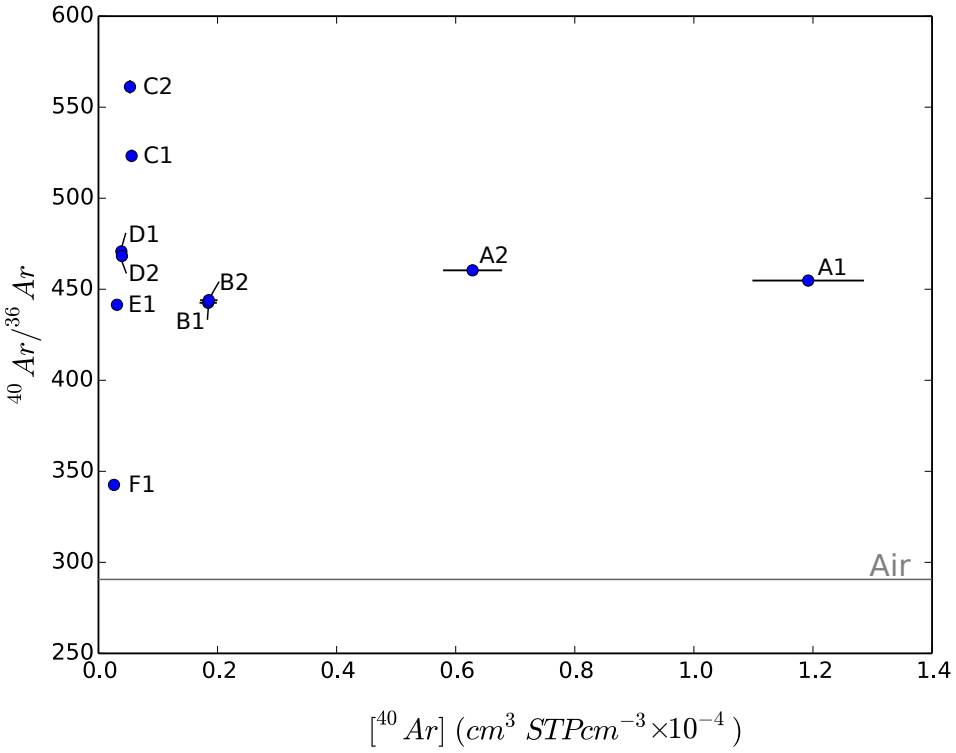

Figure 2.5: Argon concentrations and isotope ratios in the Eagle Ford gases. The isotopic ratio for air is 298.6 (Lee et al., 2006).

Krypton and xenon

Measured Kr and Xe isotope ratios are all indistinguishable from air, and are not discussed here (Torgersen and Kennedy, 1999). Krypton concentrations (^{84}Kr) range from 4.4 to 26.9 $\times10^{-10}$ cm^{3}STPcm^{-3}, and xenon concentrations (^{130}Xe) range from 1.4 to 7.5 $\times10^{-11}$ cm^{3}STPcm^{-3}. Like Ne and Ar concentrations, Kr and Xe show some correlation with sample maturity. However, samples A1 and A2, from the least mature site, both show appreciably lower Kr and Xe than some other samples, making the exact relationship with maturity unclear, and indicating that the heavy noble gases are not affected by maturity in the same way as Ne and Ar, likely due to their already high-content in the sediments themselves (Podosek et al., 1980; Podosek et al., 1981).

Sample	$^{3}He/^{4}He$	±2σ	$^{20}Ne/^{22}Ne$	±2σ	$^{21}Ne/^{22}Ne$	±2σ	$^{40}Ar/^{36}Ar$	±2σ
A1	0.138	0.007	9.77	0.08	0.0359	0.0001	454.8	2.9
A2	0.135	0.005	9.84	0.08	0.0363	0.0001	460.4	3.0
B1	0.074	0.004	9.58	0.03	0.0338	0.0001	442.6	2.8
B2	0.077	0.004	9.57	0.03	0.0339	0.0001	444.0	2.9
C1	0.053	0.003	9.63	0.03	0.0366	0.0001	523.2	3.4
C2	0.056	0.003	9.50	0.08	0.0405	0.0002	561.2	3.7
D1	0.163	0.009	9.55	0.04	0.0348	0.0001	470.8	3.1
D2	0.152	0.008	9.71	0.03	0.0343	0.0001	468.3	3.1
E1	0.048	0.004	9.61	0.03	0.0361	0.0001	441.5	2.9
F1	0.015	0.001	9.72	0.03	0.0336	0.0001	342.5	2.2

Table 2.2: Noble gas isotope ratios for Eagle Ford gases. $^{3}He/^{4}He$ ratios are reported in units of R/R_a, where R_a is the air ratio of 1.4×10^{-6} (Porcelli et al., 2002).

2.5 Discussion

2.5.1 Atmosphere-derived noble gases

The atmosphere-derived noble gases (ANG) are dominantly sourced from air (^{20}Ne, ^{36}Ar, ^{84}Kr, ^{130}Xe), and have no significant radiogenic production, primordial or cosmogenic sources (Ballentine et al., 2002; Prinzhofer, 2013; Byrne et al., 2017). These isotopes are introduced into hydrocarbon reservoirs by recharge of air-saturated water (ASW) (Aeschbach-Hertig et al., 2000; Kipfer et al., 2002), and its subsequent interaction with different hydrocarbon phases. Due to the variable solubility of the elements in different fluid phases, variations in the ratios between these isotopes ($^{20}Ne/^{36}Ar$, $^{84}Kr/^{36}Ar$, $^{130}Xe/^{36}Ar$) can be used to interpret the history of multi-component (i.e., water-gas-oil) interactions within a given hydrocarbon system (Bosch and Mazor, 1988; Zaikowski and Spangler, 1990; Ballentine et al., 1991; Ballentine et al., 1996; Barry et al., 2016).

The majority of Eagle Ford gases have $^{20}Ne/^{36}Ar$ values indistinguishable from the initial ASW (freshwater at $10^{o}C$) ratio of 0.14. This suggests quantitative partitioning of effectively 100% of the ANG's into the gas phase, in a system with a high gas-water volume ratio. However, the lower maturity oil-associated gases show fractionated $^{20}Ne/^{36}Ar$ of 0.017 to 0.10. We interpret this to represent partitioning between oil and gas phases, which is investigated further in section 2.5.5. $^{84}Kr/^{36}Ar$

Sample	^{20}Ne ($\times10^{-9}$)	±2σ	^{36}Ar ($\times10^{-9}$)	±2σ	^{84}Kr ($\times10^{-10}$)	±2σ	^{130}Xe ($\times10^{-11}$)	±2σ	^{4}He ($\times10^{-5}$)	±2σ	^{21}Ne* ($\times10^{-13}$)	±2σ	^{40}Ar* ($\times10^{-6}$)	±2σ
A1	4.54	0.36	262.10	20.59	20.14	1.58	4.96	0.39	4.69	0.37	32.56	2.56	41.75	3.28
A2	5.57	0.44	136.48	10.80	9.59	0.75	1.89	0.15	3.02	0.07	40.73	3.20	22.50	1.77
B1	4.28	0.34	41.65	3.30	26.52	2.09	7.41	0.58	5.26	0.13	24.46	1.92	6.12	0.48
B2	3.74	0.29	41.74	3.30	26.88	2.11	7.50	0.59	4.21	0.10	21.72	1.71	6.20	0.49
C1	2.20	0.17	10.63	0.84	6.15	0.48	1.77	0.14	4.47	0.11	18.40	1.45	2.42	0.19
C2	1.43	0.11	9.43	0.75	5.64	0.44	1.61	0.13	4.70	0.12	18.71	1.48	2.51	0.20
D1	1.17	0.09	8.19	0.65	5.13	0.40	1.46	0.11	2.44	0.06	7.98	0.63	1.43	0.11
D2	1.22	0.10	8.42	0.67	5.21	0.41	1.45	0.11	2.47	0.06	7.01	0.55	1.45	0.11
E1	1.12	0.09	7.03	0.56	4.43	0.35	1.38	0.11	2.40	0.06	8.93	0.70	1.03	0.08
F1	0.87	0.07	7.62	0.60	5.25	0.41	1.58	0.12	1.39	0.03	4.28	0.34	0.36	0.03

Table 2.3: Noble gas concentrations for Eagle Ford gases. Units are cm^3STPcm^{-3}, * indicates the concentration of the radiogenic component corrected for atmospheric content by comparing with non-radiogenically produced isotope.

ranges from 7.0 to 68.9 $\times 10^{-3}$ (ASW= 40×10^{-3}), and $^{130}Xe/^{36}Ar$ ranges from 1.39 to 20.7 $\times 10^{-4}$ (ASW=4.14×10^{-4}). $^{84}Kr/^{36}Ar$ and $^{130}Xe/^{36}Ar$ show a more equivocal relationship with maturity, again suggesting that the heavy noble gases are affected differently by maturity variations. All samples except those from the lowest maturity area (A1, A2) show significant excesses of Kr and Xe compared to ASW, whilst the A samples have depleted Kr and Xe. It is possible that due to their low maturity, there is still enough of an oil-phase present in samples A1 and A2 that partitioning of Kr and Xe into the oil phase has resulted in a residually depleted gas, although this is difficult to confirm. There also appears to be no clear relationship within the higher $^{84}Kr/^{36}Ar$ and $^{130}Xe/^{36}Ar$ samples.

2.5.2 Methane generation and noble gas dilution

The observation that ^{36}Ar concentrations vary by more than an order of magnitude over the range of sample maturities (Fig. 2.4) requires either drastically different hydrogeological regimes across the field, or a previously unrecognised process, innate to the hydrocarbon system, to strongly alter ANG concentrations.

We start with the simplifying assumption that the amount of ^{36}Ar delivered from groundwater into the Eagle Ford formation is approximately constant across the basin. This assumption is reasonable unless there is large-scale heterogeneity in the deep-basin groundwater movement over geological timescales. As the Eagle Ford Shale is low-permeability and relatively consistent across the basin, with no significant faulting across the area of interest (Robison, 1997), such heterogeneity would be highly unexpected. Under this assumption, the resultant concentrations in the hydrocarbon phase should be solely affected by the extent of hydrocarbon generation. The resulting reference model presented here shows that the generation of petroleum compounds and secondary cracking of those compounds will both increase the relative amount of hydrocarbon molecules compared to ^{36}Ar. This will effectively cause $[^{36}Ar]$ to be diluted as hydrocarbon generation and cracking proceeds, and can explain decreasing ^{36}Ar concentrations as a function of increasing maturity. A schematic illustration of this concept is given in Fig. 2.6. In order

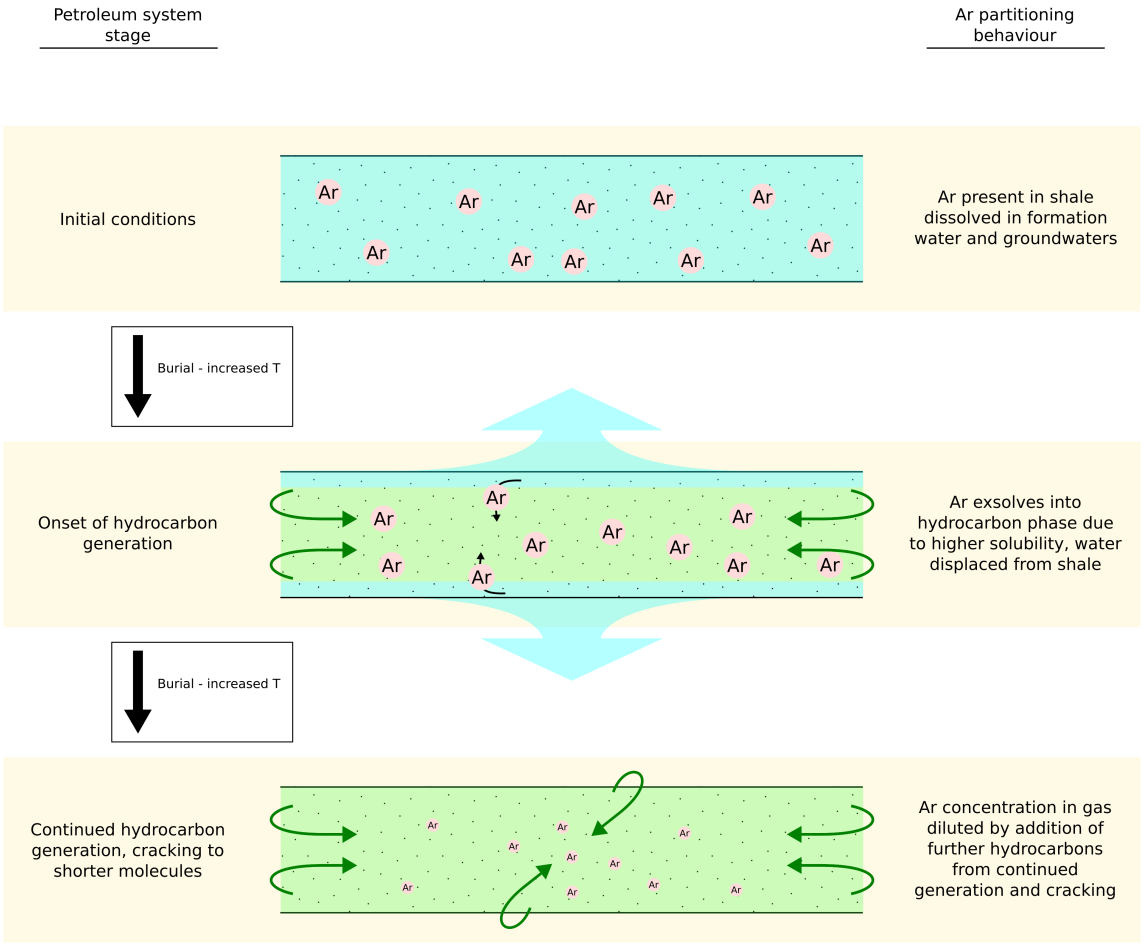

Figure 2.6: Schematic illustration of the Ar dilution model during hydrocarbon generation within the Eagle Ford shale. Argon is expected to follow methane during phase-partitioning in the subsurface, as they have similar solubilities at subsurface PT conditions (Ballentine et al., 1991). Closed system is illustrated in the final stage, whilst an open system would entail partial loss of hydrocarbon phase from the rock, along with equivalent amounts of Ar.

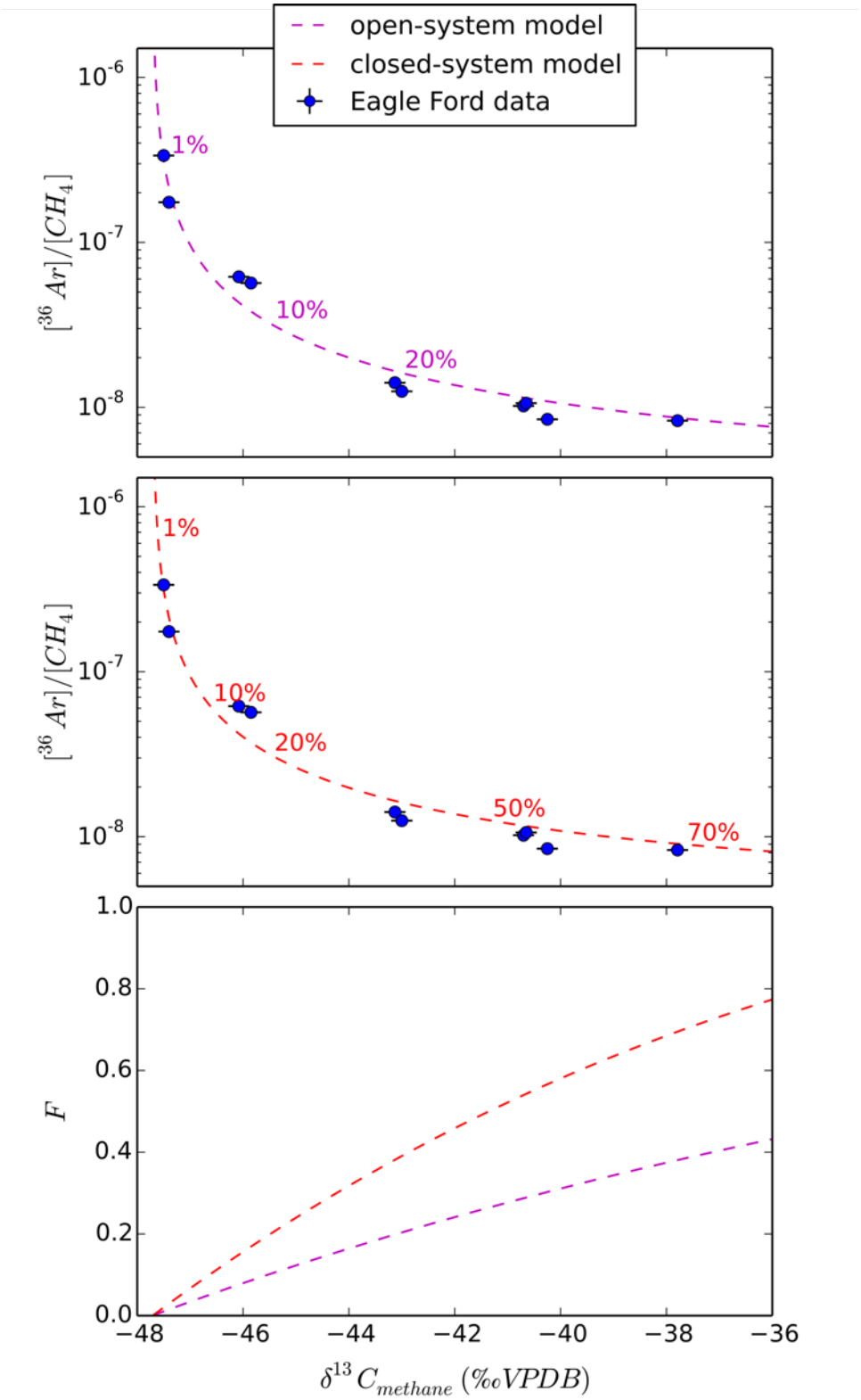

Figure 2.7: Results from Ar dilution model, for both open system and closed system calculations. The fraction of methane generated (F) is displayed as a percentage along the 2 curves. Lowermost plot displays the differing predictions for fractional methane generation for open and closed systems.

to eliminate the effects of solubility-dependent fractionation on this process, we normalise [^{36}Ar] to [CH4] in bulk gas, as both species have similar solubilities at subsurface conditions (Ballentine et al., 1991). Under the assumption that initial ^{36}Ar abundances were approximately uniform across the basin, the resultant [^{36}Ar] in the produced methane will be inversely proportional to the amount of methane produced, which can be written symbolically as follows:

$$\frac{[^{36}Ar]}{[CH_4]} \times F = c \tag{2.1}$$

Here [^{36}Ar] is the concentration of ^{36}Ar in the gas, [CH_4] is the concentration of methane in the gas, F is the amount of methane produced form the source-rock relative to the total potential production ($0 \leq F \leq 1$), and c is an arbitrary constant. We use this simple relationship to quantify the carbon-isotope fractionation associated with methane generation, the extent of methane generation within the basin, and the extent of gas loss from within the source rock.

In order to relate the extent of methane production (F) to our observable proxy for maturity, the δ^{13}C of the methane, we use a Rayleigh fractionation model (after Rooney et al., 1995). This model assumes that the product (methane) is continuously generated from an initial reservoir (kerogen) with a constant isotopic fractionation, and furthermore that the initial reservoir is homogenous and that the mechanism for methane generation is constant. Whilst methane generation in reality is a much more complex process than this, and kerogen is a complex mixture of different organic molecules, this approach has been shown to accurately reproduce observed C-isotope ratios in several case studies (see Rooney et al., 1995 for details). We consider two separate end-member scenarios. The first is a fully open-system case in which the generated methane instantaneously escapes from the source-rock, whereby the methane contained within the source rock has an isotopic composition equal to the methane being produced at that point in the generation process. The second is a fully closed-system model, in which no methane escapes from the source-rock, and the methane that is retained therefore has an isotopic composition equal to the bulk weighted average of the total produced methane that

has accumulated. These are referred to as open-system and closed-system models and designated by the subscripts 'o' and 'c' respectively.

For both cases, the δ^{13}C of methane is formulated by Rooney et al., 1995 as follows.

$$\delta^{13}C_o = \delta^{13}C_k + \epsilon(1 + ln(1 - F)) \tag{2.2}$$

$$\delta^{13}C_c = \delta^{13}C_k - \frac{\epsilon(1 - F)ln(1 - F)}{F} \tag{2.3}$$

Where $\delta^{13}C_o$, $\delta^{13}C_c$ are the carbon isotope ratios of methane generated in the open and closed-system models respectively, $\delta^{13}C_k$ is the initial carbon isotope ratio of the kerogen in the source-rock from which the hydrocarbons are being generated, ϵ is the fractionation factor that governs the isotopic fractionation between the parent kerogen and the generated methane, and F is the fraction of methane produced out of the total potential, again using subscripts 'o' and 'c' to distinguish between open and closed-system cases.

We rearrange equations 2.2 and 2.3 to isolate F.

$$F_o = 1 - exp\Big(\frac{\delta^{13}C_o - \delta^{13}C_k}{\epsilon} - 1\Big) \tag{2.4}$$

For the closed system we rearrange similarly, using the substitution $y = \frac{\delta^{13}C_c - \delta^{13}C_k}{\epsilon}$ for clarity.

$$F_c = 1 - exp\Big(\omega\Big(\frac{y}{exp(-y)}\Big) - y\Big) \tag{2.5}$$

Here $\omega(x)$ is the Lambert transcendental function (product log function).

By substituting our expressions for F_o or F_c into equation 2.1, we can directly relate the $\delta^{13}C$ of methane to the [^{36}Ar] in the produced gas, in both open and closed-system scenarios. However, we need to constrain $\delta^{13}C_k$ and ϵ, which are both assumed to be constants across the basin. The carbon isotope ratio of the kerogen in the Eagle Ford ($\delta^{13}C_k$) is well-constrained, as it has been directly measured in core sections, and although it shows some variation through the section, it averages

approximately $\delta^{13}C_k = -27‰$ (Eldrett et al., 2014). The fractionation factor for production of methane from kerogen for any given field is difficult to constrain geochemically, as reservoir conditions and timescales are challenging to recreate in laboratory conditions (Tang et al., 2005).

Using the above equations, alongside observed [^{36}Ar] and $\delta^{13}C$ data, we employ an inverse approach to estimate the ϵ parameter. For a given value of ϵ, we use the observed [^{36}Ar], $\delta^{13}C$, and [CH_4] from the 10 Eagle Ford samples to calculate 10 values of c using eq. 2.1, substituting in eq. 2.4 or 2.5 for the open and closed-systems respectively. Notably, if a perfect fit to the model were achieved, c would be constant across all data points. A goodness of fit for each trial value of ϵ can be taken from the relative variance (σ^2) in these calculated c values. Modeling results yield a best fit to the data with $\epsilon = -20.71‰$ ($\sigma^2 = 4.1\%$) for the open-system, and $\epsilon = -20.72‰$ ($\sigma^2 = 4.6\%$) for the closed-system. This is within the range of expected values for ϵ reported in previous literature, of -17 to -25‰ (Tang et al., 2000), and effectively indistinguishable for the 2 cases, suggesting that the calculated value for ϵ is relatively insensitive to the extent of the system being open or closed. Model curves for both open and closed-system cases are shown in Fig. 2.7 alongside the measured data, and both produce a close fit to the data.

The open and closed-system cases do differ in their predictions of the amount of methane generated across the field. The F-values are plotted as a percentage of total potential methane generation along the model curves in Fig. 2.7, and show that the predicted methane generation is consistently higher in the closed system model. We use these two end-member cases to place constraints on the maximum and minimum volumes of methane generated across the field. For the least mature sample (A1), the open-system predicts 1% of total methane generated, compared to 2% for the closed system. For the most mature sample (F1), the range is 38-70% of total methane generated. These results are shown in table 2.4.

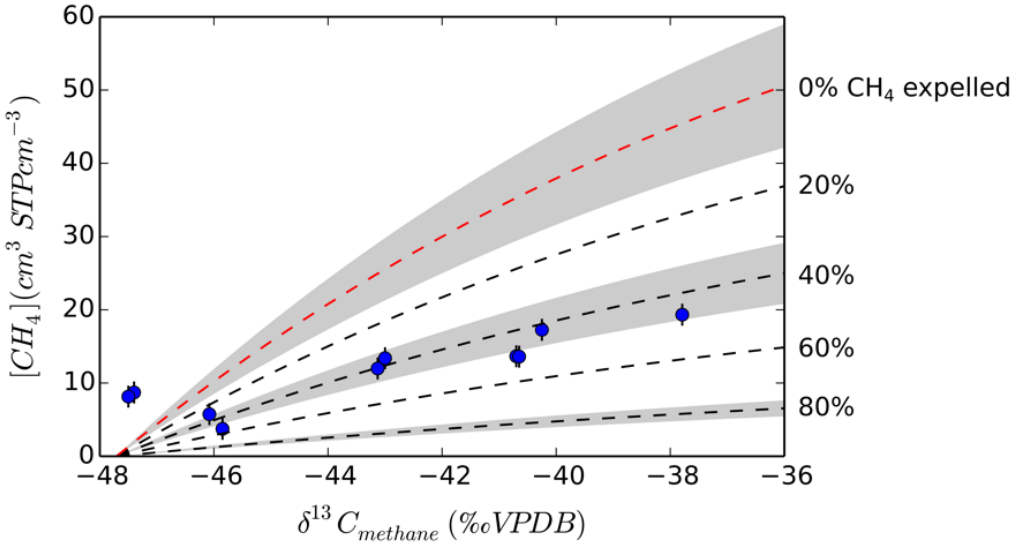

Figure 2.8: Predicted evolution of gas in-place within the Eagle Ford Shale alongside data calculated from gas compositions and reservoir PT conditions. Model evolution lines for varying amounts of system openness are displayed according to the percentage of CH_4 expelled from the shale. Dashed lines represent the midpoint of the estimates derived from the upper and lower bounds for parameters discussed in section 2.5.3, whilst shaded areas represent the areas encompassed by the upper and lower bounds (shown for openness of 0%, 40%, and 80%). Methane concentrations are per volume of rock.

2.5.3 Estimation of methane expulsion efficiency

The values calculated for the fraction of kerogen converted to methane (F) in the previous section can be converted into absolute volumes of generated methane if the generative potential of the kerogen and the organic carbon concentration is known. The total amount of methane generated in the system is calculated as follows:

$$[CH_4]_{gen} = \frac{F \times G \times TOC \times \rho_s \times V_M}{M_{CH4}} \tag{2.6}$$

Here F is the fraction of kerogen converted to methane, G is the generative potential of methane, and TOC is the weight% of organic carbon in the shale. The shale density (ρ_s), the standard molar volume (V_M) and the molar mass of methane (M_{CH4}) are used to convert the units from mass of methane per mass of rock to volume of methane per volume of rock.

G can be estimated from RockEval data, using $G = \frac{100S_2}{TOC}$ (Tissot and Welte,

1984). Edman and Pitman, 2010, publish RockEval data for the Eagle Ford, and G can be estimated at approximately $300 - 350mg$ of CH_4 per g of kerogen, in close agreement with pyrolysis experiments on other type II shales (Behar et al., 1995). TOC in the Eagle Ford is variable throughout the basin, but across the area of this study is estimated to be 5-6 wt% (Tian et al., 2013). Using these values alongside our calculated F-value curves from section 2.5.2 allows us to predict the absolute volume of methane generated with respect to $\delta^{13}C$ for both open and closed systems. This volume is converted into methane in-place volumes for a range of system 'openness' (expulsion efficiency) by interpolating between F-value curves for the open and closed system and then multiplying again by openness in order to reflect the expulsion of petroleum from the system under such conditions.

$$[CH_4]_{in-place} = ([CH_4]_{gen}^{closed} - \Theta([CH_4]_{gen}^{closed} - [CH_4]_{gen}^{open})) \times (1 - \Theta) \qquad (2.7)$$

Here Θ is system openness ($0 \leq \Theta \leq 1$). It can be seen for that a perfectly closed system (Θ=0), the amount of methane in-place is equal to that generated under a closed system, and for a perfectly open system (Θ=1), the amount of methane in-place is zero.

Using the known variability in the above-described parameters, we generate upper and lower-limit curves for $[CH_4]_{in-place}$ as a function of $\delta^{13}C$ for a range of different 'system openness'. The generated curves are then compared with in-place estimates derived empirically by converting the bulk gas composition to reservoir pressure-temperature conditions. The comparison is shown in Fig. 2.8. Due to the convergence at low maturity $\delta^{13}C$ values it is difficult to distinguish between different levels of system openness, but for the higher maturity samples the predicted vs. observed gas in-place is consistent with approximately 20-40% openness in the lower generation limit, and 40-60% in the upper generation limit. This would correspond to 20-40% of methane expelled in the lower limit scenario, and 40-60% in the upper limit scenario. Previous estimates of this figure using traditional gas-in-place estimates and hydrocarbon generation models are on the higher end of

this range, with Cooles et al., 1986 suggesting a general range of 60-90% expulsion, Ungerer, 1990 proposing >50% for mature source-rocks, and more recently Jarvie et al., 2007 calculating a range of 50-70% for the Barnett Shale.

	F		Θ		$[CH_4]_{in\text{-}place}$	$[CH_4]_{expelled}$ (cm^3STPcm^{-3})	
Sample	open	closed	min	max	(cm^3STPcm^{-3})	min	max
A1	0.01	0.02	n.a.	n.a.	8.15	-	-
A2	0.02	0.03	n.a.	n.a.	8.71	-	-
B1	0.08	0.15	0.21	0.38	5.74	1.55	3.52
B2	0.09	0.17	0.47	0.59	3.74	3.34	5.42
C1	0.20	0.38	0.32	0.47	11.99	5.62	10.58
C2	0.20	0.39	0.28	0.43	13.38	5.09	10.23
D1	0.29	0.54	0.42	0.55	13.66	9.95	16.87
D2	0.29	0.54	0.43	0.56	13.60	10.08	17.03
E1	0.30	0.57	0.34	0.48	17.26	8.75	16.19
F1	0.38	0.70	0.38	0.52	19.33	11.98	21.15

Table 2.4: Model parameter results for extent of methane generation (F) and system openness (Θ) discussed in sections 2.5.2 and 2.5.3 respectively. Values for $[CH_4]$ in-place within the reservoir (per rock volume), and model estimates for CH_4 expelled, both per rock volume, and total expelled from the shale by area. Model predictions for samples A1 and A2 are not presented as they fall outside the predicted model envelope (see Fig. 2.8).

2.5.4 Radiogenic noble gases

Radiogenically-produced noble gas isotopes (e.g. ^{4}He, ^{21}Ne, ^{40}Ar) accumulate in the subsurface over time, as daughter products of naturally occurring radioactive elements. The laws governing rates of radioactive decay are well-understood, and production rates can be calculated as a function of the concentrations of the relevant parent isotopes in the surrounding rock. For example, ^{4}He production is dominated by the α-decay of ^{235}U, ^{238}U and ^{232}Th, and the production rate can be calculated using the following equation, after Craig and Lupton, 1976:

$$J(^4He) = 0.2355 \times 10^{-6} \times [U](1 + 0.123(\frac{[Th]}{[U]} - 4)) \tag{2.8}$$

Here J(^{4}He) is the production rate of ^{4}He in units of 10^{-6}cm^{3}STPg^{-1}yr^{-1}, and concentrations of U and Th are in ppm. Analogous equations for the production of other major radiogenic noble gas species can be found in Ballentine and Burnard, 2002. The expected concentration of ^{4}He to be produced in-situ can then be calculated using the following equation, after Torgersen, 1980:

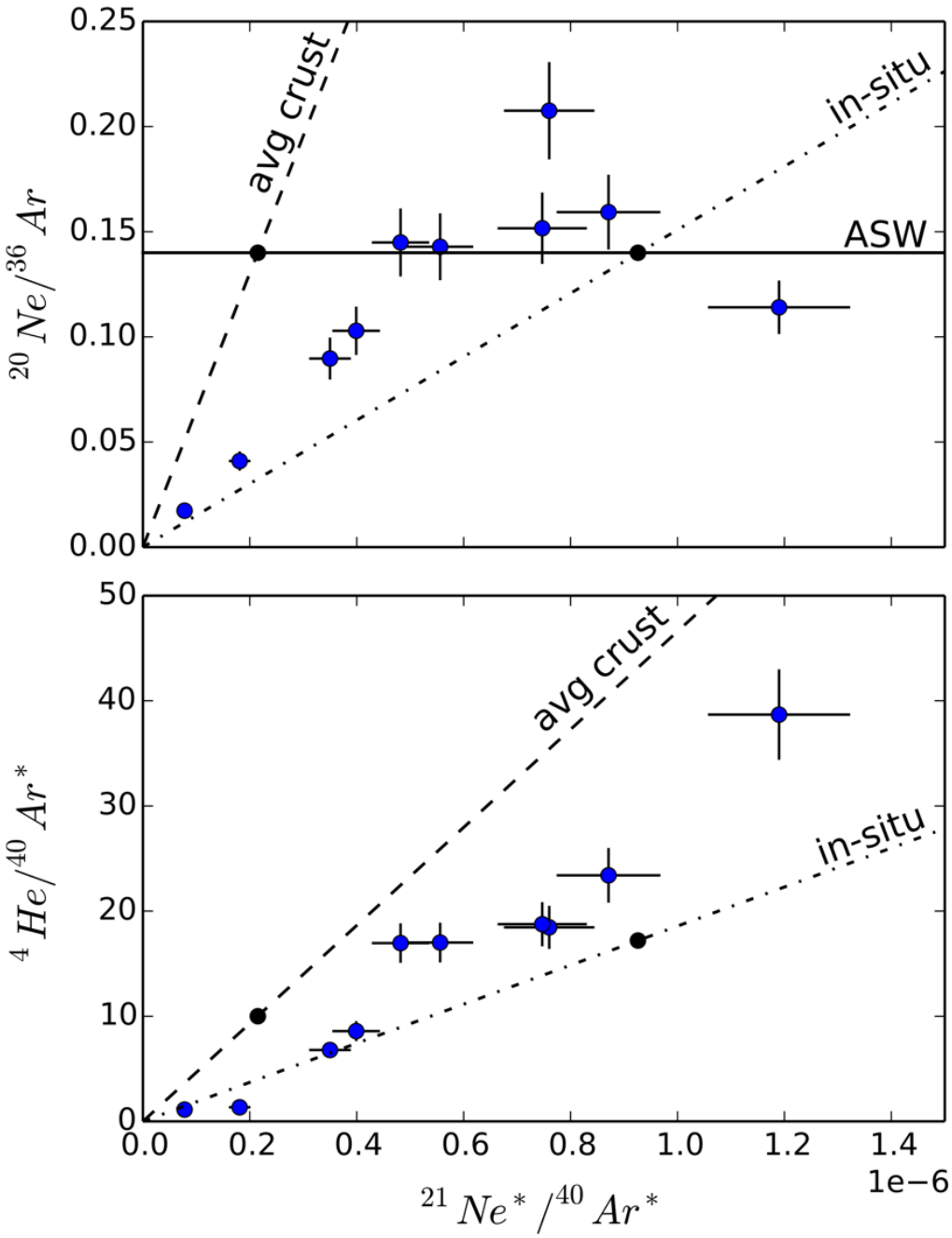

Figure 2.9: Radiogenic isotope ratios in the Eagle Ford gases. Black points indicate the calculated production ratios for typical crust and within the Eagle Ford shale, and solubility-dependent fractionation lines are drawn through the origin, assuming that He and Ne have approximately equal solubility under reservoir conditions. Dashed line indicates fractionation from average crust production ratios, and dot-dashed line is that calculated for Eagle Ford in-situ production.

$$[^4He]_{in-situ} = \frac{J(^4He) \times \rho t \Lambda R(1-\phi)}{\phi} \tag{2.9}$$

Here ρ is the rock density in gcm^{-3}, t is time in years, ϕ is porosity, and Λ is the release efficiency from the mineral grains into the surrounding pore-space ($0 \leq \Lambda \leq 1$ and $\Lambda \approx 1$ over geological timescales (Ballentine and Burnard, 2002)). R is the expansion coefficient from reservoir conditions to atmospheric conditions, needed to account for the dilution of the produced ^{4}He by pressurized CH_4 in the pore-space ($R = \frac{p_{res}T_{atm}}{p_{atm}T_{res}}$).

The expected ^{4}He concentrations in the Eagle Ford can be calculated using an average porosity of 9% (Jennings and Antia, 2013), average rock density of $2.2\mathrm{gcm}^{-3}$, U and Th concentrations of 4ppm and 6ppm respectively (Tinnin and Darmaoen, 2016), and a time of 95Myr since the deposition of the Eagle Ford. The expected ^{4}He concentration ranges from 0.95-1.2$\times 10^{-6}\mathrm{cm}^3\mathrm{STPcm}^{-3}$, an order of magnitude lower than the measured values of 1.4-5.3$\times 10^{-5}\mathrm{cm}^3\mathrm{STPcm}^{-3}$ (Table 2.3). The measured excess of ^{4}He must have been introduced from surrounding rocks, likely exsolving from groundwaters into the gas phase due to the relative insolubility of helium. This suggests there must be an external source of groundwater interaction within the Eagle Ford, despite its low permeability and porosity.

The fact that ^{4}He is so abundant in the samples compared to atmospheric noble gas species indicates that it is nearly 100% radiogenic, whereas the explicit radiogenic/nucleogenic component for Ar and Ne (^{40}Ar* or ^{21}Ne*) must be corrected for atmospheric contributions. This is done by calculating the atmospheric contribution of the isotope in question by using a purely atmospheric produced isotope (^{36}Ar or ^{20}Ne) and the atmospheric ratio. This can then be subtracted from the total concentration to give the pure radiogenic component as follows:

$$[^{40}Ar] = [^{40}Ar] * + [^{40}Ar]_{atm} \tag{2.10}$$

$$[^{40}Ar]_{atm} = [^{36}Ar] \times \left(\frac{^{40}Ar}{^{36}Ar}\right)_{air} \tag{2.11}$$

$$[^{40}Ar]* = [^{40}Ar] - [^{36}Ar] \times \left(\frac{^{40}Ar}{^{36}Ar}\right)_{air} \quad (2.12)$$

As the concentrations of the parent isotopes are heterogeneously distributed within the crust, this can be used to distinguish in-situ radiogenic production from that introduced by fluid migration. Fig. 2.9 shows a strong correlation between ^{4}He/^{40}Ar* and ^{21}Ne*/^{40}Ar*, which is consistent with solubility-dependent fractionation. Predicted solubility-dependent fractionation lines are also shown for in-situ radiogenic production (calculated from U, Th, K, O, and Mg concentrations, Tinnin and Darmaoen, 2016) and average crustal production ratios. In-situ ^{4}He/^{40}Ar* and ^{21}Ne*/^{40}Ar* production ratios are calculated as 17.2 and 9.26×10^{-7} respectively, compared to 10.0 and 2.15×10^{-7} for average crust (Leya and Wieler, 1999; Ballentine and Burnard, 2002). Fractionation lines plot as near straight lines due to the fact that He and Ne have similar Henry's constants in subsurface conditions (Fernández-Prini et al., 2003). Many of the Eagle Ford samples do not plot close to the in-situ production line, with the average crustal production line providing a better fit, especially for the more highly fractionated, higher maturity samples. This is strong evidence for the influx of externally produced radiogenic isotopes being introduced into the gas phase from groundwater in adjacent sediments. It is clear from these relationships that the Eagle Ford is exhibiting at least partially open system behaviour in a geochemical sense.

2.5.5 Solubility-dependent partitioning models

Noble gas partitioning between different fluid phases (water, oil, gas) in crustal systems follows Henry-law solubility to close approximation, even at high temperatures (Crovetto et al., 1982). Henry's constants are well constrained for water and oil across a range of temperatures, salinities, and API gravities (Smith and Kennedy, 1983; Ballentine et al., 2002). Due to their differing solubilities in water and oil, the noble gases have different affinities for water, oil, or gas phases when they contact another phase. Amongst the atmospherically-derived noble gases, ^{20}Ne is the least soluble in both oil and water, with solubility increasing with atomic number up to

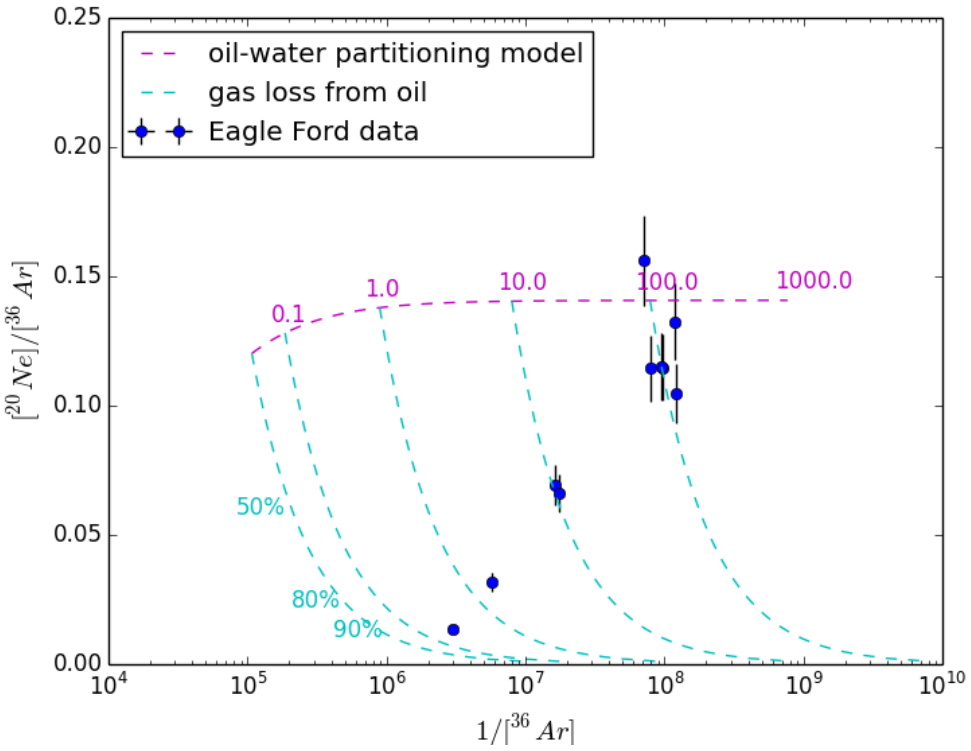

Figure 2.10: Predicted $^{20}Ne/^{36}Ar$ and $[^{36}Ar]$ evolution lines for solubility-dependent partitioning models, alongside measured data from the Eagle Ford gases. Numbers along oil-water partitioning line signify V_o/V_w and percentages along cyan line indicate the percentage of argon lost from the system.

xenon (Kharaka and Specht, 1988; Fernández-Prini et al., 2003). Fractionation of ANG's in petroleum systems is often attributed to solubility-dependent partitioning between different fluid phases (i.e., water, oil and gas). Under the assumption that all the ANG's are initially delivered into the subsurface dissolved in ASW, which has a well-defined composition, it is possible to reconstruct the phase-partitioning history of a petroleum system by looking at the ANG composition of a single phase (Zartman et al., 1961; Bosch and Mazor, 1988; Zaikowski and Spangler, 1990; Ballentine et al., 1991; Ballentine et al., 1996).

A number of different models describe water-gas, water-oil, and oil-gas partitioning in different reservoir geometries for conventional petroleum systems (see Barry et al., 2016 for a comprehensive review). In an unconventional source rock-reservoir, we predict that a simple closed-system water-oil partitioning model is most

appropriate, as the porous volume of the shale will initially be filled with ASW, which will interact with an oil phase - formed in the first stages of hydrocarbon generation. As hydrocarbon generation continues, the ratio of oil to water in the system (V_o/V_w) will increase, and the ANG partitioning and concentrations will evolve.

Upon the initial generation of an oil phase ($V_o/V_w \approx 0$), argon will preferentially partition from the ASW into the oil phase relative to neon, and the oil phase will consequently have a $^{20}Ne/^{36}Ar$ lower than the ASW ratio. As oil generation continues and V_o/V_w increases, more of the noble gases will partition into the oil phase and the $^{20}Ne/^{36}Ar$ of the oil phase will increase towards the ASW ratio. When V_o/V_w becomes large, effectively 100% of the noble gases will be partitioned into the oil phase, and the $^{20}Ne/^{36}Ar$ of the oil phase will be equal to that of the initial ASW. Concentrations of ^{20}Ne and ^{36}Ar in the oil phase will consistently decrease with increasing V_o/V_w. We can use the following equation to describe the relationship between both $^{20}Ne/^{36}Ar$ and $[^{36}Ar]$ and V_o/V_w.

$$\frac{V_o}{V_w} = \frac{C^i_{asw}}{C^i_o} - \frac{K^i_o}{K^i_w} \tag{2.13}$$

Where V_o and V_w are the volumes of oil and water respectively, C^i_{asw} and C^i_o represent the concentrations of noble gas species i in the oil phase and the initial air-saturated water, and K^i_o and K^i_w are the Henry's constants of noble gas species i in oil and water. Henry's constants are temperature-dependent and calculated after Fernández-Prini et al., 2003. ^{36}Ar concentrations can be calculated directly using eq. 2.13, and $^{20}Ne/^{36}Ar$ ratios are simply calculated by comparing the results from eq. 2.13 for both ^{20}Ne and ^{36}Ar.

Fig. 2.10 shows the modelled evolution of $^{20}Ne/^{36}Ar$ and $1/[^{36}Ar]$ with respect to V_o/V_w in the hydrocarbon phase for Eagle Ford pressure-temperature conditions, alongside data measured in the Eagle Ford samples. The mature gas samples are consistent with this model, having $^{20}Ne/^{36}Ar$ that is effectively indistinguishable from ASW, and concentrations consistent with high V_o/V_w of 100-300. However, these samples are dry gas rather than oil. In a closed system, the complete cracking of oil to gas would not affect $^{20}Ne/^{36}Ar$ of the hydrocarbon phase, but would decrease

concentrations as the hydrocarbon phase expanded; this is effectively equivalent to an apparent increase in V_o/V_w as secondary cracking progresses. However, the oil-water partitioning model clearly does not account for the extent of fractionation observed in the oil-associated gas samples.

The highly fractionated $^{20}Ne/^{36}Ar$ exhibited in the lower-maturity samples could be explained by a solubility controlled open-system Rayleigh-fractionation partitioning model between oil and gas phases. Conceptually, this describes the formation and escape of gas bubbles from the oil phase, either because of sufficient cracking of oil compounds to form a free gas phase, or gaseous hydrocarbon compounds coming out of solution in the oil phase due to changes in pressure-temperature conditions. This could happen as a result of geological processes or production effects. The Rayleigh fractionation equation describing open-system gas loss is:

$$(\frac{^{20}Ne}{^{36}Ar}) = (\frac{^{20}Ne}{^{36}Ar})_0 \times f^{(\alpha-1)} \tag{2.14}$$

Where ($^{20}Ne/^{36}Ar$) is the ratio in the oil phase, ($^{20}Ne/^{36}Ar$)0 is the initial ratio in the oil phase prior to gas loss, f is the fraction of ^{36}Ar remaining in the oil phase, and α is the fractionation factor (the ratio of the Henry's constants for Ne and Ar in oil). ^{20}Ne The cyan lines on Fig. 2.10 show the predicted evolution of the $^{20}Ne/^{36}Ar$ in the oil phase during open-system gas-oil partitioning. It can be seen that this process can account for the fractionation seen, if 90% of the argon initially present has been lost from the system.

The applied models are able to qualitatively replicate the observed patterns of [^{36}Ar] and $^{20}Ne/^{36}Ar$ observed in the Eagle Ford gas, but are likely too simplistic to represent a quantitative description of real processes. Our assumption of a simple closed system with a constant and conserved amount of ^{36}Ar present is inconsistent with observed radiogenic isotope patterns (section 2.5.4) that show the influx of external groundwater, as well as the predictions from section 2.5.3 on system openness. The open-system oil-gas partitioning required to explain the fractionated $^{20}Ne/^{36}Ar$ ratios observed in the oil-associated gases further requires deviation from this closed system. Furthermore, the processes controlling oil-gas

partitioning during hydrocarbon cracking and expulsion are likely to be more complex than the simple time-independent system we have presented using a single partitioning parameter. These noble gas partitioning models were developed to describe conventional systems, where hydrocarbons and water are in well-defined separate phases in porous reservoirs, and traps and seals provide a relatively stable closed system (Bosch and Mazor, 1988; Zaikowski and Spangler, 1990; Ballentine et al., 1991; Ballentine et al., 1996; Barry et al., 2016). We suggest that the low-porosity, more complex phase behaviour, and extensive expulsion and migration make these models difficult to apply directly into unconventional systems.

2.6 Conclusion

We present high precision noble gas (He, Ne, Ar, Kr, Xe) isotope and abundance data for 10 natural gas samples produced from the unconventional Eagle Ford shale oil and gas field. By combining these measurements with traditional bulk gas composition and stable isotope data we are able to fully investigate how the noble gas signature changes over the range of different gas compositions produced from the field. This work builds on the relatively few previous noble gas studies to advance our understanding of the physical behaviour of fluids in organic-rich shales and unconventional hydrocarbon systems (Hunt et al., 2012; Darrah et al., 2014; Darrah et al., 2015; Wen et al., 2015b; Györe et al., 2017; Cao et al., 2018). The samples span a wide range of thermal maturities, as is evident from the bulk fluid composition ranging from oil-associated gas to dry non-associated gas, and the δ^{13}C of the hydrocarbon compounds have a broad range across the sample suite. The noble gas content of the samples is dominantly radiogenic, with high concentrations of ^{4}He and high ^{40}Ar/^{36}Ar ratios, and very small amounts of putative mantle helium present in some samples.

The most striking feature in the measured samples is the large range in ^{36}Ar concentrations, which vary over several orders of magnitude, and are strongly correlated with indicators of gas maturity such as δ^{13}C. These signatures are

explained using a combination of a Rayleigh-fractionation model for methane-generation with $[^{36}Ar]/[CH_4]$ ratios to constrain hydrocarbon generation parameters, including the C-isotope fractionation factor (ϵ = -20.7‰), and the relative quantities of methane generated across the basin. This approach allows us to determine these crucial parameters using empirical data measured in gas samples produced directly from the reservoir, with the inert behaviour of the noble gases ensuring it is unaffected by extraneous chemical reactions. By comparison with measurements of methane in-place within the source rock, we use this model to constrain the extent of system openness. This allows us to quantify how much methane has been expelled from the source rock (expulsion efficiency), which we estimate to be approximately 40% for this system. This value is similar to model estimates generated for other source-rocks (Cooles et al., 1986; Jarvie et al., 2007), but the parameters controlling any noble gas variations between systems will require further investigation.

Concentrations of radiogenic ^4He are in excess of those that could be produced in-situ over the age of the strata, thus requiring external input from surrounding formations into the shale. Radiogenic $^4He/^{40}Ar^*$ and $^{21}Ne^*/^{40}Ar^*$ reveal significant exchange between the hydrocarbons within the shale and external groundwaters over geological timescales, despite their low porosity and permeability.

Combining the results from both atmospheric and radiogenic noble gas isotope systems, we conclude that the Eagle Ford shale has both expelled significant volumes of hydrocarbons and also acquired radiogenic noble gases from external groundwater. The ability to empirically constrain hydrocarbon volumes expelled may provide significant utility in the construction of basin models designed to understand the evolution of petroleum systems, specifically with regard to primary migration out of the source-rock (Ungerer, 1990). The proliferation of unconventional petroleum exploitation is subject to well-documented environmental concerns over natural gas escape and contamination of the surrounding environment, especially drinking water aquifers. Characterisation of the noble gas signature of these deep shale gases is crucial for the development of techniques designed to identify fugitive gas contamination in these systems (Darrah et al., 2014; Wen et al., 2017). As suggested

by Györe et al., 2017, high concentrations of radiogenic ^{4}He may provide evidence to distinguish between younger biogenic gas and older shale gas migrating from depth. Sediment packages similar to the Eagle Ford are proposed to act as seals for carbon or nuclear waste storage over geological time (Neuzil, 2013; Hendry et al., 2015). Our data show that they are permeable to noble gases at least over million-year timescales, although on the timescales required for sequestration this may differ, and it is possible that the internal generation of hydrocarbons has affected their integrity during burial and thermal maturation (Romero-Sarmiento et al., 2013).

3

Tracing fluid migration in the East Texas Basin

Contents

Abstract

The migration of hydrocarbons from source-rock to reservoir represents one of the critical stages of petroleum system evolution, but is challenging to study geochemically and thus remains poorly understood. Noble gas isotopes are widely

used as tracers in a variety of subsurface fluid systems, and due to their inert nature potentially provide a unique geochemical tool for understanding the effects of hydrocarbon migration. The recent proliferation of unconventional hydrocarbon production (i.e., directly from source-rocks), enables us to analyse fluids from these strata for the first time. Here we present new noble gas isotope and abundance data from 27 natural gas wells within the Haynesville basin, including (n=8) from the unconventional Haynesville source-rock. In addition, we report data from samples derived from the overlying conventional reservoirs within Cotton Valley (n=5), Travis Peak (n=9), and James Lime (n=5). Samples consist primarily of methane (>70%), with small contributions from longer chain hydrocarbons, and other gases such as CO_2 and N_2. Noble gas abundances for both atmosphere-derived and radiogenic isotopes are significantly higher in conventional reservoirs, clearly reflecting the effects of the migration process. We present a model that can be used to constrain the volumes of rock and groundwater encountered by the conventional gas accumulation. Specifically we observe progressive incorporation of mantle-sourced ^{3}He and radiogenic ^{4}He and ^{40}Ar with increasing migration distance from the source-rock. This results in a counterintuitive distribution of ^{3}He/^{4}He values, with the greatest contributions of mantle He observed in the shallowest reservoirs. We interpret this to be due to mixing between a pristine source-rock signature and an endmember characterised by elevated ^{3}He/^{4}He and ^{40}Ar/^{36}Ar, likely representative of mantle-enriched groundwater circulating in the wider hydrogeological system of the basin. In order to ascertain the processes controlling the introduction of these external noble gases into the impermeable source-rock, we model the flux of He across the basin using a finite-difference approximation of the advection-dispersion-reaction equation. We find that whilst the Haynesville source-rock is relatively impermeable to groundwater advection, groundwater flow in the overlying sandstones can transport mantle ^{3}He and radiogenic ^{4}He. Vertical diffusion from the adjacent strata can then introduce the external signatures into the source-rock.

3.1 Introduction

In petroleum systems hydrocarbons are generated within low-permeability organic-rich shales (source-rocks), before being expelled into surrounding strata and migrating into a high-permeability reservoir (Magoon and Dow, 1994). Unconventional hydrocarbon production exploits the fact that significant volumes of generated oil and gas can be retained within the source-rocks, however, the degree to which impermeable rocks can act as reservoirs and conduits for subsurface fluid flow is not well constrained.

The recent proliferation of unconventional hydrocarbon production utilises advanced techniques such as directional drilling and hydraulic fracturing (Curtis, 2002). The environmental impact of these activities has been the subject of much public concern and academic research (Rivard et al., 2014; Vengosh et al., 2014). Noble gas isotopes have been used as tracers to study the effects of unconventional production on surrounding groundwaters (Darrah et al., 2014; Barry et al., 2018b), although the effect of migration on noble gas isotope signatures is not well understood (Prinzhofer, 2013; Byrne et al., 2017).

In this study, we analyse a suite of produced natural gases from the East Texas Basin. This area is an ideal natural laboratory for studying the effects of migration on geochemical tracers due to the coexistence of unconventional production from the Haynesville source-rock, and related production from the overlying conventional reservoirs (Mancini et al., 2008; Hammes et al., 2011). By comparing the migrated hydrocarbons in the conventional reservoirs with those retained in-situ within the Haynesville, we are able to directly observe how the noble gas isotopic signature is incorporated and modified during migration, and the interaction of the petroleum system with groundwater and mantle fluids within the basin.

The recent publication of several papers reporting noble gases within unconventional reservoirs have shown that the concentrations observed cannot be explained simply by closed-system evolution of the source-rock, and in many cases, require external input of noble gas isotopes from the surrounding strata (Hunt et al., 2012;

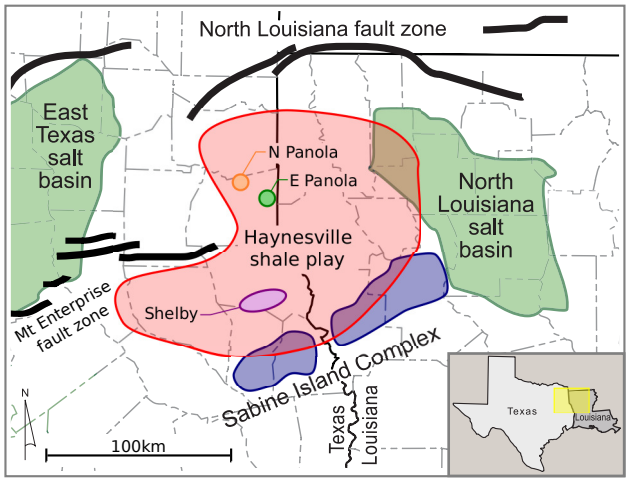

Figure 3.1: Map of study area, showing approximate locations of sampled areas. Sabine Island complex is a basement uplift feature, that would have been an emergent island chain during the deposition of much of the relevant stratigraphy, and as such is a key control on the structure of the basin. Adapted from Hammes et al., 2011.

Wen et al., 2015b; Györe et al., 2017; Byrne et al., 2018). This raises the question of what processes are responsible for delivering these external noble gas signatures into the source-rocks, and what consequences that has for the transport of fluids and volatiles within the subsurface in a wider sense.

3.2 Geological background

The Haynesville Shale was deposited in a restricted part of the wider East Texas Basin, USA, bounded to the north by continental North America, and to the south by the then-emergent Sabine Island complex that forms part of the wider Sabine Uplift basement high. The Haynesville is Upper Jurassic in age (156-151Ma) and is overlain by the Bossier Shale. For the purposes of unconventional production, the Haynesville-Bossier is often considered a single unit, referred to here within as the Haynesville (Hammes and Frébourg, 2012). Overlying the Haynesville is the Cotton Valley group sandstones, which represent a flux of terrigenous sediment from the Northern continent, extending southwards across the basin. The Cotton Valley extends from the Upper Jurassic into the Lower Cretaceous (151-140Ma), and consists primarily of fluvial deposits (Bartberger et al., 2003). The Travis Peak (Hosston) Formation is similarly a terrigenous clastic influx from the continent to

the north, of Lower Cretaceous (138-130Ma) age (Fracasso et al., 1988; Becker et al., 2010). The Travis Peak and Cotton Valley groups both thin out towards the south, where various limestones associated with the Sabine Island complex are more prevalent, including the Lower Cretaceous James Lime (120-115Ma). The layout of the Haynesville shale play and surrounding geological features are shown in Fig. 3.1.

Petroleum in the basin originated in the Haynesville shale, which is an organic-carbon rich kerogen. During burial this kerogen was subjected to thermal degradation where oil begins forms first, followed by gas with increasing temperature (thermal maturity). These petroleum phases are partially expelled from the relatively impermeable shales, and migrate through the surrounding country rock, in some cases pooling in structural or stratigraphic traps to form commercial accumulations of hydrocarbons. Oil production from these migrated accumulations, in high-porosity reservoirs, has occurred for many decades, and is known as 'conventional production' (Forgotson, 1954). This distinguishes it from the relatively recent development of production of gas directly from the source-rock, known as 'unconventional production' due to the advanced techniques required to produce commercially viable amounts of gas from such impermeable rocks (Thompson et al., 2011). In this study we present data from unconventional wells producing from the Haynesville shale, as well as overlying conventional reservoirs (Travis Peak, Cotton Valley, James Lime). The conventional reservoirs contain migrated gas that is sourced primarily from the Haynesville, with the potential for smaller contributions from in-situ production or deeper source-rocks such as the Smackover formation (Bartberger et al., 2002; Bartberger et al., 2003). The burial of the Haynesville shale is thought to coincide with a high thermal gradient resulting in early thermal maturation and generation of overpressure (Nunn, 2012). The area has since been uplifted as part of the Sabine uplift feature (Ewing, 2009).

3.3 Materials and methods

Samples were collected from three distinct zones within the Haynesville Shale play area as shown in Fig. 3.1. The first two zones are in the north and east of Panola

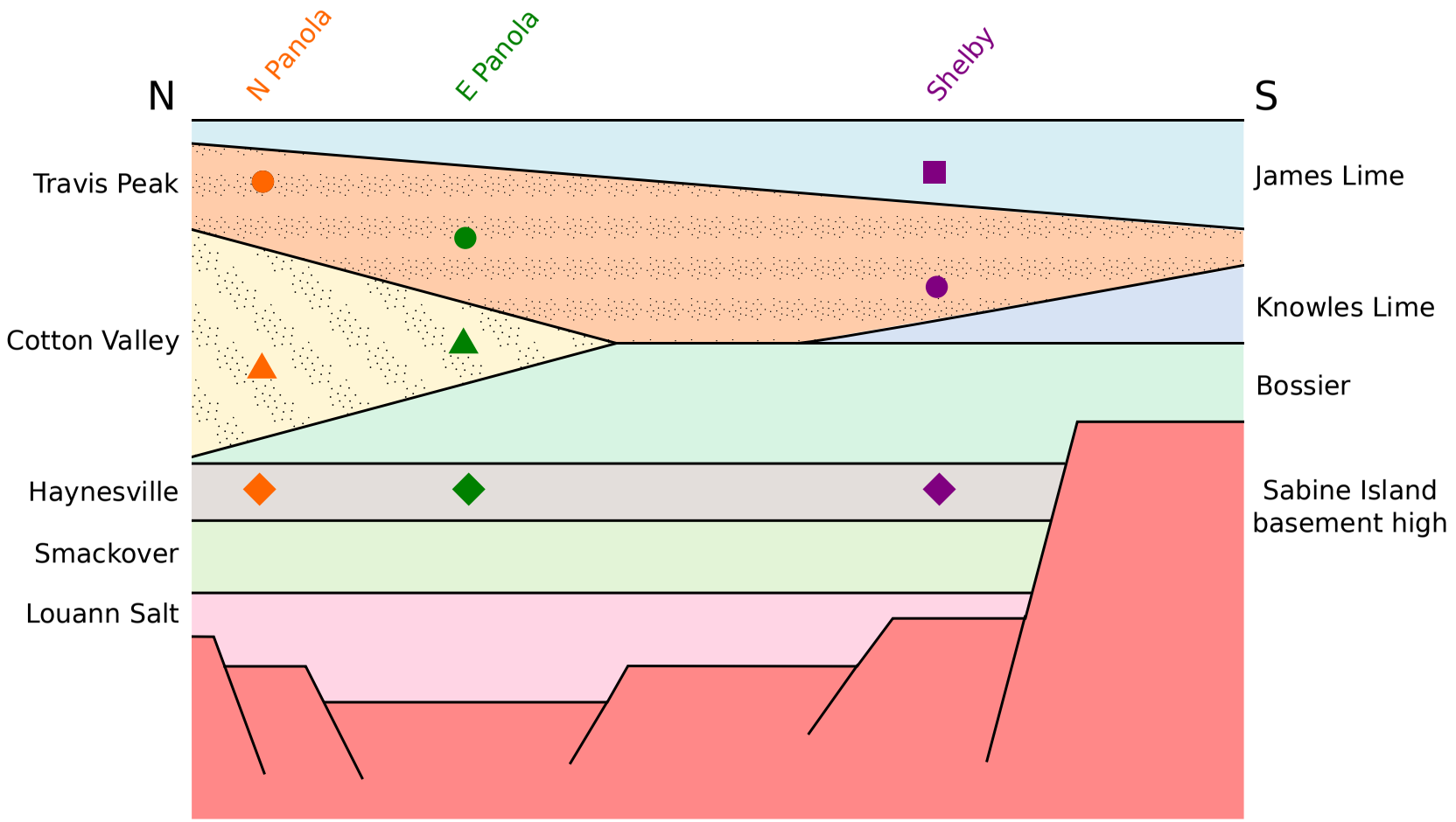

Figure 3.2: Schematic cross-section of East Texas basin, showing stratigraphy and relative position of sample areas and reservoirs.

County, where samples were collected from unconventional wells producing from the Haynesville Shale, as well as conventional wells producing from the overlying Cotton Valley and Travis Peak sandstones. In the third zone, conventional production is typically from the James Lime, and so samples were collected from wells targeting the Haynesville, James Lime, and a single well producing from the Travis Peak. Details of the geographical zone and the targeted stratigraphic unit for each sample are given in Table 3.1, as well as absolute depth of the targeted stratigraphic unit in that location. A schematic cross-section of the basin, showing reservoirs targeted in each zone and their spatial relationship, is shown in Fig. 3.2.

Samples were collected directly from producing well heads. Samples for noble gas analysis were collected in 10mm diameter, refrigeration-grade copper tubes, which were connected using tygon tubing to a 2-stage pressure regulator attached directly to the wellhead. The regulator was used to step down the pressure from the wellstream to 1-2bar. The copper tubes were then flushed with the produced gas for 10 minutes to avoid air contamination, before being sealed with stainless steel clamps (Weiss, 1968). In addition, a subset of samples for hydrocarbon gas geochemistry analysis were collected in industry-standard 300 cm^3 valve-sealed stainless-steel cylinders, which were flushed for 5 minutes to avoid air contamination. These were then shipped to GeoMark Research LTD in Lafayette, Louisiana, USA for bulk gas composition and C and H isotope analysis of major hydrocarbon species using standard procedures that are described in detail in Zumberge et al., 2012. Noble gas isotope analysis was carried out in the Noble Laboratory at the University of Oxford following procedures outlined in section 1.4.2.

3.4 Results

3.4.1 Bulk gas composition and stable isotopes

All samples exhibit a bulk composition typical for high-maturity thermogenic gas, bulk composition and isotope data are shown in Table 3.1. The gases are composed primarily of methane (C_1), with smaller contributions from longer-chain hydrocarbons ethane, propane, and butane+ (C_2, C_3, C_4+). Methane concentrations

	Composition (mole%)						δ^{13}C (‰ VPDB)				δD (‰ VSMOW)	Well
Sample	C_1	C_2	C_3	C_4+	CO_2	N_2	C_1	C_2	C_3	CO_2	C_1	depth (m)
L5	87.0	5.8	1.7	2.9	1.2	1.5	-40.5	-25.7	-23.6	-10.4	-158	2100
SM4	87.9	5.6	1.6	2.5	1.1	1.3	-40.3	-25.2	-23.1	-10.3	-161	2100
HL9	83.9	8.8	3.0	2.5	1.3	0.4	-44.1	-28.4	-26.1	-4.4	-183	2600
HL6	82.0	8.9	3.6	3.7	1.5	0.3	-44.0	-27.9	-25.7	-3.0	-182	3100
BM8	85.5	6.8	2.1	2.7	1.4	1.7	-41.5	-26.2	-24.3	-13.2	-167	3100
BC7	n.d.	n.d.	n.d.	n.d.	n.d.	n.d.	n.d.	n.d.	n.d.	n.d.	n.d.	3100
BM14	89.2	6.3	1.4	2.0	1.6	0.1	-40.9	-23.6	-19.1	2.0	-170	3600
NH1	94.0	3.2	0.4	0.9	2.0	0.1	-38.8	-19.9	-15.5	4.9	-157	3700
RE11	92.7	3.5	0.7	0.7	1.6	0.7	-39.1	-24.9	-22.7	-11.8	-160	2400
F1T	88.4	4.7	1.4	2.5	1.4	1.6	-39.2	-25.5	-23.8	-11.0	-160	1900
F13	88.6	4.7	1.4	2.2	1.6	1.4	-39.2	-25.4	-23.7	-10.2	-159	2000
AC1	n.d.	n.d.	n.d.	n.d.	n.d.	n.d.	n.d.	n.d.	n.d.	n.d.	n.d.	2000
F24	72.6	12.6	6.9	6.3	1.4	0.2	-45.3	-31.5	-28.7	-3.9	-189	2900
AA5	n.d.	n.d.	n.d.	n.d.	n.d.	n.d.	n.d.	n.d.	n.d.	n.d.	n.d.	2900
G12	n.d.	n.d.	n.d.	n.d.	n.d.	n.d.	n.d.	n.d.	n.d.	n.d.	n.d.	3500
WS13	n.d.	n.d.	n.d.	n.d.	n.d.	n.d.	n.d.	n.d.	n.d.	n.d.	n.d.	3600
MG13	93.0	4.1	0.6	1.0	1.8	0.2	-39.2	-20.5	-15.8	3.5	-160	3500
HW2	97.5	0.7	0.1	0.2	1.0	0.4	-34.8	-24.0	-23.7	-0.1	-142	2200
BR2	97.8	0.6	0.1	0.2	1.1	0.2	-34.4	-25.9	-25.3	0.1	-142	2400
RC1	97.5	0.7	0.1	0.2	1.0	0.4	-34.6	-24.1	-25.1	0.0	-146	2300
T1	n.d.	n.d.	n.d.	n.d.	n.d.	n.d.	n.d.	n.d.	n.d.	n.d.	n.d.	2300
T2	n.d.	n.d.	n.d.	n.d.	n.d.	n.d.	n.d.	n.d.	n.d.	n.d.	n.d.	2300
G1	97.4	1.0	0.0	0.1	1.1	0.4	-35.9	-18.8	n.d.	-6.8	-140	2900
C1	96.9	0.2	0.0	0.0	2.8	0.1	-35.6	-29.4	n.d.	0.4	-145	3700
LH4	96.4	0.1	0.0	0.6	3.4	0.1	-35.3	-30.5	n.d.	0.1	-141	4600
BC1	95.9	0.1	0.0	0.6	3.9	0.1	-35.4	n.d.	n.d.	0.2	-144	4100

Table 3.1: Bulk gas composition and stable isotope data for East Texas gases. Errors are ±0.1% for concentrations, and ±0.1‰ for isotope ratios. Sample locations and stratigraphic formation of targeted reservoirs are given in Table 3.2.

range from 72.7 to 97.8 mole%, with all samples apart from one being >80%. Isotope ratios of hydrocarbon compounds are consistent with a thermogenic origin, with $\delta^{13}C_{C1}$ ranging from -45.3 to -34.4‰ VPDB, and δD_{C1} from -189 to -140‰ VSMOW. Both of these ranges are consistent with a thermogenic origin of methane rather than any contribution from biogenic sources (Rice, 1983) There is a small but distinct difference in isotopic signatures between the three regions sampled. The carbon isotope composition of methane $\delta^{13}C_{C1}$ in North Panola (-44.1 to -38.8‰) and East Panola (-45.3 to -39.1‰) is consistently lighter than that of the Shelby county samples (-35.9 to -35.4‰). This suggests a slightly higher thermal maturity in the Shelby area (Whiticar, 1994), likely as a result of the Haynesville source-rock being buried to a greater depth in this area of >4000m compared to ~3500m for the Panola sites, although regional uplift has occurred (Nunn, 2012).

Non-hydrocarbon gases are present in much smaller amounts, with N_2 concentrations up to 1.7% and CO_2 up to 3.9%. Carbon isotope ratios of CO_2 exhibit a relatively wide range from -13.2 to 4.9‰, with most samples falling outside the accepted range of mantle CO_2 values (-6 to -3.5‰, Coltice et al., 2004. This makes it unlikely that there is any significant contribution of mantle CO_2 in the gases currently in the reservoirs of the basin. Again we see a difference between the North and East Panola areas (where $\delta^{13}C_{CO2}$ is variable from -11.8 to 4.9‰) and the Shelby area, where all samples are within 0.4‰ of zero except for one at -6.8‰. It is possible that the more stable values close to 0‰ in Shelby are due to a greater proportion of CO_2 sourced from thermal decomposition of carbonate minerals (again due to the greater burial depths in this area), whilst the large range seen in North and East Panola reflects a greater contribution from organic sources (Whiticar et al., 1986; Golding et al., 2013).

3.4.2 Noble gas isotopic analysis

Noble gas isotope ratios are reported in Table 3.2, and abundances are reported in Table 3.3.

Sample Name	Location	Formation	$^{3}He/^{4}He$ (R_a)	$\pm 2\sigma$	$^{20}Ne/^{22}Ne$	$\pm 2\sigma$	$^{21}Ne/^{22}Ne$	$\pm 2\sigma$	$^{40}Ar/^{36}Ar$	$\pm 2\sigma$
L5	N Panola	Travis Peak	0.203	0.008	9.51	0.03	0.0399	0.0002	851.5	4.2
SM4	N Panola	Travis Peak	0.181	0.007	9.56	0.03	0.0398	0.0002	852.4	4.4
HL9	N Panola	Travis Peak	0.085	0.004	9.51	0.03	0.0376	0.0002	729.1	3.8
HL6	N Panola	Cotton Valley	0.077	0.004	9.51	0.03	0.0374	0.0002	701.9	3.9
BM8	N Panola	Cotton Valley	0.167	0.007	9.53	0.03	0.0400	0.0002	808.4	3.9
BC7	N Panola	Cotton Valley	0.065	0.003	9.55	0.03	0.0387	0.0002	573.6	6.2
BM14	N Panola	Haynesville	0.046	0.003	9.60	0.06	0.0365	0.0002	493.4	6.5
NH1	N Panola	Haynesville	0.041	0.002	9.64	0.06	0.0348	0.0002	489.3	6.4
RE11	E Panola	Travis Peak	0.301	0.012	9.67	0.03	0.0442	0.0002	1061.2	5.8
F1T	E Panola	Travis Peak	0.311	0.013	9.61	0.03	0.0409	0.0002	1024.1	5.0
F13	E Panola	Travis Peak	0.303	0.012	9.66	0.03	0.0412	0.0002	1010.7	5.1
AC1	E Panola	Travis Peak	0.262	0.011	9.58	0.03	0.0451	0.0002	967.6	4.6
F24	E Panola	Cotton Valley	0.164	0.007	9.59	0.03	0.0396	0.0002	798.7	4.5
AA5	E Panola	Cotton Valley	0.113	0.005	9.52	0.03	0.0404	0.0002	706.4	4.4
G12	E Panola	Haynesville	0.070	0.003	9.62	0.03	0.0364	0.0002	477.5	3.3
WS13	E Panola	Haynesville	0.069	0.004	9.76	0.14	0.0377	0.0003	495.5	6.5
MG13	E Panola	Haynesville	0.070	0.004	9.66	0.06	0.0370	0.0002	476.3	6.4
HW2	Shelby	James	0.328	0.013	9.68	0.03	0.0456	0.0002	1156.6	6.2
BR2	Shelby	James	0.241	0.010	9.64	0.03	0.0445	0.0002	1002.5	6.0
RC1	Shelby	James	0.320	0.013	9.69	0.03	0.0454	0.0002	1132.9	6.3
T1	Shelby	James	0.229	0.010	9.54	0.03	0.0453	0.0002	980.9	5.4
T2	Shelby	James	0.251	0.010	9.63	0.03	0.0440	0.0002	977.6	5.4
G1	Shelby	Travis Peak	0.273	0.011	9.68	0.03	0.0462	0.0002	986.0	5.6
C1	Shelby	Haynesville	0.206	0.008	9.56	0.03	0.0386	0.0002	494.0	3.0
LH4	Shelby	Haynesville	0.173	0.009	9.70	0.14	0.0379	0.0003	477.3	6.3
BC1	Shelby	Haynesville	0.176	0.010	9.68	0.06	0.0408	0.0003	521.5	6.9
HT1	Shelby	Haynesville	0.144	0.010	9.79	0.06	0.0336	0.0003	435.9	5.8

Table 3.2: Noble gas isotope ratios for East Texas gases. $^{3}He/^{4}He$ ratios are reported in units of R_a, where R_a is the air ratio of 1.39×10^{-6} (Porcelli et al., 2002).

Sample	^{20}Ne ($\times10^{-9}$)	$\pm2\sigma$	^{36}Ar ($\times10^{-9}$)	$\pm2\sigma$	^{84}Kr ($\times10^{-10}$)	$\pm2\sigma$	^{130}Xe ($\times10^{-12}$)	$\pm2\sigma$	^{4}He ($\times10^{-5}$)	$\pm2\sigma$	^{21}Ne* ($\times10^{-12}$)	$\pm2\sigma$	^{40}Ar* ($\times10^{-6}$)	$\pm2\sigma$
L5	7.54	0.10	32.55	1.27	15.84	0.24	30.74	0.39	42.11	1.05	9.33	0.35	18.10	0.71
SM4	7.50	0.10	31.59	1.24	15.44	0.24	29.44	0.38	39.95	0.83	9.04	0.36	17.59	0.71
HL9	3.88	0.05	18.66	0.73	9.83	0.15	20.20	0.26	12.86	0.23	3.84	0.16	8.09	0.34
HL6	3.77	0.05	17.34	0.68	8.86	0.14	16.16	0.21	12.00	0.28	3.66	0.14	7.05	0.29
BM8	7.40	0.10	33.03	1.29	16.62	0.26	33.43	0.43	35.93	0.68	9.18	0.38	16.94	0.77
BC7	2.10	0.03	7.85	0.31	3.92	0.06	7.69	0.10	8.76	0.19	2.31	0.10	2.18	0.08
BM14	1.57	0.25	6.74	0.53	3.37	0.53	7.74	1.22	3.52	0.09	1.32	0.05	1.33	0.06
NH1	2.20	0.35	8.02	0.63	3.87	0.61	8.22	1.29	3.98	0.08	1.44	0.06	1.55	0.06
RE11	3.76	0.05	13.80	0.54	6.81	0.11	13.97	0.18	12.39	0.30	6.09	0.24	10.57	0.40
F1T	7.33	0.10	27.33	1.07	13.40	0.21	27.18	0.35	43.98	0.85	9.51	0.41	19.92	0.75
F13	6.82	0.09	26.69	1.04	13.54	0.21	28.47	0.37	41.43	0.91	8.91	0.38	19.09	0.76
AC1	3.77	0.05	27.11	1.06	14.55	0.22	33.10	0.42	21.13	0.44	6.58	0.26	18.22	0.72
F24	2.63	0.04	13.72	0.54	7.62	0.12	16.96	0.22	10.03	0.23	3.06	0.13	6.90	0.29
AA5	1.96	0.03	9.35	0.37	5.04	0.08	10.72	0.14	8.33	0.18	2.53	0.11	3.84	0.17
G12	1.41	0.02	5.70	0.22	2.80	0.04	5.59	0.07	2.46	0.06	1.16	0.05	1.04	0.04
WS13	1.31	0.21	6.44	0.51	3.20	0.50	7.26	1.14	3.61	0.09	1.18	0.05	1.29	0.06
MG13	1.31	0.21	6.23	0.49	3.04	0.48	6.86	1.08	3.07	0.06	1.13	0.05	1.13	0.05
HW2	3.50	0.05	13.55	0.53	6.62	0.10	12.34	0.16	34.64	0.66	6.12	0.24	11.67	0.46
BR2	2.98	0.04	10.89	0.43	4.96	0.08	9.72	0.12	25.26	0.43	4.93	0.19	7.70	0.34
RC1	3.51	0.05	13.79	0.54	6.66	0.10	12.47	0.16	33.67	0.74	6.09	0.23	11.55	0.43
T1	2.39	0.03	9.92	0.39	4.69	0.07	9.73	0.12	14.09	0.24	4.26	0.18	6.80	0.28
T2	2.92	0.04	10.83	0.42	5.04	0.08	10.04	0.13	24.69	0.59	4.70	0.19	7.39	0.30
G1	2.41	0.03	10.82	0.42	5.58	0.09	10.99	0.14	10.33	0.25	4.37	0.18	7.47	0.31
C1	0.81	0.01	5.59	0.22	3.27	0.05	7.02	0.09	3.30	0.08	0.87	0.04	1.11	0.05
LH4	0.75	0.12	5.55	0.44	3.16	0.50	7.88	1.24	2.08	0.04	0.71	0.03	1.01	0.04
BC1	0.62	0.10	4.79	0.38	2.75	0.43	6.70	1.05	2.21	0.04	0.78	0.03	1.08	0.05
HT1	1.39	0.21	6.68	0.53	3.62	0.56	8.69	1.31	1.84	0.04	0.66	0.03	0.94	0.04

Table 3.3: Noble gas concentrations for natural gas samples. Units are cm^3STPcm^{-3}, * indicates the concentration of radiogenic isotope corrected for atmospheric component.

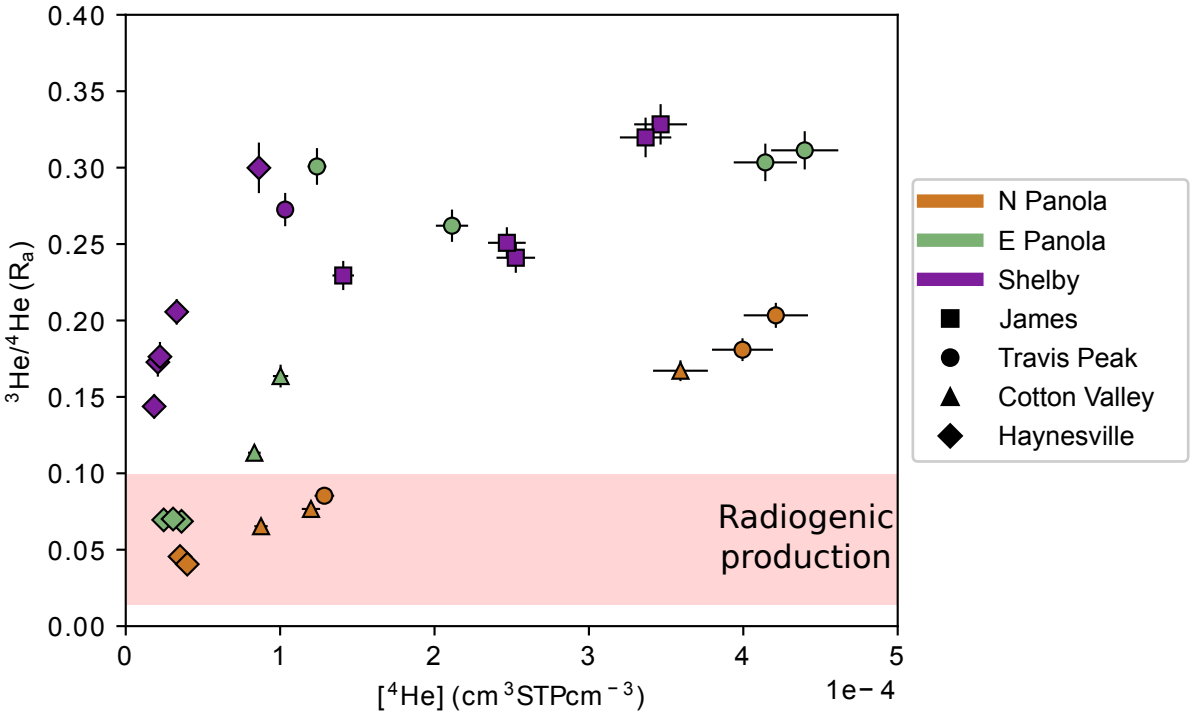

Figure 3.3: Helium concentrations and isotope ratios for collected samples. Helium isotopes are reported relative to the atmospheric ratio $R_a = 1.39 \times 10^{-6}$ (Porcelli et al., 2002). Shaded area represents plausible ratios that can be produced by radiogenic production in Earth's crust, values in excess of this are likely due to small contributions of mantle-sourced helium. Sample areas are denoted by colour, and different reservoirs by marker shape. Haynesville samples are unconventional shale gas, and the remaining reservoirs are conventional gas accumulations.

Helium

Helium concentrations (^{4}He) range from 2.08 to 43.98 ($\times 10^{-5}$cm^{3}STPcm^{-3}). In all areas, concentrations are significantly lower in samples produced from the Haynesville, compared to those produced from conventional wells. Helium isotope ratios (^{3}He/^{4}He) are reported relative to the atmospheric ratio $R_a = 1.4 \times 10^{-6}$, and range from 0.041 to 0.328R$_a$. Fig. 3.3 shows the relationship between He concentrations and helium isotope ratios. ^{4}He/^{20}Ne ratios are >6000 for all samples, which by comparison with the atmospheric ^{4}He/^{20}Ne ratio (0.32), shows that atmospheric helium contributions are negligible. Helium isotope ratios can therefore be thought of as 2-endmember mixing between crustal radiogenic helium, with ^{3}He/^{4}He = 0.02R$_a$ (Ballentine and Burnard, 2002), and small contributions of ^{3}He-

enriched mantle helium, for which sub-continental lithospheric mantle $^{3}He/^{4}He = 6.1R_a$ (Gautheron and Moreira, 2002; Day et al., 2015). Mantle helium contributions are calculated to be up to 5.1% for this dataset, with higher abundances of mantle helium observed in the shallower conventionally-producing wells. The distribution of mantle helium is detailed further in the discussion section.

Neon

For most samples, neon isotope ratios ($^{20}Ne/^{22}Ne$ and $^{21}Ne/^{22}Ne$) show an excess of the radiogenically-produced ^{21}Ne and ^{22}Ne relative to air, for which atmospheric $^{20}Ne/^{22}Ne = 9.78$, $^{21}Ne/^{22}Ne = 0.029$ (Porcelli et al., 2002). As shown in Fig. 3.4 samples predominantly follow the crustal neon production line, defined by Kennedy et al., 1990. Neon concentrations (^{20}Ne) range from 0.62 to 7.54 $\times 10^{-9} cm^3 STP cm^{-3}$, and are typically lower within the Haynesville relative to the conventional samples. Within the Haynesville samples, concentrations tend to be lower in the Shelby county area, which shows higher thermal maturity characteristics in terms of bulk composition and carbon isotope ratios. This relationship between ^{20}Ne and thermal maturity was previously observed in the Eagle Ford unconventional shale (Byrne et al., 2018), and attributed to the progressive dilution of noble gases as natural gas continues to be generated through thermal cracking at increased thermal maturities of the source interval.

Argon

Argon isotope ratios ($^{40}Ar/^{36}Ar$) show an excess of radiogenically-produced ^{40}Ar, ranging from 493 to 1157, compared with the air ratio of 298.6 (Lee et al., 2006). Like $^{3}He/^{4}He$ ratios, $^{40}Ar/^{36}Ar$ ratios are higher in the shallower conventional samples. Argon abundances (^{36}Ar) range from 4.79 to 33.0 $\times 10^{-9} cm^3 STP cm^{-3}$, and show a similar distribution to ^{20}Ne, being higher in conventional samples, and lowest in the higher maturity Haynesville samples (shown in Fig. 3.5). As ^{20}Ne and ^{36}Ar are both atmosphere-derived isotopes introduced primarily through groundwater infiltration, this paralleled behaviour is expected.

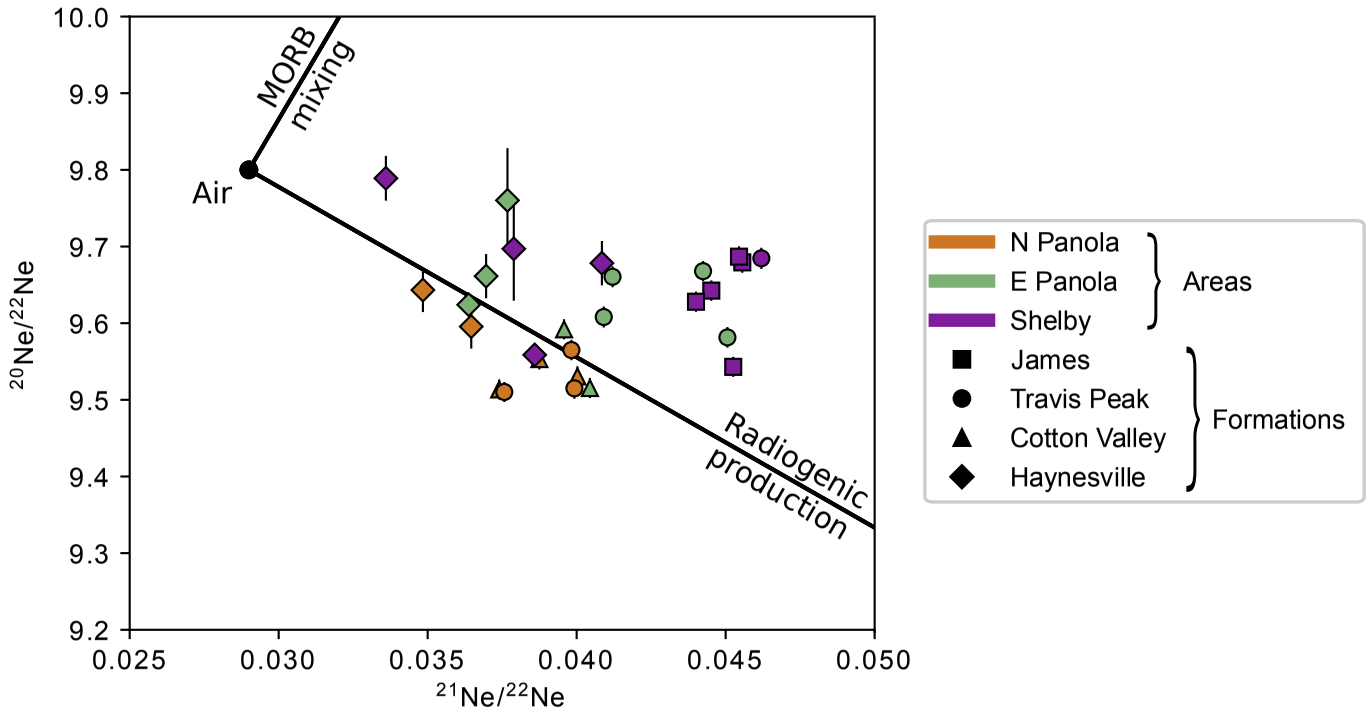

Figure 3.4: Neon isotope plot, showing isotopic composition of samples relative to atmosphere, MORB, and empirically-observed radiogenic production (Kennedy et al., 1990). Sample areas are denoted by colour, and different reservoirs by marker shape. Haynesville samples are unconventional shale gas, and the remaining reservoirs are conventional gas accumulations.

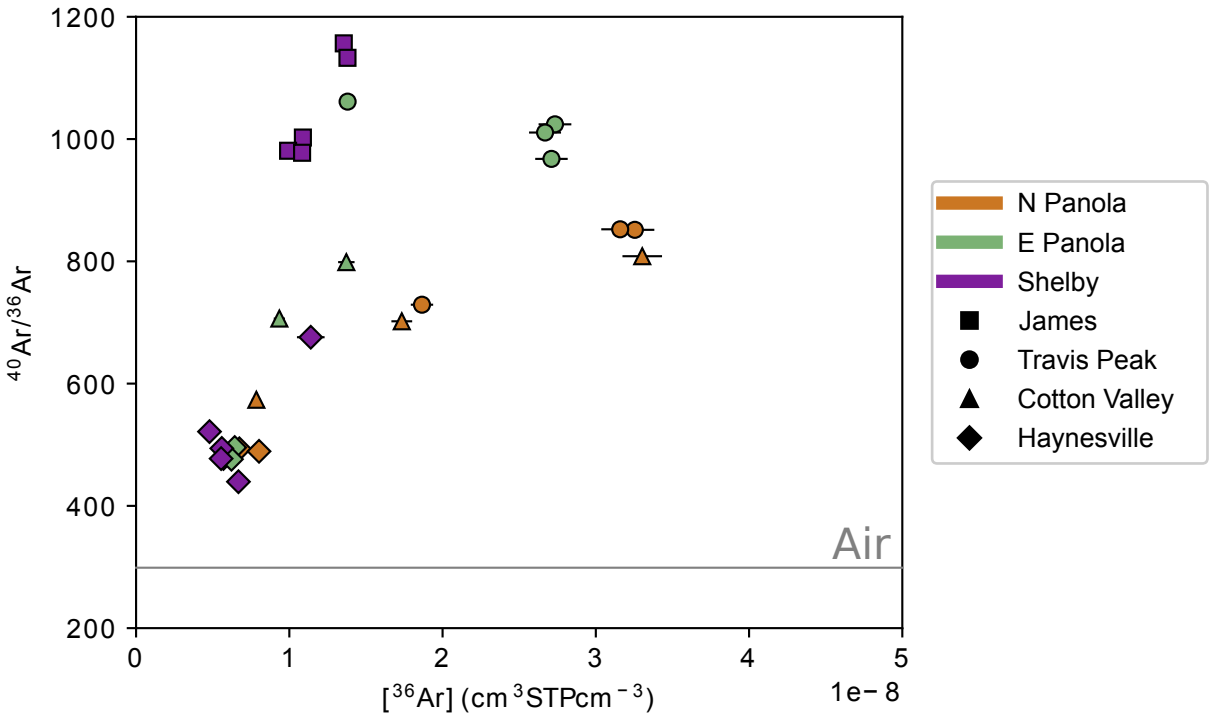

Figure 3.5: Argon isotope ratios and concentrations. Atmospheric ratio is 298.6 (Lee et al., 2006). Values in excess of atmospheric ratio are due to contribution of radiogenic ^{40}Ar produced by ^{40}K decay within the crust. ^{36}Ar is introduced into the subsurface dissolved in groundwater, and its concentration in the gas phase is controlled by solubility-dependent partitioning upon water-gas interaction (see text). Sample areas are denoted by colour, and different reservoirs by marker shape. Haynesville samples are unconventional shale gas, and the remaining reservoirs are conventional gas accumulations.

Krypton and xenon

Krypton and xenon isotope ratios are indistinguishable from air in all samples. Whilst fissiogenic production of Kr and Xe does occur in the subsurface, it is at exceedingly low rates and only observed in extremely old, isolated samples (Holland et al., 2013; Heard et al., 2018). Kr and Xe abundances (^{84}Kr, ^{130}Xe) range from 2.75 to 16.62$\times10^{-10}$cm^{3}STPcm^{-3} and 5.59 to 33.43 $\times10^{-12}$cm^{3}STPcm^{-3} respectively. As has been observed in many other petroleum systems (Bosch and Mazor, 1988; Torgersen and Kennedy, 1999; Zhou et al., 2005; Barry et al., 2018a), Kr and Xe abundances are enriched relative to Ar when compared to air or air-saturated water values. The extent of this enrichment is strongly correlated between Kr and Xe (Fig. 3.6), suggesting a common cause. Previous studies have suggested that this

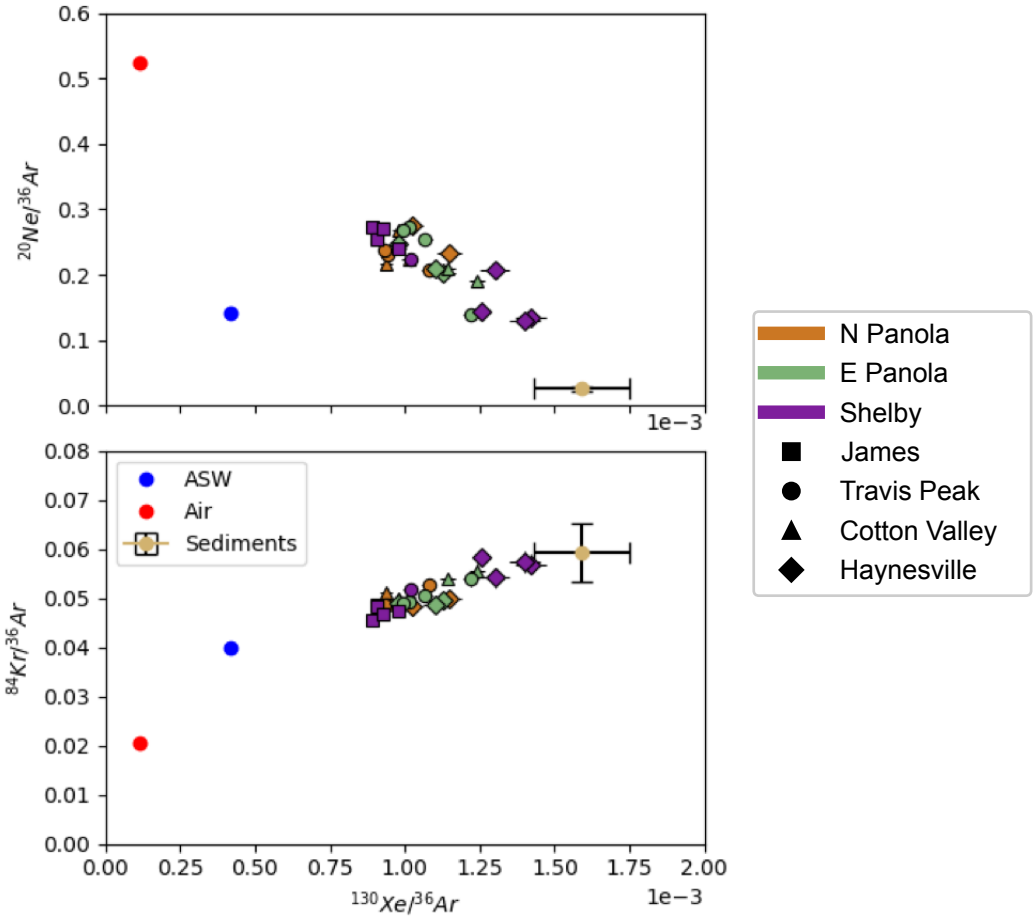

Figure 3.6: Atmosphere-derived Xe/Ar, Kr/Ar, and Ne/Ar ratios for the East Texas gases. Kr/Ar vs Xe/Ar ratios suggest mixing between sediments and Air or ASW, Ne/Ar ratios seem to suggest it is contributions from Air. Sediment endmember from data compiled by Staudacher and Allègre, 1988, error estimates on sediment endmember are 10%.

excess Kr and Xe may be sourced from the organic-rich shales themselves, due to preferential sorption of the heavier noble gases onto clay and/or kerogen (Podosek et al., 1981; Zhou et al., 2005; Marrocchi and Marty, 2013).

Fig. 3.6 shows that the Kr and Xe enrichment can be explained by mixing with a sediment endmember, with oceanic sediment data taken from Staudacher and Allègre, 1988. The Ne/Ar relationship also displayed suggests that the mixing is between sediments and air, rather than ASW. This small air contribution appears to be remarkable constant across the different samples, and is potentially introduced during production. It is also possible that this endmember represents solubility-dependent fractionation. Our samples show no clear relationship between sample

location and extent of Kr and Xe enrichment, however Haynesville samples are marked by a relatively higher Xe/Kr ratio.

3.5 Discussion

3.5.1 Source-rock to reservoir changes in noble gas isotope signature

Hydrocarbon migration is the transport of oil and/or gas from the source-rock where it is generated, into a reservoir where it may form a commercial accumulation (Stainforth, 2009). The geochemical effects of migration on hydrocarbon phases remains poorly constrained yet is an important aspect of the petroleum system (Dembicki and Anderson, 1989; Barry et al., 2017). This suite of samples allows us to directly compare migrated hydrocarbons from conventional reservoirs with the corresponding non-migrated (unconventional) phases remaining within the source-rock.

One of the most striking differences between the conventional and unconventional samples is the difference in noble gas abundances. Unconventional samples are marked by consistently lower abundances than conventional samples for all noble gas species (Table 3.3, Fig. 3.3, Fig. 3.5), suggesting that conventional hydrocarbons obtain a significant fraction of their noble gas inventory during the migration process. This systematic difference has been observed in unrelated conventional and unconventional systems before (Byrne et al., 2017), but never in the same basin. This comprehensive dataset demonstrates unequivocally that elevated noble gas abundances in conventional hydrocarbon accumulations are the direct result of a longer migration pathway relative to unconventional systems. Conversely, when hydrocarbons are effectively retained within their relatively impermeable source-rock, petroleum phases inherit a much lower noble gas inventory. Migration through the basin stratigraphy and perhaps the residence within a permeable reservoir brings the hydrocarbons into contact with groundwater to a much greater extent. During interaction with groundwater, noble gases will preferentially partition into the oil or gas phase, as they are significantly more soluble in hydrocarbon phases than in water (Kharaka and Specht, 1988; Prinzhofer, 2013).

3.5.2 Effects of migration on gas/water volume ratio calculations

One of the applications of noble gas isotopes in petroleum systems has been the calculation of volumetric gas/water or oil/water ratios in the subsurface using Henry's law solubility-dependent partitioning equations (Ballentine et al., 2002; Prinzhofer, 2013). This approach uses the atmosphere-derived noble gas (ANG) isotopes (^{20}Ne, ^{36}Ar, ^{84}Kr, ^{130}Xe; so-called because they have no radiogenic source in the subsurface), and exploits the fact that they must be introduced dissolved in groundwater, the composition of which is well-defined. The original approach was proposed using differential solubilities of the noble gas elements in the subsurface and calculating gas/water volume ratios (V_g/V_w) using the isotopic ratios ^{20}Ne/^{36}Ar, ^{84}Kr/^{36}Ar, and ^{130}Xe/^{36}Ar (Bosch and Mazor, 1988; Zaikowski and Spangler, 1990). This approach has the benefit of cancelling some of the uncertainties introduced from extrapolating the required Henry's constants to reservoir conditions . However, the observations of pervasive anomalous atmospheric Kr and Xe enrichments in petroleum (Torgersen et al., 1992; Zhou et al., 2005) alongside better constraints of Henry's constants at high temperatures (Fernández-Prini et al., 2003), and the fact that ^{20}Ne/^{36}Ar is invariant at $V_g/V_w > 0.1$ under many conditions (Barry et al., 2016) has led to reformulations using simply the concentrations of ^{36}Ar . Using ^{20}Ne concentrations is also a possible alternative/auxiliary method, but we consider this less reliable than ^{36}Ar due to the increased difficulty of measurement leading to higher errors (primarily due to mass interference with $^{40}Ar^{++}$) as well as the fact that mantle fluids are enriched in ^{20}Ne (Gautheron et al., 2005).

The observations in this system certainly lend credence to the interpretation of gas/water volume ratios using concentrations of ^{36}Ar rather than ^{20}Ne/^{36}Ar. This is due to the comparison between conventional samples that have undergone migration, and the unconventional samples which have been generated and produced in-situ. During migration, the gas phase is predicted to interact and equilibrate with much large volumes of water, leading to lower V_g/V_w values in conventional samples compared to the unconventionals. While we see a significant distinction

in ^{36}Ar concentrations between conventional and unconventional samples (Table 3.3, Fig. 3.5), ^{20}Ne/^{36}Ar ratios overlap and show no clear relationship (Fig. 3.6). Furthermore, ^{36}Ar concentrations are consistently and significantly lower in unconventional samples (Table 3.3), as is predicted for higher V_g/V_w. We therefore anticipate that using ^{36}Ar concentrations will be the most reliable method of interpreting subsurface V_g/V_w ratios using natural gas samples.

In order to calculate V_g/V_w values for the samples concerned, various geometries and sequences of gas-water interaction can be considered (see Barry et al., 2016), but a simple first-order model of a single-step gas-water equilibration can be formulated starting from Eq. 3.1 (from Ballentine et al., 2002).

$$n_i^g = n_i^{tot}\left(\frac{16T\rho_w V_w}{195\gamma_i K_i^m V_g} + 1\right)^{-1} \tag{3.1}$$

Where n_i^g is the number of moles of species i in the gas phase, n_i^{tot} is the total number of moles in the system, ρ_w is the density of water, T is reservoir temperature, K_i^m is the Henry's constant in units of atmKgmol^{-1}, γ_i is the Setschenow coefficient that accounts for the non-ideality due to salinity, and V_g and V_w are the volumes of gas and water present respectively. Here species i is ^{36}Ar. We know that all of our atmosphere-derived isotopes must have initially been delivered into the subsurface dissolved in air-saturated water, and so can make the following substitutions.

$$n_i^g = V_g C_i^{sample} \tag{3.2}$$

$$n_i^{tot} = C_i^{asw}\rho_w V_w \tag{3.3}$$

Where C_i^{sample} and C_i^{asw} are the concentrations in the sample and ASW respectively. Substituting Eq. 3.2 and 3.3 into Eq. 3.1 and rearranging results in the following equation, which can be used to predict subsurface V_g/V_w ratios given the concentration of ^{36}Ar in any sample.

$$\frac{V_g}{V_w} = \frac{\rho_w C_i^{asw}}{C_i^{sample}} - \frac{16T\rho_w}{195\gamma_i K_i^m} \tag{3.4}$$

The initial concentration in ASW used in this study is that of seawater at 10^{o}C for which [^{36}Ar] = 1.05×10^{-6}cm^{3}STPg^{-1} (Kipfer et al., 2002).

Calculated V_g/V_w ratios for each sample are shown in Table 3.4; the difference between conventional and unconventional samples is clear, demonstrating that there is significantly more groundwater interaction during conventional petroleum migration compared to unconventional systems.

3.5.3 Accumulation of radiogenic isotopes during migration

Radiogenic isotopes accumulate in the subsurface over time as a function of their parent-isotope concentrations. Here we consider ^{4}He, produced asα-particles during U, Th decay; ^{21}Ne, produced from nucleogenic reactions of ^{18}O and ^{24}Mg; ^{40}Ar, produced from the β^+ decay of ^{40}K. ^{21}Ne, and ^{40}Ar are also introduced from atmospheric sources, but their radiogenic component (denoted ^{21}Ne* or ^{40}Ar*) can be calculated by subtracting the atmospheric component using a purely atmospheric isotope as a normalisation (Byrne et al., 2017). Radiogenic isotope concentrations are given in Table 3.3. There is a clear distinction between unconventional Haynesville samples and those from the other conventional reservoirs. The unmigrated Haynesville samples have consistently lower radiogenic isotope abundances, despite being produced from the geologically oldest reservoirs. This suggests that residence time is not the primary factor controlling radiogenic isotope concentrations, and in fact migration plays a key role. By modelling predicted radiogenic production we can attempt to quantify this .

We can calculate expected in-situ production rates using the following equations (Ballentine and Burnard, 2002).

$$J(^4He) = (3.242 \times 10^6[U] + 7.710 \times 10^5[Th]) \times \frac{V_m}{N_A} \tag{3.5}$$

$$J(^{21}Ne) = ((1.48[U] + 0.186[Th])[O] + (0.105[U] + 0.0179[Th])[Mg]) \times 10^{-22} \tag{3.6}$$

Sample	Location	Formation	Well depth (m)	Z	V_g/V_w	V_R	a^2/A^2
L5	Briggs	Travis Peak	2100	167	32.4	8.77	0.40
SM4	Briggs	Travis Peak	2100	167	33.3	8.55	0.39
HL9	Briggs	Travis Peak	2600	196	56.2	4.62	0.28
HL6	Briggs	Cotton Valley	3100	224	60.8	4.57	0.52
BM8	Briggs	Cotton Valley	3100	224	31.9	11.01	1.46
BC7	Briggs	Cotton Valley	3100	224	134.0	1.41	0.06
BM14	Briggs	Haynesville	3600	248	156.1	0.95	
NH1	Briggs	Haynesville	3700	253	131.2	1.13	
RE11	Bethany	Travis Peak	2400	185	76.2	5.69	0.33
F1T	Bethany	Travis Peak	1900	154	38.5	8.93	0.39
F13	Bethany	Travis Peak	2000	160	39.4	8.92	0.41
AC1	Bethany	Travis Peak	2000	160	38.8	8.50	0.39
F24	Bethany	Cotton Valley	2900	213	76.8	4.27	0.41
AA5	Bethany	Cotton Valley	2900	213	112.5	2.38	0.17
G12	Bethany	Haynesville	3500	244	184.5	0.73	
WS13	Bethany	Haynesville	3600	248	163.3	0.92	
MG13	Bethany	Haynesville	3500	244	168.8	0.79	
HW2	Huxley	James	2200	173	77.3	5.90	0.20
BR2	Huxley	James	2400	185	96.5	4.15	0.14
RC1	Huxley	James	2300	179	76.2	6.04	0.21
T1	Huxley	James	2300	179	106.0	3.55	0.11
T2	Huxley	James	2300	179	97.4	3.84	0.12
G1	Huxley	Travis Peak	2900	213	97.4	4.63	0.22
C1	Huxley	Haynesville	3700	253	188.2	0.81	
LH4	Huxley	Haynesville	4600	291	189.5	0.85	
BC1	Huxley	Haynesville	4100	271	219.6	0.85	
HT1	Huxley	Haynesville	4400	283	157.5	0.78	

Table 3.4: Parameters calculated for the investigation of migration behaviour in the basin. Z is compression factor representative of change in relative volume between reservoir and STP conditions (see text). V_g/V_w is gas/water volume ratio calculated from atmospheric ^{36}Ar abundances. V_R is the encountered rock volume required to produce observed radiogenic ^{40}Ar abundances. a^2/A^2 is the factor representing the relative cross-sectional area of hydrocarbon generation to migration conduit, discussed in text. As such this is not shown for unconventional samples that have not undergone migration.

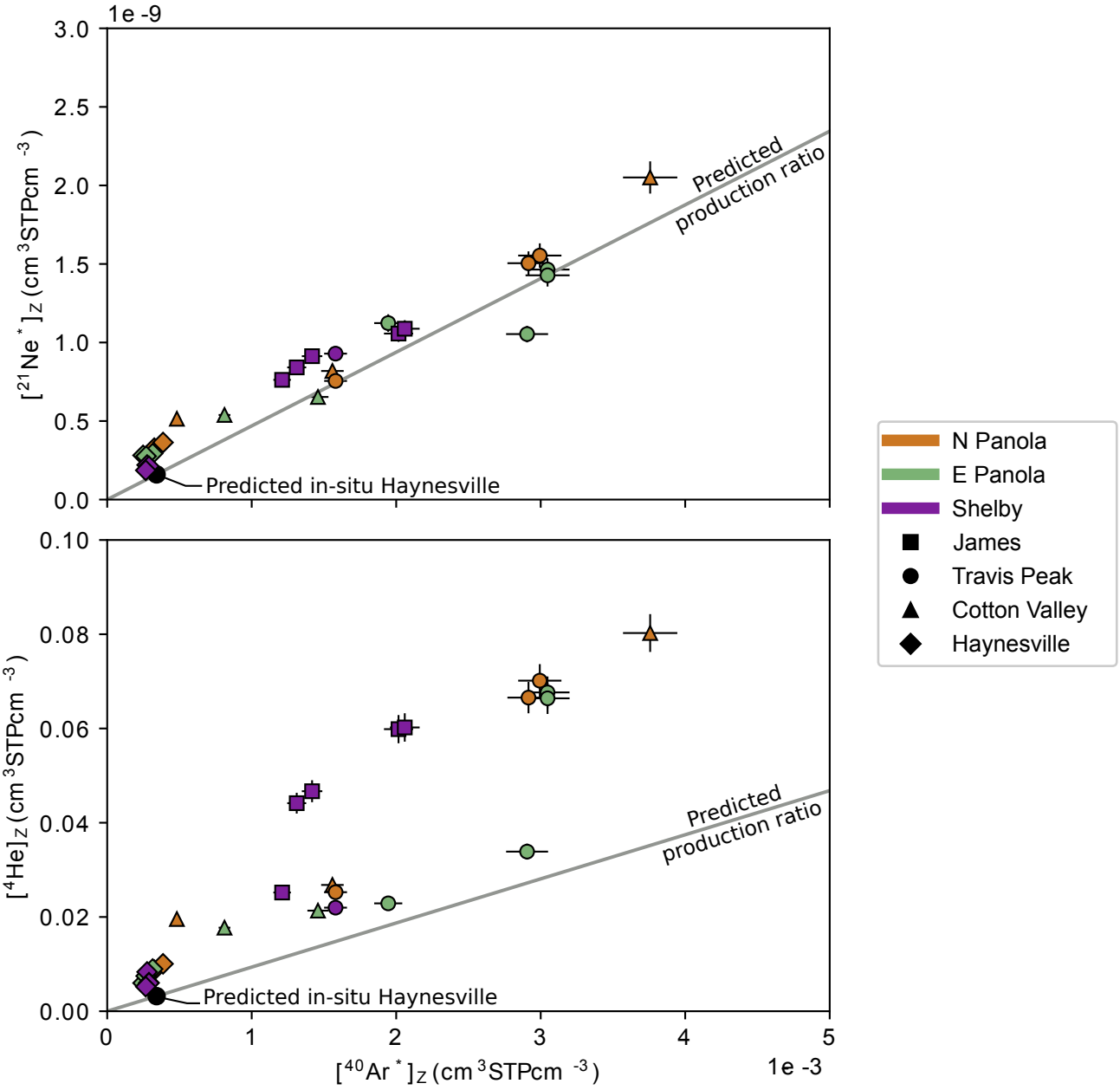

Figure 3.7: Radiogenic isotope abundances in samples, subscript Z denotes that samples have been normalised to reservoir pressure and temperature conditions, and as such concentrations are per unit volume of pore-space rather than per unit of the produced natural gas. Asterisk indicates that abundances have been corrected for atmospheric contributions. Grey lines indicate predicted radiogenic isotope production ratio, with calculations detailed in the text. Black circle is predicted total accumulation within the Haynesville source-rock over the 150Myr since its deposition. Sample areas are denoted by colour, and different reservoirs by marker shape. Haynesville samples are unconventional shale gas, and the remaining reservoirs are conventional gas accumulations.

Parameter	Value
[U]	$4ppm$
[Th]	$8ppm$
[K]	$20,000ppm$
[O]	48%
[Mg]	1%
ϕ	10%
$[^4\mathrm{He}]_M$	3.20×10^{-3}
$[^{21}\mathrm{Ne}^*]_M$	1.60×10^{-10}
$[^{40}\mathrm{Ar}^*]_M$	3.42×10^{-4}

Table 3.5: Haynesville Shale parameters used for radiogenic production calculations

$$J(^{40}Ar) = 102.2[K] \times \frac{V_m}{N_A} \tag{3.7}$$

Where $J(i)$ is the production of species i in $\mathrm{cm^3STPg^{-1}yr^{-1}}$, U, Th, and K concentrations are in ppm, O and Mg concentrations are in wt%, and V_m and N_A are the molar gas volume and Avogadro's number, required to convert from atoms into $\mathrm{cm^3STP}$. Chemical analysis of Haynesville shale cores show typical $[U]$ = 4ppm, $[Th]$ = 8ppm (Sano et al., 2013a), and typical sedimentary values for other elements are $[K]$ = 20,000ppm, $[O]$ = 48wt%, $[Mg]$ = 2wt% (Plank and Langmuir, 1998; Ballentine and Burnard, 2002). The predicted concentration of the radiogenic isotope in the gas phase can then be calculated from the flux:

$$[i] = \frac{J(i) \times t}{\phi} \tag{3.8}$$

Where $[i]$ is the concentration of species i in the pore-space in $\mathrm{cm^3STPcm^{-3}}$, t is the elapsed time, and ϕ is the porosity, for which the average in the Haynesville is 10% (Hammes and Frébourg, 2012). Predicted concentrations of radiogenic isotopes accumulated since the deposition of the Haynesville Shale (~150Ma) are given in Table 3.5.

In order to compare our calculated concentrations with those measured in the samples, we must take into account the gas compression experienced at reservoir

depth. Our calculated radiogenic production rates are in cm^3STP per unit volume of reservoir pore-space, but our measurements in cm^3STP per unit volume of sample gas. We can account for the difference by simply compressing the sample gas back down to reservoir conditions using the ideal gas law to derive a correction factor 'Z'.

$$Z = \frac{V_{res}}{V_0} = \frac{T_{res} p_0}{T_0 p_{res}} \tag{3.9}$$

$$[^{40}Ar^*]_Z = [^{40}Ar^*] \times Z \tag{3.10}$$

Where subscript '0' indicates STP and 'res' indicates reservoir conditions. We can estimate reservoir temperature and pressure using typical temperature and pressure gradients of 35^oCkm^{-1} and $100atmkm^{-1}$ respectively. Calculated correction factors for each sample are given in Table 3.4.

We can now compare our predicted radiogenic isotope concentrations with the measured values, plotted in Fig. 3.7. Measured [^{21}Ne*] and [^{40}Ar*] are strongly correlated, and their production ratio is in closed agreement with predicted production rates. [^{4}He] shows more variability when compared to [^{40}Ar*], and production is mostly in excess of the predicted ^{4}He/^{40}Ar production rate. This could be due to several factors. ^{4}He/^{40}Ar is more likely to be affected by diffusive or solubility-controlled fractionation than ^{21}Ne/^{40}Ar, and further fractionation can occur on release of radiogenic isotopes from mineral phases, as ^{4}He undergoes α-recoil upon production, facilitating its expulsion (Ziegler, 1977; Farley et al., 1996). We therefore consider ^{40}Ar* to be a more reliable indicator of radiogenic isotope abundance.

Fig. 3.7 clearly shows that the unconventional Haynesville samples that have not undergone migration plot relatively close to the predicted in-situ accumulation abundances of ^{21}Ne and ^{40}Ar. However, the samples that have migrated into shallower reservoirs have radiogenic isotope abundances far in excess of what could have accumulated in-situ, despite being in geologically younger reservoirs. This indicates that the radiogenic isotopes must have been entrained into the gas phase during migration, as the gas phase was exposed to a larger volume of rock. We

can compare the observed [^{40}Ar*] to the predicted and define a 'volume of rock', V_R, representative of this increased exposure.

$$V_R = \frac{[^{40}Ar^*]_Z}{[^{40}Ar^*]_M} \tag{3.11}$$

Where V_R is the volume of rock from which the sample is inferred to have acquired radiogenic isotopes, $[^{40}Ar^*]_M$ is the predicted in-situ radiogenic isotope concentration, given in Table 3.5. Calculated V_R for each sample is shown in Table 3.4. The unmigrated Haynesville samples have an average V_R of 0.87, compared to 5.87 for the conventional samples.

3.5.4 Insights into migration behaviour from combined radiogenic-atmospheric isotope approaches

In the previous 2 sections, we derived 2 independent parameters that can both be related to migration distance from the source-rock. The gas-water volume ratio V_g/V_w, derived from atmospheric ^{36}Ar, is expected to decrease with increasing migration distance, as more groundwater equilibrates with the gas phase. The radiogenic rock volume V_R is derived from radiogenic ^{40}Ar* and is expected to increase with increasing migration distance. Both parameters show marked distinctions between conventional and unconventional samples, indicative of the greater migration distance experienced by conventional accumulations.

If we consider a conceptual model of gas migration, we might expect a gas phase to originate in the source rock, having some initial V_g/V_w ratio , and an initial V_R of around 1. Upon expulsion from the source-rock into the surrounding strata we would expect the gas to equilibrate with surrounding groundwater, acquiring both atmospheric ^{36}Ar and radiogenic ^{40}Ar*, and consequently decreasing V_g/V_w and increasing V_R. This concept is illustrated in Fig. 3.8. In a simple system with little variation in radiogenic production and groundwater age we can directly equate the change in V_g/V_w and V_R, as they are inversely proportional. Further, we can consider V_w/V_g instead to get a simple relationship of direct proportionality. Fig. 3.9 shows a plot of the computed V_w/V_g vs V_R for our sample suite. The samples

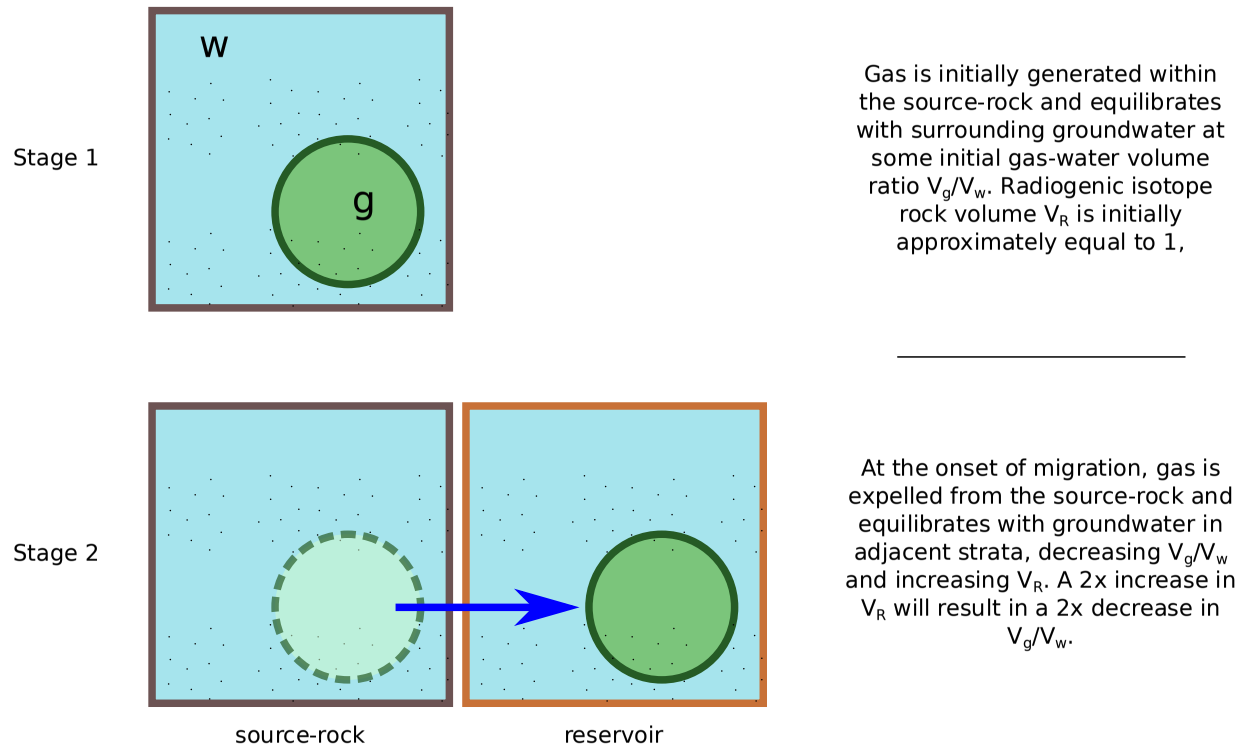

Figure 3.8: Conceptual model showing the relationship between gas/water volume ratios and total rock volume interaction. Assuming gas volume remains constant and groundwater flow is relatively static compared to hydrocarbon migration timescales, the recorded gas/water volume ratio (V_g/V_w) in the gas phase should be inversely proportional to the total rock volume (V_R) encountered.

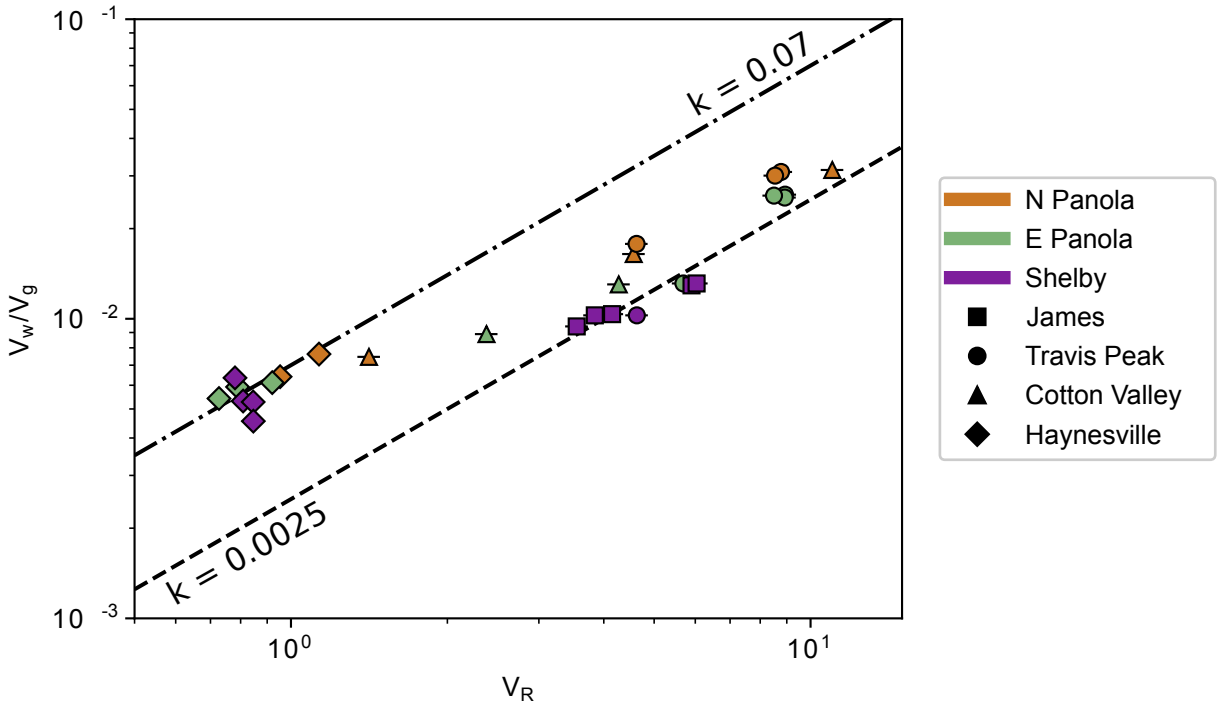

Figure 3.9: Calculated relative rock volumes encountered (V_R) versus recorded water/gas ratio (V_w/V_g) for measured samples. Lines plotted are models considering direct proportionality between the 2 variables with different coefficients k. See text for definitions and calculations of parameters. Sample areas are denoted by colour, and different reservoirs by marker shape. Haynesville samples are unconventional shale gas, and the remaining reservoirs are conventional gas accumulations.

are remarkably well correlated, suggesting that this simple conceptual model is broadly accurate. We can compare the samples to our model by formulating it mathematically.

$$\frac{V_w}{V_g} = k \times V_R \tag{3.12}$$

Where V_w/V_g is the water-gas volume ratio (inverse of V_g/V_w calculated in section 5.1.2), V_R is the radiogenic rock volume calculated in Section 3.5.3, and k is a constant that conceptually represents the initial V_w/V_g inside the source-rock, when V_R=1. We plot 2 model lines for values of $k = 0.0025$ and $k = 0.07$ in Fig. 3.9. It is impossible to fit the dataset with a single k-value, however, samples trend towards a line with a lower k-value as their V_R increases. This could be due to several reasons, including changes in porosity or parent isotope concentrations from

source-rock to reservoir affecting radiogenic isotope production, lateral migration of older groundwaters increasing radiogenic isotope concentrations, instead of a simple static system, or the result of secondary cracking increasing relative gas volumes either in the reservoir or source-rock. Nevertheless, the general trends exhibited in this approach show clear and consistent effects of migration, and indicate that the noble gases have real potential for investigating migration in petroleum systems.

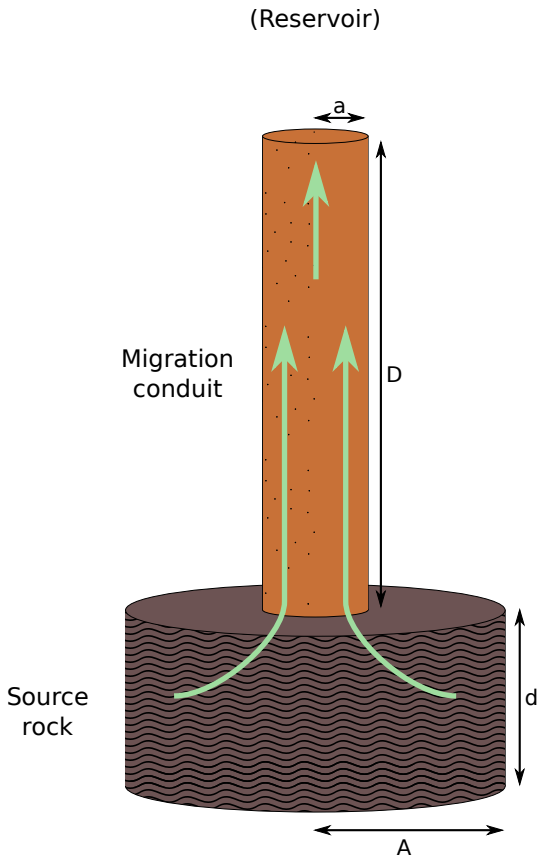

Figure 3.10: Conceptual model showing migration conduit from source-rock to reservoir. The calculation of relative radii of source-rock to migration conduit volumes are discussed in the text, as a proxy for the extent of localisation of hydrocarbon migration.

We can gain further insight into migration behaviour by comparing our calculated parameters with observed differences in stratigraphic depth. Conventional wisdom

dictates that cross-formational hydrocarbon migration occurs along relatively constrained pathways (Dembicki and Anderson, 1989). We can investigate this hypothesis by comparing the difference in depth between source-rock and reservoir, along with the volume of rock required by our radiogenic isotope calculations, V_R. In a simple single-conduit model of migration, we can assume gas is generated in some source-rock volume V_{source} and migrates along a pathway with a volume V_{path}. A schematic representation of this model is shown in Fig. 3.10.

$$V_{source} = \pi A^2 d \tag{3.13}$$

Where d is the thickness of the source-package and A is the radius. The thickness of the Haynesville source-rock is typically around 80m (Hammes et al., 2011). The volume experienced along the migration pathway can also be calculated.

$$V_{path} = \pi a^2 D \tag{3.14}$$

Where D is the migration path length (calculated by taking the difference between the reservoir depth and source-rock depth), and a is the radius of the migration conduit. In our definition of V_R we stated that with zero migration the gas phase would acquire $V_R = 1$, and that the observed V_R represented the total volumes of rock seen relative to the expected source-rock production in-situ. We can therefore equate V_R to the ratio of the source-rock volume V_{source} to the total rock volume experienced by the gas phase ($V_{source} + V_{path}$). We can then rearrange the equations to solve for a^2/A^2 which represents the theoretical ratio of the conduit cross-sectional area to the cross-sectional area of the associated source-rock. In reality, hydrocarbon migration occurs in a more complex fashion, and over is not a single-stage process. As such, this parameter does not directly represent any physical property, but is a useful derived parameter for comparison of migration style.

$$V_R = \frac{V_{source} + V_{path}}{V_{source}} \tag{3.15}$$

$$\frac{a^2}{A^2} = \frac{(V_R - 1)d}{D} \tag{3.16}$$

If $a^2/A^2 < 1$, then the gas will have migrated along a narrow conduit relative to the associated source-rock volume from which the gas was generated. Calculated values for all conventional samples are shown in Table 3.4, and we show that for all samples apart from 1, a^2/A^2 is indeed less than 1. It should be noted that this value represents an upper limit for the migration conduit size, as it makes the assumption that all radiogenic isotopes are acquired during migration, and neglects any additional equilibration that might take place whilst the gas is stored in the reservoir. These results suggest that hydrocarbon migration occurs along relatively localised conduits. Interestingly, the different locations sampled display different values, with Shelby county samples having the lowest a^2/A^2 of around 0.1-0.2, whilst Panola county samples are generally higher at a range of around 0.4-0.6. This could be reflective of migration process, and suggests that migration in the Shelby county region has occurred to a greater extent along a few localised conduits such as fault planes. In the Panola county areas the migration appears to be more diffuse, perhaps indicating a more connected or extensive fracture network.

3.5.5 Helium and Argon isotope relationships

Helium and argon isotopes show a clear positive correlation with unconventional samples, which are consistently lower in both $^3He/^4He$ than their unconventional counterparts, and shallower conventional samples showing the strongest enrichment (Fig. 3.11). Within the conventional North and East Panola sample suites, the data show a parabolic trend indicative of 2-endmember mixing.

One endmember (A) is clearly characterised by strongly radiogenic $^3He/^4He$ values, and atmospheric $^{40}Ar/^{36}Ar$ values. This endmember can be interpreted as the result of a closed-system radiogenic accumulation within a typical crustal system. Starting from an initial ASW composition, <10 Myr of radiogenic ingrowth will skew the $^3He/^4He$ ratio heavily towards the radiogenic endmember of $0.02R_a$ (Ballentine and Burnard, 2002), but the $^{40}Ar/^{36}Ar$ will stay relatively unchanged

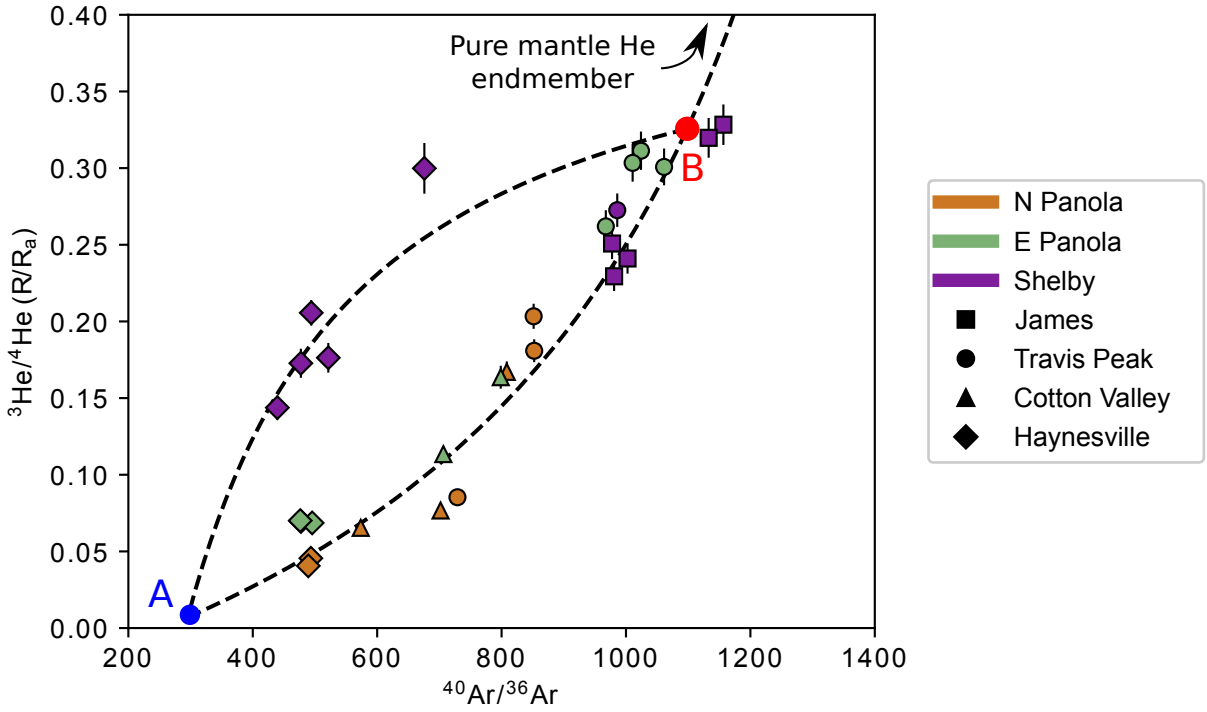

Figure 3.11: Helium and Argon isotope ratios for measured samples. Mixing lines are plotted between endmember A, representative of a closed-system source-rock evolution, and endmember B, interpreted to represent groundwater circulation in the wider hydrogeological system. Sample areas are denoted by colour, and different reservoirs by marker shape. Haynesville samples are unconventional shale gas, and the remaining reservoirs are conventional gas accumulations.

from air. This is due to the higher production rate of ^{4}He (roughly an order of magnitude higher than ^{40}Ar), but also because the much higher initial abundance of argon in ASW makes impacting the ratio more difficult (Kipfer et al., 2002).

The second endmember (B) clearly has elevated ^{3}He/^{4}He approaching mantle values, and elevated ^{40}Ar/^{36}Ar, due to an excess of radiogenically produced ^{40}Ar. Excess radiogenic ^{40}Ar can be source from the crust or the mantle, as both have high ^{40}Ar/^{36}Ar ratios. However, in the previous section we showed a clear correlation between crustal-radiogenic ^{40}Ar, ^{21}Ne, and ^{4}He, making a crustal source for ^{40}Ar much more likely. Furthermore, mantle ^{4}He/^{40}Ar* varies between 1.6 to 4.2 (Graham, 2002), while sediments (particularly organic-carbon rich source-rocks) are typically higher, ranging from 10-20 (Ballentine and Burnard, 2002). Samples in this study are more commensurate with the latter source, ranging from 11.7 up to 40.6. However,

it is difficult to exclude the possibility of $^{4}He/^{40}Ar^{*}$ fractionation during mineral release or due to solubility-dependent partitioning (Ballentine and Burnard, 2002).

In Fig. 3.11 North and East Panola county data are plotted along with a mixing line starting from the well-defined endmember A. Mixing with a pure mantle helium endmember, for which sub-continental lithospheric mantle $^{3}He/^{4}He = 6.1R_a$ (Day et al., 2015), would lead to an argon isotope ratio of $^{40}Ar/^{36}Ar = 1700$. However, this is an unrealistic endmember for a number of reasons. Firstly, as observed in the previous section and shown in Fig. 3.3, radiogenic ^{4}He abundances also increase with $^{3}He/^{4}He$ ratios. Furthermore, a pure mantle endmember would have a much higher $^{40}Ar/^{36}Ar$ of around 10,000 (Graham, 2002), and would not correlate with other radiogenic isotopes as shown in Fig. 3.7. A better conceptual model is that of mixing between pure source-rock endmember A, and endmember B as a hybrid between mantle, radiogenic, and sedimentary signatures representative of the general groundwater circulation through the stratigraphy, which lies somewhere along the mixing line displayed in Fig. 3.11. As such, the mixing can be thought of as the extent of influence from the wider hydrogeological regime within the basin.

If we choose endmember B to have $^{3}He/^{4}He$ ratio similar to the highest observed in our samples, at around 0.33, this corresponds to a $^{40}Ar/^{36}Ar$ ratio of 1100 on the mixing trajectory for the Panola County area samples. We can then explain the Shelby area samples which have relatively higher $^{3}He/^{4}He$ ratios than those further north. If we allow the r-value of the mixing curve to vary we can fit the Shelby samples with the same 2 endmembers. This conceptually means raising the He/Ar ratio of endmember B in the Shelby area, which does make sense given the observed distribution of mantle He ratios, which consistently increase towards the south. We can therefore fully explain the observed He and Ar isotope relationships with a 2-endmember mixing model, with increased migration distance leading to a greater mixing towards endmember B.

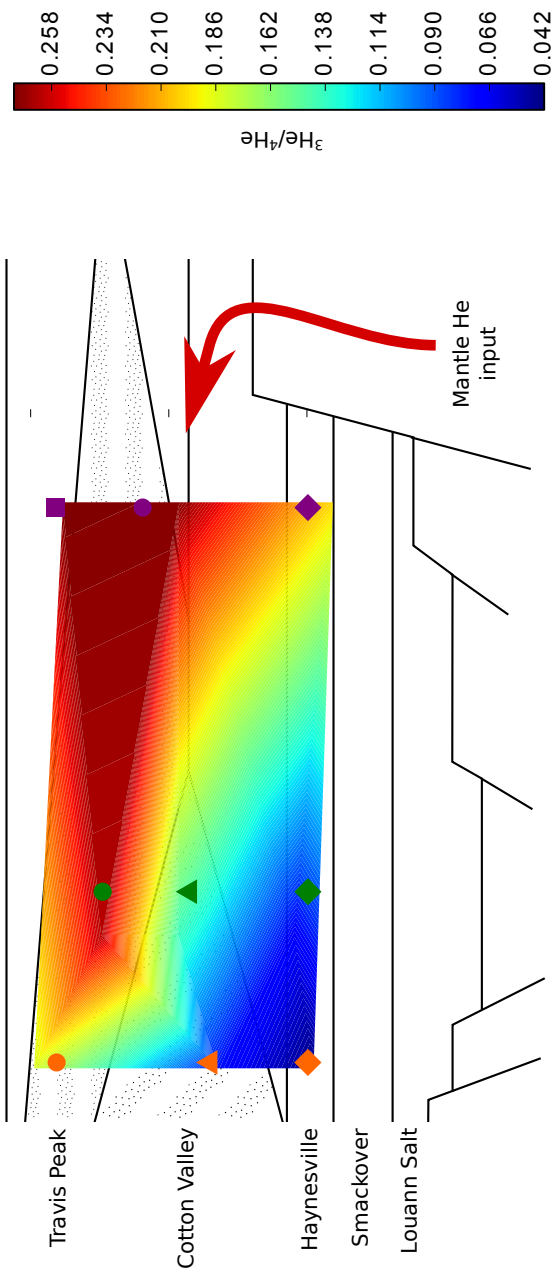

Figure 3.12: Illustration of distribution of ^{3}He/^{4}He isotope ratios within the basin, along with interpreted introduction pathway of mantle He, see text for full explanation.

3.5.6 Numerical modelling of mantle helium input

The unintuitive distribution of helium isotopes described in the previous section leads to the question of how these exotic isotopes are introduced into the various reservoirs, in such a fashion as to produce the observed data. The behaviour of helium within groundwater must obey the laws of solute transport in porous media. These are well-understood and encapsulated in the advection-diffusion-reaction equation in Eq. 3.17 as follows.

$$\frac{\partial c}{\partial t} = \nabla \cdot (\tau D \nabla c) - \nabla \cdot (\phi \mathbf{u} c) + R \tag{3.17}$$

Where c is the concentration of the species of interest in the groundwater, D is the diffusion coefficient, $\mathbf{u}$ is the velocity vector, ϕ is porosity, and R is the net result of any reactions that contribute or remove the species from solution. Being inert, helium does not participate in any chemical reactions, but the radiogenic production of helium must be considered as source in the subsurface over geological time. The effects of the porous media on diffusion are represented by the tortuosity τ, which can be defined in several ways but is often approximated as ϕ^2 (Dullien, 1979).

In the system under consideration, we make the assumption that mantle helium is delivered from depth along the southern edge of the basin, through the Sabine Island basin uplift (see Fig. 3.1 and 3.2). This assumption is justified by: (i) the observed pattern of $^3He/^4He$ ratios being consistently higher in the south, (ii) several previous studies showing that fault-bounded basement blocks are associated with high $^3He/^4He$ ratios (Hooker et al., 1985; Oxburgh et al., 1986), and (iii) the presence of the thick impermeable Louann Salt in the centre of the basin, likely precluding any vertical migration here. An illustration of the distribution of mantle helium isotopes and the interpreted transport pathway is shown in Fig. 3.12. This assumption infers that mantle helium must be transported 10's of kilometres across the basin from the Southern edge.

A simple 1D consideration of helium diffusion in sediments tells us that purely diffusive mechanisms are incapable of providing the transport flux necessary. The

characteristic timescale for diffusion, $t = L^2/(\tau D)$, is much higher than could be considered reasonable. The diffusion coefficient of helium at 400K is 24×10^{-5}cm^{2}s^{-1} (Jähne et al., 1987), and tortuosity in a shale with porosity of 10% would be 0.01. For transport over a distance L=10km this results in a characteristic timescale of t=12Gyr, and even a conservative estimate of 40% porosity in a sandstone would result in t=800Myr, much older than the basin itself.

We can also consider advection under Darcy's law.

$$u = -\frac{k}{\mu\phi}\delta p \tag{3.18}$$

Where u is velocity, k is permeability, δp is pressure gradient, μ is the viscosity of water (~8.9×10^{-4}Pas), and ϕ is porosity. To achieve a velocity of 1kmMyr^{-1} a typical shale with k=1×10^{-11}cm^2 requires a pressure gradient of 2100Pakm^{-1}, whereas for a sandstone it will be considerably smaller. To investigate fluid flow mechanisms, we utilised a finite-element model implemented in crunchflow - a specialised software package for solving reactive-transport equations in porous media (Steefel and Lasaga, 1994).

Firstly, we input a representative cross-sectional stratigraphic representation of the region, produced from basin-modelling and gridded it into a 100x100 2D space (Fig. 3.13). We then populated porosity, permeability, and tortuosity properties for the different stratigraphic layers using well-established methods for estimating these parameters as a function of depth, and lithology (Athy, 1930; Pittman, 1992). The upper edge of the model space is treated as an open boundary to the atmosphere, and the Louann Salt, being impermeable, acts as an effectively closed boundary along the bottom edge.

Evolution of the model under a purely diffusive regime failed to introduce significant quantities of ^{3}He into the relevant strata, even over Myr timescales. However, the introduction of even a small pressure gradient of 10Pakm^{-1} across the basin, results in an evolution towards a distribution close to that observed in the data (Fig. 3.13). The key features of the behaviour of the model under these conditions are that horizontal advection is effectively confined to the more

permeable sandstone layers. As expected, there is no significant advection in the impermeable shales. However, the movement of fluids in adjacent permeable strata, allows vertical diffusion of ^{3}He into the impermeable layers over Myr timescales. The combination of these effects produces the observed wedge-shaped intrusion of mantle ^{3}He into the basin, with highest ^{3}He/^{4}He in the shallower, more permeable zones.

3.6 Conclusion

In summary, we present new noble gas isotope and abundance data for natural gases sampled from 27 wells in East Texas, USA. The presence of both unconventional source-rock reservoirs and associated conventional gas accumulations in this basin allows us to use these data to investigate the geochemical effects and behaviour of natural gas migration and gain insight into the interconnectivity of these systems. There are significant differences in both noble gas abundance and isotope ratios between unconventional and conventional samples. Abundances of both atmosphere-derived isotopes and radiogenic isotopes increase dramatically in conventional accumulations, demonstrating the importance of migration in the acquisition of these isotopes. Helium isotopes are also higher in conventional samples, showing that mantle fluids are correspondingly incorporated during migration.

We combine air-derived and radiogenic noble gas data to calculate gas-water volume ratios, as well as the total encountered rock volume during migration. We extend these models to validate conceptual models of migration behaviour (Schowalter, 1979; Allan, 1989), and conclude that gas migration occurs along relatively confined pathways. These observations improve our understanding of gas migration behaviour and provide insight into wider basin dynamics and the connectivity of hydrocarbon reservoirs. In a petroleum systems context, oil and/or natural gas forms one part of a complex multi-phase regime including groundwater and CO_2-rich mantle fluids (Magoon and Dow, 1994; Prinzhofer et al., 2010; Vengosh et al., 2014). Understanding the interplay between these has crucial implications not only for hydrocarbon production, but also for contamination (Darrah et al., 2014; Woda et al., 2018), and containment of CO_2 (Gilfillan et al., 2009; Györe

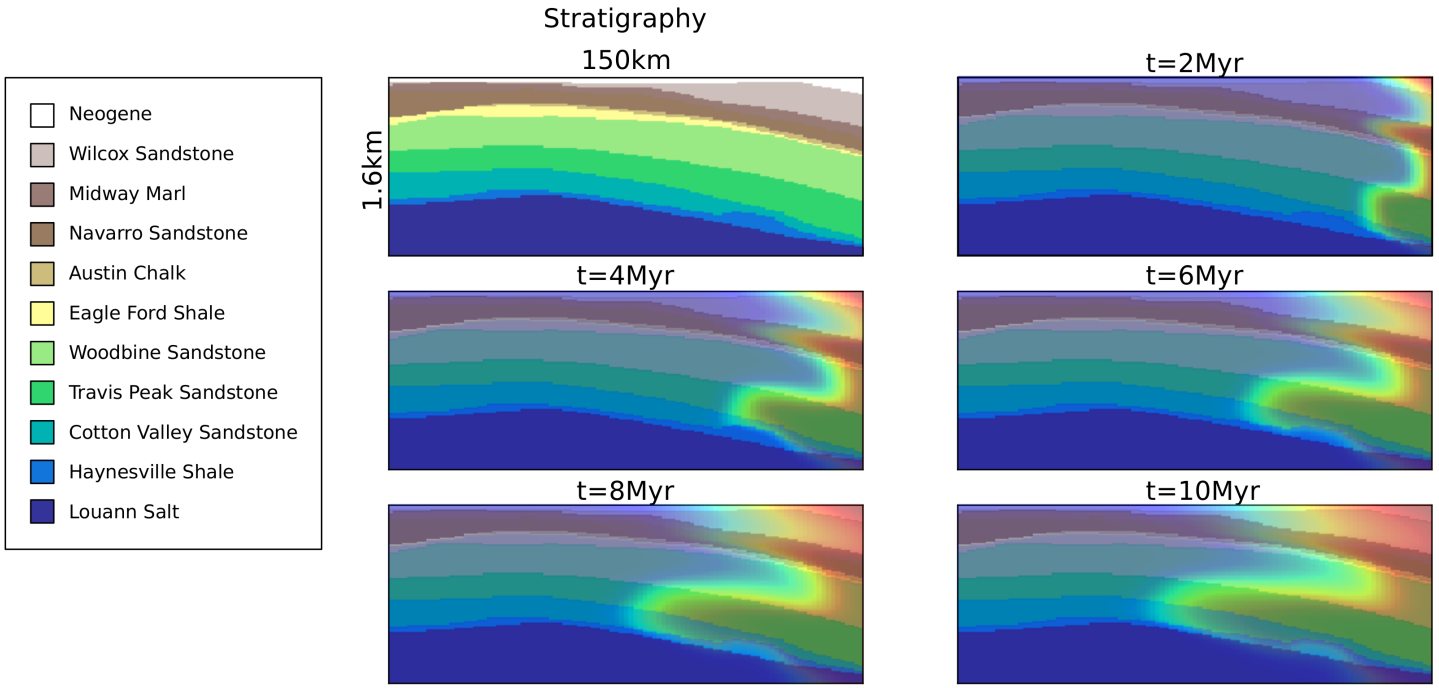

Figure 3.13: Model of mantle helium influx into the East Texas basin. Stratigraphy is shown in top-left panel, with other panels showing He influx over time. Colour ramp indicates input of mantle He on an arbitrary scale, ranging from zero to mantle endmember composition.

et al., 2015) or nuclear waste (Osenbrück et al., 1998; Hendry et al., 2015). The results from this study show clearly that mantle fluid incorporation is a function of migration distance from the source-rock for natural gases, and that input of mantle-sourced fluids could be across lengthscales of up to 100's of km. The high abundance of radiogenic isotopes further suggest interaction with large volumes of old groundwater. Together these are indicative of a remarkably well-connected and intrinsically interlinked subsurface fluid system in the basin as a whole.

4

Behaviour of geothermal fluids in Iceland

Contents

Abstract

Geothermal fluids are a key geochemical component in volcanic systems. Noble gases are ideal tracers of fluid provenance and processes in the subsurface. We present new data for complete noble gas isotope and abundance data (He, Ne, Ar, Kr, Xe) from 29 geothermal gases: 16 from geothermal power boreholes and 13

from naturally-degassing fumaroles. Samples are taken from both the Northern Rift Zone (NRZ) and Western Rift Zone (WRZ) of Iceland. Helium isotope ratios are MORB-like in the NRZ, with values in excess of MORB up to $16.92R_a$ in the WRZ. Neon isotopes show enrichment in primordial $^{20}Ne/^{22}Ne$, plotting close to the solar-air mixing line. Helium and neon isotope systematics are decoupled, consistent with previous studies. Argon, krypton and xenon isotopes are indistinguishable from air. Atmosphere-derived noble gas (ANG) isotopes (^{20}Ne, ^{36}Ar, ^{84}Kr, ^{130}Xe) are strongly correlated and show evidence for solubility-controlled fractionation. A pure air-saturated water source for these ANG isotopes is not consistent with our observations, and instead a small (10%) external contribution with a similar composition to that observed in sediments is required. Multiple-stage gas-water equilibration is required to explain the observed magnitudes of ANG fractionation, supporting repeated boiling/condensation/degassing episodes in the subsurface geothermal system. Concentrations and stable isotope ratios of other major geochemical species show relationships with $^3He/^4He$ ratios. In some cases (δD and $\delta^{18}O$ of H_2O) this is likely to be a superficial relationship due to the geographic distribution of MORB vs OIB signals. However, other observed correlations (e.g. δD and $\delta^{13}C$ of methane) may be indicative of deeper source or process controls.

4.1 Introduction

Fluids in geothermal systems represent the conduits by which key geochemical fluxes are transferred between the interior of the Earth and its surface. Understanding the composition and behaviour of these fluids informs us about the nature of the interior reservoirs of the planet, and the processes of volatile element cycling between them. Geochemistry reveals that domains within the mantle have undergone different evolutionary histories (Zindler and Hart, 1986; Hofmann, 1997). The mechanisms by which these reservoirs transfer volatiles has crucial implications for the chemical inventories and state of the surface of the Earth's oceans and atmospheres (Varekamp et al., 1992; Canfield, 2004; Dasgupta and Hirschmann, 2010; Anderson and Poland, 2017).

Noble gases are ideal tracers in geochemical systems due to their inert nature, and distinct isotopic composition between different terrestrial reservoirs (Porcelli and Ballentine, 2002). They have been widely applied in terrestrial chemistry both to identify and delineate different volatile reservoirs (Sano et al., 1985; Poreda et al., 1992; Hilton et al., 1998; Marty and Zimmermann, 1999; Cartigny et al., 2001; Marty, 2012), and to estimate fluxes of volatile elements (Marty and Jambon, 1987; Marty and Tolstikhin, 1998; Barry et al., 2014; Lowenstern et al., 2014; Day et al., 2015; Boucher et al., 2018; Broadley et al., 2018). Furthermore, noble gases have a wide range of uses as tracers of fluid movement, age and interaction in the subsurface, allowing process and timing to be distinguished from source features (Ballentine and Hall, 1999; Kulongoski et al., 2003; Lehmann et al., 2003; Gilfillan et al., 2008; Gumm et al., 2015; Barry et al., 2016).

Iceland is an ideal natural laboratory for studying geothermal fluids. It exhibits a wide range of different geochemical environments and processes across a small region, as evidenced in the wide range of geochemical signatures observed in both fluids and lavas, for noble gases as well as as a number of other chemical tracers (Sigmarsson and Steinthórsson, 2007; Sigmarsson et al., 2008). It also has an abundance of geothermal fluid activity, with primary fluids composed of dilute meteoric water, making it easier to distinguish primary sources and processes affecting volatiles (Stefánsson et al., 2017). Finally, geothermal energy production from boreholes is widespread, as are many vigorously-degassing fumaroles, providing ample sampling opportunities with minimal atmospheric contamination (Füri et al., 2010).

In this study we present full noble gas isotope and abundance data from 13 fumarole and 16 borehole fluids (He, Ne, Ar, Kr and Xe). Samples are taken from a range of geographic locations in Iceland, representing different geothermal regimes. We discuss fluid provenance, and investigate geothermal fluid behaviour using elemental ratios of atmosphere-derived noble gas isotopes. We also compare noble gas isotope data to major gas geochemistry and stable isotope data.

4.2 Geological setting and background

4.2.1 Overview

The unique geology of Iceland is a result of the interaction between the Mid-Atlantic divergent plate boundary and the Iceland mantle plume. The island itself represents a subaerial section of the Mid-Atlantic ridge, emergent from the ocean due to enhanced crustal thickness from the increased melting associated with the mantle hotspot (White et al., 1995; Darbyshire et al., 2000). Seismic tomography studies show a clear region of anomalously low P- and S-wave velocities beneath central Iceland, indicative of an underlying mantle hotspot (Bjarnason et al., 1993; Wolfe et al., 1997). The ultimate source of this hotspot is not completely resolved, with some studies claiming a shallow source (Ritsema et al., 1999), and others suggesting that it may extend as deep as the core-mantle boundary (Helmberger et al., 1998; Bijwaard and Spakman, 1999; Zhao, 2004). The geological landscape has also been relatively dynamic on geological timescales. The plate boundary itself is migrating westward relative to the mantle plume (Bjarnason, 2008), and there is both geochemical and geophysical evidence for dynamic mantle plume behaviour over time (Marty et al., 1998; Poore et al., 2009; Parnell-Turner et al., 2014).

4.2.2 Neovolcanism

Current volcanic activity on Iceland is ubiquitous, and falls primarily into two types of neovolcanic zones. Axial rift zones connect the Mid-Atlantic ridge across the island from the Kolbeinsey ridge in the North to the Reykjanes ridge in the South. In Northern Iceland the axial rift is constrained to a single Northern Rift Zone (NRZ), whilst in the Southern part of the island it is separated into distinct Eastern and Western Rift Zones (ERZ and WRZ), separated by a seismically-active transform fault region known as the South Iceland Seismic Zone (SISZ) (Einarsson, 2008). Off-axis volcanic flank zones lying around the central rifts include the South Iceland Volcanic Zone (SIVZ), Snæfellsnes Volcanic Zone (SNVZ), the Öræfajökull Volcanic Zone (OVZ) and the older Vestfirðir region (Óskarsson et al., 1982; Jakobsson

et al., 2008). See Fig. 4.1 for a map of the different volcanic zones showing their distribution and relationship to the island.

4.2.3 Geochemical background

The geochemical evolution of Iceland is often interpreted as a result of mixing between a depleted MORB mantle endmember (DMM) and a mantle-hotspot endmember characteristic of ocean-island basalts (OIB). This mixing is evidenced in several geochemical parameters including La/Sm, $^{206}Pb/^{204}Pb$, $^{87}Sr/^{86}Sr$, $^{143}Nd/^{144}Nd$, and $^{3}He/^{4}He$ (Hart et al., 1973; Schilling, 1973; Sun et al., 1975; Taylor et al., 1997; Hilton et al., 2000; Thirlwall et al., 2004; Peate et al., 2010). However, other studies attribute trace element and Sr-Nd-Pb-Hf isotope variations to chemical and isotopic heterogeneities within the mantle source itself (Mertz et al., 1991; Hards et al., 1995; Kerr, 1995; Thirlwall, 1995; Chauvel and Hémond, 2000; Kempton et al., 2000; Fitton et al., 2003; Macpherson et al., 2005b).

In terms of the noble gases, $^{3}He/^{4}He$ ratios are supportive of MORB-OIB mixing, with values averaging ~8R_a in the NRZ, typical of MORB samples worldwide (Moreira et al., 1998; Graham, 2002; Harðardóttir et al., 2018), and higher ratios up to 24R_a in central Iceland and the ERZ, where the centre of the plume is inferred to be (Condomines et al., 1983; Tryggvason et al., 1983; Kurz et al., 1985; Breddam et al., 2000; Macpherson et al., 2005a). However, the highest $^{3}He/^{4}He$ ratios are reported from Vestfirðir, up to 34R_a (Hilton et al., 1999; Ellam and Stuart, 2004), although this region is also associated with a Bouguer gravity anomaly (Kaban et al., 2002). For a comprehensive review of helium isotope distributions across the island (in geothermal fluids, volcanic glasses and phyric lavas) as well as their relationship to the wider geochemical and geophysical characteristics of the region, see Harðardóttir et al., 2018.

4.2.4 Geothermal activity and geothermal fluids

Geothermal activity in Iceland is classified into low- and high-temperature systems, where high-temperature systems experience temperatures $\geq 150^{o}$C at depths of 1km (Bödvarsson, 1961; Fridleifsson, 1979). The majority of high-temperature systems

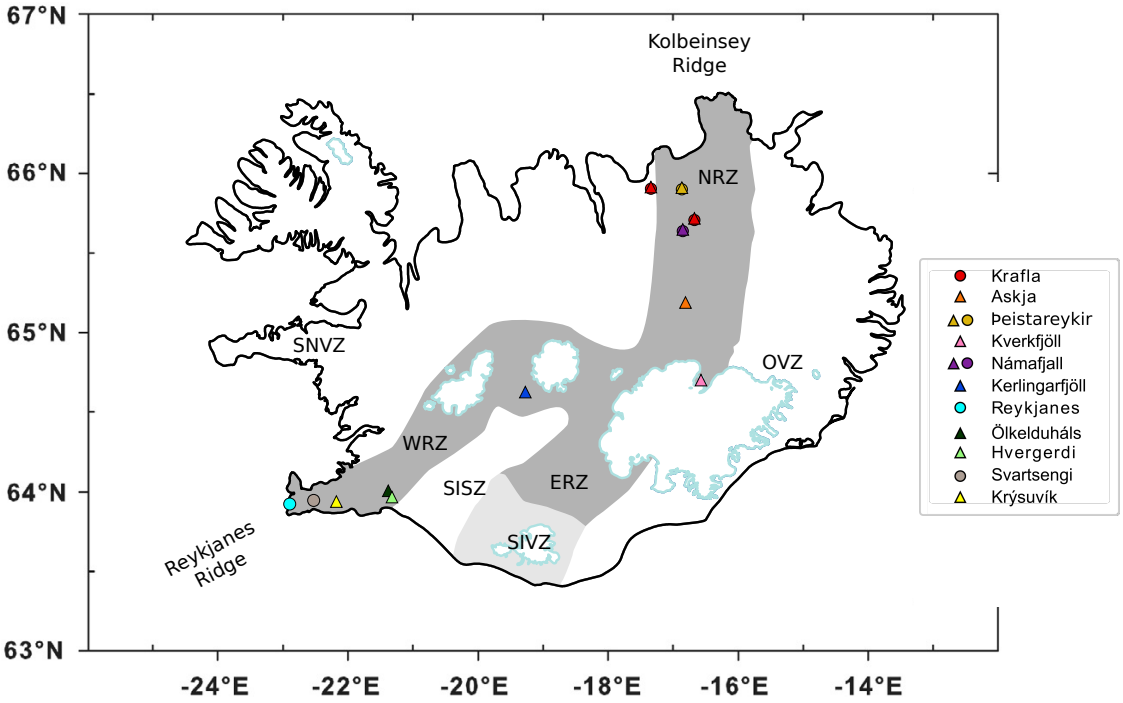

Figure 4.1: Map of Iceland, showing sample locations alongside principal volcanic provinces and areas of glacial coverage. In several cases multiple samples were taken in close proximity, and are represented with a single symbol. Locations where fumarole samples were taken are marked with a triangle, and borehole samples with a circle. Dark grey region is the main rift zone area across the island, connecting the Reykjanes and Kolbeinsey ridges. NRZ=Northern Rift Zone, WRZ=Western Rift Zone, ERZ = Eastern Rift Zone, SISZ = South Iceland Seismic Zone, SIVZ = South Iceland Volcanic Zone, SNVZ = Snæfellsnes Volcanic Zone, OVZ = Öræfajökull Volcanic Zone. Adapted from Barry et al., 2014.

are associated with the axial rift volcanic zones. Iceland makes extensive use of geothermal energy for district heating and electricity production, around 53% of the total energy consumed in Iceland comes from geothermal energy (Kristmannsdóttir and Ármannsson, 2003). For a classification of the different geothermal areas and their associated energy production, see Stefánsson et al., 2017.

4.3 Materials and Methods

Samples were collected across 3 sampling campaigns (2015, 2016, 2017), from both fumarole and borehole gases. Sample locations are shown in Fig. 4.1. Samples were collected in 10mm refrigeration-grade copper tubes, following procedures outlined in section 1.3.1. For borehole samples, a regulator was used to decrease the sampling

pressure down to 1-2bar. For fumarole samples a plastic funnel was used to seal around the degassing vent, and the exhaust tubing submerged in water to assist with flushing of air. A selection of samples were also collected for analysis of major gas geochemistry and stable isotopes, in both water and vapour phases. Noble gas abundance and isotope ratio measurements were carried out at the University of Oxford, following procedures outlined in section 1.4.2. Major gas abundance and stable isotope ratios were carried out at the University of Iceland.

4.4 Results

We report noble gas abundance data in Table 4.1 and noble gas isotope ratio data in Table 4.2. Abundances are reported for the wet gas bulk sample, including any water vapour that was present during sample collection. As such, the presence of variable contributions of steam to gas will be the cause of much of the variation in noble gas abundance.

4.4.1 Helium

Measured helium isotope ratios (^{3}He/^{4}He) are reported relative to the atmospheric ratio (where air = 1R$_a$) and show a range from 7.29 to 16.92. These values can be corrected for atmospheric helium in order to better represent the mantle isotope ratio itself. Helium isotopes show a clear distinction between NRZ sample sites (Krafla, Askja, Kverkfjöll, Námafjall, Þeistareykir) and WRZ (Kerlingarfjöll, Reykjanes, Ölkelduháls, Hvergerdi). NRZ samples range from 7.29 to 10.53R_a, consistent with typical MORB values from the Mid-Atlantic Ridge. The compilation by Graham, 2002 of 236 Mid-Atlantic MORB glass samples has a median=8.08, mean=9.58 with $\sigma = 2.94$. WRZ samples range from 11.41 to 16.92R$_a$, suggesting a greater mantle plume influence, where OIB values are typically elevated compared to MORB, up to 50R$_a$ (Stuart et al., 2003). Samples 15-AS-10, 16-AS-01 and 17-NM-3 are all produced from the same borehole, and their range from 7.51 to 9.44R$_a$ shows the potential for some variability in He isotope ratios through time. Overall, these new data are consistent with previous observations of the regional distribution of

Sample ID	Type	Location	Well	^{4}He ($\times10^{-7}$)	$\pm1\sigma$	^{20}Ne ($\times10^{-8}$)	$\pm1\sigma$	^{36}Ar ($\times10^{-7}$)	$\pm1\sigma$	^{84}Kr ($\times10^{-10}$)	$\pm1\sigma$	^{130}Xe ($\times10^{-10}$)	$\pm1\sigma$
17-ÞEI-1	B	Þeistareykir	w7	0.81	0.03	1.51	0.03	1.33	0.03	27.44	0.10	0.31	0.01
17-ÞEI-H	F	Þeistareykir		0.27	0.01	43.60	0.88	37.81	0.87	325.97	1.23	2.38	0.04
17-KRA-4	B	Krafla	w20	124.42	5.09	57.30	1.16	19.11	0.44	552.86	2.09	5.48	0.09
17-KRA-2	B	Krafla	w31	45.67	1.87	7.87	0.16	2.75	0.06	95.00	0.36	1.29	0.02
17-KRA-5	B	Krafla	w1	23.02	0.94	7.40	0.15	6.48	0.15	140.23	0.53	1.70	0.03
17-KRA-B	F	Krafla		256.49	10.48	49.30	1.00	18.72	0.43	603.47	2.28	7.24	0.13
17-KRA-1	B	Krafla	w34	115.00	4.70	6.81	0.14	18.18	0.42	337.29	1.27	4.01	0.07
17-ASK-3	F	Askja		43.31	1.77	1.24	0.03	0.98	0.02	27.02	0.10	0.33	0.01
17-ASK-1	F	Askja		47.10	1.93	1.45	0.03	1.08	0.02	23.71	0.09	0.28	0.00
17-KVE-2	F	Kverkfjöll		111.51	4.56	7.69	0.16	6.00	0.14	69.51	0.26	0.69	0.01
17-KVE-K	F	Kverkfjöll		107.74	4.40	3.02	0.06	2.41	0.06	39.64	0.15	0.46	0.01
17-KVE-1	F	Kverkfjöll		126.50	5.17	32.70	0.66	10.08	0.23	272.86	1.03	2.95	0.05
17-NM-3	B	Námafjall	w9	63.74	2.61	49.20	0.99	20.69	0.48	726.62	2.75	8.72	0.15
15-AS-02	F	Krýsuvík		62.96	1.69	23.29	0.47	8.06	0.19	243.35	0.92	2.75	0.05
15-AS-17	B	Reykjanes	w15	371.78	9.96	95.65	1.93	29.94	0.69	738.98	2.79	8.64	0.15
15-AS-06	F	Kerlingarfjöll		36.07	0.97	23.72	0.48	10.21	0.24	275.51	1.04	3.42	0.06
15-AS-08	B	Krafla	w16	56.07	1.50	19.11	0.39	6.62	0.15	190.40	0.72	2.15	0.04
15-AS-10	B	Námafjall	w9	47.02	1.26	54.27	1.10	21.39	0.49	n.d.		8.63	0.15
16-AS-01	B	Namafjall	w9	34.58	0.93	32.46	0.66	13.92	0.32	466.24	1.76	5.70	0.10
16-AS-02	B	Námafjall	w13	2.35	0.06	16.83	0.34	5.55	0.13	170.96	0.65	1.88	0.03
16-AS-08	F	Námafjall		31.71	0.85	189.93	3.84	43.09	0.99	n.d.		9.79	0.17
16-AS-03	B	Krafla	w37	4.53	0.12	1.02	0.02	0.44	0.01	16.31	0.06	0.24	0.01
16-AS-04	B	Krafla	w31	32.57	0.87	37.96	0.77	11.78	0.27	329.24	1.24	3.76	0.07
16-AS-10	F	Ölkelduháls		115.15	3.08	25.68	0.52	8.90	0.21	270.27	1.02	3.17	0.05
16-AS-11	F	Hvergerdi		19.90	0.53	79.89	1.62	25.95	0.60	661.24	2.50	7.96	0.14
16-AS-12	F	Hvergerdi		99.81	2.67	116.55	2.36	40.99	0.94	n.d.		14.52	0.25
16-AS-13	B	Svartsengi	w9	1.82	0.05	0.73	0.01	0.95	0.02	45.67	0.17	0.64	0.01
16-AS-14	B	Svartsengi	w11	0.39	0.01	0.29	0.01	0.34	0.01	14.12	0.05	0.21	0.01
16-AS-17	B	Reykjanes	w11	55.24	1.48	17.85	0.36	5.63	0.13	177.25	0.67	1.95	0.03

Table 4.1: Concentrations of noble gases in Iceland geothermal gas samples. Concentration units are in cm^3STPcm^{-3}. B = Borehole sample, F = Fumarole sample.

Sample ID	Type	Location	Well	$^{3}He/^{4}He$ (R/R_a)	$\pm1\sigma$	$^{20}Ne/^{22}Ne$	$\pm1\sigma$	$^{21}Ne/^{22}Ne$	$\pm1\sigma$	$^{40}Ar/^{36}Ar$	$\pm1\sigma$
17-ÞEI-1	Borehole	Þeistareykir	w7	9.60	0.42	10.07	0.05	0.0335	0.0003	260.8	2.6
17-ÞEI-H	Fumarole	Þeistareykir		9.67	0.44	10.01	0.05	0.0325	0.0003	267.0	3.0
17-KRA-4	Borehole	Krafla	w20	7.29	0.35	9.83	0.05	0.0302	0.0003	302.6	3.5
17-KRA-2	Borehole	Krafla	w31	7.41	0.34	9.92	0.05	0.0283	0.0003	307.3	4.0
17-KRA-5	Borehole	Krafla	w1	10.53	0.48	9.76	0.05	0.0311	0.0003	272.6	2.8
17-KRA-B	Fumarole	Krafla		9.28	0.33	9.48	0.05	n.d.		297.0	3.3
17-KRA-1	Borehole	Krafla	w34	9.19	0.35	n.d.		n.d.		n.d.	
17-ASK-3	Fumarole	Askja		10.15	0.40	9.96	0.05	0.0294	0.0003	295.2	3.6
17-ASK-1	Fumarole	Askja		10.33	0.48	10.01	0.05	0.0276	0.0003	316.1	4.0
17-KVE-2	Fumarole	Kverkfjöll		8.42	0.30	9.53	0.05	0.0270	0.0003	306.6	3.7
17-KVE-K	Fumarole	Kverkfjöll		8.46	0.35	9.72	0.05	0.0282	0.0003	299.6	3.6
17-KVE-1	Fumarole	Kverkfjöll		8.30	0.32	9.34	0.05	0.0260	0.0003	300.4	3.7
17-NM-3	Borehole	Námafjall	w9	9.44	0.42	9.71	0.05	0.0264	0.0003	302.7	3.5
15-AS-02	Fumarole	Krýsuvík		11.41	0.39	9.94	0.05	0.0292	0.0003	301.2	3.2
15-AS-17	Borehole	Reykjanes	w15	14.61	0.54	9.86	0.05	0.0291	0.0003	305.1	3.3
15-AS-06	Fumarole	Kerlingarfjöll		14.26	0.59	9.86	0.05	0.0291	0.0003	303.9	3.0
15-AS-08	Borehole	Krafla	w16	8.77	0.31	9.92	0.05	0.0292	0.0003	300.0	3.8
15-AS-10	Borehole	Námafjall	w9	7.51	0.33	9.78	0.05	0.0290	0.0003	307.0	3.2
16-AS-01	Borehole	Námafjall	w9	7.98	0.36	9.77	0.05	0.0289	0.0003	306.1	4.2
16-AS-02	Borehole	Námafjall	w13	8.55	0.33	10.00	0.05	0.0293	0.0003	303.5	4.0
16-AS-08	Fumarole	Námafjall		10.28	0.45	9.67	0.05	0.0288	0.0003	307.1	3.5
16-AS-03	Borehole	Krafla	w37	10.19	0.44	10.35	0.05	0.0293	0.0003	273.1	3.5
16-AS-04	Borehole	Krafla	w31	9.04	0.43	9.89	0.05	0.0292	0.0003	301.1	3.9
16-AS-10	Fumarole	Ölkelduháls		15.62	0.58	9.90	0.05	0.0292	0.0003	302.9	3.6
16-AS-11	Fumarole	Hvergerdi		15.90	0.71	9.81	0.05	0.0290	0.0003	304.4	3.4
16-AS-12	Fumarole	Hvergerdi		16.92	0.76	9.80	0.05	0.0290	0.0003	305.6	3.2
16-AS-13	Borehole	Svartsengi	w9	14.47	0.67	9.87	0.05	0.0284	0.0003	n.d.	
16-AS-14	Borehole	Svartsengi	w11	13.28	0.60	10.04	0.05	0.0241	0.0002	n.d.	
16-AS-17	Borehole	Reykjanes	w11	14.73	0.52	9.92	0.05	0.0292	0.0003	304.9	3.2

Table 4.2: Noble gas isotope ratios for Iceland geothermal gas samples. Helium isotope ratios are reported relative to the atmospheric ratio $R_a = 1.4 \times 10^{-6}$ (Porcelli et al., 2002)

helium isotope ratios in Icelandic geothermal fluids (Torgersen and Jenkins, 1982; Sano et al., 1985; Hilton et al., 1990; Marty et al., 1991; Poreda et al., 1992; Hilton et al., 1998; Füri et al., 2010; Harðardóttir et al., 2018). Helium concentrations (^{4}He) range from 0.39 to 371.78 $\times 10^{-7}$cm^{3}STPcm^{-3}

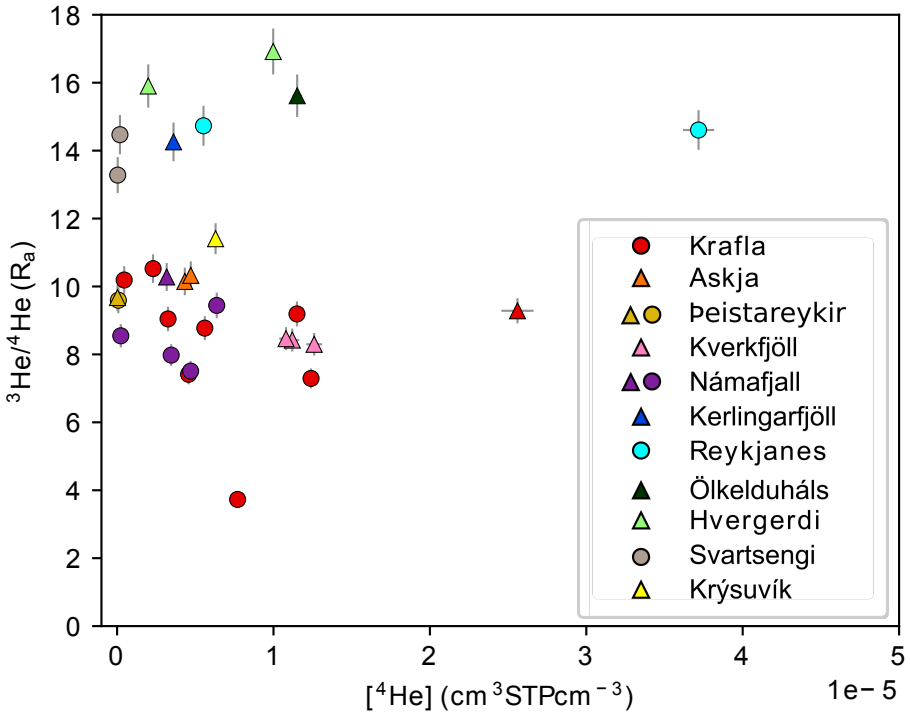

Figure 4.2: Plot of helium isotope and concentration data for Iceland geothermal fluid samples. Fumarole samples are denoted by triangles, and borehole samples by circles. Isotope ratios are reported relative to the atmpspheric ratio $R_a = 1.4 \times 10^{-6}$.

4.4.2 Neon

Neon isotope ratios (^{20}Ne/^{22}Ne and ^{21}Ne/^{22}Ne) in volcanic systems are typically interpreted as mixing between atmospheric values, for which ^{20}Ne/^{22}Ne = 9.78 and ^{21}Ne/^{22}Ne = 0.029 (Sano et al., 2013b), and a variety of different mantle endmembers (Craig and Lupton, 1976). The primordial neon isotope composition of the Earth is assumed to be approximately that of solar values, which are strongly elevated in ^{20}Ne/^{22}Ne (=13.78) and moderately in ^{21}Ne/^{22}Ne (=0.0329) when compared to air (Heber et al., 2009). This results in a steep mixing slope when plotted on a 3-isotope neon plot, as in Fig. 4.3. Radiogenic production of ^{21}Ne

and ^{22}Ne through Wetherill reactions (Wetherill, 1954), will decrease ^{20}Ne/^{22}Ne and increase ^{21}Ne/^{22}Ne over time. OIB samples typically plot closer to the solar neon mixing line, with MORB samples following a distinct, shallower trend (Sarda et al., 1988; Trieloff et al., 2000; Graham, 2002).

The majority of our samples plot close to, but slightly below the solar neon mixing line, as shown in Fig. 4.3, although there is some scatter in other samples. This is consistent with measurements of glasses by Trieloff et al., 2000, and previous studies of Icelandic neon isotopes (Füri et al., 2010). Interestingly, both samples from Þeistareykir appear to plot along the MORB mixing line. This might be expected, as their He isotope ratios support a predominantly MORB source, but He and Ne isotope systematics in Iceland are often observed to be uncorrelated (Dixon et al., 2000; Trieloff et al., 2000; Moreira et al., 2001; Dixon, 2003). This 'decoupling' of He and Ne isotopes is likely due to mixing of distinct mantle endmembers, degassing fractinoation, and interaction with atmospheric sources (Füri et al., 2010).

4.4.3 Argon

Argon isotope ratios (^{40}Ar/^{36}Ar) are predominantly similar to the atmospheric ratio of 298.6 (Lee et al., 2006). There are however several samples that have measured ratios significantly lower than the atmospheric value. As there is no known reservoir with such low Ar isotope ratios it is likely that these were fractionated during sample collection and/or storage. Several of the affected samples (e.g. 17-KRA-1) that have anomalous Ar isotope ratios also have anomalous Ne isotope ratios. The presence of mantle argon would be indicated by elevated ^{40}Ar/^{36}Ar, as the mantle reservoir has ^{40}Ar/^{36}Ar$\approx 10,000$ (Graham, 2002). The lack of elevated argon isotope ratios in our sample suggests that the argon is overwhelmingly introduced from an atmospheric source, likely the shallow circulation of air-saturated water (ASW). Ar abundances (^{36}Ar) range from 0.39 to 43.09 $\times 10^{-7}$cm^{3}STPcm^{-3}.

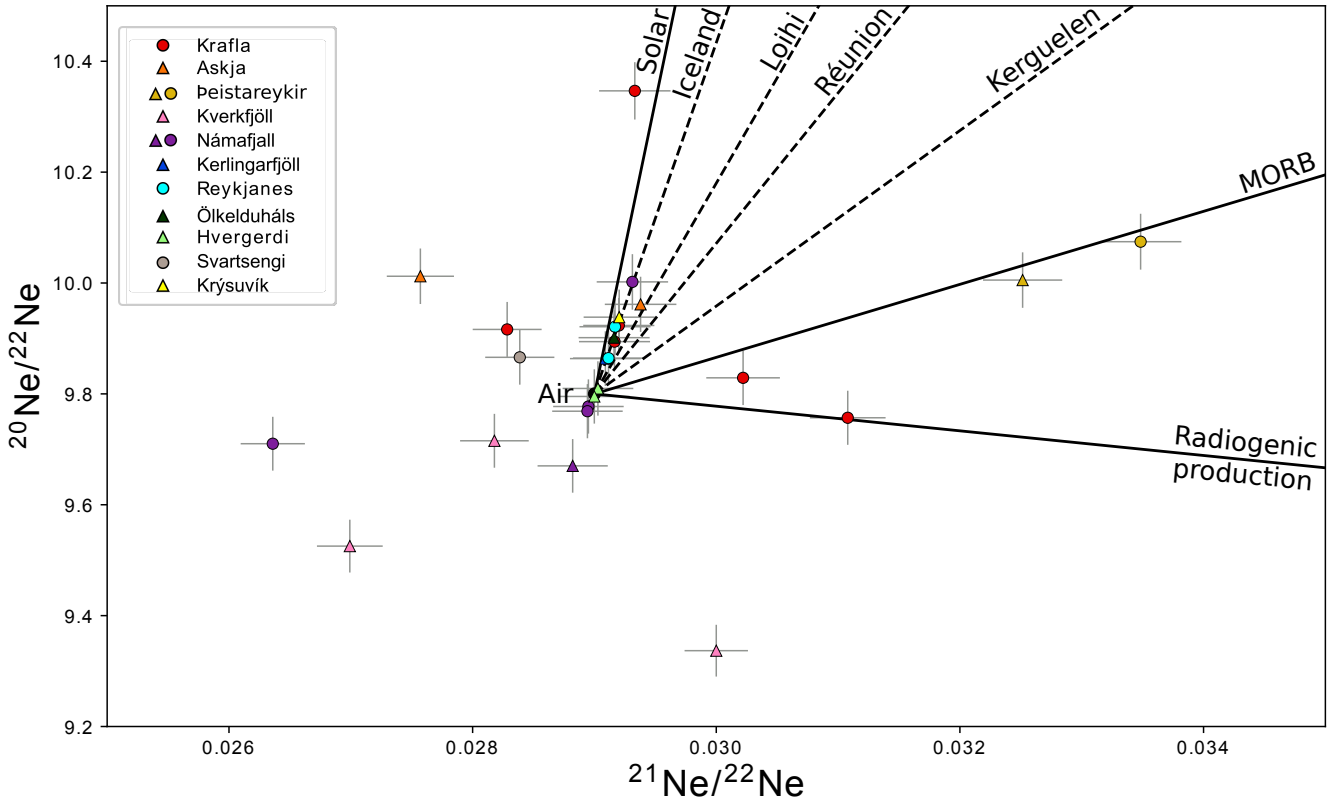

Figure 4.3: Neon 3-isotope plot for Iceland geothermal fluids. Mixing lines are shown between the isotopic composition of the atmosphere and a series of different endmembers, including MORB, Solar, and a series of different OIB's. These different mixing trajectories are calculated from a series of datasets compiled in Graham, 2002. Fumarole samples are plotted as triangles, and borehole samples as circles.

4.4.4 Krypton and xenon

Krypton and xenon isotope ratios are all indistinguishable from air, and are not reported here. Kr abundances (^{84}Kr) range from 14.12 to 738.98 $\times 10^{-10}$cm^{3}STPcm^{-3}, and Xe abundances (^{130}Xe) from 0.28 to 14.52 $\times 10^{-10}$cm^{3}STPcm^{-3}.

4.5 Discussion

4.5.1 Atmosphere-derived noble gas isotopes

The distribution of atmosphere-derived noble gas (ANG) isotopes (^{20}Ne, ^{36}Ar, ^{84}Kr, ^{130}Xe) has previously been successfully applied to investigate gas-water phase interactions and partitioning in subsurface groundwater and petroleum systems (Mazor, 1972; Ballentine et al., 1996; Castro et al., 1998a; Barry et al., 2016; Tolstikhin et al., 2017) . ANG isotopes are not produced radiogenically in the subsurface, nor are they found in significant amounts in other endmembers (Ballentine et al., 2002). Their provenance in geothermal fluids can therefore be attributed completely to processes delivering atmospheric isotopes into the subsurface. This is principally dissolved in air-saturated water, which equilibrates at the surface and then flows through subsurface aquifers (Aeschbach-Hertig et al., 2000). The composition of ASW is well-constrained (Kipfer et al., 2002). Once in the subsurface, this initial distribution can be fractionated by solubility-controlled processes such as dissolution, exsolution, boiling and condensation (Ballentine et al., 2002).

In Fig. 4.4, we plot concentrations of the ANG isotopes. Their abundances are all strongly correlated, and range across several orders of magnitude. Very low concentrations are observed in 2 samples from the Krafla geothermal plant, 2 boreholes from the Reykjanes region (both from the Svartsengi geothermal plant), fumarole samples from Askja and Kverkfjöll and the Þeistareykir borehole sample.

In Fig. 4.5 we show inter-elemental ratios of ANG isotopes (^{20}Ne/^{36}Ar, ^{84}Kr/^{36}Ar, ^{130}Xe/^{36}Ar and ^{84}Kr/^{130}Xe). These ratios show clear relationships, strongly suggestive of solubility-controlled processes. ^{84}Kr/^{36}Ar vs ^{130}Xe/^{36}Ar is very strongly

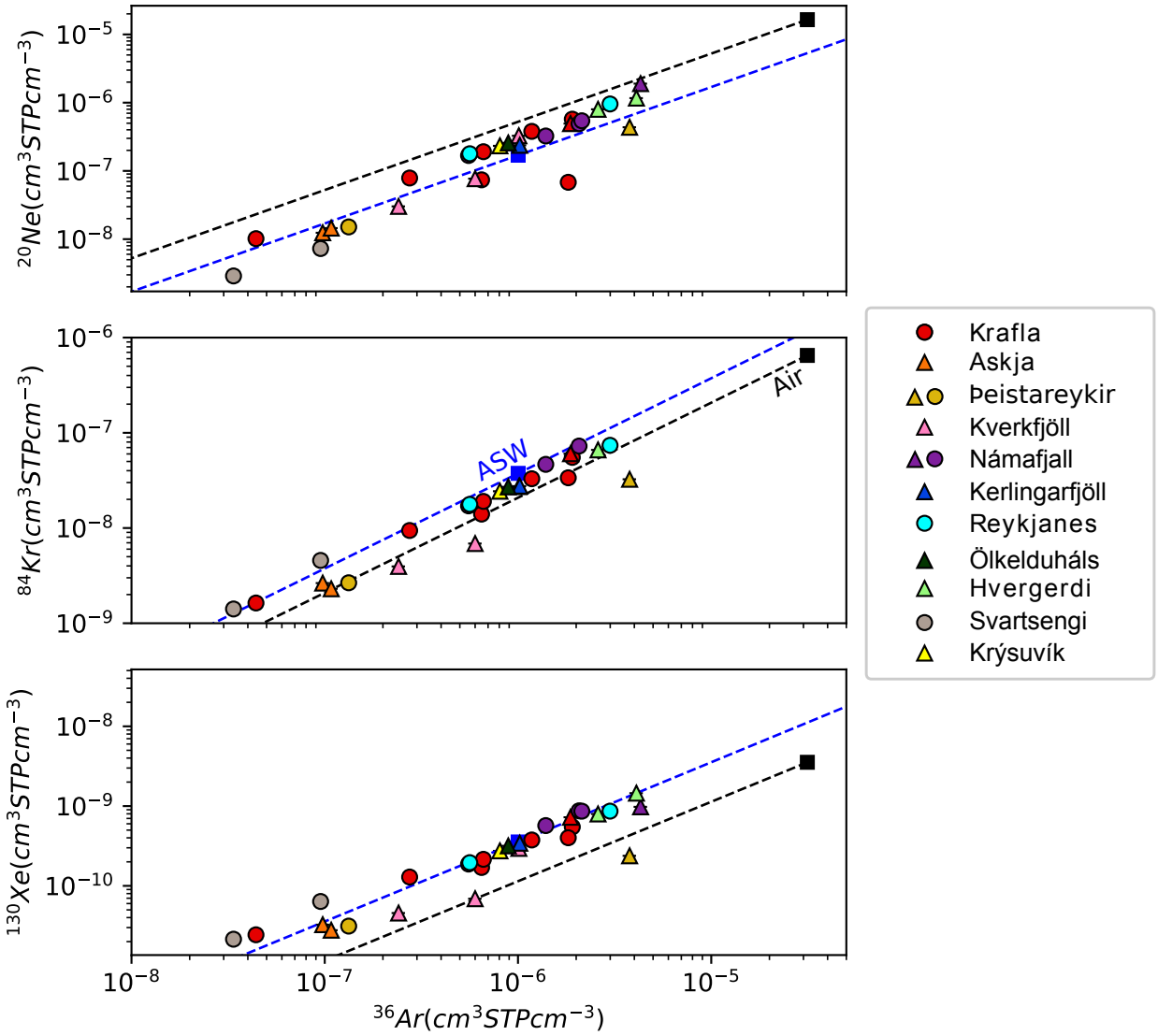

Figure 4.4: Concentrations of atmosphere-derived noble gas isotopes. Atmospheric and ASW (freshwater at 10°C) compositions are marked by the black and blue squares respectively. Dotted lines are 1:1 trajectories of dilution/concentration and represent the effects of addition/removal of carrier gas phases without fractionating the elemental ratios. Fumarole samples are plotted as triangles, and borehole samples as circles.

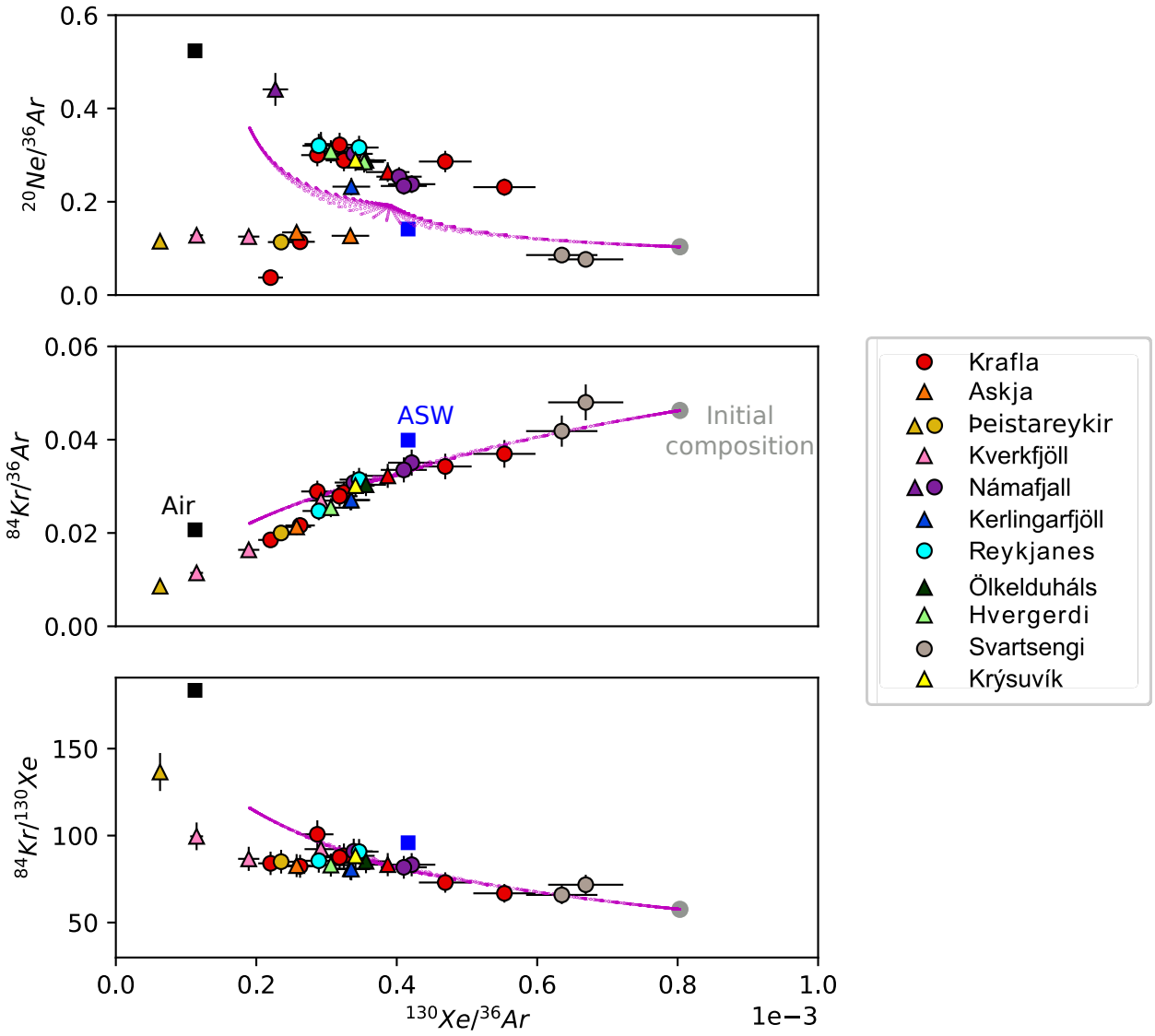

Figure 4.5: Inter-elemental ratios of atmosphere-derived noble gas isotopes in Iceland geothermal fluids. Atmospheric and ASW (freshwater at 10^{o}C) compositions are marked by black and blue squares respectively. Sedimentary endmember is off-scale, and has a composition of ^{20}Ne/^{36}Ar=0.026, ^{84}Kr/^{36}Ar=0.059, ^{130}Xe/^{36}Ar=0.0016, ^{84}Kr/^{130}Xe=37 (Staudacher and Allègre, 1988). Pink domain represents the range of potential compositions that can be achieved by 2-stage gas-water partitioning starting from a composition of ASW plus a 10% sediment contribution, at a temperature of 300K.

correlated for all samples. The gradient of the trend is almost exactly the same as the offset between air and the initial ASW composition, which is expected for solubility-dependent fractionation. However, there is a clear offset showing a small Xe-enrichment relative to the air-ASW line. This, alongside the fractionations in excess either side of air and ASW rule out simple mixing to explain the trend.

The relationship for $^{20}Ne/^{36}Ar$ vs $^{130}Xe/^{36}Ar$ is similar for the majority of samples. However, there is a subset that show strongly ASW-like Ne/Ar, whilst still preserving fractionated Xe/Ar. This could be due to a later addition of pristine ASW, which due to being enriched in Ne and Ar, could strongly affect Ne/Ar ratios whilst still preserving Kr and Xe variations. The samples which have ASW-like Ne/Ar are also the samples which were observed to have the lowest abundances in Fig. 4.4. It is possible that these samples were collected from boreholes producing very little gas and large amounts of water/steam rich in ASW-like Ne/Ar.

The observed trends can be explained by the presence of a small contribution of sedimentary noble gases to the initial ASW composition. Sedimentary noble gases are enriched in Kr and Xe, which would account for the shifting of the data to higher Xe/Ar values (Staudacher and Allègre, 1988) . Iceland is primarily composed of volcanic rather than sedimentary rocks, making the presence of 'sedimentary' noble gases puzzling. However, the process responsible for the acquisition of enriched Xe and Kr in sediments is thought to be adsorption (Podosek et al., 1980), and it is possible that Icelandic basalts also experience this sorptive enrichment to some extent. Alternatively, groundwaters may acquire this component whilst flowing through surficial soils, which would have a high sorptive capacity.

If we allow our initial composition to contain 10% of a sedimentary composition in addition to ASW, we can explain the majority of the data using solubility-controlled models. The partitioning of a noble gas species following Henry's law between a gas and an initial water phase can be calculated using Eq. (4.1), after Ballentine et al., 2002, and Barry et al., 2016.

$$[i]_g = \left(\frac{224T}{2730\gamma_i K_i \times (V_g/V_w)} + 1\right)^{-1} \times [i]_{asw} \tag{4.1}$$

Where $[i]_g$ and $[i]_{asw}$ are the number of moles of noble gas i in the gas and initial air-saturated water phase respectively, γ_i is the salinity-dependent Setschenow coefficient (Smith and Kennedy, 1983), K_i is the Henry's coefficient (Fernández-Prini et al., 2003), V_g/V_w is the gas to water volume ratio, and T is temperature. It can be seen that for large V_g/V_w the number of moles in the gas phase is equal to the initial number of moles in the water phase, maximum fractionation occurs at low V_g/V_w. We can calculate predicted fractionation of inter-elemental ratios simply by performing the above calculation for each species and comparing. Here we assume that the effects of salinity are minimal, and that $\gamma_i \approx 1$.

In Fig. 4.5 the pink domain represents the possible compositions that can be attained in the gas phase using a double-stage gas-water equilibrium partitioning model, starting from a dissolved composition of ASW plus 10% sediments, and equilibrating at a temperature of 300K. The trajectory of the fractionation is in the correct direction for all the observed ratios. However, the magnitude of the observed fractionation is greater for a number of samples. This indicates several episodes of solubility-dependent partitioning in a multi-stage process, which could be caused by repeated boiling and condensation of geothermal fluids in the subsurface, a phenomenon that has been investigated using other geochemical tools (Stefánsson et al., 2016b). Further work will be needed to reconcile noble gas observations with these existing methods, and to explore the additional insights that could be gained from an additional noble gas based constraint on these processes.

4.5.2 Major gas chemistry and stable isotopes

Geothermal fluids in Iceland are dominantly composed of H_2O (Stefánsson et al., 2017), but a range of minor components are used for the investigation of different processes within the system using both abundances and isotope ratios (Friedman et al., 1963; Aggarwal et al., 2000; Arnórsson et al., 2006; Stefánsson and Barnes, 2016; Thomas et al., 2016). In Fig. 4.6 we show the abundances of several important chemical species in both the gas and aqueous phases, alongside helium isotope ratios. In terms of the gas phase, samples from the NRZ show consistently higher

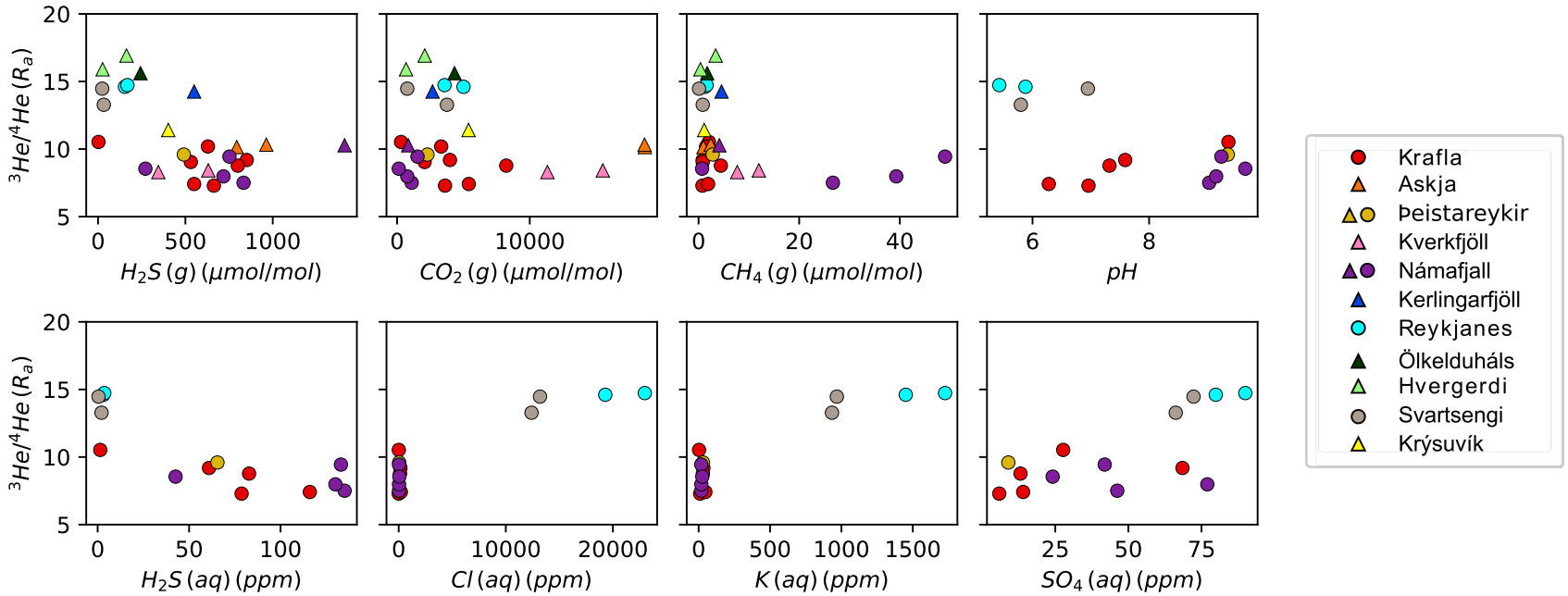

Figure 4.6: Relationships between helium isotope ratios and the abundance of major chemical species in both gas (top row) and aqueous (bottom row) phases. Fumarole samples are plotted as triangles, and borehole samples as circles. Aqueous phase chemistry is not taken from fumarole samples, due to the lack of a significant liquid phase. Major gas and solute chemistry values from Stefánsson (unpublished data).

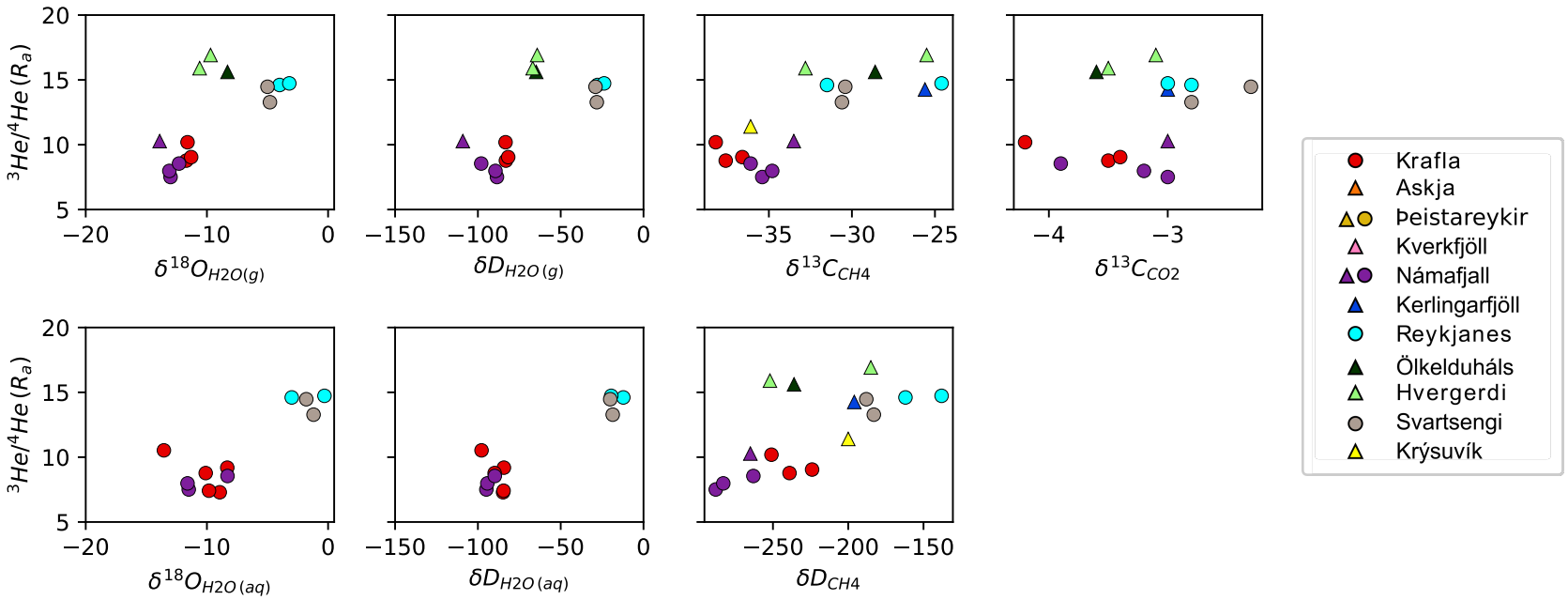

Figure 4.7: Relationships between helium isotope ratios and the stable isotope ratios for C, O, and H for several major species present in Icelandic geothermal fluids. Fumarole samples are plotted as triangles, and borehole samples as circles. Aqueous phase chemistry is not taken from fumarole samples, due to the lack of a significant liquid phase. Stable isotope values from Stefánsson (unpublished data).

abundances of H_2S, and fumarole samples tend to have higher H_2S concentrations as well. CO_2 abundance follows a similar pattern, with NRZ zone with MORB-like helium isotopes having highest concentrations of CO_2, especially in fumarole samples. In terms of CH_4, the fumarole samples from Kverkfjöll have elevated abundances, alongside borehole samples from Námafjall, which has been reported previously (Ólafsson and Ármannsson, 2013).

For the associated aqueous phases, both Cl and K are present at much higher abundances in WRZ samples, likely as a result of seawater infiltration (Arnórsson and Andrésdóttir, 1995; Ármannsson, 2016). The aqueous concentrations of sulfur species H_2S and SO_4 are also correlated with helium isotopes, with the higher $^3He/^4He$ samples from the WRZ showing consistently high SO_4 and low H_2S, indicative of a more oxidised environment (Björke et al., 2015; Stefánsson et al., 2015; Stefánsson and Barnes, 2016). NRZ samples with MORB-like $^3He/^4He$ have a wider range of concentrations of both.

Isotope ratios for major elements C, H and O in different species and phases are shown in Fig. 4.7, with many showing a clear relationship with helium isotope ratios. For H_2O in both aqueous and vapour phases, both $\delta^{18}O$ and δD are consistently heavier in WRZ samples with high $^3He/^4He$ ratios. However, this is likely a circumstance of geography due to the fact that the precipitation happens to be isotopically heavier in the Northern half of Iceland, and especially further from the coast, as the majority of our NRZ samples are situated (Arnason, 1977).

Of greater interest is the relationship between helium isotope ratios and the $\delta^{13}C$ and δD in methane. The source of methane in geothermal fluids is not well understood (Stefánsson et al., 2017). Some studies have supported an abiogenic origin using isotopic data (Lollar et al., 2008; Proskurowski et al., 2008), while others have suggested that isotopic equilibrium is unlikely to have been reached even at high temperatures (Stefánsson and Arnórsson, 2002). Several authors have suggest that methane must derive from both mantle/basaltic sources and the thermal degradation of organic matter (Poreda et al., 1992; Botz et al., 1999). These data show a clear positive correlation between $^3He/^4He$ isotope ratios and

both δ^{13}C and δD of methane. Helium isotopes are typically viewed as a definitive indicator of source rather than process, suggesting the possibility of source-control on the methane isotopes. A similar pattern is also observed in the δ^{13}C of CO_2, although the variation is much smaller at only ~2‰. It is possible there is some influence from CO_2 isotopes on methane, even without reaching equilibrium.

4.6 Conclusion

We present new high precision noble gas isotope and abundance data for 29 geothermal fluid samples from Iceland. Samples are taken both from boreholes drilled for geothermal power plants, and naturally-degassing fumaroles. Noble gas isotopes have been used extensively in Iceland previously for investigating the different deep mantle endmembers that contribute to the volcanic regimes (Poreda et al., 1992; Hilton et al., 1999; Barry et al., 2014; Colin et al., 2015). These data corroborate the observations concerning the distribution of helium isotope ratios between the different volcanic zones of the island (Torgersen and Jenkins, 1982; Condomines et al., 1983; Kurz et al., 1985; Harðardóttir et al., 2018), as well as the decoupling of neon and helium isotope systematics (Dixon et al., 2000; Moreira et al., 2001; Füri et al., 2010).

However, there has been relatively little use of noble gases as tracers of physical fluid processes in the subsurface. This is a crucial aspect of the wider geochemical system that has been studies using a number of different geochemical tools (Aggarwal et al., 2000; Stefánsson et al., 2015; Halldórsson et al., 2016; Stefánsson et al., 2016a). Here we seek to both reconcile noble gas observations with different geochemical abundance and stable isotope data, as well as to utilise the behaviour of atmosphere-derived noble gas isotopes to better understand the gas-water phase interactions of geothermal fluids at depth.

We show that the distribution of ANG's is strongly correlated for all measured samples. The inter-elemental ratios ^{20}Ne/^{36}Ar, ^{84}Kr/^{36}Ar and ^{130}Xe/^{36}Ar show clear trends suggestive of solubility-dependent fractionation. However, certain samples, particularly those with very low concentrations, appear to have ^{20}Ne/^{36}Ar ratios

that are overprinted by a later addition of meteoric ASW, possibly introduced during fluid exhumation and/or sample collection. We show that the observed trends can be satisfied with a multi-stage solubility-dependent fractionation at temperatures of 300-500K, starting from a composition that is ASW-like with a small sedimentary-type addition. One issue is the difficulty in distinguishing a large number of small fractionations from a few large fractionations. However, these promising results suggest several avenues that could be explored, especially the possibility of combining the noble gas observations and constraints with the other geochemical tools and models that have been used to investigate these processes (Björke et al., 2015; Stefánsson et al., 2016b).

Finally, we show that helium isotopes are correlated with a number of traditional geochemical parameters, including abundances of Cl, K. H_2S, as well as δD, δ^{18}O in H_2O, and δD and δ^{13}C in methane. Whilst some of these correlations are likely circumstantial and due to geography, others are potentially representative of deeper source and process controls on the geothermal fluids themselves. Again, further work and collaboration will be required to properly understand what information these relationships may provide.

5 Conclusion

Contents

5.1 Summary and impact

This study presents the first comprehensive investigation of noble gas isotopes in unconventional shale gas systems, and their relation to wider subsurface fluid regimes in the subsurface. The ability to measure natural gas samples that have been produced directly from the source-rocks in which they were generated leads to several promising avenues of research. We exploit this in a number of case studies to directly analyse different aspects of the petroleum system that were previously unreachable. Previous work in conventional petroleum systems and groundwater studies has laid the foundations for this project. The use of noble gas isotopes in the crustal fluids has been previously established for investigating fluid provenance (Hooker et al., 1985; Oxburgh et al., 1986; Ballentine and Holland, 2008) partitioning (Bosch and Mazor, 1988; Zaikowski and Spangler, 1990; Ballentine et al., 1996), and residence times (Torgersen and Clarke, 1985; Zaikowski et al., 1987; Zhou

et al., 2005). We adapt and develop these approaches to the novel environment of unconventional source-rock reservoirs, and then to geothermal fluids.

In Chapter 2 we use noble gas analysis of unconventional gas samples to investigate the generation of hydrocarbons in a natural system. This is a critical stage in the development of any petroleum system, but one which is challenging to study in a natural environment due to the time extent of the process (Lewan, 1993; Bernard and Horsfield, 2014; Peters et al., 2015). As the Eagle Ford is buried to variable depths across the basin, it has experienced different time-temperature histories which manifests as a range of thermal maturities of produced gases (Tian et al., 2013). We make the novel observation that atmosphere-derived noble gas isotope abundances are strongly affected by the extent of gas generation, being diluted as gas generation proceeds with increased thermal maturity. This phenomenon is evidenced most clearly in the inverse relationship between $[^{36}\mathrm{Ar}]$ and $\delta^{13}\mathrm{C}$ in methane, a traditional thermal maturitiy indicator (Berner and Faber, 1988). By combining this observation with existing studies using geochemical proxies for gas generation, we are able to place additional constraints and deduce previously unknown parameters describing gas generation in-situ. We calculate that the isotopic fractionation imparted during methane generation, $\epsilon = -27‰$. We use the constraints provided by the noble gas isotope observations to extend previous models of hydrocarbon generation. From this, we deduce quantitative estimates of proportional volumes of gas generated within and expelled from the source-rock. To our knowledge these are the first inferences of their kind based on direct empirical measurements derived from in-situ gases.

In Chapter 3 we compile an original dataset consisting of natural gases derived from related source-rocks and conventional reservoirs. This allows us, for the first time, to directly assess the effects of gas migration on noble gas isotopic signatures, another crucial stage in petroleum system development that is difficult to constrain (Stainforth and Reinders, 1990; Hindle, 1997). We find that abundances of both atmosphere-derived and radiogenic isotopes are greatly increased during the migration process, and that their relative enrichments are consistently related. For

both atmospheric and radiogenic isotopes, we apply simple models to determine the extent of enrichment due to migration distance. We conclude that migration occurs through relatively constrained conduits, but that the extent of this localisation is variable across the basin. This observation validates laboratory simulations of migration processes (Dembicki and Anderson, 1989), and suggests consequences for potential pathways of fluid migration. Additionally, we observe a correlated enrichment in conventional samples for both mantle-derived ^{3}He and radiogenic ^{40}Ar. Using a mixing model we ascertain that this isotopic enrichment is likely a result of increased exposure to the wider hydrogeological system within the basin. Finally, we investigate the spatial distribution of helium isotope ratios within the basin using a numerical approach, and conclude that introduction of mantle-derived ^{3}He into impermeable shale gas reservoirs requires a combination of lateral migration in adjacent porous layers, alongside the occurrence of vertical diffusion. This transport behaviour raises questions about the ability of low-permeability shales to act as seals over geological time, which could have implications for trapping of hydrocarbons, but also for CO_2 sequestration or radioactive waste storage (Osenbrück et al., 1998; Zhou et al., 2012; Neuzil, 2013; Warr, 2013).

In Chapter 4, we focus on a different environment, but one which shares many features with the petroleum systems discussed in previous chapters. Geothermal fluids are known to undergo a complex history of phase changes in the subsurface, involving boiling, degassing, condensation and mixing (Stefánsson et al., 2016b). Noble gases are an under-utilised tool for determining and quantifying these behaviours, the physical basis of which is analagous to many of the processes occurring in the petroleum systems discussed in Chapters 1 and 2 (Mazor et al., 1981; Ballentine et al., 2002). We measure the full suite of noble gas isotopes in a large range of geothermal fluids from Iceland. Helium and neon isotope systematics confirm a strong mantle signature, enriched in primordial ^{3}He and ^{20}Ne (Füri et al., 2010). Atmosphere-derived noble gases show clear signatures of fractionation from an initial composition that appears to be similar to ASW but with a small component enriched in Kr and Xe, which we infer to be from a

sorbed, sedimentary-style endmember (Staudacher and Allègre, 1988). We show that the observed fractionation is consistent with multi-stage equilibration, suggesting several stages of boiling, mixing and phase-partitioning in the subsurface (Björke et al., 2015). We also compare noble gas isotope data with a range of traditional stable isotope and abundance geochemical data. We anticipate that continued integration of noble gas analysis alongside these methods has the potential for significant impacts into our understanding of the physical behaviour of geothermal fluids. This is important not only for energy in the form of geothermal power, but also as one of the critical geochemical interfaces between the volatile reservoirs of the planet, controlling the geochemical evolution and distribution of elements of the surface (Ármannsson et al., 1982; Zindler and Hart, 1986; Fitton et al., 2003; Barry et al., 2014; Stefánsson et al., 2016a)

5.2 Outlook and future work

Overall, this work constitutes a solid basis for using noble gas isotopes to understand fluid behaviour in unconventional shale gas systems. We build on the data and methods developed in other subsurface fluid systems, and extend their use into a significant new subsurface environment. We provide case studies that demonstrate the general mechanisms controlling both hydrocarbon generation/expulsion from source-rocks, as well as migration from source-rock to reservoir. We anticipate that the efficacy of noble gases as tracers in unconventional reservoirs and other low-porosity subsurface systems will be greatly enhanced by the findings presented herein, alongside the work done by others in the field (Hunt et al., 2012; Darrah et al., 2014; Wen et al., 2016; Györe et al., 2017; Moore et al., 2018; Pujol et al., 2018). However, further studies will surely elucidate the finer details that control these processes, and only by combining multiple studies will the universal picture become more apparent.

In terms of progress and future work, several potential avenues of research present themselves. Analyses in this project were all measured from gas-phase samples, however water and/or oil phases are also often significant hosts of noble gases in the crust (Pinti and Marty, 1995; Barry et al., 2018a). Whilst the broad picture

of the subsurface conditions can be reconstructed purely from gas phase data, it relies on several assumptions inherent in the model reconstructions (Crovetto et al., 1982). The measurement of high-precision noble gas isotope data in produced water and oil phases will provide multiple additional constraints on their partitioning behaviour in the subsurface, and allow the investigation of areas where there is no significant gas phase present (Prinzhofer, 2013). The extraction of noble gases from a liquid phase presents a much more challenging experimental procedure, especially with oils as they can introduce contaminants into measurement apparatus (Tyne et al., 2018). Reproduction and study of subsurface conditions in a controlled laboratory environment would also give much greater confidence in the assumptions and extrapolations inherent in these types of analysis (Byrne et al., 2017). Whilst a base of literature does exist for these sources many are limited in scope or rendered inaccurate by the capabilities of modern instrumentation (Smith and Kennedy, 1983; Kharaka and Specht, 1988). It would be timely for a renewed effort to constrain these parameters with an expanded scope and increased precision, as has been done for CO_2-water systems (Warr et al., 2015a; Warr et al., 2015b). The ubiquity and potential of the noble gases as tracers means that the extension of noble gas isotope analysis to a range of systems is an intrinsic part of the field. In Chapter 4 of this work, we show the promise of some of these techniques in geothermal fluids in Iceland. However, integrating the noble gas analysis within the context of other geochemical tools is required to maximise the impact and utility of our findings. This will be a collaborative effort with geochemists from a range of backgrounds, and has the potential for significant contributions to our understanding of these environments.

Ultimately, this study makes a number of original contributions to the field. The laboratory capability to measure the full suite of noble gas isotopes to a high precision in a large number of samples results in a step change in the quality and quantity of data available. The utility of noble gases as tracers in unconventional shale-gas reservoirs, and other crustal fluids, is underlined by the wealth of information available in a large number of isotopes with diverse histories. As such, we expect

noble gas isotope geochemistry to continue to be an important tool in the analysis of these environments, and hope that this volume assists in that endeavour.

Appendices

A

Is excess Xe in hydrocarbons associated with type III kerogen?

Contents

Abstract

No. The presence of anomalously high xenon and krypton abundances in some produced hydrocarbons is well-documented, yet the process controlling it is not well understood. This 'excess' Kr and Xe is always air-like in isotopic composition, often well-correlated, and appears in oils and gases of certain petroleum systems but not others. The source of this excess is often attributed to a trapped component within sediments, with preferential adsorption of Kr and Xe responsible for the enrichment in the heavy noble gases. Laboratory studies into the sorptive processes confirm that this process does enrich Kr and Xe, but fails to explain the variability in this signature between petroleum systems. If sorption is the controlling process, we

might expect the kerogen type of the host source-rock to play a role. Here, we compare noble gas isotopic composition from two hydrocarbon fields determined to be sourced by type III source-rocks. The Hogsback field is part of the LaBarge platform in Wyoming, USA, and the Sable Island field is part of the Scotian Basin offshore of Canada. Our results show that both fields are strongly enriched in radiogenic noble gas isotopes (^{4}He, ^{21}Ne, ^{22}Ne, ^{40}Ar) and that no discernible traces of primordial mantle fluids are present. Abundances of atmosphere-derived argon are similar in the 2 fields. The Sable Island ^{130}Xe/^{36}Ar ratios are similar to atmosphere or air-saturated water, $<0.6\times10^{-3}$. However, the Hogsback samples show strong enrichments in ^{130}Xe/^{36}Ar of up to 2.4×10^{-3}, and corresponding enrichments in ^{84}Kr/^{36}Ar. We compare our dataset with previous literature studies and find that the nearly all systems which exhibit excess Kr and Xe are consistent with the influence of a sedimentary-style component. However, we conclude that the kerogen type is not a primary factor in determining the presence or extent of this enrichment.

A.1 Introduction

The presence of xenon enrichments in natural gases and oils was first reported by Torgersen and Kennedy, 1999, from hydrocarbons in the Elk Hills field, California. They observed Xe/Ar ratios up to 567 times that of air, but with definitively atmospheric xenon isotopes. In the intervening years, many further studies have been made, and only occasionally is the same xenon enrichment observed. Some studies find Xe/Ar similar to air or air-saturated water (Gilfillan et al., 2008; Holland et al., 2009), others highly variable enriched Xe/Ar which does not correlate with Kr/Ar (Pinti and Marty, 1995; Zhou et al., 2005). However, several studies have observed a closely-correlated enrichment in both Kr/Ar and Xe/Ar, with values extending up to several times that of air (Barry et al., 2016; Wen et al., 2017; Barry et al., 2018a; see also Chapter 3 of this volume). What is clear is that these enrichments are not observed in non-hydrocarbon fluids, with both deep crustal brines (Heard et al., 2018) and degassing volcanic fluids (Lowenstern et al., 2014) showing Kr/Ar and Xe/Ar ranging between air and ASW, but not extending beyond it.

This naturally leads to the question of what is controlling this behaviour? It has been suggested that the preferential adsorption of xenon and krypton onto sediments during deposition could lead to a sedimentary endmember rich in the heavy noble gases (Torgersen and Kennedy, 1999). Measured data from sediments show enrichments in Kr and Xe relative to air (Podosek et al., 1980; Staudacher and Allègre, 1988), and laboratory experiments show that Kr and Xe are more-easily sorbed than the lighter noble gases, especially on kerogen, and kerogen-rich shales (Podosek et al., 1981; Marrocchi et al., 2005).

However, what is causing the inconsistent behaviour observed in produced gases? One possibility is the type of shale which serves as the source-rock for the hydrocarbons. Source-rocks are classified into 3 main types based on the source of the kerogen found within, type I for lacustrine algal, type II for marine algal, and type III for terrestrial plant matter. Here, we measure 9 gases produced from 2 fields thought to be generated from type III source-rocks, in order to examine the potential effect on Kr/Ar and Xe/Ar enrichments.

A.2 Geological background

The Hogsback field is part of the LaBarge platform in Wyoming, and produces from the Jurassic Nugget Sandstone (Dunnewald and Gorton, 1977; Picard, 1977). The reservoir primarily consists of eolian deposits, but has relatively low-porosity, averaging around 13% , and highly variable permeability (Picard, 1975; Lindquist, 1988). The reservoir itself is around 180m thick and at an average depth of 3000m where produced (Webel, 1977). The source-rock is thought to be primarily rich in type III kerogen, rich in terrestrial plant matter and prone to gas rather than oil generation (Romer et al., 2007).

The Sable Island field is in the Scotian Basin, off the Atlantic coast of Canada, and has been an area of active and continuous deposition since the Triassic (Purcell et al., 1979). While the basin contains both type II and type III source-rocks, Rock-Eval pyrolysis in the Sable Island field supports a type III source (Mukhopadhyay et al., 1995).

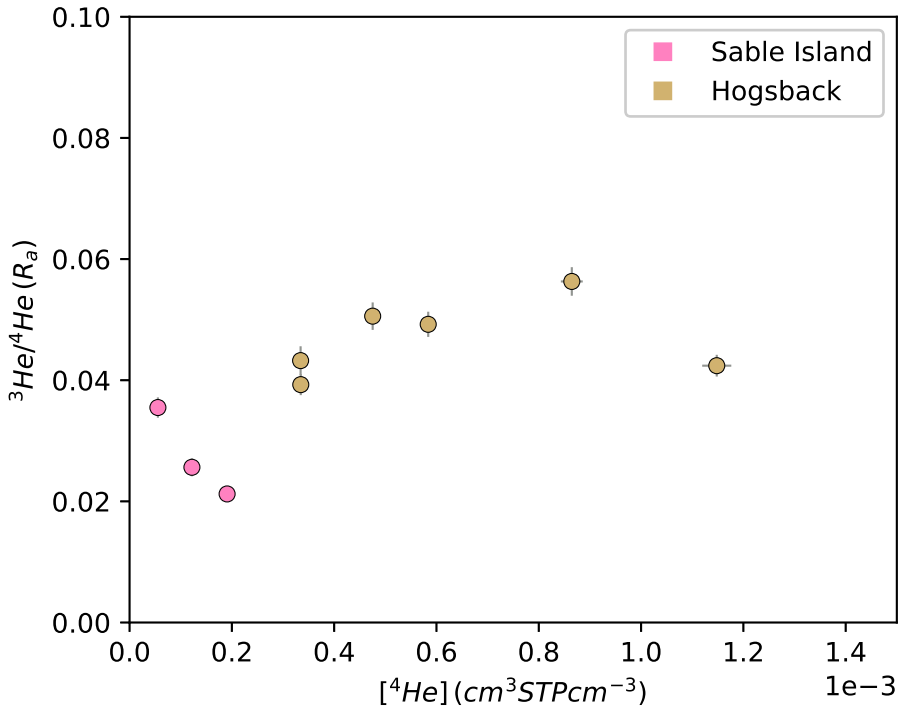

Figure A.1: Plot of helium isotope and abundance data for Hogsback and Sable Island samples.

A.3 Results

The measured noble gas abundances are reported in Table A.1, and isotope ratios in Table A.2. Helium isotope ratios are strongly radiogenic in all samples (<0.05R_a), with no evidence for mantle ^{3}He input. ^{4}He concentrations are slightly higher in the Hogsback samples, up to 1.2×10^{-3} cm^{3}STPcm^{-3}, as shown in Fig. A.1. Neon isotope ratios are shown in Fig. A.2, and plot close to the expected crustal production line for radiogenic ^{21}Ne and ^{22}Ne (Kennedy et al., 1990). Argon isotopes are also predominantly radiogenic, with ^{40}Ar/^{36}Ar ratios enriched up to ^{40}Ar/^{36}Ar=1714 compared with the atmospheric ratio of 298.6 (Lee et al., 2006). Argon abundances range from 0.63 to 8.36 $\times10^{-8}$cm^{3}STPcm^{-3}, with no clear distinction between the 2 fields. Of particular note is sample A6589, which shows air-like argon isotope ratios, and atmospheric ^{36}Ar, ^{20}Ne enrichments of several orders of magnitude compared to other samples. As a result it is considered to be air-contaminated and excluded from discussions. Overall, both Sable Island and Hogsback samples

Sample	Location	^{4}He ($\times 10^{-4}$)	$\pm 2\sigma$	^{20}Ne ($\times 10^{-8}$)	$\pm 2\sigma$	^{36}Ar ($\times 10^{-8}$)	$\pm 2\sigma$	^{84}Kr ($\times 10^{-9}$)	$\pm 2\sigma$	^{130}Xe ($\times 10^{-11}$)	$\pm 2\sigma$
A6589	Sable Island	0.55	0.01	98.98	2.50	179.25	4.53	38.87	0.98	23.96	0.61
A6591	Sable Island	1.22	0.03	1.81	0.04	3.00	0.07	0.77	0.02	0.82	0.02
A6443	Sable Island	1.91	0.05	0.28	0.01	0.63	0.02	0.20	0.01	0.34	0.01
HO2217	Hogsback	3.34	0.08	1.40	0.03	5.44	0.13	3.04	0.08	9.66	0.24
HB6823	Hogsback	5.84	0.14	0.47	0.01	2.05	0.05	1.24	0.03	4.57	0.11
HB487	Hogsback	3.35	0.08	0.42	0.01	1.81	0.04	1.17	0.03	4.18	0.10
HB43761	Hogsback	8.65	0.21	0.84	0.02	3.68	0.09	2.07	0.05	5.90	0.15
HB158	Hogsback	4.75	0.12	0.53	0.01	2.07	0.05	1.28	0.03	4.06	0.10
HB6436	Hogsback	11.48	0.28	1.81	0.04	8.38	0.21	3.85	0.10	8.05	0.20

Table A.1: Abundances of noble gas isotopes in Hogsback and Sable Island natural gases. Units are in $cm^3STPcm-3$. Anomalously high concentrations of atmospheric isotopes in sample A6589 are interpreted to be due to atmospheric contamination of the sample.

SampleID	Location	$^{3}He/^{4}He$ (R_a)	$\pm 2\sigma$	$^{40}Ar/^{36}Ar$	$\pm 2\sigma$	$^{20}Ne/^{22}Ne$	$\pm 2\sigma$	$^{21}Ne/^{22}Ne$	$\pm 2\sigma$
A6589	Sable Island	0.035	0.002	301.1	0.7	9.50	0.04	n.d.	
A6591	Sable Island	0.026	0.001	493.9	1.3	9.63	0.04	0.0300	0.0006
A6443	Sable Island	0.021	0.001	1714.3	5.4	9.45	0.04	0.0458	0.0010
HO2217	Hogsback	0.043	0.002	640.2	1.7	9.52	0.04	0.0338	0.0007
HB6823	Hogsback	0.049	0.002	1041.7	2.7	9.24	0.04	0.0460	0.0010
HB487	Hogsback	0.039	0.002	824.2	2.2	9.40	0.04	0.0420	0.0009
HB43761	Hogsback	0.056	0.002	1066.3	2.7	9.30	0.04	0.0444	0.0009
HB158	Hogsback	0.051	0.002	1030.6	2.8	9.38	0.04	0.0439	0.0009
HB6436	Hogsback	0.042	0.002	584.2	1.4	9.32	0.04	0.0384	0.0008

Table A.2: Noble gas isotope ratio data for Hogsback and Sable Island natural gases. Helium isotope ratios are reported relative to the atmospheric ratio, where $R_a = 1.4 \times 10^{-6}$ (Porcelli et al., 2002).

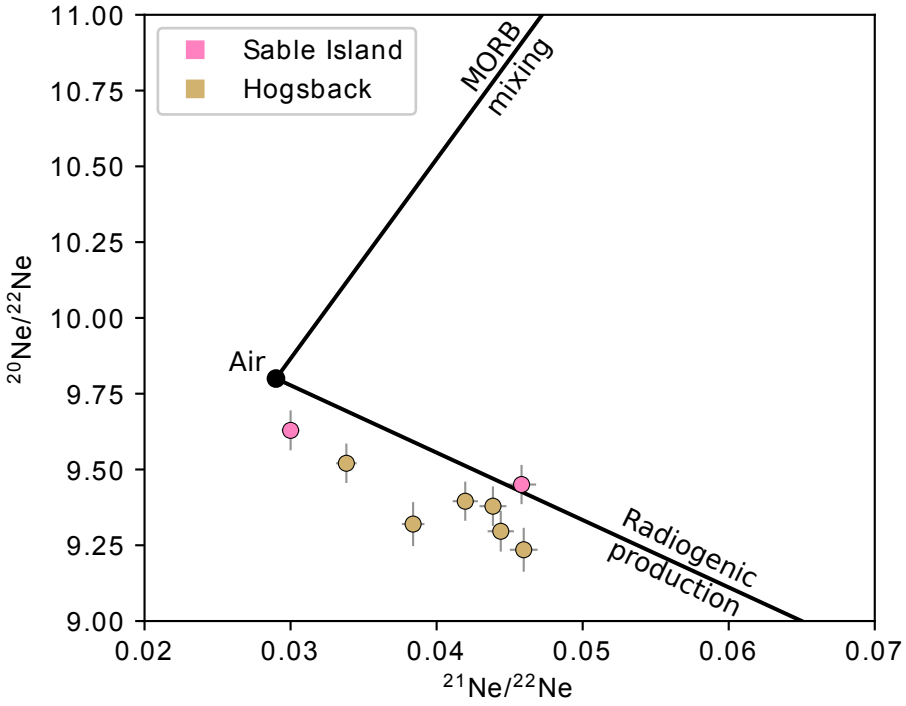

Figure A.2: Plot of neon isotope data for Hogsback and Sable Island samples. Atmospheric endmember is shown, alongside mixing lines towards MORB, and evolution due to production of radiogenic isotopes (Kennedy et al., 1990).

show strongly radiogenic isotope signatures, and aside from differences in ^{4}He abundances, have very similar characteristics.

A.4 Discussion

In Fig. A.4, we plot atmosphere-derived noble gas (^{20}Ne, ^{36}Ar, ^{84}Kr, ^{130}Xe) elemental ratios, for Hogsback and Sable Island datasets, as well as a selection of data from previously published literature. It can be seen that Sable Island samples show no Kr/Ar or Xe/Ar enrichments, plotting between air and ASW endmembers. However Hogsback samples show a consistent enrichment towards and even beyond measured sedimentary values for both Kr/Ar and Xe/Ar. Clearly if the source-rock type is indeed similar between the 2 fields, then source-rock type cannot be a major controlling factor on the presence of Xe/Ar and Kr/Ar enrichments in produced gases.

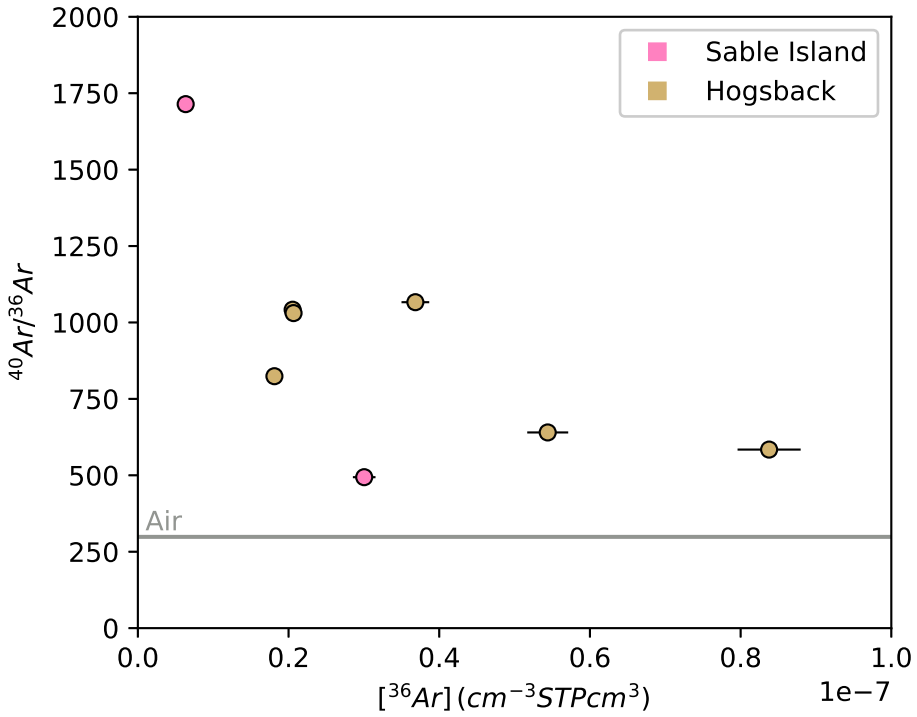

Figure A.3: Plot of argon isotope and abundance data for Hogsback and Sable Island samples. Sample A6589 is not shown as it is off-scale due to presumed contamination with atmospheric Ar.

The assorted literature data do show a remarkably clear and consistent trend suggestive of mixing between the atmospheric, ASW, and measured sedimentary endmembers. $^{20}Ne/^{36}Ar$ is never appreciably lower than ASW, and it seems unlikely that there is much sedimentary contribution affecting Ne and Ar systems. Measured Ne and Ar abundances in sediments are much lower than the heavy noble gases (Staudacher and Allègre, 1988). $^{84}Kr/^{36}Ar$ and $^{130}Xe/^{36}Ar$ shows a strong influence of the sedimentary endmember component, although its significance varies between systems. The volcanic Yellowstone dataset (Lowenstern et al., 2014), and the deep ancient brines from Kaapvaal (Heard et al., 2018), show no significant input of sedimentary Kr and Xe, and can likely be explained purely by ASW-air mixing or solubility-dependent fractionation. The Sleipner and Alberta hydrocarbon systems (Hiyagon and Kennedy, 1992; Barry et al., 2016) show moderate and consistent enrichments in Kr and Xe, with the Haynesville slightly higher. Gulf of Mexico (Barry et al., 2018a), Eagle Ford and Hogsback all show consistently high enrichments

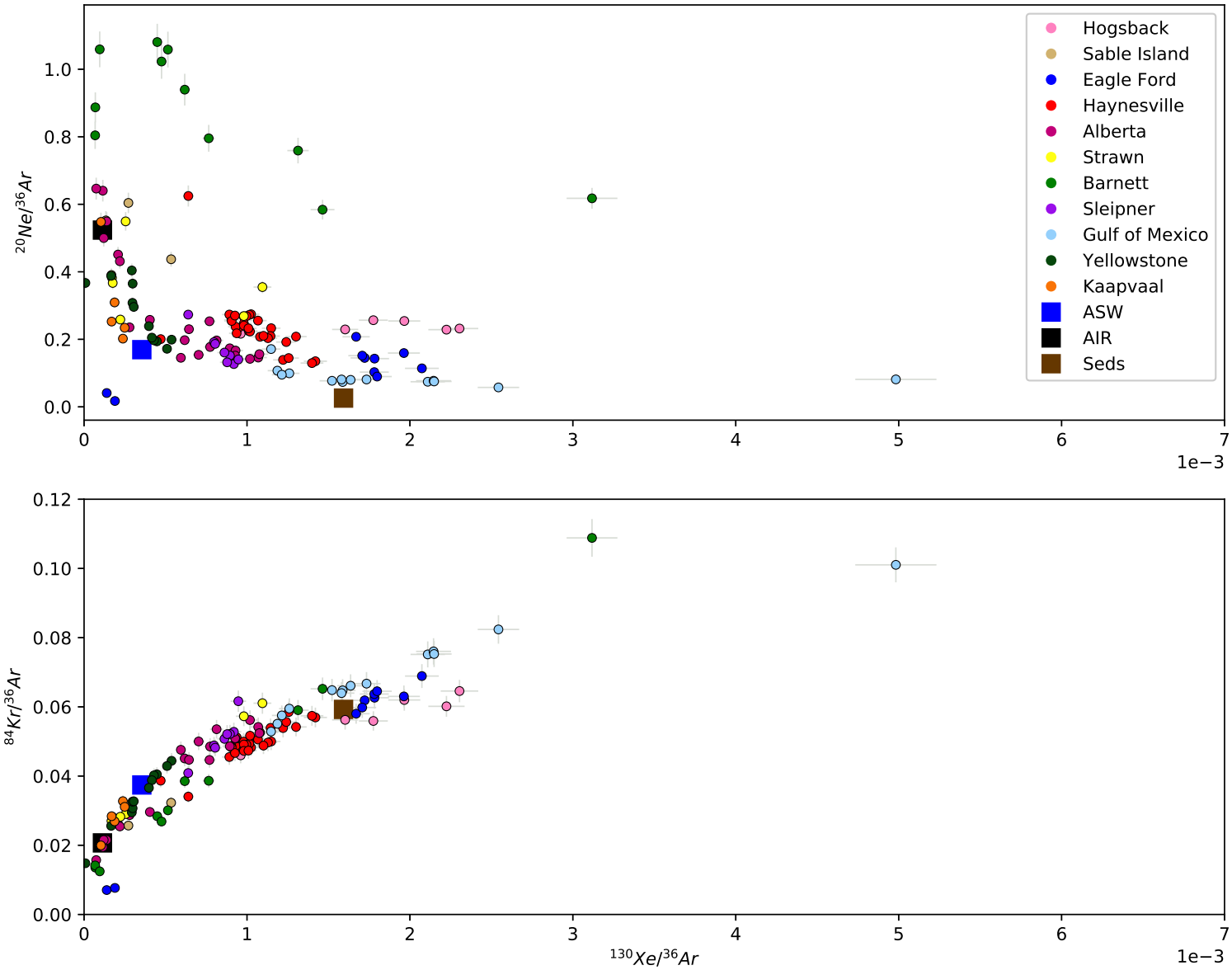

Figure A.4: Compilation of atmosphere-derived noble gas ratios in studies conducted as part of this project and elsewhere. Mixing with sedimentary endmember is clearly seen. Data sources: Hogsback and Sable Island (this study); Eagle Ford (Byrne et al., 2018); Haynesvile (Chapter 3); Alberta (Hiyagon and Kennedy, 1992); Strawn and Barnett (Wen et al., 2017); Sleipner (Barry et al., 2016); Gulf of Mexico (Barry et al., 2018a); Yellowstone (Lowenstern et al., 2014); Kaapvaal (Heard et al., 2018). Errorbars are shown for illustration only and represent a 5% error typical of measurements of this type.

around and even in excess of the sedimentary endmember. Barnett and Strawn systems (Wen et al., 2017) show some of the highest, enrichments, but are highly variable and some plot lower than ASW. Not shown are samples from San Juan (Zhou et al., 2005) and the Paris Basin (Pinti and Marty, 1995). These 2 systems show much greater Kr and Xe enrichments to the extent that the rest of the data would be obscured by the larger scale. However their enrichments are not well-correlated, and so not necessarily the result of a sorbed sedimentary process.

Comparison of the fields which do exhibit a Kr and Xe enrichment shows that we can rule out some obvious potential controls on its presence. The signature is seen in both oil-associated gases (Gulf of Mexico) and in single-phase non-associated gas reservoirs (Hogsback), indicating that the presence of a significant oil phase does not necessarily contribute to the heavy noble gases. Furthermore, both unconventional source-rock reservoirs (Eagle Ford), and conventional reservoirs show enrichments, suggesting that migration is not the cause, but also does not necessarily overprint the excess Kr and Xe. If the source of Kr and Xe is from the source-rocks themselves we might expect the greatest enrichments to be in the unconventional reservoirs, but that does not seem to be the case. The Haynesville dataset (Chapter 3) consists of conventional and unconventional reservoirs from the same area, with no apparent distinction between the two in terms of Kr/Ar and Xe/Ar. In some ways this strengthens the case for source-rocks being the principal source of excess Kr and Xe, as both conventional and unconventional samples from this dataset share the same source-rock. However, the observed enrichment is no greater in the source-rocks, and as migrated samples have generally higher abundances of all atmosphere-derived isotopes, the signal is clearly not being diluted during migration. If both conventional reservoir rocks and source-rock reservoirs can equally be considered as sources of excess Kr and Xe, then this raises the question of why some hydrocarbon fields show a complete lack of sedimentary endmember enrichment (Sable Island).

A.5 Conclusion

This data compilation strongly suggests that Kr and Xe sorbed during sediment deposition control the observed enrichments in the majority of petroleum systems. However the exact reasons for the observed inconsistent behaviour between different systems is still unexplained. Our new data from the Hogsback and Sable Island systems strongly suggest that a control by sediment type or organic kerogen type can be ruled out as a possibility. Comparison between other datasets also shows that there is no clear distinction between fluid type (oil vs gas), or conventional vs unconventional reservoirs.

References

Aeschbach-Hertig, W., Peeters, F., Beyerle, U., & Kipfer, R. (2000). Palaeotemperature reconstruction from noble gases in ground water taking into account equilibration with entrapped air. *Nature*, *405*(6790), 1040–1044.

Aeschbach-Hertig, W., El-Gamal, H., Wieser, M., & Palcsu, L. (2008). Modeling excess air and degassing in groundwater by equilibrium partitioning with a gas phase. *Water Resources Research*, *44*(8).

Aggarwal, J. K., Palmer, M. R., Bullen, T. D., Arnórsson, S., & Ragnarsdóttir, K. V. (2000). The boron isotope systematics of Icelandic geothermal waters: 1. Meteoric water charged systems. *Geochimica et Cosmochimica Acta*, *64*(4), 579–585.

Allan, U. S. (1989). Model for Hydrocarbon Migration and Entrapment Within Faulted Structures. *AAPG Bulletin*, *73*(7), 803–811.

Allègre, C. J., Hofmann, A., & O'Nions, K. (1996). The argon constraints on mantle structure. *Geophysical Research Letters*, *23*(24), 3555–3557.

Anders, E., & Grevesse, N. (1989). Abundances of the elements: Meteoritic and solar. *Geochimica et Cosmochimica Acta*, *53*(1), 197–214.

Anderson, K. R., & Poland, M. P. (2017). Abundant carbon in the mantle beneath Hawai'i. *Nature Geoscience*, *10*(9), 704–708.

Apotria, T., Kaiser, C. J., & Cain, B. A. (1994). Fracturing and Stress History of the Devonian Antrim Shale, Michigan Basin, American Rock Mechanics Association.

Ármannsson, H., Gíslason, G., & Hauksson, T. (1982). Magmatic gases in well fluids aid the mapping of the flow pattern in a geothermal system. *Geochimica et Cosmochimica Acta*, *46*(2), 167–177.

Ármannsson, H. (2016). The fluid geochemistry of Icelandic high temperature geothermal areas. *Applied Geochemistry*, *66*, 14–64.

Arnason, B. (1977). Hydrothermal systems in Iceland traced by deuterium. *Geothermics*, *5*(1), 125–151.

Arnórsson, S., Bjarnason, J. Ö., Giroud, N., Gunnarsson, I., & Stefánsson, A. (2006). Sampling and analysis of geothermal fluids. *Geofluids*, *6*(3), 203–216.

Arnórsson, S., Gunnlaugsson, E., & Svavarsson, H. (1983). The chemistry of geothermal waters in Iceland. II. Mineral equilibria and independent variables controlling water compositions. *Geochimica et Cosmochimica Acta*, *47*(3), 547–566.

Arnórsson, S., & Andrésdóttir, A. (1995). Processes controlling the distribution of boron and chlorine in natural waters in Iceland. *Geochimica et Cosmochimica Acta*, *59*(20), 4125–4146.

Athy, L. F. (1930). Density, Porosity, and Compaction of Sedimentary Rocks. *AAPG Bulletin*, *14*(1), 1–24.

Avice, G., Marty, B., Burgess, R., Hofmann, A., Philippot, P., Zahnle, K., & Zakharov, D. (2018). Evolution of atmospheric xenon and other noble gases inferred from Archean to Paleoproterozoic rocks. *Geochimica et Cosmochimica Acta*, *232*, 82–100.

Bach, W., Naumann, D., & Erzinger, J. (1999). A helium, argon, and nitrogen record of the upper continental crust (KTB drill holes, Oberpfalz, Germany): Implications for crustal degassing. *Chemical Geology*, *160*(1–2), 81–101.

Ballentine, C. J., O'Nions, R. K., Oxburgh, E. R., Horvath, F., & Deak, J. (1991). Rare gas constraints on hydrocarbon accumulation, crustal degassing and groundwater flow in the Pannonian Basin. *Earth and Planetary Science Letters*, *105*(1–3), 229–246.

Ballentine, C. J., & O'nions, R. K. (1993). The use of natural He, Ne and Ar isotopes as constraints on hydrocarbon transport. *Geological Society, London, Petroleum Geology Conference series*, *4*, 1339–1345.

Ballentine, C. J., O'Nions, R. K., & Coleman, M. L. (1996). A Magnus opus: Helium, neon, and argon isotopes in a North Sea oilfield. *Geochimica et Cosmochimica Acta*, *60*(5), 831–849.

Ballentine, C. J., & Hall, C. M. (1999). Determining paleotemperature and other variables by using an error-weighted, nonlinear inversion of noble gas concentrations in water. *Geochimica et Cosmochimica Acta*, *63*(16), 2315–2336.

Ballentine, C. J., & Burnard, P. G. (2002). Production, Release and Transport of Noble Gases in the Continental Crust. *Reviews in Mineralogy and Geochemistry*, *47*(1), 481–538.

Ballentine, C., & O'Nions, R. (1992). The nature of mantle neon contributions to Vienna Basin hydrocarbon reservoirs. *Earth and Planetary Science Letters*, *113*(4), 553–567.

Ballentine, C. J., & Sherwood Lollar, B. (2002). Regional groundwater focusing of nitrogen and noble gases into the Hugoton-Panhandle giant gas field, USA. *Geochimica et Cosmochimica Acta*, *66*(14), 2483–2497.

Ballentine, C. J., Burgess, R., & Marty, B. (2002). Tracing Fluid Origin, Transport and Interaction in the Crust. *Reviews in Mineralogy and Geochemistry*, *47*(1), 539–614.

Ballentine, C. J., Marty, B., Sherwood Lollar, B., & Cassidy, M. (2005). Neon isotopes constrain convection and volatile origin in the Earth's mantle. *Nature*, *433*(7021), 33–38.

Ballentine, C. J., & Holland, G. (2008). What CO2 well gases tell us about the origin of noble gases in the mantle and their relationship to the atmosphere. *Philosophical Transactions of the Royal Society of London A: Mathematical, Physical and Engineering Sciences*, *366*(1883), 4183–4203.

Barry, P. H., Hilton, D. R., Füri, E., Halldórsson, S. A., & Grönvold, K. (2014). Carbon isotope and abundance systematics of Icelandic geothermal gases, fluids and subglacial basalts with implications for mantle plume-related CO2 fluxes. *Geochimica et Cosmochimica Acta*, *134*, 74–99.

Barry, P. H., Lawson, M., Meurer, W. P., Warr, O., Mabry, J. C., Byrne, D. J., & Ballentine, C. J. (2016). Noble gases solubility models of hydrocarbon charge mechanism in the Sleipner Vest gas field. *Geochimica et Cosmochimica Acta*, *194*, 291–309.

Barry, P. H., Lawson, M., Meurer, W. P., Cheng, A., & Ballentine, C. J. (2018a). Noble Gases in Deepwater Oils of the U.S. Gulf of Mexico. *Geochemistry, Geophysics, Geosystems*, *19*(11), 4218–4235.

Barry, P. H., Kulongoski, J. T., Landon, M. K., Tyne, R. L., Gillespie, J. M., Stephens, M. J., ... Ballentine, C. J. (2018b). Tracing enhanced oil recovery signatures in casing gases from the Lost Hills oil field using noble gases. *Earth and Planetary Science Letters*, *496*, 57–67.

Barry, P. H., Lawson, M., Meurer, W. P., Danabalan, D., Byrne, D. J., Mabry, J. C., & Ballentine, C. J. (2017). Determining fluid migration and isolation times in multiphase crustal domains using noble gases. *Geology*, *45*(9), 775–778.

Bartberger, C. E., Dyman, T. S., & Condon, S. M. (2002). *Is there a basin-centered gas accumulation in Cotton Valley Group Sandstones, Gulf Coast Basin, U.S.A.?* (USGS Numbered Series No. 2184-D).

Bartberger, C. E., Dyman, T. S., & Condon, S. M. (2003). *Potential for deep basin-centered gas accumulation in Travis Peak (Hosston) Formation, Gulf Coastal Basin* (tech. rep. No. 2184-E). USGS.

Battani, A., Sarda, P., & Prinzhofer, A. (2000). Basin scale natural gas source, migration and trapping traced by noble gases and major elements: The Pakistan Indus basin. *Earth and Planetary Science Letters*, *181*(1–2), 229–249.

Baxter, E. F., DePaolo, D. J., & Renne, P. R. (2002). Spatially correlated anomalous 40ar/39ar "age" variations in biotites about a lithologic contact near Simplon Pass, Switzerland: A mechanistic explanation for excess Ar. *Geochimica et Cosmochimica Acta*, *66*(6), 1067–1083.

Becker, S. P., Eichhubl, P., Laubach, S. E., Reed, R. M., Lander, R. H., & Bodnar, R. J. (2010). A 48 my history of fracture opening, temperature, and fluid pressure: Cretaceous Travis Peak Formation, East Texas basin. *Bulletin*, *122*(7-8), 1081–1093.

Behar, F., Vandenbroucke, M., Teermann, S. C., Hatcher, P. G., Leblond, C., & Lerat, O. (1995). Experimental simulation of gas generation from coals and a marine kerogen. *Chemical Geology*. Processes of Natural Gas Formation, *126*(3), 247–260.

Behar, F., Vandenbroucke, M., Tang, Y., Marquis, F., & Espitalie, J. (1997). Thermal cracking of kerogen in open and closed systems: Determination of kinetic parameters and stoichiometric coefficients for oil and gas generation. *Organic Geochemistry*, *26*(5), 321–339.

Bekaert, D. V., Broadley, M. W., Delarue, F., Avice, G., Robert, F., & Marty, B. (2018). Archean kerogen as a new tracer of atmospheric evolution: Implications for dating the widespread nature of early life. *Science Advances*, *4*(2), eaar2091.

Ben-Naim, A., & Egel-Thal, M. (1965). Thermodynamics of Aqueous Solutions of Noble Gases. III. Effect of Electrolytes. *The Journal of Physical Chemistry*, *69*(10), 3250–3253.

Bernard, B. B., Brooks, J. M., & Sackett, W. M. (1976). Natural gas seepage in the Gulf of Mexico. *Earth and Planetary Science Letters*, *31*(1), 48–54.

Bernard, S., & Horsfield, B. (2014). Thermal Maturation of Gas Shale Systems. *Annual Review of Earth and Planetary Sciences*, *42*(1), 635–651.

Berner, U., & Faber, E. (1988). Maturity related mixing model for methane, ethane and propane, based on carbon isotopes. In L. Mattavelli & L. Novelli (Eds.), *Organic Geochemistry In Petroleum Exploration* (pp. 67–72).

Bijwaard, H., & Spakman, W. (1999). Tomographic evidence for a narrow whole mantle plume below Iceland. *Earth and Planetary Science Letters*, *166*(3), 121–126.

Bjarnason, I. (2008). An Iceland hotspot saga. *Jökull*, *58*, 3–16.

Bjarnason, I. T., Menke, W., Flóvenz, Ó. G., & Caress, D. (1993). Tomographic image of the Mid-Atlantic Plate Boundary in southwestern Iceland. *Journal of Geophysical Research: Solid Earth*, *98*(B4), 6607–6622.

Björke, J. K., Stefánsson, A., & Arnórsson, S. (2015). Surface water chemistry at Torfajökull, Iceland—Quantification of boiling, mixing, oxidation and water–rock

interaction and reconstruction of reservoir fluid composition. *Geothermics*, *58*, 75–86.

Blanc, P., & Connan, J. (1994). Preservation, degradation, and destruction of trapped oil. *Memoirs-American Association of Petroleum Geologists*, 237–237.

Bödvarsson, G. (1961). Physical characteristics of natural heat resources in Iceland. *Jökull*, *11*, 29–38.

Bojesen-Koefoed, J. A., Christiansen, F. G., Nytoft, H. P., & Pedersen, A. K. (1999). Oil seepage onshore West Greenland: Evidence of multiple source rocks and oil mixing. *Geological Society, London, Petroleum Geology Conference series*, *5*, 305–314.

Bosch, A., & Mazor, E. (1988). Natural gas association with water and oil as depicted by atmospheric noble gases: Case studies from the southeastern Mediterranean Coastal Plain. *Earth and Planetary Science Letters*, *87*(3), 338–346.

Botz, R., Winckler, G., Bayer, R., Schmitt, M., Schmidt, M., Garbe-Schönberg, D., ... Kristjansson, J. K. (1999). Origin of trace gases in submarine hydrothermal vents of the Kolbeinsey Ridge, north Iceland. *Earth and Planetary Science Letters*, *171*(1), 83–93.

Boucher, C., Lan, T., Marty, B., Burnard, P. G., Fischer, T. P., Ayalew, D., ... Zimmermann, L. (2018). Atmospheric helium isotope composition as a tracer of volcanic emissions: A case study of Erta Ale volcano, Ethiopia. *Chemical Geology. The noble gases as geochemical tracers – in celebration of Pete Burnard*, *480*, 3–11.

Breddam, K., Kurz, M. D., & Storey, M. (2000). Mapping out the conduit of the Iceland mantle plume with helium isotopes. *Earth and Planetary Science Letters*, *176*(1), 45–55.

Broadley, M. W., Barry, P. H., Ballentine, C. J., Taylor, L. A., & Burgess, R. (2018). End-Permian extinction amplified by plume-induced release of recycled lithospheric volatiles. *Nature Geoscience*, *11*(9), 682.

Brooker, R. A., Wartho, J.-A., Carroll, M. R., Kelley, S. P., & Draper, D. S. (1998). Preliminary UVLAMP determinations of argon partition coefficients for olivine and clinopyroxene grown from silicate melts. *Chemical Geology*, *147*(1–2), 185–200.

Brown, H. (1949). Rare gases and the formation of the Earth's atmosphere. In *The atmospheres of the Earth and planets* (Vol. 1, p. 258).

Burnard, P. G., & Farley, K. A. (2000). Calibration of pressure-dependent sensitivity and discrimination in Nier-type noble gas ion sources. *Geochemistry, Geophysics, Geosystems*, *1*(7).

Burnard, P., Graham, D., & Turner, G. (1997). Vesicle-Specific Noble Gas Analyses of Popping Rock: Implications for Primordial Noble Gases in Earth. *Science*, *276*(5312), 568–571.

Burnard, P., Zimmermann, L., & Sano, Y. (2013). The Noble Gases as Geochemical Tracers: History and Background. In P. Burnard (Ed.), *The Noble Gases as Geochemical Tracers* (pp. 1–15). Advances in Isotope Geochemistry.

Byrne, D. J., Barry, P. H., Lawson, M., & Ballentine, C. J. (2018). Determining gas expulsion vs retention during hydrocarbon generation in the Eagle Ford Shale using noble gases. *Geochimica et Cosmochimica Acta*, *241*, 240–254.

Byrne, D. J., Barry, P. H., Lawson, M., & Ballentine, C. J. (2017). Noble gases in conventional and unconventional petroleum systems. *Geological Society, London, Special Publications*, *468*, SP468.5.

Cady, H. P., & McFarland, D. F. (1906). Helium in Natural Gas. *Science*, *24*(611), 344–344.

Canfield, D. E. (2004). The evolution of the Earth surface sulfur reservoir. *American Journal of Science*, *304*(10), 839–861.

Cao, C., Zhang, M., Tang, Q., Yang, Y., Lv, Z., Zhang, T., ... Li, L. (2018). Noble gas isotopic variations and geological implication of Longmaxi shale gas in Sichuan Basin, China. *Marine and Petroleum Geology*. Gas Geochemistry: from conventional to unconventional domains, *89*(Part 1), 38–46.

Cartigny, P., Jendrzejewski, N., Pineau, F., Petit, E., & Javoy, M. (2001). Volatile (C, N, Ar) variability in MORB and the respective roles of mantle source heterogeneity and degassing: The case of the Southwest Indian Ridge. *Earth and Planetary Science Letters*, *194*(1), 241–257.

Castro, M. C., Jambon, A., de Marsily, G., & Schlosser, P. (1998a). Noble gases as natural tracers of water circulation in the Paris Basin: 1. Measurements and discussion of their origin and mechanisms of vertical transport in the basin. *Water Resources Research*, *34*(10), 2443–2466.

Castro, M. C., Goblet, P., Ledoux, E., Violette, S., & de Marsily, G. (1998b). Noble gases as natural tracers of water circulation in the Paris Basin: 2. Calibration of a groundwater flow model using noble gas isotope data. *Water Resources Research*, *34*(10), 2467–2483.

Chauvel, C., & Hémond, C. (2000). Melting of a complete section of recycled oceanic crust: Trace element and Pb isotopic evidence from Iceland. *Geochemistry, Geophysics, Geosystems*, *1*(2).

Clarke, P. R., Portis, D. H., Barzola, G. J., Bello, H., & Basu, N. K. (2016). Assessing Well Performance in a Prolific Liquids-rich Shale Play—An Eagle Ford Case Study. In J. Breyer (Ed.), *The Eagle Ford Shale* (pp. 213–240).

Clarkson, C. R., Jensen, J. L., & Chipperfield, S. (2012). Unconventional gas reservoir evaluation: What do we have to consider? *Journal of Natural Gas Science and Engineering*. Unconventional Natural Gas, *8*, 9–33.

Clayton, C. (1991). Carbon isotope fractionation during natural gas generation from kerogen. *Marine and Petroleum Geology*, *8*(2), 232–240.

Colin, A., Moreira, M., Gautheron, C., & Burnard, P. (2015). Constraints on the noble gas composition of the deep mantle by bubble-by-bubble analysis of a volcanic glass sample from Iceland. *Chemical Geology*, *417*, 173–183.

Coltice, N., Simon, L., & Lécuyer, C. (2004). Carbon isotope cycle and mantle structure. *Geophysical Research Letters*, *31*(5), n/a–n/a.

Condomines, M., Grönvold, K., Hooker, P. J., Muehlenbachs, K., O'Nions, R. K., Óskarsson, N., & Oxburgh, E. R. (1983). Helium, oxygen, strontium and neodymium isotopic relationships in Icelandic volcanics. *Earth and Planetary Science Letters*, *66*, 125–136.

Cooles, G. P., Mackenzie, A. S., & Quigley, T. M. (1986). Calculation of petroleum masses generated and expelled from source rocks. *Organic Geochemistry*, *10*(1–3), 235–245.

Craig, H., & Lupton, J. E. (1976). Primordial neon, helium, and hydrogen in oceanic basalts. *Earth and Planetary Science Letters*, *31*(3), 369–385.

Crovetto, R., Fernández-Prini, R., & Japas, M. L. (1982). Solubilities of inert gases and methane in H2o and in D2o in the temperature range of 300 to 600 K. *The Journal of Chemical Physics*, *76*(2), 1077–1086.

Crowhurst, P. V., Green, P. F., & Kamp, P. J. J. (2002). Appraisal of (U-Th)/He apatite thermochronology as a thermal history tool for hydrocarbon exploration: An example from the Taranaki Basin, New Zealand. *AAPG bulletin*, *86*(10).

Curiale, J. A., & Curtis, J. B. (2016). Organic geochemical applications to the exploration for source-rock reservoirs – A review. *Journal of Unconventional Oil and Gas Resources*, *13*, 1–31.

Curtis, J. B. (2002). Fractured shale-gas systems. *AAPG bulletin*, *86*(11), 1921–1938.

Darbyshire, F. A., White, R. S., & Priestley, K. F. (2000). Structure of the crust and uppermost mantle of Iceland from a combined seismic and gravity study. *Earth and Planetary Science Letters*, *181*(3), 409–428.

Darrah, T. H., Vengosh, A., Jackson, R. B., Warner, N. R., & Poreda, R. J. (2014). Noble gases identify the mechanisms of fugitive gas contamination in drinking-water wells overlying the Marcellus and Barnett Shales. *Proceedings of the National Academy of Sciences of the United States of America*, *111*(39), 14076–81.

Darrah, T. H., Jackson, R. B., Vengosh, A., Warner, N. R., Whyte, C. J., Walsh, T. B., ... Poreda, R. J. (2015). The evolution of Devonian hydrocarbon gases in shallow aquifers of the northern Appalachian Basin: Insights from integrating noble gas and hydrocarbon geochemistry. *Geochimica et Cosmochimica Acta*, *170*, 321–355.

Dasgupta, R., & Hirschmann, M. M. (2010). The deep carbon cycle and melting in Earth's interior. *Earth and Planetary Science Letters*, *298*(1), 1–13.

Dauphas, N. (2003). The dual origin of the terrestrial atmosphere. *Icarus*, *165*(2), 326–339.

Day, J. M. D., Barry, P. H., Hilton, D. R., Burgess, R., Pearson, D. G., & Taylor, L. A. (2015). The helium flux from the continents and ubiquity of low-3he/4he recycled crust and lithosphere. *Geochimica et Cosmochimica Acta*, *153*, 116–133.

Demaison, G., & Huizinga, B. J. (1991). Genetic Classification of Petroleum Systems (1). *AAPG Bulletin*, *75*(10), 1626–1643.

Dembicki, H. J., & Anderson, M. J. (1989). Secondary Migration of Oil: Experiments Supporting Efficient Movement of Separate, Buoyant Oil Phase Along Limited Conduits. *AAPG Bulletin*, *73*(8), 1018–1021.

Dixon, E. T., Honda, M., McDougall, I., Campbell, I. H., & Sigurdsson, I. (2000). Preservation of near-solar neon isotopic ratios in Icelandic basalts. *Earth and Planetary Science Letters*, *180*(3), 309–324.

Dixon, E. T. (2003). Interpretation of helium and neon isotopic heterogeneity in Icelandic basalts. *Earth and Planetary Science Letters*, *206*(1), 83–99.

Donovan, A. D., Staerker, T. S., Gardner, R., Pope, M. C., Pramudito, A., & Wehner, M. (2016). Findings from the Eagle Ford Outcrops of West Texas and Implications to the Subsurface of South Texas. In J. Breyer (Ed.), *The Eagle Ford Shale* (pp. 301–336).

Dow, W. G. (1974). Application of Oil-Correlation and Source-Rock Data to Exploration in Williston Basin. *AAPG Bulletin*, *58*(7), 1253–1262.

Downey, M. W. (1984). Evaluating Seals for Hydrocarbon Accumulations. *AAPG Bulletin*, *68*(11), 1752–1763.

Dullien, F. (1979). *Porous Media*. San Diego: Academic Press.

Dunnewald, J. B., & Gorton, K. A. (1977). Nugget Oil Accumulations at Dry Piney, Tip Top, and Hogsback Fields, Sublette County, Wyoming. *AAPG Search and Discovery*.

Dymond, J. H., & Smith, E. B. (1980). Virial coefficients of pure gases and mixtures. A critical compilation.

Edman, J. D., & Pitman, J. K. (2010). Geochemistry of Eagle Ford Group source rocks and oils from the First Shot field area, Texas. *Gulf Coast Association of Geological Societies Transactions*, *60*, 217–234.

EIA. (2018). Annual Energy Outlook. U.S. Department of Energy - Energy Information Administration.

Einarsson, P. (2008). Plate boundaries, rifts and transforms in Iceland. *Jökull*, *58*(12), 35–58.

Eldrett, J. S., Minisini, D., & Bergman, S. C. (2014). Decoupling of the carbon cycle during Ocean Anoxic Event 2. *Geology*, *42*(7), 567–570.

Ellam, R. M., & Stuart, F. M. (2004). Coherent He–Nd–Sr isotope trends in high 3he/4he basalts: Implications for a common reservoir, mantle heterogeneity and convection. *Earth and Planetary Science Letters*, *228*(3), 511–523.

Ewing, T. E. (2009). The Ups and Downs of the Sabine Uplift and the Northern Gulf of Mexico Basin: Jurassic Basement Blocks, Cretaceous Thermal Uplifts, and Cenozoic Flexure.

Fanale, F. P., & Cannon, W. A. (1971). Physical adsorption of rare gas on terrigenous sediments. *Earth and Planetary Science Letters*, *11*(1–5), 362–368.

Farley, K. A., Wolf, R. A., & Silver, L. T. (1996). The effects of long alpha-stopping distances on (U,Th)/He ages. *Geochimica et Cosmochimica Acta*, *60*(21), 4223–4229.

Farley, K. A. (2002). (U-Th)/He Dating: Techniques, Calibrations, and Applications. *Reviews in Mineralogy and Geochemistry*, *47*(1), 819–844.

Fernández-Prini, R., Alvarez, J. L., & Harvey, A. H. (2003). Henry's Constants and Vapor–Liquid Distribution Constants for Gaseous Solutes in H2o and D2o at High Temperatures. *Journal of Physical and Chemical Reference Data*, *32*(2), 903–916.

Fitton, J. G., Saunders, A. D., Kempton, P. D., & Hardarson, B. S. (2003). Does depleted mantle form an intrinsic part of the Iceland plume? *Geochemistry, Geophysics, Geosystems*, *4*(3).

Forgotson, J. M. (1954). Regional Stratigraphic Analysis of Cotton Valley Group of Upper Gulf Coastal Plain. *AAPG Bulletin*, *38*(12), 2476–2499.

Fracasso, M. A., Dutton, S. R., & Finley, R. J. (1988). Depositional Systems and Diagenesis of Travis Peak Tight Gas Sandstone Reservoirs, Sabine Uplift Area, Texas. *SPE Formation Evaluation*, *3*(01), 105–115.

Fridleifsson, I. (1979). Geothermal activity in Iceland. *Jökull*, *29*, 47–56.

Friedman, I., Sigurgeirsson, T., & Gardarsson, Ö. (1963). Deuterium in Iceland waters. *Geochimica et Cosmochimica Acta*, *27*(6), 553–561.

Füri, E., Hilton, D. R., Halldórsson, S. A., Barry, P. H., Hahm, D., Fischer, T. P., & Grönvold, K. (2010). Apparent decoupling of the He and Ne isotope systematics of the Icelandic mantle: The role of He depletion, melt mixing, degassing fractionation and air interaction. *Geochimica et Cosmochimica Acta*, *74*(11), 3307–3332.

Gautheron, C., & Moreira, M. (2002). Helium signature of the subcontinental lithospheric mantle. *Earth and Planetary Science Letters*, *199*(1), 39–47.

Gautheron, C., Moreira, M., & Allègre, C. (2005). He, Ne and Ar composition of the European lithospheric mantle. *Chemical Geology*, *217*(1), 97–112.

Gilfillan, S. M. V., Ballentine, C. J., Holland, G., Blagburn, D., Lollar, B. S., Stevens, S., ... Cassidy, M. (2008). The noble gas geochemistry of natural CO2 gas reservoirs

from the Colorado Plateau and Rocky Mountain provinces, USA. *Geochimica et Cosmochimica Acta*, *72*(4), 1174–1198.

Gilfillan, S. M. V., Lollar, B. S., Holland, G., Blagburn, D., Stevens, S., Schoell, M., ... Ballentine, C. J. (2009). Solubility trapping in formation water as dominant CO2 sink in natural gas fields. *Nature*, *458*(7238), 614–618.

Gluyas, J., & Swarbrick, R. (2013). *Petroleum geoscience*. John Wiley & Sons.

Göbel, R., Ott, U., & Begemann, F. (1978). On trapped noble gases in ureilites. *Journal of Geophysical Research: Solid Earth*, *83*(B2), 855–867.

Golding, S. D., Boreham, C. J., & Esterle, J. S. (2013). Stable isotope geochemistry of coal bed and shale gas and related production waters: A review. *International Journal of Coal Geology*, *120*, 24–40.

Graham, D. W. (2002). Noble Gas Isotope Geochemistry of Mid-Ocean Ridge and Ocean Island Basalts: Characterization of Mantle Source Reservoirs. *Reviews in Mineralogy and Geochemistry*, *47*(1), 247–317.

Grimberg, A., Baur, H., Bochsler, P., Bühler, F., Burnett, D. S., Hays, C. C., ... Wieler, R. (2006). Solar Wind Neon from Genesis: Implications for the Lunar Noble Gas Record. *Science*, *314*(5802), 1133–1135.

Gumm, L. P., Bense, V. F., Dennis, P. F., Hiscock, K. M., Cremer, N., & Simon, S. (2015). Dissolved noble gases and stable isotopes as tracers of preferential fluid flow along faults in the Lower Rhine Embayment, Germany. *Hydrogeology Journal*, *24*(1), 99–108.

Györe, D., Stuart, F. M., Gilfillan, S. M., & Waldron, S. (2015). Tracing injected CO2 in the Cranfield enhanced oil recovery field (MS, USA) using He, Ne and Ar isotopes. *International Journal of Greenhouse Gas Control*, *42*, 554–561.

Györe, D., McKavney, R., Gilfillan, S. M. V., & Stuart, F. M. (2017). Fingerprinting coal-derived gases from the UK. *Chemical Geology*.

Halldórsson, S. A., Hilton, D. R., Barry, P. H., Füri, E., & Grönvold, K. (2016). Recycling of crustal material by the Iceland mantle plume: New evidence from nitrogen elemental and isotope systematics of subglacial basalts. *Geochimica et Cosmochimica Acta*, *176*, 206–226.

Halliday, A. N. (2013). The origins of volatiles in the terrestrial planets. *Geochimica et Cosmochimica Acta*, *105*, 146–171.

Hammes, U., Hamlin, H. S., & Ewing, T. E. (2011). Geologic analysis of the Upper Jurassic Haynesville Shale in east Texas and west Louisiana. *AAPG Bulletin*, *95*(10), 1643–1666.

Hammes, U., & Frébourg, G. (2012). Haynesville and Bossier mudrocks: A facies and sequence stratigraphic investigation, East Texas and Louisiana, USA. *Marine and Petroleum Geology*. Insights into Shale Gas Exploration and Exploitation, *31*(1), 8–26.

Harðardóttir, S., Halldórsson, S. A., & Hilton, D. R. (2018). Spatial distribution of helium isotopes in Icelandic geothermal fluids and volcanic materials with implications for location, upwelling and evolution of the Icelandic mantle plume. *Chemical Geology*, *480*, 12–27.

Hards, V. L., Kempton, P. D., & Thompson, R. N. (1995). The heterogeneous Iceland plume: New insights from the alkaline basalts of the Snaefell volcanic centre. *Journal of the Geological Society*, *152*(6), 1003–1009.

Harkness, J. S., Darrah, T. H., Warner, N. R., Whyte, C. J., Moore, M. T., Millot, R., ... Vengosh, A. (2017). The geochemistry of naturally occurring methane and saline

groundwater in an area of unconventional shale gas development. *Geochimica et Cosmochimica Acta*, *208*, 302–334.

Hart, S. R., Schilling, J.-G., & Powell, J. L. (1973). Basalts from Iceland and Along the Reykjanes Ridge: Sr Isotope Geochemistry. *Nature Physical Science*, *246*(155), 104–107.

Heard, A. W., Warr, O., Borgonie, G., Linage, B., Kuloyo, O., Fellowes, J. W., … Ballentine, C. J. (2018). South African crustal fracture fluids preserve paleometeoric water signatures for up to tens of millions of years. *Chemical Geology*, *493*, 379–395.

Heaton, T., & Vogel, J. (1981). "Excess air" in groundwater. *Journal of Hydrology*, *50*, 201–216.

Heber, V. S., Wieler, R., Baur, H., Olinger, C., Friedmann, T. A., & Burnett, D. S. (2009). Noble gas composition of the solar wind as collected by the Genesis mission. *Geochimica et Cosmochimica Acta*, *73*(24), 7414–7432.

Helmberger, D. V., Wen, L., & Ding, X. (1998). Seismic evidence that the source of the Iceland hotspot lies at the core–mantle boundary. *Nature*, *396*(6708), 251–255.

Hendry, M. J., Solomon, D. K., Person, M., Wassenaar, L. I., Gardner, W. P., Clark, I. D., … Hasegawa, T. (2015). Can argillaceous formations isolate nuclear waste? Insights from isotopic, noble gas, and geochemical profiles. *Geofluids*, *15*(3), 381–386.

Herzberg, O., & Mazor, E. (1979). Hydrological applications of noble gases and temperature measurements in underground water systems: Examples from Israel. *Journal of Hydrology*, *41*(3), 217–231.

Hilton, D. R., Thirlwall, M. F., Taylor, R. N., Murton, B. J., & Nichols, A. (2000). Controls on magmatic degassing along the Reykjanes Ridge with implications for the helium paradox. *Earth and Planetary Science Letters*, *183*(1), 43–50.

Hilton, D. R., Grönvold, K., O'Nions, R. K., & Oxburgh, E. R. (1990). Regional distribution of 3he anomalies in the Icelandic crust. *Chemical Geology*, *88*(1), 53–67.

Hilton, D. R., Gronvold, K., Sveinbjornsdottir, A. E., & Hammerschmidt, K. (1998). Helium isotope evidence for off-axis degassing of the Icelandic hotspot. *Chemical Geology*, *149*(3), 173–187.

Hilton, D. R., Grönvold, K., Macpherson, C. G., & Castillo, P. R. (1999). Extreme 3he/4he ratios in northwest Iceland: Constraining the common component in mantle plumes. *Earth and Planetary Science Letters*, *173*(1), 53–60.

Hindle, A. D. (1997). Petroleum Migration Pathways and Charge Concentration: A Three-Dimensional Model. *AAPG Bulletin*, *81*(9), 1451–1481.

Hiyagon, H., & Kennedy, B. M. (1992). Noble gases in CH4-rich gas fields, Alberta, Canada. *Geochimica et Cosmochimica Acta*, *56*(4), 1569–1589.

Hoefs, J. (1997). *Stable isotope geochemistry*. Springer.

Hofmann, A. W. (1997). Mantle geochemistry: The message from oceanic volcanism. *Nature*, *385*(6613), 219–229.

Holland, G., & Gilfillan, S. M. V. (2013). Application of Noble Gases to the Viability of CO2 storage. In *The Noble Gases as Geochemical Tracers*. Springer.

Holland, G., Lollar, B. S., Li, L., Lacrampe-Couloume, G., Slater, G. F., & Ballentine, C. J. (2013). Deep fracture fluids isolated in the crust since the Precambrian era. *Nature*, *497*(7449), 357–360.

Holland, G., Cassidy, M., & Ballentine, C. J. (2009). Meteorite Kr in Earth's Mantle Suggests a Late Accretionary Source for the Atmosphere. *Science*, *326*(5959), 1522–1525.

Holzner, C. P., McGinnis, D. F., Schubert, C. J., Kipfer, R., & Imboden, D. M. (2008). Noble gas anomalies related to high-intensity methane gas seeps in the Black Sea. *Earth and Planetary Science Letters*, *265*(3–4), 396–409.

Honda, M., Kurita, K., Hamano, Y., & Ozima, M. (1982). Experimental studies of He and Ar degassing during rock fracturing. *Earth and Planetary Science Letters*, *59*(2), 429–436.

Hooker, P. J., O'Nions, R. K., & Oxburgh, E. R. (1985). Helium isotopes in North Sea gas fields and the Rhine rift. *Nature*, *318*(6043), 273–275.

Hornafius, J. S., Quigley, D., & Luyendyk, B. P. (1999). The world's most spectacular marine hydrocarbon seeps (Coal Oil Point, Santa Barbara Channel, California): Quantification of emissions. *Journal of Geophysical Research: Oceans*, *104*(C9), 20703–20711.

Horstad, I., Larter, S. R., & Mills, N. (1992). A quantitative model of biological petroleum degradation within the Brent Group reservoir in the Gullfaks Field, Norwegian North Sea. *Organic Geochemistry*, *19*(1), 107–117.

Hughes, W. B., Holba, A. G., & Dzou, L. I. P. (1995). The ratios of dibenzothiophene to phenanthrene and pristane to phytane as indicators of depositional environment and lithology of petroleum source rocks. *Geochimica et Cosmochimica Acta*, *59*(17), 3581–3598.

Hunt, A. G., Darrah, T. H., & Poreda, R. J. (2012). Determining the source and genetic fingerprint of natural gases using noble gas geochemistry: A northern Appalachian Basin case study. *AAPG Bulletin*, *96*(10), 1785–1811.

Jackson, R. B., Vengosh, A., Darrah, T. H., Warner, N. R., Down, A., Poreda, R. J., ... Karr, J. D. (2013). Increased stray gas abundance in a subset of drinking water wells near Marcellus shale gas extraction. *Proceedings of the National Academy of Sciences*, *110*(28), 11250–11255.

Jähne, B., Heinz, G., & Dietrich, W. (1987). Measurement of the diffusion coefficients of sparingly soluble gases in water. *Journal of Geophysical Research: Oceans*, *92*(C10), 10767–10776.

Jakobsson, S., Jónasson, K., & Sigurdsson, I. (2008). The three igneous rock series of Iceland. *Jökull*, *58*, 117–138.

Jarvie, D. M., Hill, R. J., Ruble, T. E., & Pollastro, R. M. (2007). Unconventional shale-gas systems: The Mississippian Barnett Shale of north-central Texas as one model for thermogenic shale-gas assessment. *AAPG Bulletin*, *91*(4), 475–499.

Jennings, D., & Antia, J. (2013). Petrographic characteri- zation of the Eagle Ford Shale, South Texas: Mineralogy, common constituents, and distribution of nanometer-scale pore types. In *Electron microscopy of shale hydrocarbon reservoirs* (102, pp. 102–113). AAPG Memoir.

Kaban, M. K., Flóvenz, Ó. G., & Pálmason, G. (2002). Nature of the crust-mantle transition zone and the thermal state of the upper mantle beneath Iceland from gravity modelling. *Geophysical Journal International*, *149*(2), 281–299.

Kempton, P. D., Fitton, J. G., Saunders, A. D., Nowell, G. M., Taylor, R. N., Hardarson, B. S., & Pearson, G. (2000). The Iceland plume in space and time: A Sr–Nd–Pb–Hf study of the North Atlantic rifted margin. *Earth and Planetary Science Letters*, *177*(3), 255–271.

Kennedy, B., Hiyagon, H., & Reynolds, J. (1990). Crustal neon: A striking uniformity. *Earth and Planetary Science Letters*, *98*(3-4), 277–286.

Kerr, A. C. (1995). The melting processes and composition of the North Atlantic (Iceland) plume: Geochemical evidence from the Early Tertiary basalts. *Journal of the Geological Society*, *152*(6), 975–978.

Kharaka, Y. K., & Specht, D. J. (1988). The solubility of noble gases in crude oil at 25–100°C. *Applied Geochemistry*, *3*(2), 137–144.

Kipfer, R., Aeschbach-Hertig, W., Peeters, F., & Stute, M. (2002). Noble Gases in Lakes and Ground Waters. *Reviews in Mineralogy and Geochemistry*, *47*(1), 615–700.

Kristmannsdóttir, H., & Ármannsson, H. (2003). Environmental aspects of geothermal energy utilization. *Geothermics*. Selected Papers from the European Geothermal Conference 2003, *32*(4), 451–461.

Kulongoski, J. T., Hilton, D. R., & Izbicki, J. A. (2003). Helium isotope studies in the Mojave Desert, California: Implications for groundwater chronology and regional seismicity. *Chemical Geology*, *202*(1), 95–113.

Kurz, M. D., Meyer, P. S., & Sigurdsson, H. (1985). Helium isotopic systematics within the neovolcanic zones of Iceland. *Earth and Planetary Science Letters*, *74*(4), 291–305.

Lafargue, E., & Barker, C. (1988). Effect of water washing on crude oil compositions. *AAPG Bulletin*, *72*(3), 263–276.

Leahy, J. G., & Colwell, R. R. (1990). Microbial degradation of hydrocarbons in the environment. *Microbiological Reviews*, *54*(3), 305–315.

Lee, J.-Y., Marti, K., Severinghaus, J. P., Kawamura, K., Yoo, H.-S., Lee, J. B., & Kim, J. S. (2006). A redetermination of the isotopic abundances of atmospheric Ar. *Geochimica et Cosmochimica Acta*, *70*(17), 4507–4512.

Lee, K. K. M., & Steinle-Neumann, G. (2006). High-pressure alloying of iron and xenon: "Missing" Xe in the Earth's core? *Journal of Geophysical Research: Solid Earth*, *111*(B2), B02202.

Lehmann, B. E., Love, A., Purtschert, R., Collon, P., Loosli, H. H., Kutschera, W., … Gröning, M. (2003). A comparison of groundwater dating with 81kr, 36cl and 4he in four wells of the Great Artesian Basin, Australia. *Earth and Planetary Science Letters*, *211*(3–4), 237–250.

Lewan, M. D. (1993). Laboratory Simulation of Petroleum Formation. In M. H. Engel & S. A. Macko (Eds.), *Organic Geochemistry* (11, pp. 419–442). Topics in Geobiology.

Leya, I., & Wieler, R. (1999). Nucleogenic production of Ne isotopes in Earth's crust and upper mantle induced by alpha particles from the decay of U and Th. *Journal of Geophysical Research: Solid Earth*, *104*(B7), 15439–15450.

Lindquist, S. J. (1988). Practical characterization of eolian reservoirs for development: Nugget Sandstone, Utah—Wyoming thrust belt. *Sedimentary Geology*, *56*(1), 315–339.

Lollar, B. S., Lacrampe-Couloume, G., Voglesonger, K., Onstott, T. C., Pratt, L. M., & Slater, G. F. (2008). Isotopic signatures of CH4 and higher hydrocarbon gases from Precambrian Shield sites: A model for abiogenic polymerization of hydrocarbons. *Geochimica et Cosmochimica Acta*, *72*(19), 4778–4795.

Lorant, F., Prinzhofer, A., Behar, F., & Huc, A.-Y. (1998). Carbon isotopic and molecular constraints on the formation and the expulsion of thermogenic hydrocarbon gases. *Chemical Geology*, *147*(3–4), 249–264.

Lowenstern, J. B., Evans, W. C., Bergfeld, D., & Hunt, A. G. (2014). Prodigious degassing of a billion years of accumulated radiogenic helium at Yellowstone. *Nature*, *506*(7488), 355–358.

Lupton, J., & Evans, L. (2013). Changes in the atmospheric helium isotope ratio over the past 40 years. *Geophysical Research Letters*, *40*(23), 6271–6275.

Mabry, J., Burnard, P., Blard, P.-H., & Zimmermann, L. (2012). Mapping changes in helium sensitivity and peak shape for varying parameters of a Nier-type noble gas ion source. *Journal of Analytical Atomic Spectrometry*, *27*(6), 1012–1017.

Macpherson, C. G., Hilton, D. R., Day, J. M. D., Lowry, D., & Grönvold, K. (2005a). High-3he/4he, depleted mantle and low-18o, recycled oceanic lithosphere in the source of central Iceland magmatism. *Earth and Planetary Science Letters*, *233*(3), 411–427.

Macpherson, C. G., Hilton, D. R., Mertz, D. F., & Dunai, T. J. (2005b). Sources, degassing, and contamination of CO2, H2o, He, Ne, and Ar in basaltic glasses from Kolbeinsey Ridge, North Atlantic. *Geochimica et Cosmochimica Acta*, *69*(24), 5729–5746.

Magoon, L. B., & Dow, W. G. (1994). The petroleum system. *The petroleum system—From source to trap: AAPG Memoir*, *60*, 3–24.

Mahara, Y., Habermehl, M. A., Hasegawa, T., Nakata, K., Ransley, T. R., Hatano, T., … Ohta, T. (2009). Groundwater dating by estimation of groundwater flow velocity and dissolved 4he accumulation rate calibrated by 36cl in the Great Artesian Basin, Australia. *Earth and Planetary Science Letters*, *287*(1–2), 43–56.

Mancini, E. A., Li, P., Goddard, D. A., Ramirez, V., & Talukdar, S. C. (2008). Mesozoic (Upper Jurassic–Lower Cretaceous) deep gas reservoir play, central and eastern Gulf coastal plain. *AAPG Bulletin*, *92*(3), 283–308.

Mark, D. F., Barfod, D., Stuart, F. M., & Imlach, J. (2009). The ARGUS multicollector noble gas mass spectrometer: Performance for 40ar/39ar geochronology. *Geochemistry, Geophysics, Geosystems*, *10*(10).

Marrocchi, Y., Razafitianamaharavo, A., Michot, L. J., & Marty, B. (2005). Low-pressure adsorption of Ar, Kr, and Xe on carbonaceous materials (kerogen and carbon blacks), ferrihydrite, and montmorillonite: Implications for the trapping of noble gases onto meteoritic matter. *Geochimica et Cosmochimica Acta*, *69*(9), 2419–2430.

Marrocchi, Y., Marty, B., Reinhardt, P., & Robert, F. (2011). Adsorption of xenon ions onto defects in organic surfaces: Implications for the origin and the nature of organics in primitive meteorites. *Geochimica et Cosmochimica Acta*, *75*(20), 6255–6266.

Marrocchi, Y., & Marty, B. (2013). Experimental determination of the xenon isotopic fractionation during adsorption. *Geophysical Research Letters*, *40*(16), 4165–4170.

Martel, D. J., O'Nions, R. K., Hilton, D. R., & Oxburgh, E. R. (1990). The role of element distribution in production and release of radiogenic helium: The Carnmenellis Granite, southwest England. *Chemical Geology*, *88*(3), 207–221.

Marty, B., & Jambon, A. (1987). C3he in volatile fluxes from the solid Earth: Implications for carbon geodynamics. *Earth and Planetary Science Letters*, *83*(1–4), 16–26.

Marty, B., Gunnlaugsson, E., Jambon, A., Oskarsson, N., Ozima, M., Pineau, F., & Torssander, P. (1991). Gas geochemistry of geothermal fluids, the Hengill area, southwest rift zone of Iceland. *Chemical Geology*, *91*(3), 207–225.

Marty, B., Torgersen, T., Meynier, V., O'Nions, R. K., & de Marsily, G. (1993). Helium isotope fluxes and groundwater ages in the Dogger Aquifer, Paris Basin. *Water Resources Research*, *29*(4), 1025–1035.

Marty, B., & Tolstikhin, I. N. (1998). CO2 fluxes from mid-ocean ridges, arcs and plumes. *Chemical Geology*, *145*(3), 233–248.

Marty, B., Upton, B. G. J., & Ellam, R. M. (1998). Helium isotopes in early Tertiary basalts, northeast Greenland: Evidence for 58 Ma plume activity in the North Atlantic–Iceland volcanic province. *Geology*, *26*(5), 407–410.

Marty, B., & Zimmermann, L. (1999). Volatiles (He, C, N, Ar) in mid-ocean ridge basalts: Assesment of shallow-level fractionation and characterization of source composition. *Geochimica et Cosmochimica Acta*, *63*(21), 3619–3633.

Marty, B. (2012). The origins and concentrations of water, carbon, nitrogen and noble gases on Earth. *Earth and Planetary Science Letters*, *313–314*, 56–66.

Mazor, E. (1972). Paleotemperatures and other hydrological parameters deduced from noble gases dissolved in groundwaters; Jordan Rift Valley, Israel. *Geochimica et Cosmochimica Acta*, *36*(12), 1321–1336.

Mazor, E., Kharaka, Y. K., Bebout, D. G., & Bachman, A. L. (1981). Atmospheric and Radiogenic Noble Gases in Geopressured-Geothermal Fluids: Northern Gulf of Mexico Basin.

McGlade, C., Speirs, J., & Sorrell, S. (2013). Methods of estimating shale gas resources – Comparison, evaluation and implications. *Energy*, *59*, 116–125.

McMahon, P. B., Thomas, J. C., & Hunt, A. G. (2013). Groundwater Ages and Mixing in the Piceance Basin Natural Gas Province, Colorado. *Environmental Science & Technology*, *47*(23), 13250–13257.

Merrihue, C., & Turner, G. (1966). Potassium-argon dating by activation with fast neutrons. *Journal of Geophysical Research*, *71*(11), 2852–2857.

Mertz, D. F., Devey, C. W., Todt, W., Stoffers, P., & Hofmann, A. W. (1991). Sr-Nd-Pb isotope evidence against plume-asthenosphere mixing north of Iceland. *Earth and Planetary Science Letters*, *107*(2), 243–255.

Moore, M. T., Vinson, D. S., Whyte, C. J., Eymold, W. K., Walsh, T. B., & Darrah, T. H. (2018). Differentiating between biogenic and thermogenic sources of natural gas in coalbed methane reservoirs from the Illinois Basin using noble gas and hydrocarbon geochemistry. *Geological Society, London, Special Publications*, *468*, SP468.8.

Moreira, M., Kunz, J., & Allègre, C. (1998). Rare Gas Systematics in Popping Rock: Isotopic and Elemental Compositions in the Upper Mantle. *Science*, *279*(5354), 1178–1181.

Moreira, M., Breddam, K., Curtice, J., & Kurz, M. D. (2001). Solar neon in the Icelandic mantle: New evidence for an undegassed lower mantle. *Earth and Planetary Science Letters*, *185*(1), 15–23.

Morgan, L. E. (2015). Noble Gas Mass Spectrometer. In W. Jack Rink & J. W. Thompson (Eds.), *Encyclopedia of Scientific Dating Methods* (pp. 608–608).

Mukhopadhyay, P. K., Wade, J. A., & Kruge, M. A. (1995). Organic facies and maturation of Jurassic/Cretaceous rocks, and possible oil-source rock correlation based on pyrolysis of asphaltenes, Scotian Basin, Canada. *Organic Geochemistry*, *22*(1), 85–104.

Neuzil, C. E. (1994). How permeable are clays and shales? *Water Resources Research*, *30*(2), 145–150.

Neuzil, C. E. (2013). Can Shale Safely Host U.S. Nuclear Waste? *Eos, Transactions American Geophysical Union*, *94*(30), 261–262.

Niedermann, S., Graf, T., & Marti, K. (1993). Mass spectrometric identification of cosmic-ray-produced neon in terrestrial rocks with multiple neon components. *Earth and Planetary Science Letters*, *118*(1), 65–73.

Nier, A. O. (1981). Some reminiscences of isotopes, geochronology, and mass spectrometry. *Annual Review of Earth and Planetary Sciences*, *9*(1), 1–18.

Nunn, J. A. (2012). Burial and Thermal History of the Haynesville Shale: Implications for Overpressure, Gas Generation, and Natural Hydrofracture. *GCAGS Journal*, *1*, 81–96.

Ólafsson, M., & Ármannsson, H. (2013). The Námafjall High Temperature System, NE Iceland; Chemical Characteristics of the Fluid for a Power Plant. *Procedia Earth and Planetary Science*. Proceedings of the Fourteenth International Symposium on Water-Rock Interaction, WRI 14, *7*, 640–643.

Osborn, S. G., Vengosh, A., Warner, N. R., & Jackson, R. B. (2011). Methane contamination of drinking water accompanying gas-well drilling and hydraulic fracturing. *Proceedings of the National Academy of Sciences*, *108*(20), 8172–8176.

Osenbrück, K., Lippmann, J., & Sonntag, C. (1998). Dating very old pore waters in impermeable rocks by noble gas isotopes. *Geochimica et Cosmochimica Acta*, *62*(18), 3041–3045.

Óskarsson, N., Sigvaldason, G. E., & Steinthórsson, S. (1982). A Dynamic Model of Rift Zone Petrogenesis and the Regional Petrology of Iceland. *Journal of Petrology*, *23*(1), 28–74.

Owen, T., Bar-Nun, A., & Kleinfeld, I. (1992). Possible cometary origin of heavy noble gases in the atmospheres of Venus, Earth and Mars. *Nature*, *358*(6381), 43–46.

Oxburgh, E. R., O'Nions, R. K., & Hill, R. I. (1986). Helium isotopes in sedimentary basins. *Nature*, *324*(6098), 632.

Ozima, M., & Podosek, F. A. (2002). *Noble gas geochemistry*. Cambridge University Press.

Parnell-Turner, R., White, N., Henstock, T., Murton, B., Maclennan, J., & Jones, S. M. (2014). A continuous 55-million-year record of transient mantle plume activity beneath Iceland. *Nature Geoscience*, *7*(12), 914–919.

Patriarche, D., Castro, M. C., & Goblet, P. (2004). Large-scale hydraulic conductivities inferred from three-dimensional groundwater flow and 4he transport modeling in the Carrizo aquifer, Texas. *Journal of Geophysical Research: Solid Earth*, *109*(B11), B11202.

Peate, D. W., Breddam, K., Baker, J. A., Kurz, M. D., Barker, A. K., Prestvik, T., ... Skovgaard, A. C. (2010). Compositional Characteristics and Spatial Distribution of Enriched Icelandic Mantle Components. *Journal of Petrology*, *51*(7), 1447–1475.

Pepin, R. O. (1991). On the origin and early evolution of terrestrial planet atmospheres and meteoritic volatiles. *Icarus*, *92*(1), 2–79.

Pepin, R. O. (2006). Atmospheres on the terrestrial planets: Clues to origin and evolution. *Earth and Planetary Science Letters*, *252*(1–2), 1–14.

Pepin, R. O., & Porcelli, D. (2006). Xenon isotope systematics, giant impacts, and mantle degassing on the early Earth. *Earth and Planetary Science Letters*, *250*(3–4), 470–485.

Peters, K. E. (1986). Guidelines for Evaluating Petroleum Source Rock Using Programmed Pyrolysis. *AAPG Bulletin*, *70*(3), 318–329.

Peters, K. E., & Cassa, M. R. (1994). Applied Source Rock Geochemistry: Chapter 5: Part II. Essential Elements. *77*, 93–120.

Peters, K. E., Burnham, A. K., & Walters, C. C. (2015). Petroleum generation kinetics: Single versus multiple heating-ramp open-system pyrolysis. *AAPG Bulletin*, *99*(04), 591–616.

Philp, R. P. (1993). Oil-Oil and Oil-Source Rock Correlations: Techniques. In M. H. Engel & S. A. Macko (Eds.), *Organic Geochemistry* (11, pp. 445–460). Topics in Geobiology.

Picard, M. D. (1975). Facies, Petrography and Petroleum Potential of Nugget Sandstone (Jurassic), Southwestern Wyoming and Northeastern Utah. *Symposium on Deep Drilling Frontiers in the Central Rocky Mountains*.

Picard, M. D. (1977). Petrology of the Jurassic Nugget Sandstone, Northeast Utah and Southwest Wyoming. *Rocky Mountain Thrust Belt Geology and Resources; 29th Annual Field Conference Guidebook*, 239–258.

Pierce, A. P., Gott, G. B., & Mytton, J. W. (1964). *Uranium and helium in the Panhandle gas field, Texas, and adjacent areas* (USGS Numbered Series No. 454-G). U.S. Govt. Print. Off.,

Pinti, D. L., & Marty, B. (1995). Noble gases in crude oils from the Paris Basin, France: Implications for the origin of fluids and constraints on oil-water-gas interactions. *Geochimica et Cosmochimica Acta*, *59*(16), 3389–3404.

Pittman, E. D. (1992). Relationship of Porosity and Permeability to Various Parameters Derived from Mercury Injection-Capillary Pressure Curves for Sandstone (1). *AAPG Bulletin*, *76*(2), 191–198.

Plank, T., & Langmuir, C. H. (1998). The chemical composition of subducting sediment and its consequences for the crust and mantle. *Chemical geology*, *145*(3), 325–394.

Podosek, F., Honda, M., & Ozima, M. (1980). Sedimentary noble gases. *Geochimica et Cosmochimica Acta*, *44*(11), 1875–1884.

Podosek, F., Bernatowicz, T., & Kramer, F. (1981). Adsorption of xenon and krypton on shales. *Geochimica et Cosmochimica Acta*, *45*(12), 2401–2415.

Podosek, F. A., Woolum, D. S., Cassen, P., & Nichols, R. H. (2000). Solar gases in the Earth by solar wind irradiation. In *J. Conf. Abstr* (Vol. 5, p. 804).

Poore, H. R., White, N., & Jones, S. (2009). A Neogene chronology of Iceland plume activity from V-shaped ridges. *Earth and Planetary Science Letters*, *283*(1), 1–13.

Porcelli, D., Ballentine, C. J., & Wieler, R. (2002). An Overview of Noble Gas Geochemistry and Cosmochemistry. *Reviews in Mineralogy and Geochemistry*, *47*(1), 1–19.

Porcelli, D., & Ballentine, C. J. (2002). Models for Distribution of Terrestrial Noble Gases and Evolution of the Atmosphere. *Reviews in Mineralogy and Geochemistry*, *47*(1), 411–480.

Poreda, R. J., Craig, H., Arnórsson, S., & Welhan, J. A. (1992). Helium isotopes in Icelandic geothermal systems: I. 3he, gas chemistry, and 13c relations. *Geochimica et Cosmochimica Acta*, *56*(12), 4221–4228.

Prinzhofer, A., Dos Santos Neto, E. V., & Battani, A. (2010). Coupled use of carbon isotopes and noble gas isotopes in the Potiguar basin (Brazil): Fluids migration and mantle influence. *Marine and Petroleum Geology*, *27*(6), 1273–1284.

Prinzhofer, A. (2013). Noble Gases in Oil and Gas Accumulations. In P. Burnard (Ed.), *The Noble Gases as Geochemical Tracers* (pp. 225–247). Advances in Isotope Geochemistry.

Proskurowski, G., Lilley, M. D., Seewald, J. S., Früh-Green, G. L., Olson, E. J., Lupton, J. E., … Kelley, D. S. (2008). Abiogenic Hydrocarbon Production at Lost City Hydrothermal Field. *Science*, *319*(5863), 604–607.

Pujol, M., Marty, B., & Burgess, R. (2011). Chondritic-like xenon trapped in Archean rocks: A possible signature of the ancient atmosphere. *Earth and Planetary Science Letters*, *308*(3–4), 298–306.

Pujol, M., Van den Boorn, S., Bourdon, B., Brennwald, M., & Kipfer, R. (2018). Physical processes occurring in tight gas reservoirs from Western Canadian Sedimentary Basin: Noble gas signature. *Chemical Geology*. The noble gases as geochemical tracers – in celebration of Pete Burnard, *480*, 128–138.

Purcell, L. P., Rashid, M. A., & Hardy, I. A. (1979). Geochemical Characteristics of Sedimentary Rocks in Scotian Basin. *AAPG Bulletin*, *63*(1), 87–105.

Renne, P. R., Mundil, R., Balco, G., Min, K., & Ludwig, K. R. (2010). Joint determination of 40k decay constants and 40ar/40k for the Fish Canyon sanidine standard, and improved accuracy for 40ar/39ar geochronology. *Geochimica et Cosmochimica Acta*, *74*(18), 5349–5367.

Reynolds, J. H. (1963). Xenology. *Journal of Geophysical Research*, *68*(10), 2939–2956.

Reynolds, J. H. (1956). High Sensitivity Mass Spectrometer for Noble Gas Analysis. *Review of Scientific Instruments*, *27*(11), 928–934.

Rice, D. D. (1983). Relation of Natural Gas Composition to Thermal Maturity and Source Rock Type in San Juan Basin, Northwestern New Mexico and Southwestern Colorado. *AAPG Bulletin*, *67*(8), 1199–1218.

Ritsema, J., Heijst, H. J. v., & Woodhouse, J. H. (1999). Complex Shear Wave Velocity Structure Imaged Beneath Africa and Iceland. *Science*, *286*(5446), 1925–1928.

Rivard, C., Lavoie, D., Lefebvre, R., Séjourné, S., Lamontagne, C., & Duchesne, M. (2014). An overview of Canadian shale gas production and environmental concerns. *International Journal of Coal Geology*. Environmental geology and the unconventional gas revolution, *126*, 64–76.

Robison, C. R. (1997). Hydrocarbon source rock variability within the Austin Chalk and Eagle Ford Shale (Upper Cretaceous), East Texas, U.S.A. *International Journal of Coal Geology*, *34*(3–4), 287–305.

Romer, M. C., Phi, M. V., Barber, C., & Huynh, D. V. (2007). Well Stimulation Technology Progression in Horizontal Frontier Wells, Tip Top/Hogsback Field, Wyoming.

Romero-Sarmiento, M.-F., Ducros, M., Carpentier, B., Lorant, F., Cacas, M.-C., Pegaz-Fiornet, S., … Moretti, I. (2013). Quantitative evaluation of TOC, organic porosity and gas retention distribution in a gas shale play using petroleum system modeling: Application to the Mississippian Barnett Shale. *Marine and Petroleum Geology*, *45*, 315–330.

Rooney, M. A., Claypool, G. E., & Moses Chung, H. (1995). Modeling thermogenic gas generation using carbon isotope ratios of natural gas hydrocarbons. *Chemical Geology*. Processes of Natural Gas Formation, *126*(3), 219–232.

Ross, D. J. K., & Bustin, M. R. (2007). Impact of mass balance calculations on adsorption capacities in microporous shale gas reservoirs. *Fuel*, *86*(17), 2696–2706.

Rutherford, E. (1906). *Radioactive transformations*. Yale University Press.

Ryder, R. T. (1996). *Fracture patterns and their origin in the upper Devonian Antrim Shale gas reservoir of the Michigan basin; a review* (USGS Numbered Series No. 96-23). U.S. Geological Survey,

Sanloup, C., Schmidt, B. C., Perez, E. M. C., Jambon, A., Gregoryanz, E., & Mezouar, M. (2005). Retention of Xenon in Quartz and Earth's Missing Xenon. *Science*, *310*(5751), 1174–1177.

Sano, J. L., Ratcliffe, K. T., & Spain, D. R. (2013a). Chemostratigraphy of the Haynesville Shale. *AAPG Memoir*, *105*, 137–154.

Sano, Y., Urabe, A., Wakita, H., Chiba, H., & Sakai, H. (1985). Chemical and isotopic compositions of gases in geothermal fluids in Iceland. *Geochemical Journal*, *19*(3), 135–148.

Sano, Y., Marty, B., & Burnard, P. (2013b). Noble Gases in the Atmosphere. In P. Burnard (Ed.), *The Noble Gases as Geochemical Tracers* (pp. 17–31). Advances in Isotope Geochemistry.

Sarda, P., Staudacher, T., & Allegre, C. (1988). Neon isotopes in submarine basalts. *Earth and Planetary Science Letters*, *91*(1-2), 73–88.

Schilling, J.-G. (1973). Iceland Mantle Plume: Geochemical Study of Reykjanes Ridge. *Nature*, *242*(5400), 565–571.

Schlegel, M. E., Zhou, Z., McIntosh, J. C., Ballentine, C. J., & Person, M. A. (2011). Constraining the timing of microbial methane generation in an organic-rich shale using noble gases, Illinois Basin, USA. *Chemical Geology*, *287*(1–2), 27–40.

Schmoker, J. W. (2002). Resource-assessment perspectives for unconventional gas systems. *AAPG Bulletin*, *86*(11), 1993–1999.

Schoell, M. (1980). The hydrogen and carbon isotopic composition of methane from natural gases of various origins. *Geochimica et Cosmochimica Acta*, *44*(5), 649–661.

Schowalter, T. T. (1979). Mechanics of Secondary Hydrocarbon Migration and Entrapment. *AAPG Bulletin*, *63*(5), 723–760.

Sigmarsson, O., & Steinthórsson, S. (2007). Origin of Icelandic basalts: A review of their petrology and geochemistry. *Journal of Geodynamics*. Hotspot Iceland, *43*(1), 87–100.

Sigmarsson, O., Maclennan, J., & Carpentier, M. (2008). Geochemistry of igneous rocks in Iceland: A review. *Jökull*, *58*.

Smith, S. P., & Kennedy, B. M. (1983). The solubility of noble gases in water and in NaCl brine. *Geochimica et Cosmochimica Acta*, *47*(3), 503–515.

Smith, S. (1985). Noble gas solubility in water at high temperature. *Eos*, *66*, 397.

Solomon, D. K., Hunt, A., & Poreda, R. J. (1996). Source of radiogenic helium 4 in shallow aquifers: Implications for dating young groundwater. *Water Resources Research*, *32*(6), 1805–1813.

Stacey, J. S., Sherrill, N. D., Dalrymple, G. B., Lanphere, M. A., & Carpenter, N. V. (1981). A five-collector system for the simultaneous measurement of argon isotope ratios in a static mass spectrometer. *International Journal of Mass Spectrometry and Ion Physics*, *39*(2), 167–180.

Stahl, W. J. (1978). Source rock-crude oil correlation by isotopic type-curves. *Geochimica et Cosmochimica Acta*, *42*(10), 1573–1577.

Stainforth, J. G., & Reinders, J. E. A. (1990). Primary migration of hydrocarbons by diffusion through organic matter networks, and its effect on oil and gas generation. *Organic Geochemistry*, *16*(1), 61–74.

Stainforth, J. G. (2009). Practical kinetic modeling of petroleum generation and expulsion. *Marine and Petroleum Geology*. Thematic Set on Basin Modeling Perspectives, *26*(4), 552–572.

Staudacher, T., Sarda, P., Richardson, S. H., Allègre, C. J., Sagna, I., & Dmitriev, L. V. (1989). Noble gases in basalt glasses from a Mid-Atlantic Ridge topographic high at 14°N: Geodynamic consequences. *Earth and Planetary Science Letters*, *96*(1), 119–133.

Staudacher, T., & Allègre, C. J. (1988). Recycling of oceanic crust and sediments: The noble gas subduction barrier. *Earth and Planetary Science Letters*, *89*(2), 173–183.

Steefel, C. I., & Lasaga, A. C. (1994). A coupled model for transport of multiple chemical species and kinetic precipitation/dissolution reactions with application to reactive flow in single phase hydrothermal systems. *American Journal of Science*, *294*(5), 529–592.

Stefánsson, A., & Arnórsson, S. (2002). Gas pressures and redox reactions in geothermal fluids in Iceland. *Chemical Geology*. Geochemistry of Crustal Fluids-Fluids in the Crust and Chemical Fluxes at the Earth's Surface, *190*(1), 251–271.

Stefánsson, A., Keller, N. S., Robin, J. G., & Ono, S. (2015). Multiple sulfur isotope systematics of Icelandic geothermal fluids and the source and reactions of sulfur in volcanic geothermal systems at divergent plate boundaries. *Geochimica et Cosmochimica Acta*, *165*, 307–323.

Stefánsson, A., & Barnes, J. D. (2016). Chlorine isotope geochemistry of Icelandic thermal fluids: Implications for geothermal system behavior at divergent plate boundaries. *Earth and Planetary Science Letters*, *449*, 69–78.

Stefánsson, A., Sveinbjörnsdóttir, Á. E., Heinemeier, J., Arnórsson, S., Kjartansdóttir, R., & Kristmannsdóttir, H. (2016a). Mantle CO2 degassing through the Icelandic crust: Evidence from carbon isotopes in groundwater. *Geochimica et Cosmochimica Acta*, *191*, 300–319.

Stefánsson, A., Keller, N. S., Robin, J. G., Kaasalainen, H., Björnsdóttir, S., Pétursdóttir, S., … Hreggvidsson, G. Ó. (2016b). Quantifying mixing, boiling, degassing, oxidation and reactivity of thermal waters at Vonarskard, Iceland. *Journal of Volcanology and Geothermal Research*, *309*, 53–62.

Stefánsson, A., Hilton, D. R., Sveinbjörnsdóttir, Á. E., Torssander, P., Heinemeier, J., Barnes, J. D., … Arnórsson, S. (2017). Isotope systematics of Icelandic thermal fluids. *Journal of Volcanology and Geothermal Research*, *337*, 146–164.

Stolper, D. A., Lawson, M., Davis, C. L., Ferreira, A. A., Neto, E. V. S., Ellis, G. S., … Eiler, J. M. (2014). Formation temperatures of thermogenic and biogenic methane. *Science*, *344*(6191), 1500–1503.

Stolper, D. A., Lawson, M., Formolo, M. J., Davis, C. L., Douglas, P. M. J., & Eiler, J. M. (2017). The utility of methane clumped isotopes to constrain the origins of methane in natural gas accumulations. *Geological Society, London, Special Publications*, *468*, SP468.3.

Stuart, F. M., Lass-Evans, S., Godfrey Fitton, J., & Ellam, R. M. (2003). High 3he/4he ratios in picritic basalts from Baffin Island and the role of a mixed reservoir in mantle plumes. *Nature*, *424*(6944), 57–59.

Stute, M., Forster, M., Frischkorn, H., Serejo, A., Clark, J. F., Schlosser, P., … Bonani, G. (1995). Cooling of Tropical Brazil (5°C) During the Last Glacial Maximum. *Science*, *269*(5222), 379–383.

Sun, S.-S., Tatsumoto, M., & Schilling, J.-G. (1975). Mantle Plume Mixing Along the Reykjanes Ridge Axis: Lead Isotopic Evidence. *Science*, *190*(4210), 143–147.

Sweeney, J. J., & Burnham, A. K. (1990). Evaluation of a Simple Model of Vitrinite Reflectance Based on Chemical Kinetics (1). *AAPG Bulletin*, *74*(10), 1559–1570.

Takahata, N., & Sano, Y. (2000). Helium flux from a sedimentary basin. *Applied Radiation and Isotopes*, *52*(4), 985–992.

Takaoka, N. (1983). Noble gas mass spectrometry. *Shitsuryo Bunseki*, *31*(1), 21–33.

Tang, Y., Perry, J. K., Jenden, P. D., & Schoell, M. (2000). Mathematical modeling of stable carbon isotope ratios in natural gases†. *Geochimica et Cosmochimica Acta*, *64*(15), 2673–2687.

Tang, Y., Huang, Y., Ellis, G. S., Wang, Y., Kralert, P. G., Gillaizeau, B., ... Hwang, R. (2005). A kinetic model for thermally induced hydrogen and carbon isotope fractionation of individual n-alkanes in crude oil. *Geochimica et Cosmochimica Acta*, *69*(18), 4505–4520.

Taylor, R. N., Thirlwall, M. F., Murton, B. J., Hilton, D. R., & Gee, M. A. M. (1997). Isotopic constraints on the influence of the Icelandic plume. *Earth and Planetary Science Letters*, *148*(1), E1–E8.

Thirlwall, M. F. (1995). Generation of the Pb isotopic characteristics of the Iceland plume. *Journal of the Geological Society*, *152*(6), 991–996.

Thirlwall, M. F., Gee, M. A. M., Taylor, R. N., & Murton, B. J. (2004). Mantle components in Iceland and adjacent ridges investigated using double-spike Pb isotope ratios. *Geochimica et Cosmochimica Acta*, *68*(2), 361–386.

Thomas, D. L., Bird, D. K., Arnórsson, S., & Maher, K. (2016). Geochemistry of CO2-rich waters in Iceland. *Chemical Geology*, *444*, 158–179.

Thompson, J., Fan, L., Grant, D., Martin, R. B., Kanneganti, K. T., & Lindsay, G. J. (2011). An Overview of Horizontal-Well Completions in the Haynesville Shale. *Journal of Canadian Petroleum Technology*, *50*(06), 22–35.

Tian, Y., Ayers, W., & D. Jr. McCain, W. (2013). The Eagle Ford Shale Play South Texas: Regional Variations in Fluid Types Hydrocarbon Production and Reservoir Properties.

Tinnin, B. M., & Darmaoen, S. T. R. (2016). Chemostratigraphic Variability of the Eagle Ford Shale, South Texas: Insights into Paleoredox and Sedimentary Facies Changes. In J. Breyer (Ed.), *The Eagle Ford Shale* (pp. 259–283).

Tissot, B. P., & Welte, D. H. ( ) (1984). Petroleum formation and occurrence.

Tolstikhin, I., Lehmann, B. E., Loosli, H. H., & Gautschi, A. (1996). Helium and argon isotopes in rocks, minerals, and related ground waters: A case study in northern Switzerland. *Geochimica et Cosmochimica Acta*, *60*(9), 1497–1514.

Tolstikhin, I., Ballentine, C., Polyak, B., Prasolov, E., & Kikvadze, O. (2017). The noble gas isotope record of hydrocarbon field formation time scales. *Chemical Geology*, *471*, 141–152.

Torgersen, T., & Ivey, G. N. (1985). Helium accumulation in groundwater. II: A model for the accumulation of the crustal 4he degassing flux. *Geochimica et Cosmochimica Acta*, *49*(11), 2445–2452.

Torgersen, T., & Jenkins, W. J. (1982). Helium isotopes in geothermal systems: Iceland, The Geysers, Raft River and Steamboat Springs. *Geochimica et Cosmochimica Acta*, *46*(5), 739–748.

Torgersen, T., & Clarke, W. (1985). Helium accumulation in groundwater, I: An evaluation of sources and the continental flux of crustal 4he in the Great Artesian Basin, Australia. *Geochimica et Cosmochimica Acta*, *49*(5), 1211–1218.

Torgersen, T. (1989). Terrestrial helium degassing fluxes and the atmospheric helium budget: Implications with respect to the degassing processes of continental crust. *Chemical Geology: Isotope Geoscience section*, *79*(1), 1–14.

Torgersen, T., Habermehl, M. A., & Clarke, W. B. (1992). Crustal helium fluxes and heat flow in the Great Artesian Basin, Australia. *Chemical Geology*, *102*(1–4), 139–152.

Torgersen, T., & Kennedy, B. M. (1999). Air-Xe enrichments in Elk Hills oil field gases: Role of water in migration and storage. *Earth and Planetary Science Letters*, *167*(3–4), 239–253.

Torgersen, T. (1980). Controls on pore-fluid concentration of 4he and 222rn and the calculation of 4he/222rn ages. *Journal of Geochemical Exploration*, *13*(1), 57–75.

Toth, J. (1980). Cross-Formational Gravity-Flow of Groundwater: A Mechanism of the Transport and Accumulation of Petroleum (The Generalized Hydraulic Theory of Petroleum Migration). *29*, 121–167.

Trieloff, M., Kunz, J., Clague, D. A., Harrison, D., & Allègre, C. J. (2000). The Nature of Pristine Noble Gases in Mantle Plumes. *Science*, *288*(5468), 1036–1038.

Tryggvason, K., Husebye, E. S., & Stefánsson, R. (1983). Seismic image of the hypothesized Icelandic hot spot. *Tectonophysics*. Continental Tectonics: Structure, Kinematics and Dynamics, *100*(1), 97–118.

Tucker, J. M., & Mukhopadhyay, S. (2014). Evidence for multiple magma ocean outgassing and atmospheric loss episodes from mantle noble gases. *Earth and Planetary Science Letters*, *393*, 254–265.

Tyne, R. L., Barry, P. H., Kulongoski, J. T., Landon, M. K., Hillegonds, D. J., McMahon, P. B., & Ballentine, C. J. (2018). Noble Gas Characterisation of Produced Waters from the Fruitvale and Lost Hills Oil Fields, CA, USA. In *Goldschmidt Abstracts 2018* (Vol. 2592).

Ungerer, P., Burrus, J., Doligez, B., Chenet, P. Y., & Bessis, F. (1990). Basin Evaluation by Integrated Two-Dimensional Modeling of Heat Transfer, Fluid Flow, Hydrocarbon Generation, and Migration (1). *AAPG Bulletin*, *74*(3), 309–335.

Ungerer, P. (1990). State of the art of research in kinetic modelling of oil formation and expulsion. *Organic Geochemistry*. Proceedings of the 14th International Meeting on Organic Geochemistry, *16*(1), 1–25.

Varekamp, J. C., Kreulen, R., Poorter, R. P. E., & Bergen, M. J. V. (1992). Carbon sources in arc volcanism, with implications for the carbon cycle. *Terra Nova*, *4*(3), 363–373.

Vengosh, A., Jackson, R. B., Warner, N., Darrah, T. H., & Kondash, A. (2014). A Critical Review of the Risks to Water Resources from Unconventional Shale Gas Development and Hydraulic Fracturing in the United States. *Environmental Science & Technology*, *48*(15), 8334–8348.

Waples, D. W. (1980). Time and Temperature in Petroleum Formation: Application of Lopatin's Method to Petroleum Exploration. *AAPG Bulletin*, *64*(6), 916–926.

Waples, D. W. (1994). Maturity modeling: Thermal indicators, hydrocarbon generation, and oil cracking. *Memoirs-American Association of Petroleum Geologists*, 285–285.

Warr, O., Rochelle, C. A., Masters, A., & Ballentine, C. J. (2015a). Determining noble gas partitioning within a CO2–H2o system at elevated temperatures and pressures. *Geochimica et Cosmochimica Acta*, *159*, 112–125.

Warr, O., Ballentine, C. J., Mu, J., & Masters, A. (2015b). Optimizing Noble Gas–Water Interactions via Monte Carlo Simulations. *The Journal of Physical Chemistry B*, *119*(45), 14486–14495.

Warr, O. W. P. (2013). Understanding phase behaviour in the geological storage of carbon dioxide.

Wasserburg, G. J., Mazor, E., & Zartman, R. E. (1963). Isotopic and Chemical Composition of Some Terrestrial Natural Gases. In J. Geiss & E. D. Goldberg (Eds.), *Earth science and meteoritics* (pp. 219–240). Amsterdam: North-Holland Pub. Co.

Webel, S. (1977). Some New Perspectives on the Old Nugget Oil Fields of the LaBarge Platform. *Rocky Mountain Thrust Belt Geology and Resources; 29th Annual Field Conference Guidebook*, 665–671.

Weiss, R. F. (1968). Piggyback sampler for dissolved gas studies on sealed water samples. *Deep Sea Research and Oceanographic Abstracts*, *15*(6), 695–699.

Wen, T., Castro, M. C., Hall, C. M., Pinti, D. L., & Lohmann, K. C. (2015a). Constraining groundwater flow in the glacial drift and saginaw aquifers in the Michigan Basin through helium concentrations and isotopic ratios. *Geofluids*.

Wen, T., Castro, M., Nicot, J.-P., Hall, C., Pinti, D., Mickler, P., … Larson, T. (2017). Characterizing the Noble Gas Isotopic Composition of the Barnett Shale and Strawn Group and Constraining the Source of Stray Gas in the Trinity Aquifer, North-Central Texas. *Environmental Science and Technology*, *51*(11), 6533–6541.

Wen, T., Castro, M. C., Ellis, B. R., Hall, C. M., & Lohmann, K. C. (2015b). Assessing compositional variability and migration of natural gas in the Antrim Shale in the Michigan Basin using noble gas geochemistry. *Chemical Geology*, *417*, 356–370.

Wen, T., Castro, M. C., Nicot, J.-P., Hall, C. M., Larson, T., Mickler, P., & Darvari, R. (2016). Methane Sources and Migration Mechanisms in Shallow Groundwaters in Parker and Hood Counties, Texas—A Heavy Noble Gas Analysis. *Environmental Science & Technology*.

Wetherill, G. W. (1954). Variations in the Isotopic Abundances of Neon and Argon Extracted from Radioactive Minerals. *Physical Review*, *96*(3), 679–683.

White, R. S., Bown, J. W., & Smallwood, J. R. (1995). The temperature of the Iceland plume and origin of outward-propagating V-shaped ridges. *Journal of the Geological Society*, *152*(6), 1039–1045.

Whiticar, M. J., Faber, E., & Schoell, M. (1986). Biogenic methane formation in marine and freshwater environments: CO2 reduction vs. acetate fermentation—Isotope evidence. *Geochimica et Cosmochimica Acta*, *50*(5), 693–709.

Whiticar, M. J. (1994). Correlation of natural gases with their sources. *Memoirs-American Association of Petroleum Geologists*, 261–261.

Wieler, R., & Eikenberg, J. (1999). An upper limit on the spontaneous fission decay constant of 232th derived from xenon in monazites with extremely high Th/U ratios. *Geophysical research letters*, *26*(1), 107–110.

Wieler, R. (2002). Noble Gases in the Solar System. *Reviews in Mineralogy and Geochemistry*, *47*(1), 21–70.

Wiprut, D., & Zoback, M. D. (2000). Fault reactivation and fluid flow along a previously dormant normal fault in the northern North Sea. *Geology*, *28*(7), 595–598.

Woda, J., Wen, T., Oakley, D., Yoxtheimer, D., Engelder, T., Castro, M. C., & Brantley, S. L. (2018). Detecting and explaining why aquifers occasionally become degraded near hydraulically fractured shale gas wells. *Proceedings of the National Academy of Sciences*.

Wolfe, C. J., Bjarnason, I. T., VanDecar, J. C., & Solomon, S. C. (1997). Seismic structure of the Iceland mantle plume. *Nature*, *385*(6613), 245–247.

Zaikowski, A., Kosanke, B. J., & Hubbard, N. (1987). Noble gas composition of deep brines from the Palo Duro Basin, Texas. *Geochimica et Cosmochimica Acta*, *51*(1), 73–84.

Zaikowski, A., & Spangler, R. R. (1990). Noble gas and methane partitioning from ground water: An aid to natural gas exploration and reservoir evaluation. *Geology*, *18*(1), 72–74.

Zartman, R. E., Wasserburg, G. J., & Reynolds, J. H. (1961). Helium, argon, and carbon in some natural gases. *Journal of Geophysical Research*, *66*(1), 277–306.

Zhao, D. (2004). Global tomographic images of mantle plumes and subducting slabs: Insight into deep Earth dynamics. *Physics of the Earth and Planetary Interiors*. Plumes and Superplumes, *146*(1), 3–34.

Zhou, Z., Ballentine, C. J., Kipfer, R., Schoell, M., & Thibodeaux, S. (2005). Noble gas tracing of groundwater/coalbed methane interaction in the San Juan Basin, USA. *Geochimica et Cosmochimica Acta*, *69*(23), 5413–5428.

Zhou, Z., & Ballentine, C. J. (2006). 4he dating of groundwater associated with hydrocarbon reservoirs. *Chemical Geology*, *226*(3-4), 309–327.

Zhou, Z., Ballentine, C. J., Schoell, M., & Stevens, S. H. (2012). Identifying and quantifying natural CO2 sequestration processes over geological timescales: The Jackson Dome CO2 Deposit, USA. *Geochimica et Cosmochimica Acta*, *86*, 257–275.

Ziegler, J. F. (1977). *Helium: Stopping powers and ranges in all elemental matter*. pergamon.

Zindler, A., & Hart, S. (1986). Chemical geodynamics. *Annual review of earth and planetary sciences*, *14*(1), 493–571.

Zumberge, J., Ferworn, K., & Brown, S. (2012). Isotopic reversal ('rollover') in shale gases produced from the Mississippian Barnett and Fayetteville formations. *Marine and Petroleum Geology*. Insights into Shale Gas Exploration and Exploitation, *31*(1), 43–52.